

**Generative Reciprocity: A Computational Approach for Performance-Based and
Fabrication-Aware Design of Reciprocal Systems**

by

Omid Oliyan Torghabehi

A dissertation submitted in partial fulfillment
of the requirements for the degree of
Doctor of Philosophy
(Architecture)
in the University of Michigan
2020

Doctoral Committee:

Professor Peter D. von Buelow, Chair
Professor Karl Daubmann, Lawrence Technological University
Associate Professor Lars Junghans
Professor Emeritus Richard E. Robertson
Associate Professor Kathy Velikov

Omid Oliyan Torghabehi

oliyan@umich.edu

ORCID iD: 0000-0003-2074-5109

© Omid Oliyan Torghabehi 2020

DEDICATION

To my parents for their endless support and love, my brother Ehsan, and most of all to Sarah, the love of my life.

TABLE OF CONTENTS

DEDICATION	ii
LIST OF TABLES	vi
LIST OF FIGURES	vii
ABSTRACT	xxvii
Chapter 1: Introduction	1
1.1 Historical context for reciprocal structures	1
1.2 Contemporary applications of the reciprocal structures	3
1.3 Thesis structure	10
Chapter 2: Theoretical Framework and Application of Computational Design	14
2.1 Form and form-finding in architecture	15
2.2 Morphogenesis and generative design in architecture	18
2.3 Constraint-based modelling in fabrication-aware design	21
2.3.1 Definition of constraint-based modelling	21
2.3.2 Types of design constraints: Hard and soft constraints	22
2.4 Rationalization in architecture	24
2.4.1 Definition and necessity of rationalization	24
2.4.2 Timing and strategies in architectural rationalization	27
2.5 performance-based and fabrication-aware design process for reciprocal systems	34
2.6 Conclusions	35
Chapter 3: Generative Design and Form-Finding of Reciprocal Systems	41
3.1 Introduction	41
3.2 Chapter Methodology	42
3.3 General approaches for design and form-finding of reciprocal systems as discrete systems	42
3.4 Review of modeling methods for generation of reciprocal patterns	44

3.5	Proposed mesh-based generative formulation for reciprocal pattern generation	48
3.6	Review of form-finding methods for reciprocal systems	56
3.7	Proposed method for form-finding of reciprocal systems	58
3.7.1	Methodology	58
3.7.2	Constraint-based modelling formulation	61
3.7.3	The dynamic relaxation method for constraint resolution	63
3.7.4	Numerical formulation of dynamic relaxation method	65
3.8	Quantitative study of the results for the proposed form-finding method	68
3.9	Conclusions	74
Chapter 4: Design Parameters, Simulation and Structural Behavior		78
4.1	Reciprocal structures as discrete systems: Introduction to analytical study of reciprocal behavior	79
4.2	Methodology	82
4.3	Simulating the reciprocal behavior	83
4.3.1	Module analysis	91
4.3.2	Parametric study of the structural behavior of the reciprocal module	104
4.3.3	Parametric study of the structural behavior of flat reciprocal systems	109
4.3.4	Comparative study of the determinacy and member connectivity conditions	120
4.4	Comparative study of reciprocal systems and grid shells	128
4.5	Optimization of flat reciprocal systems	131
4.5.1	Methodology	131
4.5.2	Geometry definition and parametric modeling	132
4.5.3	Simulation model	135
4.5.4	Form exploration	137
4.5.5	Optimization results and post processing	140
4.6	Discussion	148
Chapter 5: Physical Prototyping, Destructive Structural Tests, and Scaled Model Fabrication		155
5.1	Introduction	155
5.2	Fabrication data generation and analytical model development	157
5.2.1	Generating 3-D reciprocal member geometry	157
5.2.2	Generating analytical model from the wireframe geometry	160
5.3	Reciprocal connections	162

5.3.1	Design parameters and types of reciprocal connections	162
5.3.2	Physical prototyping of the reciprocal modules	172
5.3.3	Application and types of connection fasteners	175
5.4	Destructive structural tests	178
5.4.1	Fabrication of test samples	178
5.4.2	Structural setup and results	179
5.5	Detailed finite elements analysis and results	187
5.6	Scaled model fabrication	193
5.6.1	Scaled model definition	193
5.6.2	Fabrication process_ Test 01	194
5.6.3	Fabrication process_ Test 02	200
5.6.4	Fabrication process_ Test 03	203
5.7	Discussion and conclusion	210
Chapter 6: Computational Design Process and the Fabrication Case Study		214
6.1	The complexity of the reciprocal systems: the need for an integrative design process	214
6.2	Computational design process: the need for computational tooling	216
6.3	Case study: design to fabrication of the Reciprocal Shades project	218
6.4	Implementation of the computational design process	222
6.4.1	Computational model: The geometry module	222
6.4.2	Computational model: the form-finding module	223
6.4.3	Computational model: the 3-D geometry generation module	225
6.4.4	Computational model: the structural simulation module	227
6.4.5	Computational model: the shading estimation module	230
6.4.6	Computational model: the fabrication data generation module	231
6.5	Design exploration: multi-objective exploration of the design space	234
6.6	Fabrication process for the Reciprocal Shades project	258
6.7	Post-construction inspections	271
6.8	Discussion and conclusions	279
Chapter 7: Conclusions		282
7.1	Summary	282
7.2	Conclusions, Contributions and synthesis	282
7.3	Outlook and future works	288

LIST OF TABLES

Table 1_ Material properties of plywood based on the Engineered Wood Association standard.	96
Table 2_ Optimization formulation definition for the first case study.	138
Table 3_ Optimization formulation definition for the second case study.....	139
Table 4_ Material properties of Plywood based on APA (Engineered Wood Association) standard.	188
Table 6_ Design parameters and their variation ranges defined for design exploration.	236
Table 7_ Numerical output generated for each design solution in the form exploration process.	240
Table 8_ Numerical design data for the selected arch geometry.	258

LIST OF FIGURES

Figure 1_ Rainbow Bridge only exists in a 900-year-old painting that shows the capital city of Kaifeng in Song dynasty. (Chen, 2008).....	1
Figure 2_ da Vinci’s temporary bridge sketch. (Anon, 1956)	2
Figure 3_ a) Villard de Honnecourt (1250 C.E.), b) Sebastiano Serlio (1545 C.E.), c) Leonardo da Vinci (1452–1519 C.E.), d) John Wallis (1695 C.E.).....	3
Figure 4_ Bamboo roof, Shigeru Ban, School of Architecture, Rice University. 2002	4
Figure 5_ a) European Quality Award. The sphere is constructed by the precise fit of 24 identical components. One of a series of 4 different awards made for EFQM, Brussels (1990). b) Dagen van de WISKUNST, LUCA, Brussel, Belgium, 2013.....	4
Figure 6_ a) KREOD Pavilion Chun Li architects, Ramboll Engineering 2015. b) Quasi-reciprocal timber and discontinuous post-tensioned concrete structure and fabrication constraints. Utzon 40 Pavilion, 2015.	5
Figure 7_ An example of connection detailing in a spatial structure. Canopy roof of Fiera Milano, Architectural design by studio Fuksas. Engineering by Schlaich Bergermann Partners. .	6
Figure 8_ Structural joint conditions: a) a knot with multiple bars meeting in one point with or b) without an additional joint element, c) an expanded node with a minimum expansion and d) expanded node with larger expansion (Apolinarska, 2018).....	6
Figure 9_ Left: Development of eccentricities between member centerlines in generation of free-form reciprocal systems. Right: reciprocal system after minimizing eccentricities using form-finding method.	7

Figure 10_ Expanding a four-valent connection node and generating two-valent connections as in a reciprocal system (Mesnil et al., 2018), Eccentricities between the centerline of concurrent members in reciprocal structures.	8
Figure 11_ Classification for reciprocal structure families and their respective design and form-finding methods (Danz, 2014).	9
Figure 12_ Figure 1. Soap film experiments by the Institute for Lightweight Structures at the University of Stuttgart, German Pavilion Expo 1967, Frei Otto and Rolf Gutbrod.	16
Figure 13_ Design and manufacturing of bio-degradable hydrogel material for robotic additive manufacturing (Mogas-Soldevila et al., 2015).	16
Figure 14_ Antonio Gaudi’s application of catenary arches in designing of a church at Colonia Guell in Barcelona, Spain 1883. Candela’s High Life Textile factory in Coyoacan, Mexico City in 1955 consisting of concrete hyperbolic Parabolas.	18
Figure 15_ Pier Luigi Nervi Lanificio Gatti, 1951-53 Rome, Italy, application of principal stress patterns in designing concrete ribbed shells. Frei Otto’s Olympic Stadium in Munich in 1972, using a steel cable net with acrylic panels.	18
Figure 16_ Frequency of appearance for different fabrication constraints in the fabrication-aware design (Austern et al., 2018).	23
Figure 17_ Types of rationalization strategies within temporal categories of rationalization (Austern et al., 2018).	27
Figure 18_ ICD/ITKE Research Pavilion 2010 and application of bending active simulation using FEM to find the global geometry of the interconnected system based on the material behavior under large defamations with predefined connection points (Fleischmann and Menges, 2011).	29

Figure 19_ Computational design and robotic fabrication of thin timber plate shell.
ICD/ITKE/IIGS Landesgartenschau exhibition hall. Application of packing algorithm with a
novel integrated edge connection detailing to inform the paneling patterns and fabrication
process for a timber plate shell (Schwinn and Menges, 2015). 29

Figure 20_ Quasi-reciprocal timber and discontinuous post-tensioned concrete structure and
fabrication constraints. Completed Utzon 40 Pavilion (Maxwell et al., 2014)..... 30

Figure 21_ The Ongreening Pavilion, Schematic diagram showing the overall process of form
generation and co-rationalization of interweaving members and their structural performance.
(Harding et al., 2015). 31

Figure 22_ FABPOD: A design-to-fabrication system integrating early sound performance
prediction and fabrication constraints in a co-rationalization process. (Williams et al., 2015).... 32

Figure 23_ The interconnected structure of the reciprocal systems. 41

Figure 24_ Sketches of Leonardo da Vinci in sheet 898 of the Codex Atlanticus (1452-1519).
Three Fishes tessellation. Robert Fathauer, screen print made in 1994..... 45

Figure 25_ From the left: Translation method, rotation method, extended translation method. .. 46

Figure 26_ Mapping procedure for mapping of a 2-D reciprocal pattern to the 3-D space (Song et
al., 2013). 46

Figure 27_ Mesh based tessellation method for generation of reciprocal patterns on a 3-d surface
(Anastas et al., 2016). 47

Figure 28_ Sample discretization of a doubly curve surface using quadrilateral meshes. 49

Figure 29_ Numbering mesh faces, mesh vertices and generating mesh half-edge data. 50

Figure 30_ Application of homogeneous dilation and generation of scaled quadrilateral cells. .. 51

Figure 31_ Generating reciprocal patterns on each cell based on the scaled cells. Notations of the geometric entities on a cell.	52
Figure 32_ Intersections between the four elements are found and used to generate the segmented reciprocal modules. Left: notations of the geometric entities on a cell, right: numbering of the intersection points after pattern generation.	52
Figure 33_ Left: independent modules on the pseudo-plane of cells, right: continuous network of interconnected reciprocal members with eccentricities.	53
Figure 34_ Generation of continuous network of reciprocal modules on the predefined surface and introduction of eccentricities between the elements.	54
Figure 35_ Calculation of member eccentricities in the reciprocal system.	54
Figure 36_ Left: False color visualization of Gaussian surface curvature. Right: False color visualization of the eccentricities size and distribution.	55
Figure 37_ Refining the mesh density and distribution of eccentricities on the doubly curve surface.	56
Figure 38_ Reciprocal polyhedra generated by expanding the vertices. Variation in a dodeca-icosahedron for rotation angles 5, 10, and 20 degrees (Sénéchal et al., 2011).	57
Figure 39_ mapping a 2-D pattern to 3-D space and least-square optimization for 1-D members. (Song et al., 2013).	58
Figure 40_ Fabrication of reciprocal connections. From the left: clamped connection, notched connection, T-joint connection.	59
Figure 41_ Pair assignment in a reciprocal module. Each module will have four pairing constraints.	62

Figure 42_ Figure a: Reciprocal pattern generation. Figure b: Definition of the constrained model, boundary conditions, member pairings and rigid body definition.....	66
Figure 43_ Member to member eccentricities in reciprocal systems before (on the left) and after (on the right) the form-finding process.....	67
Figure 44_ Variation in eccentricities during the form-finding process in a four by four reciprocal grid. Left: minimization of the maximum eccentricity. Right: minimization of the average eccentricity.....	68
Figure 45_ The overlay of maximum and average eccentricities.....	68
Figure 46_ Figure 27_ Variation in eccentricities during the form-finding process for different grid densities. Top: Minimization of maximum and average eccentricity in a three by three grid. bottom: Minimization of maximum and average eccentricity in a five by five.....	69
Figure 47_ Variation in maximum eccentricities during the form-finding process for different grid densities.....	70
Figure 48_ Variation in average eccentricities during the form-finding process for different grid densities.....	71
Figure 49_ Distribution of the divergence of the reciprocal system from the designed geometry after the form-finding process.....	72
Figure 50_ Comparison of distribution of eccentricities before (on the left) and after (on the right) the form-fining process.....	73
Figure 51. Eccentricities between the centerline of concurrent members in reciprocal structures.....	80
Figure 52_ Decomposition of a reciprocal module. From left: load transmission within the unit, unit assembly, force diagram of reciprocal member with corresponding fabrication cuts.....	81

Figure 53_ Examples of a non-flat reciprocal structure and the inherent eccentricities between members.....	84
Figure 54_ The extended structure by John Wallis. Wallis’s 25 simultaneous equations. Detail from Opera Mathematica.	85
Figure 55_ Example of a basic system ($n = 4$). (a) statics system; (b) sub-system. Example of three iterative steps: first red, second blue, third green; (b) right: Example of a cyclical and a diffused iteration step progression.	86
Figure 56_ Finite element analysis of reciprocal module with four members.	87
Figure 57_ Kinematic scheme of connectors accounting for eccentricities. Local equilibrium of the reciprocal member subjected to bending.	87
Figure 58_ Structural reciprocal element discretized to three beam elements with 12 degrees of freedom in each element six displacement and six rotation degrees of freedom.....	89
Figure 59_ The side beams can be restrained to define the connection behavior.....	90
Figure 60_ From left: Fat surface and reciprocal pattern, reciprocal module with 2-D elements in relation to the mesh geometry, reciprocal module.....	92
Figure 61_ Controlling parameters. From left: Engagement ratio, rotation angle, member thickness, and member depth.....	92
Figure 62_ Structural model: reciprocal member discretization, structural nodes numbering, beam numbering, structural model with external loads and supports.	93
Figure 63_ APA specification for classification of species.....	94
Figure 64_ APA specification for allowable stress and section properties.	95
Figure 65_ Member numbering, beam element numbering, node numbering.	97

Figure 66_Local member axis and moment releases around the y-axis of members in a reciprocal module.....	98
Figure 67_Structural model, boundary conditions, and the external loading used in analysis of a reciprocal module.....	98
Figure 68_Internal force distribution. From the top: moment distribution, shear force distribution, torsional moment distribution.	99
Figure 69_ Lateral torsional buckling based on the Wood Council Association’s National Design Specification.	100
Figure 70_ Utilization calculation in reciprocal members under combined forces.....	103
Figure 71_ Stress distribution in reciprocal members under combined forces.....	103
Figure 72_ Variation in reciprocal module geometry based on variation in engagement length. From left: EL=0.2, EL=0.4, EL=0.6.	104
Figure 73_ Parametric study of the effect of engagement length on the structural behavior of a single reciprocal module.	105
Figure 74_ Variation in the reciprocal module geometry based on variation in rotation angle (RA) From left: RA=-40, RA=0, EL=40.	106
Figure 75_ Parametric study of the effect of the rotation angle on the structural behavior of a single reciprocal module.	107
Figure 76_ Variation in reciprocal module geometry based on variation in member depth. From left: D=5 in, D=7.5 in, D=10 in.	108
Figure 77_ Parametric study of the effect of the member depth on the structural behavior of a single reciprocal module.	109
Figure 78_ Sample flat reciprocal system as a roof system.....	111

Figure 79_ Generation of analytical model. From left: structural node numbering, beam elements numbering, joint release definition.	112
Figure 80_ Distributed loading and boundary conditions for a flat reciprocal system.....	112
Figure 81_ Visualization of the internal forces in the flat reciprocal system.	113
Figure 82_ Discretization of reciprocal member to three beams and creating five design check points on each beam.....	114
Figure 83_ Iterative structural design process to find the minimum weight cross-section for each beam element.	114
Figure 84_ Cross-section geometric information of IPE; table of design properties for flanged steel profiles.....	115
Figure 85_ Structural analysis and member design process.	116
Figure 86_ Visualizing utilization factor after member sizing.	117
Figure 87_ Variation in reciprocal geometry based on variation in engagement length (EL). From left: EL=0.1, EL=0.5, EL=0.9.....	117
Figure 88_ Parametric study of the reciprocal system’s behavior based on the variations in the engagement length.	118
Figure 89_ Increase in member sizing due to local shear forces in reciprocal systems with very small engagement length. Top: reciprocal system with 0.1, bottom: reciprocal system with 0.5.	119
Figure 90_ Variation in reciprocal geometry based on variation in engagement length (EL). From left: EL=0.1, EL=0.5, EL=0.9.....	121
Figure 91_ Comparative study of a structural behavior of the reciprocal systems with semi-rigid and rigid connections.	121

Figure 92_ Comparative study of structural behavior of reciprocal systems with semi-rigid and rigid connections.....	122
Figure 93_ Variation in mesh density with constant engagement length and a 0.4 scale factor.	123
Figure 94_ Parametric study of the effect of mesh density on the structural behavior of flat reciprocal systems. Reciprocal system with engagement length of 0.4.....	124
Figure 95_ Parametric study of the effect of mesh density on the structural behavior of flat reciprocal systems. Reciprocal systems with engagement lengths of 0.2, 0.4, 0.6, and 0.8.....	125
Figure 96_ Reciprocal system with variations in mesh density (D) and engagement length (EL).	126
Figure 97_ Parametric study of the effect of mesh density on the structural behavior of flat reciprocal systems with engagement lengths of 0.4 and 0.6.....	127
Figure 98_ Left: Mannheim Multihalle (Happold and Liddell, 1975), Right: The great court grid shell at the British Museum.	128
Figure 99_ Geometry and structural design of the model reciprocal system and its grid shell counterpart.	129
Figure 100_ Comparing the efficiency of reciprocal geometry and grid shell counterpart.....	130
Figure 101_ Form exploration workflow and design considerations.	131
Figure 102_ First case study, 2-D parametric pattern.....	132
Figure 103_ Reciprocal module and the global geometry.....	132
Figure 104_ Design parameters: reciprocal parameter (left), depth parameter (middle), thickness parameter (right), geometric variations based on the reciprocal changes (bottom).....	134
Figure 105_ Rotational parameter and transformation of the reciprocal system to a non-orthogonal configuration.....	135

Figure 106_ Analytical model.	136
Figure 107_ Structural model and FE analysis results.....	137
Figure 108_ Iterative optimization process toward minimization of the total mass based on performance feedback.....	140
Figure 109_ Optimization results for the first case study.	141
Figure 110_ Variation of member thickness through the optimization process.	142
Figure 111_ Variation of the edge depth through the optimization process.....	143
Figure 112_ Variation of structural depth through the optimization process.	144
Figure 113_ Variation of the engagement length through the optimization process.	145
Figure 114_ Optimization results for the second case study and geometric transformation.	147
Figure 115_ Classification of woven structures based on their characteristics and bending stiffness. (Baverel and Popovic, 2011).	156
Figure 116_ Left: Generating reference and storage data for the reciprocal members in each reciprocal module of the reciprocal system. Right: Generating reference and storage data for the four intersecting members to each reciprocal member for fabrication purposes.....	158
Figure 117_ Left. Member orientation is generated based on the Darboux-frame convention. Right Rotation parameter controls the angle between the Darboux-frame vector and the member orientation.	159
Figure 118_ Solid geometry of the reciprocal members. Left: Members following the Darboux-frame convention, right: application of the rotation parameter.	160
Figure 119_ Regeneration of reciprocal members based on the calculated connection points. And generation of three beam elements for structural analysis.....	161
Figure 120_ 50 digital wood joints project by Jochen Gros. www.flexiblestream.org	163

Figure 121_ A. single-layer reciprocal frame, Gramazio Kohler Research, ETH, Zurich, 2018.	165
Figure 122_ A. Conventional reciprocal connection adapted for rotated reciprocal members, b. T-joint member connection, c. modified conventional connection, d. 3-D printed connection.	166
Figure 123_ Conventional reciprocal connection adapted for rotated reciprocal members.	167
Figure 124_ modified conventional connection adapted for rotated reciprocal members.....	168
Figure 125_ T-joint member connection.	169
Figure 126_ Robotic fabrication with elevated members for Utzon 40 Pavilion.	170
Figure 127_ 3-D printed connection.	171
Figure 128_ Topology optimization of metal connection for optimal distribution of material and weight reduction (Galjaard et al., 2014).	172
Figure 129_ Conventional reciprocal connection for orthogonal flat members with four different engagement lengths (EL) with different fabrication tolerances (TL).	173
Figure 130_ Modified connection detailing for orthogonal flat members with four different engagement lengths with different fabrication tolerances.	174
Figure 131_ Modified connection detailing for rotated flat members.....	175
Figure 132_ Initial detailing for orthogonal connection with end grain screws.	175
Figure 133_ Standard guidelines for screw penetration based on the material thickness. (https://www.kregtool.com/files/newsletters/kregplus/Images/february12/selecting-the-correct- screw).....	176
Figure 134_ Application of Kreg jig to drill the connection holes.	177
Figure 135_ Modified connection detailing for rotated flat members with Kreg screws.	177

Figure 136_ Modified connection detailing for orthogonal flat members with end grain screw fasteners.	178
Figure 137_ reciprocal modules are fabricated for structural testing using 3-Axis CNC machine.	179
Figure 138_ Test setup for the destructive structural test.	180
Figure 139_ Destructive structural testing using displacement control with Universal machine.	180
Figure 140_ Failure of test samples under displacement control loading. Left: 13-layer Birch plywood material, right: MDF material.	181
Figure 141_ Slight rotation of the reciprocal module and warping of the reciprocal members under symmetric loading.....	182
Figure 142_ Load-displacement graph for 8 sample tests with bilinear slopes.	183
Figure 143_ Top: force deformation graphs for six test samples with maximum ultimate force and deformation. Bottom: Cumulative regression model for the force-displacement data.	184
Figure 144_ Box plot of the loading data for 9 test samples.	185
Figure 145_ Box plot of the displacement data for 9 test samples.	185
Figure 146_ Connection detailing and fabrication tolerances in the reciprocal module before loading.....	186
Figure 147_ Solid modelling and assembly of a four membered reciprocal module.	189
Figure 148_ Solid modelling of the reciprocal connection (member cuts and dog bones) and fabrication tolerances.	189
Figure 149_ Definition of contact faces for the connecting members and 3-D finite element mesh. Four contact surfaces (CS) are shown in the picture.	190

Figure 150_ Solid modelling and assembly of a four membered reciprocal module. 3-D Finite Element Mesh of the reciprocal module including contact elements and boundary conditions.	190
Figure 151_ Finite Element analysis results of the structural module. Left: Von Mises stress distribution, right: Deformations.	191
Figure 152_ Finite Element analysis results the structural module under distributed loading on the engagement area. Von Mises stress distribution.	192
Figure 153_ Detailed 3-D finite element analysis of reciprocal module with three different engagement lengths. Von Mises stress distribution.	192
Figure 154_ Detailed 3-D finite element analysis of the reciprocal module with exaggerated deformations.	193
Figure 155_ Scaled prototype. The geometry and measurements of a half arch reciprocal system with rotated planar elements.	194
Figure 156_ Swarf cuts tool pathing.	195
Figure 157_ Contour cuts tool pathing.	195
Figure 158_ Full tool pathing for the 5-axis CNC cutting.	195
Figure 159_ 5-axis CNC bed and the test cut results for the fabrication test one.	196
Figure 160_ Fabrication results for the fabrication test one.	197
Figure 161_ Excess heat in swarf cuts: Left, burning in the spoil board. right, successful cuts.	197
Figure 162_ Collision of the drill collet with material.	198
Figure 163_ 1/4 inch down shear drill bit extension capacity.	199
Figure 164_ 5-axis CNC bed and the test cut results for the fabrication test two.	200
Figure 165_ Fabrication results for the fabrication test two.	201
Figure 166_ Drill bit failure in swarf cuts in test two.	202

Figure 167_ 5-axis CNC bed and the test cut results for the fabrication test three.	203
Figure 168_ Using swarf cuts to test the full member cutting in one toolpath.	204
Figure 169_ Swarf cut tool pathing and depth cut consideration.	205
Figure 170_ Comparing dog bone cuts vs drilling. Top: drilling the corners, bottom: dog bone detailing.....	206
Figure 171_ Using 3/8 inch and 1/2 inch drill holes based on the connection angle.	206
Figure 172_ Bottom up assembly process for the scaled half arch.....	208
Figure 173_ Half Arch reciprocal geometry with planar rotated members.	209
Figure 174_ The interconnected structure of the reciprocal systems illustrating he relationship between member, module, and system.	214
Figure 175_ Depiction of the digital dataflow: different methods and file formats to store and view design objects and the corresponding data in each module within the digital dataflow.	217
Figure 176_ Implemented software and programming tools differentiating between self-made (custom) and commercial (standard) components.	218
Figure 177_ Reciprocal Shades dimensions.	219
Figure 178_ Designated site for construction of the Reciprocal Shades at Matthaei Botanical Gardens, Ann Arbor, Michican.....	220
Figure 179_ Accessibility from the north entrance and arch location and orientation.	220
Figure 180_ Comparison of different material properties for wood, plywood, MDF, PVC and PC (Asefi and Bahremandi-Tolou, 20019).	221
Figure 181_ Implementation of the reciprocal pattern generation module in the computational design process.	223
Figure 182_ Generation of the system network data.	224

Figure 183_ Implementation of the form-finding module in the computational design process.	225
Figure 184_ Implementation of the geometry generation module in the computational design process.....	227
Figure 185_ Implementation of the structural analysis module in the computational design process.....	229
Figure 186_ Visualization of the structural analysis results a) Stress Distribution b) Member utilization generated by a custom code c) Displacement Distribution d) Bending moment distribution.	229
Figure 187_ Implementation of the shading estimation module in the computational design process.....	230
Figure 188_ Comparing shading capacity and shading pattern of two different designs. A) shading ratio 14.7% b) shading ratio 85%.	231
Figure 189_ Lapped notched joint: modified conventional connection adapted for rotated reciprocal members.	231
Figure 190_ Implementation of the fabrication data generation module in the computational design process.	232
Figure 191_ Fabrication module visual outputs: a) Sample of the design geometry with connection detailing. b) Sample of the fabrication cut patterns nested on a 4 by 8 sheet for toolpath generation.....	233
Figure 192_ Definition of inputs and outputs and the digital dataflow between different modules in the computational design process.	235
Figure 193_ Samples of design solutions generated by manual exploration showing the variation of form based on the design parameters.	236

Figure 194_ ParaGen process for a GA based exploration of the design space.	238
Figure 195_ Visual output generated for each design solution in the form exploration process. a) 3-D Geometry and shading pattern b) Stress Distribution c) Member utilization.	239
Figure 196_ Visualization of the design exploration cycle.	241
Figure 197_ Design exploration using design parameters: design solutions with lowest mesh density in the design space, sorted using the ParaGen interface.	242
Figure 198_ Design exploration using design parameters: design solutions with the highest mesh density in the design space, sorted using the ParaGen interface.	242
Figure 199_ Design exploration using design parameters: design solutions with the smallest engagement length in the design space, sorted using the ParaGen interface.	243
Figure 200_ Design exploration using design parameters: design solutions with the largest engagement length in the design space, sorted using the ParaGen interface.	243
Figure 201_ Design exploration using design parameters: design solutions with the smallest rotation angle in the design space, sorted using the ParaGen interface.	244
Figure 202_ Design exploration using design parameters: design solutions with the largest rotation angle in the design space, sorted using the ParaGen interface.	244
Figure 203_ Design exploration using performance criteria: design solutions with the smallest total weight in the design space, sorted using the ParaGen interface.	245
Figure 204_ Design exploration using performance criteria: design solutions with largest total weight in the design space, sorted using the ParaGen interface.	245
Figure 205_ Design exploration using performance criteria: design solutions with the smallest form-finding error in the design space, sorted using the ParaGen interface.	246

Figure 206_ Design exploration using performance criteria: design solutions with the largest form-finding error in the design space, sorted using the ParaGen interface.....	247
Figure 207_ 2-D graph describing shading capacity vs. engagement length. The design solutions with maximum shading capacity are visualized for each engagement length value.	248
Figure 208_ 2-D graph describing shading capacity vs. rotation angle. The design solutions with maximum shading capacity are visualized for each rotation angle.	249
Figure 209_ 2-D graph describing total arch weight vs. engagement length. The heaviest arch geometries and shading patterns are visualized for each engagement length value.	250
Figure 210_ 2-D graph describing total arch weight vs. rotation angle. The design solutions with minimum weight are visualized for each rotation angle.	251
Figure 211_ 2-D graph describing estimated machine time vs. mesh density.....	252
Figure 212_ 2-D graph describing shading capacity vs. mesh density.....	253
Figure 213_ 2-D graph describing estimated 4 by 8 sheet material use vs. mesh density.....	254
Figure 214_ Application of multiple queries in ParaGen to explore the design space.....	255
Figure 215_ Visualization of the design space reduction due to the application of different design constraints.	256
Figure 216_ Final arch geometry and the design process: a) mesh approximation of the base geometry b) reciprocal pattern generation and form-finding results c) 3-D member geometry generation d) analytical model and finite element analysis results e) 3-D member geometry... ..	256
Figure 217_ Visual data for the selected arch geometry. a) 3-D Geometry and shading pattern b) Stress Distribution c) Member utilization d) Displacement Distribution e) Bending moment distribution f) Member geometry and labeling.	257

Figure 218_ Sample of lapped reciprocal connection design stabilized with two Kreg screws using MDF material.	259
Figure 219_ Arch geometry and the members layout and the final arch geometry 112 reciprocal members.	260
Figure 220_ Cutting the reciprocal members out of plywood sheets using 5-Axis CNC.	260
Figure 221_ Labeling and storage of the members.	261
Figure 222_ Predrilling the screws and pre-assembly of connecting members.	262
Figure 223_ Assembling the arch at the Taubman College of Architecture. Assembled arch with temporary supports.	263
Figure 224_ Application of waterproof and anti UV sealant to the arch.	264
Figure 225_ Custom support palate design.	264
Figure 226_ Fabrication of the support plates using water jet cutter.	265
Figure 227_ Bending the supports plates to custom angles using break.	265
Figure 228_ Connection detailing of the support members and the base plates.	265
Figure 229_ Base plate connection detailing and connection pieces.	266
Figure 230_ Moving the preassembled pieces of the arch to the site location for setup.	267
Figure 231_ a) Erecting the arch from three pre-assembled pieces using two support ladders. b) assembling the connecting pieces using screws c) assembling the last pre-assembled piece of the arch. d) supporting the arch using bracing ropes.	267
Figure 232_ Connecting the base plates to the arch support members.	268
Figure 233_ Base plate connection detailing.	268
Figure 234_ The arch geometry (South view), Matthaei Botanical Gardens, Ann Arbor, Michigan.	269

Figure 235_ The arch geometry (North view), Matthaei Botanical Gardens, Ann Arbor, Michigan.	269
Figure 236_ Arch connection detailing.....	270
Figure 237_ Arch connection detailing.....	270
Figure 238_ Convex and concave reciprocal modules in the system.	271
Figure 239_ Discoloration due to UV exposure. a) Arch condition after eight months. b) Arch condition after sixteen months.	272
Figure 240_ a) Reciprocal member deformations after sixteen months, b) warping of reciprocal members.....	272
Figure 241_ a) Connection failure due to excessive deformations, b) connection failure due to material defect.....	273
Figure 242_ Using the radial distance measurement data to generate the digital arch geometry. The deformed geometry is depicted in blue and the initial arc geometry is depicted in red.	274
Figure 243_ Comparison of the measured geometry and the initial geometry.....	274
Figure 244_ Support displacement scheme to retrieve the initial height. Gradual and simultaneous movement of the right support to the left side (30 cm) and the top center members upwards (15 cm).	275
Figure 245_ Internal member moments in the arch structure induced by the gradual support movements. a) step one: support movements 15 cm to left and 5 cm upwards. b) step two: support movements 30 cm to left and 10 cm upwards. c) step three: support movements 45 cm to left and 15 cm upwards.	275

Figure 246_ Internal member forces in the arch induced by the support movements (30 cm to left, 15 cm upwards). a) axial member forces, b) bending moments, c) stress distribution, d) member utilization factor..... 276

Figure 247_ Using the simulation results to reinforce the joints with maximum utilizations prior to supports displacement..... 277

Figure 248_ Support displacement scheme and target support locations. 277

Figure 249_ Arch geometry: a) deformed arch (blue) vs initial arch (red), b) arch geometry after moving the supports to the target locations (purple) vs initial arch (red). 278

Figure 250_ Arch geometry. a) initial arch geometry right after erection, b) arch geometry after moving the supports to the target locations. 278

ABSTRACT

Using the capabilities of computation and digital fabrication this thesis provides a basis for a novel process of design to fabrication for reciprocal systems.

In the traditional sense, reciprocal structures combine the advantages of timber as a renewable source of construction material and low-energy production with the modular fabrication, fabrication efficiency, structural capacities, and elegance of reciprocal interconnection of members. The unique benefits of reciprocal systems come from their discrete geometry, which simplifies the connection detailing and provides freedom for local and global variations in the system. However, this reduction in construction complexity and flexibility of local variation is replaced with geometrical complexity due to numerous compatibility constraints coupled with the structural behavior of the system. This research therefore identifies the key design parameters and design constraints of reciprocal systems. The results demonstrate the complex coupling of geometry, structural performance and fabrication in these systems, hence an essential need for application of an integrative design process. Through the application of computation, simulation, and digital fabrication this research proposes an integrative computational design process which can effectively address the coupling of design, analysis and fabrication of reciprocal systems and accommodate design exploration and optimization.

First, a novel computational method for geometric modelling and form-finding is presented to resolve the compatibility constraints and generate the essential geometric and topological data for analysis and fabrication. Second, a flexible and scalable analysis method is implemented to

study the interplay of the design parameters and the structural behavior of reciprocal systems. A comprehensive parametric study reveals a complex relationship between the geometric parameters and the structural performance and demonstrates the essential need for a real-time performance feedback for optimal design of free-form reciprocal systems. Third, a generalizable and efficient fabrication process is proposed for reciprocal systems with 3-D module geometry using 5-axis CNC machinery. Towards this goal, four different connection types are proposed, and different fabrication parameters are studied through digital and physical prototyping, destructive structural testing, detailed finite element simulation, and fabrication of a scaled structure. The results are summarized as a guideline for selection of the main fabrication parameters including joint detailing and fabrication tolerances. The computational design process is then developed by rethinking and replacing the conventional direct incremental development by a modular integrative computational process using multi-directional dataflow between different design phases. Finally, the proposed framework is used for a full-scale design to fabrication case study to validate the applicability of the proposed design process.

Chapter 1: Introduction

1.1 Historical context for reciprocal structures

The principle of structural reciprocity is based on the 3-D assembly of loadbearing members that mutually support each other along their span and create a self-supporting spatial configuration without any structural hierarchy and which can span multiple times the length of members. The primitive concept initially emerged in the East, in the Song dynasty in China, at least 900 years ago as a bridge construction system to span longer than the length of available timbers and became a practical approach for construction in different parts of the world (Popovic, 2008) (Figure 1 and Figure 2).

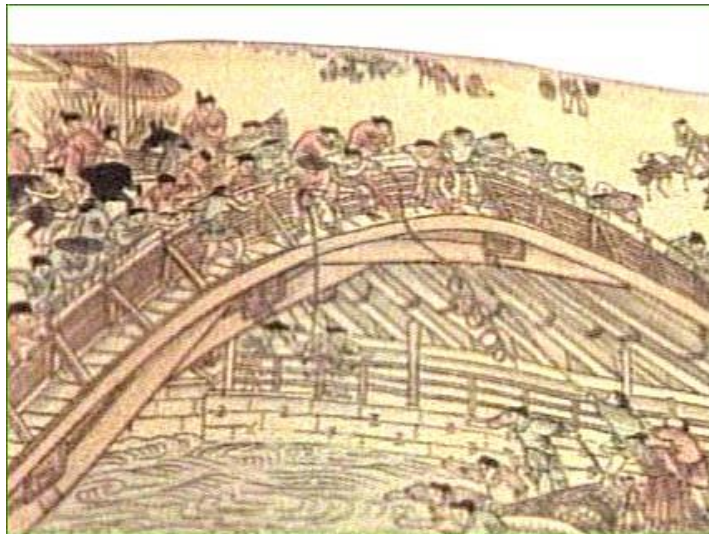


Figure 1_ Rainbow Bridge only exists in a 900-year-old painting that shows the capital city of Kaifeng in Song dynasty. (Chen, 2008)

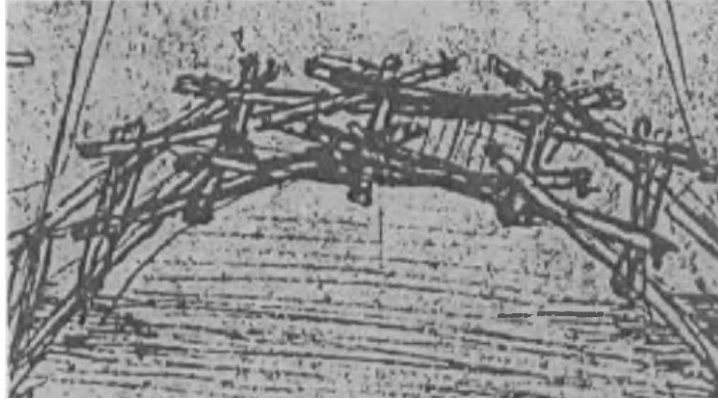
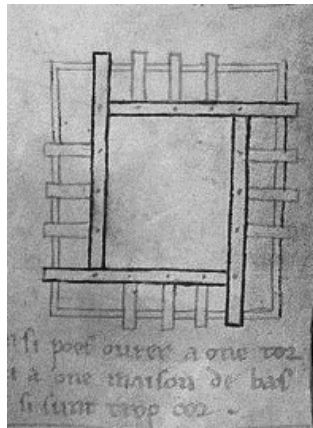
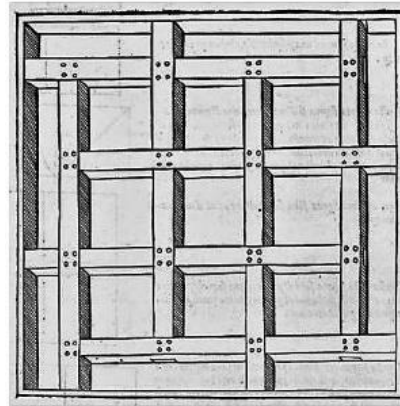


Figure 2_ da Vinci's temporary bridge sketch. (Anon, 1956)

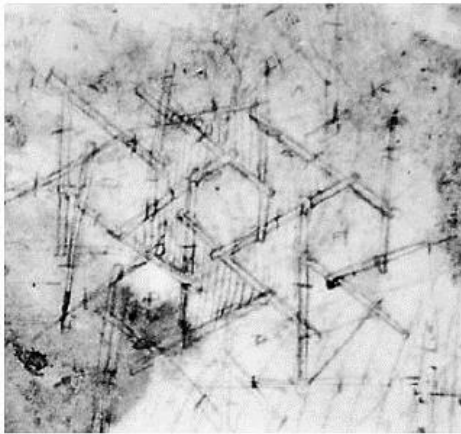
The simplicity of connection detailing and use of relatively short members to cover a large area are some of the construction benefits of these systems. For that matter, such systems have been adapted into flat systems to covers larger spaces since medieval architecture, for example, by Villard de Honnecourt (1250 C.E.) in designing flat interlocking structures, by Leonardo da Vinci in a sketch on sheet 898 of the Codesx Atlanticus (1452–1519 C.E.), in an aligned axis floor system by Sebastiano Serlio (1545 C.E.), and flat roof systems by John Wallis (1695 C.E.), as shown in Figure 3 (Houlsby, 2014).



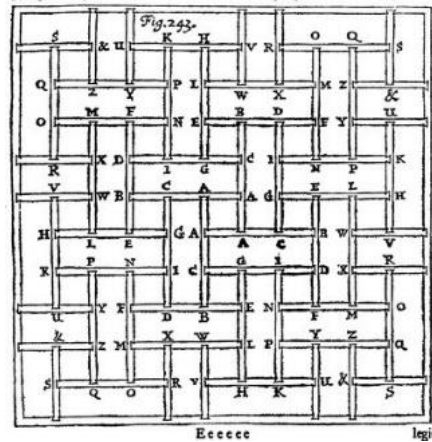
a)



b)



c)



d)

Figure 3_ a) Villard de Honnecourt (1250 C.E.), b) Sebastiano Serlio (1545 C.E.), c) Leonardo da Vinci (1452–1519 C.E.), d) John Wallis (1695 C.E.).

1.2 Contemporary applications of the reciprocal structures

In contemporary architectural design, reciprocal systems have been a source of inspiration for architects such as Shigeru Ban (Figure 4) or artists like Rinus Roelofs (McQuaid, 2006. Roelofs, 2007) shown in Figure 4 and Figure 5.



Figure 4_ Bamboo roof, Shigeru Ban, School of Architecture, Rice University. 2002



a)



b)

Figure 5_ a) European Quality Award. The sphere is constructed by the precise fit of 24 identical components. One of a series of 4 different awards made for EFQM, Brussels (1990). b) Dagen van de WISKUNST, LUCA, Brussel, Belgium, 2013.

However, with the advent of digital technologies for modelling and simulation, as well as the availability of digital fabrication technologies for architecturally scaled fabrication, the concept of reciprocal systems has been revisited by engineers and designers as a light-weight and

modular system with high capacities for performance integration, prefabrication and low-cost construction (Figure 6) (Apolinarska, 2018).



a)



b)

Figure 6_ a) KREOD Pavilion Chun Li architects, Ramboll Engineering 2015. b) Quasi-reciprocal timber and discontinuous post-tensioned concrete structure and fabrication constraints. Utzon 40 Pavilion, 2015.

Moreover, while reciprocal structures are considered a practical way to reduce the complexity of member connections, this reduction in construction complexity is replaced with geometrical complexity due to numerous compatibility constraints (Sénéchal et al., 2011).

Member connectivity is an important issue in design and fabrication of free-form structures. On one hand connectors are usually complex and often expensive being strongly depend on the geometry of the structure. On the other hand, the mechanical behavior of these connections has a significant effect on the structural performance of the system, and due to the concentration of stresses, it becomes the most vulnerable aspect of the structure (Figure 7) (Schlaich et al., 2005).

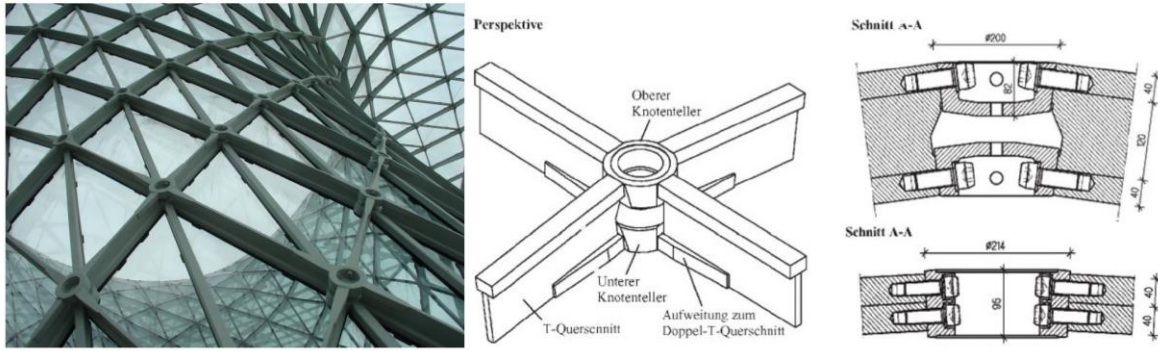


Figure 7_ An example of connection detailing in a spatial structure. Canopy roof of Fiera Milano, Architectural design by studio Fuksas. Engineering by Schlaich Bergermann Partners.

One effective way to design safer and more cost-effective connections is to reduce the complexity of connections by reducing the number of members connecting at each node Figure 8.

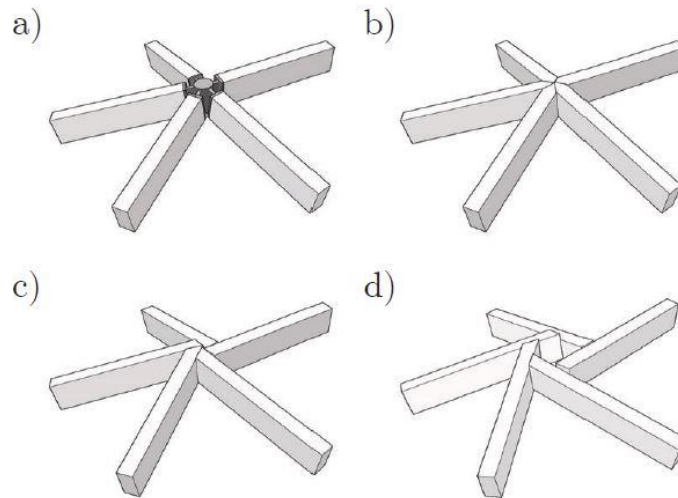


Figure 8_ Structural joint conditions: a) a knot with multiple bars meeting in one point with or b) without an additional joint element, c) an expanded node with a minimum expansion and d) expanded node with larger expansion (Apolinarska, 2018).

This is one of the benefits of reciprocal systems, as by definition, connections in reciprocal systems are two-valent. This means that only two members meet at a connection, which reduces

both the complexity of the connection needing to be designed for minimal material use, and also expedite the assembly process (Mesnil et al., 2018).

However, minimization of the eccentricities in an interconnected network such as a reciprocal system cannot be achieved through manual geometric manipulation. A systematic approach is needed which can simultaneously minimize the eccentricities in the system. As a result, with reciprocal systems, the problem of connecting numerous members shifts from technological complexity to geometrical complexity (Sénéchal et al., 2011).

In this research, we use a constraint-based modeling technique to mathematically define the eccentricities between the intersecting members, and then use a dynamic form-finding method to reduce the member eccentricities and keep them within the bounds of fabrication tolerances (Figure 9).

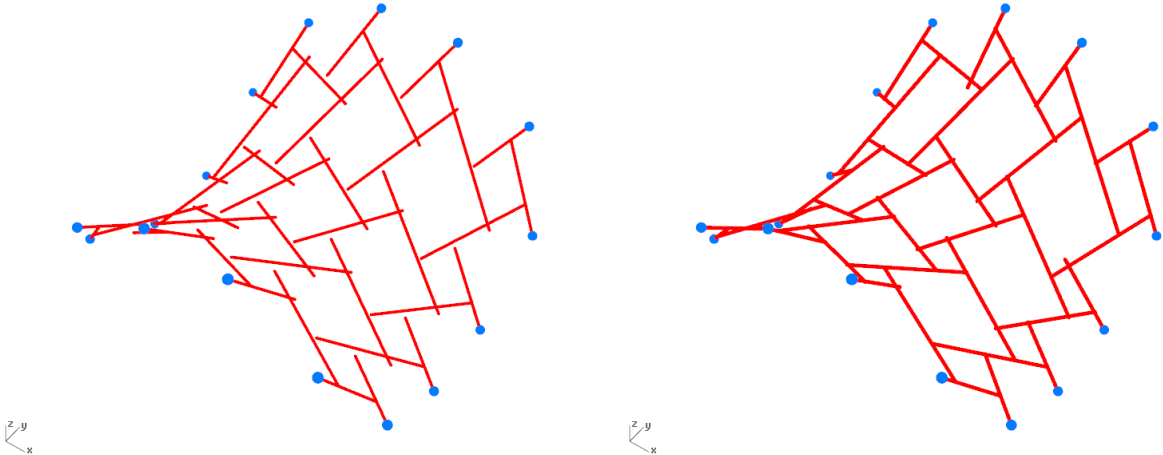


Figure 9_ Left: Development of eccentricities between member centerlines in generation of free-form reciprocal systems. Right: reciprocal system after minimizing eccentricities using form-finding method.

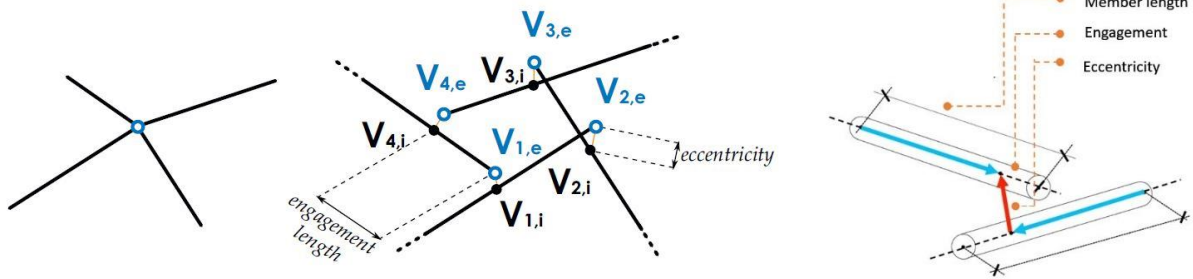


Figure 10_ Expanding a four-valent connection node and generating two-valent connections as in a reciprocal system (Mesnil et al., 2018), Eccentricities between the centerline of concurrent members in reciprocal structures.

As shown in Figure 10, the members of conventional reciprocal systems do not intersect at the connections points but are resting either on or below each other by pairs.

A generalization of the multi-reciprocal grids concept was proposed by Baverel et al. and called “nexorade” according to a neologism of Nooshin (Baverel et al., 2000). The general idea of this generalization is that, contrary to historical reciprocal systems, the connections between the members must not necessary be in compression. One can thus vary the respective positions of the members, and build grids with an even wider variety of forms, from flat grids to free-form shapes (Sénéchal et al., 2011).

However, in contemporary reciprocal systems the goal is to minimize the eccentricities between the reciprocal members and ideally have all the members to intersect at their connections (Mesnil et al., 2018). This is important in terms of practical realization of connection detailing for 2-D and 3-D member geometries, moreover, minimization of eccentricities enhances the structural performance of reciprocal systems.

Danz proposed a classification for reciprocal structure families and categorized their respective design and form-finding methods and their limitations (Danz, 2014).

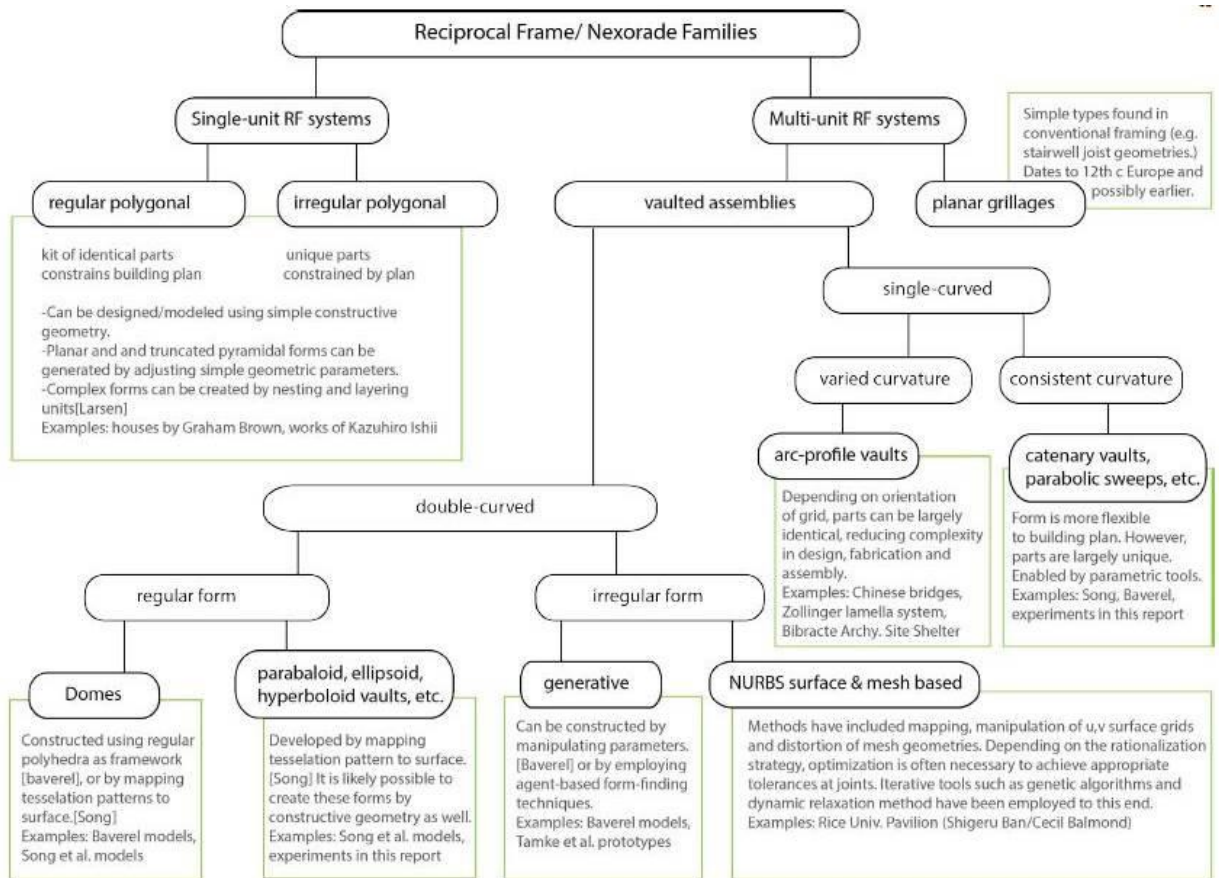


Figure 11_ Classification for reciprocal structure families and their respective design and form-finding methods (Danz, 2014).

As shown in Figure 11, the classification by Danz explains the complexity of reciprocal structures and their design requirements in relation to their geometric complexity. Significant limitations of existing design methods for reciprocal systems, such as case specificity and lack of generalizability, limitations in formal complexity, lack of capacity for the integration of performance and fabrication parameters, make these methods unsuitable for design purposes. Moreover, these methods do not accommodate the integration of fabrication requirements of these systems in the process of design which causes a disconnection in the design to construction process.

In this dissertation we introduce a unified design method for design and form-finding of reciprocal systems accommodating varying degrees of formal complexities. Moreover, this research investigates different aspects of complexity related to design, form-finding, analysis and fabrication of reciprocal structures. A generalizable and scalable performance-based and fabrication-aware design method is proposed to address these complexities in free-form design of reciprocal system.

1.3 Thesis structure

The research in this thesis is developed and presented in 7 chapters.

Chapter 2 introduces some of the main concepts and strategies in the field of computational design and explores their scope and application within academic and industry driven research. In this regard, architectural representations of generative design are explained through the ways the geometry and organization of space is informed based on the underlying rules defined by the main design drivers including performance, tectonic, material, and fabrication. The application of these design methods is investigated through the study of pre-, post-, and co-rationalization methods in academic and industrial research and qualities, timing and the scope of application of each of these methods are investigated. The review shows the necessity for the implementation of flexible computational design processes with capacities to integrate real-time and continuous data feedback including performance goals (performance-based design) and fabrication constraints (fabrication-aware design). This analytical review establishes the theoretical framework for the proposed performance-based and fabrication-aware design process of reciprocal systems.

Chapter 3 deals with the complexities of the design and form-finding of reciprocal systems. The limitations of the existing design methods are studied, and a generalizable and scalable design

method is proposed for design and form-finding of these systems which accommodates varying degrees of formal complexity. The proposed design method consists of two steps, a generative modelling process and a dynamic form-finding process. The modelling process introduces a geometric formulation using the quadrilateral mesh data derived from the rationalization of the base geometry to generate the reciprocal patterning. The form-finding process uses the dynamic relaxation method to solve the constraint-based model, which iteratively and simultaneously minimizes the eccentricities between the members to generate the proper geometric model for analysis and fabrication of 2-D and 3-D reciprocal systems. Finally, effectiveness and speed of the proposed method is studied quantitatively, and visualization techniques are developed for post-processing of the form-finding results.

Chapter 4 investigates the structural behavior of the reciprocal systems. A flexible and scalable analysis method is implemented to study the effect of design parameters (mesh density, engagement length, rotational angle and member connectivity conditions) on the structural behavior and flexibility of the reciprocal systems. Through application of the proposed method a comprehensive parametric study of reciprocal structures is carried out on different scales including: reciprocal member, reciprocal module, and reciprocal structure.

These results show, the multiple levels of interconnection between the structural performance and the constructability (fabrication parameters) of reciprocal systems. It becomes clear that, due to the high level of complexity in analysis and fabrication of these systems the optimal configuration of the design parameters is neither trivial nor intuitive. As a result, a design process with real-time fabrication and performance feedback is essential to address the design complexity of reciprocal systems.

Chapter 5 studies the fabrication process for reciprocal structures with 2-D and 3-D configurations. In this chapter, four different connection types are proposed for reciprocal systems with 2-D and 3-D member connections, and applications and limitations of each connection design is explained. This information is helpful in decision making for connection design in different scenarios in relation to: the function of the reciprocal system, choice of the digital fabrication technology, and choice of material.

Finally, a modified notched connection design is chosen for further studies. Different design considerations of this connection type are studied through digital and physical prototyping, destructive structural testing, detailed finite element simulation, and fabrication of a scaled structure. These studies define the key parameters for fabrication of reciprocal systems based on the proposed connection detailing. Also, a generalizable and efficient fabrication process is proposed for fabrication of reciprocal systems with 3-D module geometry using 5-axis CNC machinery. The fabrication and assembly process of the proposed method is tested through the design and fabrication of a scaled half-arch reciprocal geometry.

Chapter 6 explains the structure of the computational design process for design to fabrication of reciprocal systems with planar elements. A modular computational method is developed in an associative parametric environment to address the interconnected design constraints of the reciprocal systems. Multiple design modules were developed and connected with an efficient digital dataflow to create an integrative design to fabrication process. Finally, the proposed computational model is paired with a design exploration method to address the complexity of the interconnected design parameters and the conflicting design constraints in a full-scale design to fabrication case study project.

Chapter 7 presents an overall discussion of the results and contributions of each chapter and provides a synthesis of the dissertation research.

References

Anon, A. "Leonardo Da Vinci, a memorial edition based on the 'Leonardo Exposition' held in Milan in 1939." (1956).

Apolinarska, Aleksandra A. "Complex Timber Structures from Simple Elements: Computational Design of Novel Bar Structures for Robotic Fabrication and Assembly." PhD diss., ETH Zurich, 2018.

Baverel, O., H. Nooshin, Y. Kuroiwa, and G. A. R. Parke. "Nexorades." *International Journal of Space Structures* 15, no. 2 (2000): 155-159.

Chen, Pei-Shan. "A Study Report on an Ancient Chinese Wooden Bridge Hongqiao." *Structural Engineering International* 18, no. 1 (2008): 84-87.

Danz, Calder. "Reciprocal Frames, Nexorades and Lamellae: An Investigation into Mutually Supporting Structural Forms." *University of Washington* (2014).

Houlsby, Guy T. "John Wallis and the numerical analysis of structures." *Nexus Network Journal* 16, no. 1 (2014): 207-217.

Larsen, Olga Popovic. *Reciprocal frame architecture*. Routledge, 2008.

Mesnil, Romain, Cyril Douthe, Olivier Baverel, and Tristan Gobin. "Form finding of nexorades using the translations method." *Automation in Construction* 95 (2018): 142-154.

Sénéchal, B., Cyril Douthe, and Olivier Baverel. "Analytical investigations on elementary nexorades." *International Journal of Space Structures* 26, no. 4 (2011): 313-320.

Schlaich, Jörg, Hans Schober, and Kai Kürschner. "New trade fair in Milan—grid topology and structural behaviour of a free-formed glass-covered surface." *International Journal of Space Structures* 20, no. 1 (2005): 1-14.

Chapter 2: Theoretical Framework and Application of Computational Design

This chapter studies some of the main concepts and strategies in the field of computational design and situates them within the context of architectural and engineering design. The study defines different computational strategies and explores their scope and application within academic and industry driven research. This analytical review is conducted to establish the theoretical framework for the proposed performance-based and fabrication-aware design process of reciprocal systems.

Taking on the notion of “form follows force” the relationship between form, material and performance is explored through historical investigation of form-finding methods and significant works of contemporary architects and engineers. Inspired by biological systems, the process of digital morphogenesis is explained within the context of generative design. Subsequently, architectural representations of generative design are explained through the ways that the geometry and organization of space is informed based on the underlying rules defined by the main design drivers including performance, tectonic, material, and fabrication. The application of these design methods is investigated through study of pre-, post-, and co-rationalization methods in academic and industrial research, and the qualities, timing, and scope of application for each of these methods are investigated. The critical review shows the necessity for the implementation of flexible computational design processes with capacities to integrate real-time

and continuous data feedback including performance goals (performance-based design) and fabrication constraints (fabrication-aware design).

2.1 Form and form-finding in architecture

Conception and generation of form is one of the fundamental questions in architectural design and practice. In a nonlinear design process architectural form is generated in response to the connection between the form and function, context and structure, user needs, construction cost, etc. The response to the question of form has been influenced with a variety of theories in the history of architecture. Within the naturalist movement in 20th century there was significant desire to understand the “universal laws of form” to explain the forms of living organisms.

D’Arcy Wentworth Thompson, in *On Growth and Form*, explained the understanding that there are universal laws which arise from fundamental math and physics that reflect the growth and form in biological systems (Thompson, 1952). His book became an important basis in the study of nature which later contributed to the emergence of the field of biomimetics.

Thompson’s work became a growing field of interest especially as researchers and designers learned more about the implications of correlation between natural systems, form and structure, and their embedded rules. As an example, studies of soap film provided insights into minimal surface behavior and informed the design and engineering of membrane structures as shown in Figure 12.

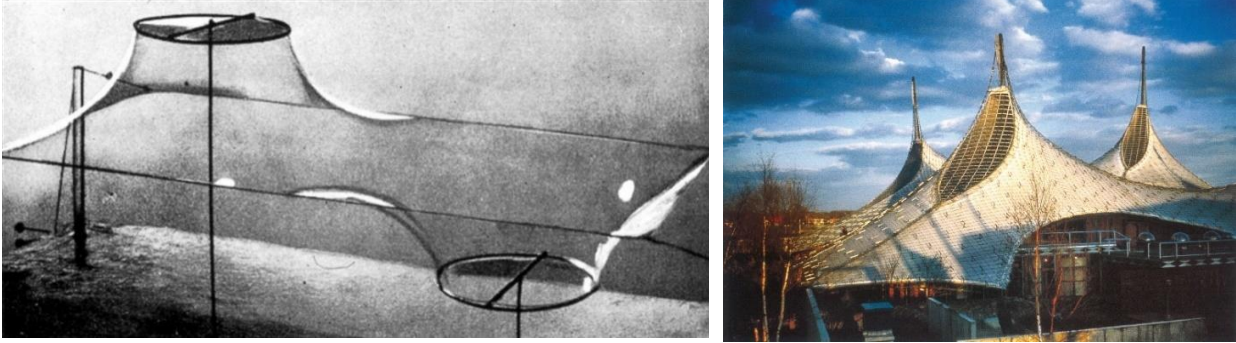


Figure 12_Figure 1. Soap film experiments by the Institute for Lightweight Structures at the University of Stuttgart, German Pavilion Expo 1967, Frei Otto and Rolf Gutbrod.

Studies into the relation between natural patterns and their function has been an attractive topic for biomimetic research in functional material distributions. Figure 13 shows an example of such research by Mogas-Soldevila et al., where structural patterning and material chemistry and distribution is inspired by natural processes.

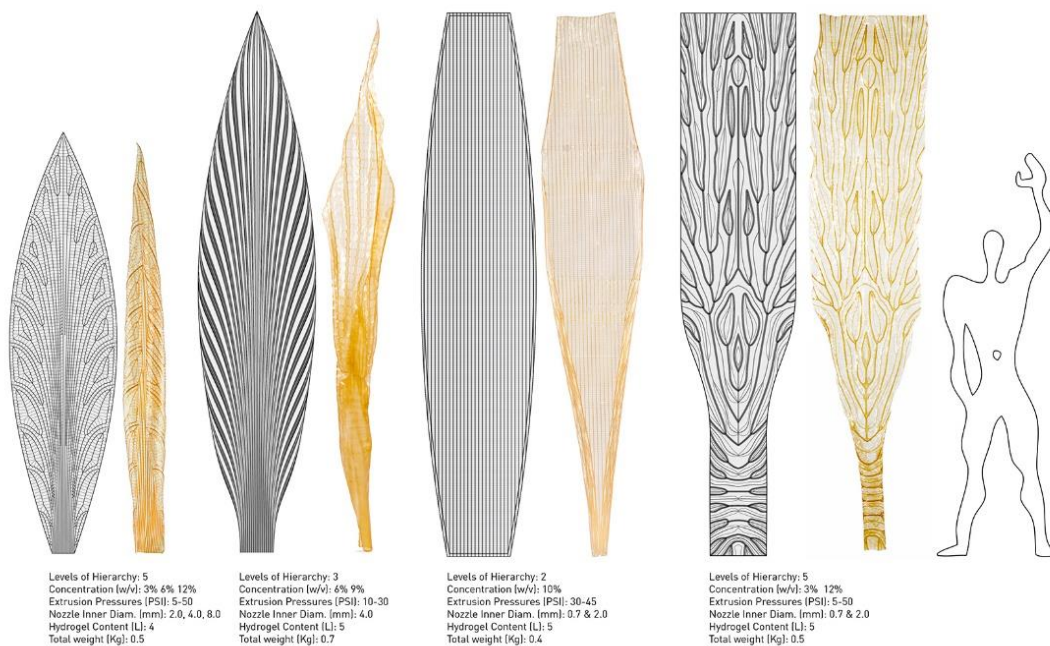


Figure 13_Design and manufacturing of bio-degradable hydrogel material for robotic additive manufacturing (Mogas-Soldevila et al., 2015).

The structural patterning was inspired by the structural patterning of dragonfly wing and of the venation pattern of an Acer leaf (Mogas-Soldevila et al., 2015).

In design and engineering, form-finding processes are inspired by natural processes in a way that the form emerges from the interactions within a designed system. Christopher Alexander calls these design systems “generating systems”, and differentiates them from what he calls “system as a whole”. In his description, a generating system is not a view of a single thing; it is a kit of parts with rules about the way these parts may be combined (Alexander, 1964).

Unlike the traditional methods of making, such as cutting, carving, folding or weaving, which use the known limitations of the material and physical forces to produce the designed form. Form-finding processes embed a considerable level of material and structural intent within active design modeling processes. As an example, Robert Hooke’s anecdotal inversion of the suspended chain, sets the context for a technique-based approach for development of funicular (compression only) geometries (Pedersen et al., 2014).

Application of form-finding methods in design produces a natural aesthetic which is derived by the internal interactions of the system components and governing rules. Historical examples of form-finding can be seen in the manifestation of “form follows force” in the works of Antonio Gaudi in Spain, Felix Candela in Mexico, Pier Luigi Nervi in Italy, and Frei Otto in Germany (Figure 14 and Figure 15).

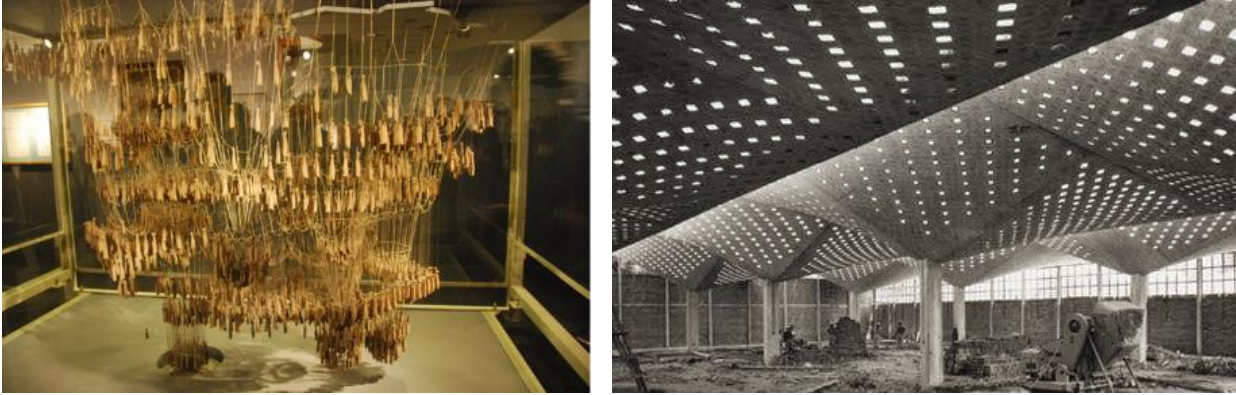


Figure 14_ Antonio Gaudi’s application of catenary arches in designing of a church at Colonia Guell in Barcelona, Spain 1883. Candela’s High Life Textile factory in Coyoacun, Mexico City in 1955 consisting of concrete hyperbolic Paraboloids.

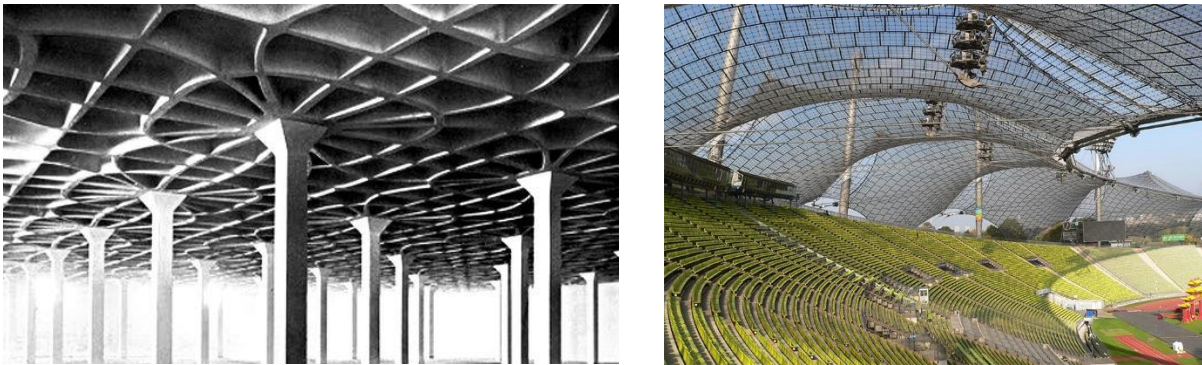


Figure 15_ Pier Luigi Nervi Lanificio Gatti, 1951-53 Rome, Italy, application of principal stress patterns in designing concrete ribbed shells. Frei Otto’s Olympic Stadium in Munich in 1972, using a steel cable net with acrylic panels.

2.2 Morphogenesis and generative design in architecture

Inspired by historical form-finding techniques, digital modelling and computational simulation tools have revolutionized the concept of form-finding. Historical prototyping and form-finding techniques, such as funicular shape design using catenary curves or soap film modelling for minimal surface design, set the context for development of interactive computational modelling tools that enable designers to simulate these systems digitally. The academic world made significant contributions to the development of theoretical frameworks for these new processes, and paved the way towards the development of new modes of design process such as computational design and design methods such as generative design.

Kostas Terzidis (2006) argues that the creative process of design must be based on computation rather than computerization. Computerization is a relatively static process of inputting predefined data and it is characteristic of CAAD systems that merely automate the drawing tools. On the other hand, computation takes advantage of a machine's capacity to analyze a very large amount of data. This computational power makes it possible to control (e.g., by means of analyzing, constructing and visualizing) architectural objects that go beyond human conceptualization.

Similar to the conceptual relation between digital form-finding methods and historical form-finding techniques, many contemporary generative design methods are derived from the same theories applied in the progressive pre-digital design processes. In early 90's Peter Eisenman pioneered the application of these theories, especially through the application of scaling, fractals, overlay and superposition in relation to rules of order. Later, as the computational tools advanced, Greg Lynn started applying new tools such as splines, NURBS and isomorphic polysurfaces influencing a new wave of architectural production often described as "blob architecture" (Asterios Agkathidis, 2015). Celestino Soddu defines generative design as "a morphogenetic process using algorithm structured as nonlinear system for endless unique and unpredictable results, performed by an idea code as in nature", and describes the strong association between the notion of generative design and digital morphogenesis (Soddu, 1994). Michael Hensel describes digital morphogenesis as a self-organizing process, underling the growth of living organisms from which architects can learn (Hensel, 2006). Branko Kolarevic describes digital morphogenesis as a process where models of design capable of consistent and dynamic transformation are replacing the static norms of conventional processes which brings about significant formal flexibility and creates alternatives through mass-customization (Kolarevic, 2003). In that sense architectural morphology is focusing on the emergent and

adaptable qualities of form. Form is no longer being made, but found, based on set of rules or algorithms in association with mainly digital, but also physical, tools and techniques (Agkathidis, 2015).

Oxman categorizes form generation into six dominant models in relation to its main driver: mathematical, tectonic, material, natural, fabrication and performative (Rivka and Robert Oxman, 2014). In their view digital morphogenesis is “the exploitation of generative media for the derivation of material form and its evolutionary mutation”, which includes manipulation of topological relations in the geometry, application of evolutionary algorithms, and integration of performance analysis using computational design methods.

Computational design offers a systematic approach to translation of the design problem into a computational model which is iteratively informed by data feedback. Moreover, computational technologies along with digital and robotic fabrication technologies have enabled designers and engineers to develop integrative design processes which not only inform the design based on the governing rules and performance metrics but can also take account of fabrication and constructability constraints throughout the design process. In some sense, computational design became the gateway for the introduction of a broad range of concepts and design modeling techniques into the design fields including concepts and methods from computational geometry, computer graphics, computer science, mechanical engineering and material science.

Since early 2000 the industry has been active in case-based adoption of these technologies, mainly out of necessity, for delivery of special projects which could not have been delivered with existing conventional methods. However, academia had the main role in theorizing these design processes and expansion of their application in all phases of design through research and design-

build projects. These new aspirations in design created the need for acquisition of new technologies from neighboring industries such as aerospace, ship building, and the automotive industry where the desired materials, analysis and fabrication methods were already well established. At the beginning of this period these technologies were acquired and applied in a project-based fashion and mainly developed piecemeal in service of the need for realization of the already designed project. Some leading companies like Gehry Technologies contributed to these efforts through research and development in digital modelling and simulation of non-conventional design forms (Sheldon, 2002).

Introduction of new computational concepts, modelling and simulation methods on one hand, and development of new materials, ubiquity of computational power in form of cloud-computing and web-based storage and availability and applicability of new fabrication methods for architecture scale construction on the other, opened new venues for a more integrative design processes under the umbrella of computational design. The evolution of computational design as a design process and the integration of these new technologies into this design process has become a growing field of interest in academia and industry for application of new design methods such as generative-design, performance-based design and fabrication-aware design.

2.3 Constraint-based modelling in fabrication-aware design

2.3.1 Definition of constraint-based modelling

In the context of architectural structures, constraint-based modeling or constraint-aware modeling refers to modelling approaches which directly integrate the design constraints in the design process, leading to a bottom-up generation of form based on the generative rules and the design constraints (Deuss, 2015). Different applications of constraint-based modelling can exist

depending on the type of constraints involved and the constraint resolution process defined by the computational model. The power of constraint-based modelling depends on the mathematical definition of design constraints and the efficiency and efficacy of the constraint resolution process. A lot of the vocabulary in computational design is derived from the field of computer graphics. It is perceived that computer graphics with its rich history in digital 3D modeling is a promising field of research to tackle the interdisciplinary challenges of computer-aided methods in computational design processes. In fact, a part of the computer graphics community started to study potentials of incorporating fabrication constraints into the computational 3-D modeling under the topic of architectural geometry in close collaboration with geometric mathematicians (Pottman et al., 2015).

2.3.2 Types of design constraints: Hard and soft constraints

The concept of design constraint is often used in two fundamentally different meanings. Hard constraints express types of constraints which need to be satisfied for a feasible design solution. Any deviation from a hard constraint can result in an impractical or meaningless design solution. A typical example of a hard constraint is the static equilibrium of an architectural structure or constructability in terms of member connection design. Soft constraints express something desirable to have. They are also called objectives. They are often formalized as an objective function to be optimized which assigns a satisfying enough measure to each result. Typical examples of soft constraints are ease of fabrication and assembly, material use, machine time and cost. Soft constraints can be converted into hard constraints by setting a hard limit on the objective function, for example, to formulate the fact that a flat glass panel can be deformed with a margin without breaking. In their research on fabrication-aware methods in computer-aided design Austern et al. categorized the constraints in the fabrication-aware design process (Figure

16) based on the stages of the design process and the frequency of appearance of these constraints in projects related to practice and academia (Austern et al., 2018).

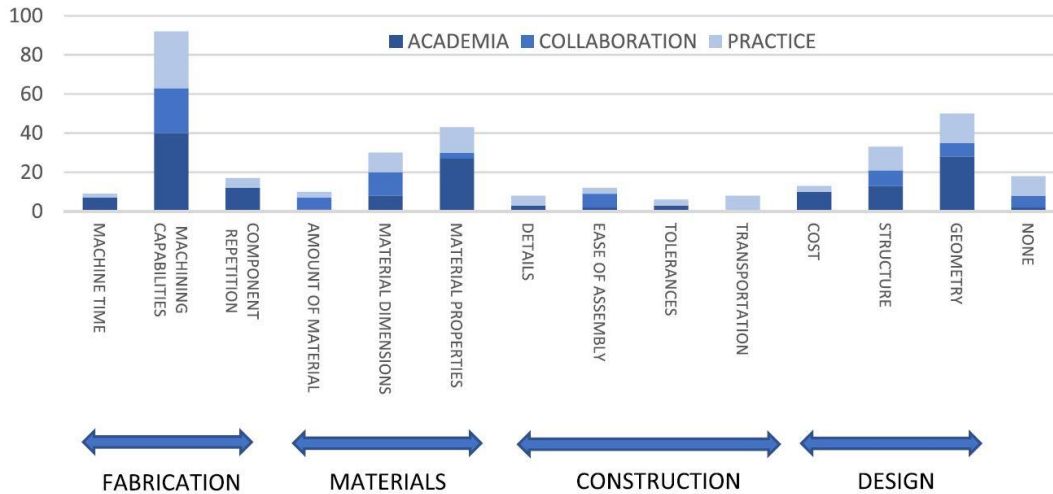


Figure 16_Frequency of appearance for different fabrication constraints in the fabrication-aware design (Austern et al., 2018).

Depending on the nature of the design problem, material properties, performance requirements, capabilities of fabrication machinery and the necessities of the construction process, the computational design approach can be implemented to integrate these design requirements into the design process based on the priorities of hard and soft constraints. The results show that capabilities of fabricating machinery are the most common targets in constraint-based modeling applications and research. This shows the importance of the application of fabrication-aware design especially with respect to digital and robotic fabrication. Also, adherence to the design geometry, material properties, and structural requirements appear frequently as the targets of rationalization in constraint-based modelling, however, these requirements appear more in industry related projects.

2.4 Rationalization in architecture

2.4.1 Definition and necessity of rationalization

In the traditional sense, architectural rationalization refers to the process of making a complex design possible to fabricate within the limitations of available machinery and affordable by changing the geometry of the design. However, introduction of advanced technologies for design and fabrication in the field of architecture has changed this notion significantly. In this section we explain the evolution of architectural rationalization in relation with computational design and digital and robotic fabrication. The goal is to define and categorize the existing practices of rationalization in academia and in the AEC industry and develop a theoretical framework for application of fabrication-aware design.

In the medieval period the master builder was responsible for designing of the building as well as realization of the design which made the practicalities of the construction an inherent consideration in all stages of the design (Kolarevic 2003 and 2005). This formed a deep connection between the geometry, structure, materiality and construction in masterpieces of human creation such as, the Pyramids, the Pantheon and the Gothic cathedrals. Separation between the architect and the builder, advocated by Alberti, was in fact the separation between the fields of structure and construction and the stylistic and aesthetic craft of the architect (Carpo, 2011). In this regard geometry evolved to a basic tool (language) for communication between the fields. However, with the increase in the geometric complexity the need for the architectural rationalization became apparent (Austern et al., 2018).

Gaudi, as a pioneer of classic geometric rationalization, was a leading figure in the introduction of complex geometries into architectural design, this included the application of mathematically

described ruled surfaces which could better conform to the practicalities of construction methods without compromising the design (Fischer, 2012 and Burry, 2011). This type of mathematical rationalization of geometry is also evident in the works of great architects/engineers of the mid-20th century such as Felix Candela with his application of hyperbolic paraboloids as doubly curved concrete systems (Pedreschi, 2008), or Dieste and his application of catenary surfaces in designing thin brickwork shells (Dieste, 1992). A classic method of geometric rationalization is the design of the Sydney Opera House (1956-1973) where the architect Jørn Utzon had to change the design from free-form geometry into the repetitive, spherical segments which were possible to produce with the technologies of the time (Schodek et al., 2005). The practices of these architects/engineers are quite relatable to the architect/builders of the medieval period in the sense that for them rationalization of the geometry and empirical buildability feedback is a crucial factor and an economic necessity.

With the availability of digital modeling tools in the contemporary architectural practice, rationalization has gained significant attention. Companies like Gehry Partners and Foster and Partners in early 2000 were the pioneers of the application of geometric rationalization processes in practice. Glymph describes the rationalization process at Gehry Partners as a process where physical models are approximated by digital models with programmed geometric constraints which guarantee their constructability (Glymph et al., 2004). Whitehead used the terms pre-rationalization and post-rationalization to categorize rationalization methods based on when they are performed in the design process (Whitehead, 2003). Hudson described post-rationalization as a top-down approach where the final geometry is defined, and the parametric design task is to find rational geometry that gives a very close match, and pre-rationalization as a bottom up or generative method where the parts and the constraints and interactions between the parts are

defined and the building geometry is the result of these interactions (Hudson, 2010). Fisher added a new temporal category as co-rationalization where the system composition is redefined through the design process (Fischer, 2007).

From the field of computational geometry, Pottman defined pre-rationalization as construction-aware design and post-rationalization as design optimization which provides a meaningful distinction between the targets of the rationalization process, the timing of the rationalization, and the identity of the agency performing the rationalization (Pottman, 2010; Pottman et al., 2007).

Large architectural forms are often technically impossible or overly expensive to build in one piece. They are therefore commonly realized as an assembly of components. Post-rationalization is the centralized approach for realization of the complex geometry of the architectural form by discretizing the elaborate form into constructible and assemblable modules (Jonas, 2014 and Shepherd et al., 2014). Paneling is an instance of rationalization and refers to the approximation of a surface by a set of surface components, so-called panels, producible at reasonable cost.

There are also many advantages to subdividing an architectural system. Individual components can be fabricated remotely at the most suitable facility and can be optimized for fabrication with minimum energy use and material waste. Transporting components is easier than the whole structure. Moreover, in the life cycle of the structure individual components are easier to replace and can even be recycled and reused (Austern et al., 2018). Due to the need for fabrication of elaborate architectural form, many smart computational methods have been developed to take account of different fabrication constraints such as digital fabrication constraints, assembly logics, material properties, and modules connectivity.

2.4.2 Timing and strategies in architectural rationalization

As has been mentioned earlier, researchers traditionally categorize rationalization methods based on the timing in the design sequence, often referred to as pre-, post- or co-rationalization (Lindsey et al., 2001; Whitehead, 2003; Attar et al., 2010). In this regard, academic researchers have a strong bias towards pre-rationalization with a more generalizable approach. On the other hand, designers, engineers and fabricators, usually address rationalization during the design development stage, while fabricators use rationalization when they get involved in the process which is usually at the final stages of the design. Dritsas suggested an alternative categorization, in which rationalization methods are divided based on the type of the strategy they use such as, description, analysis and evaluation (Dritsas, 2012). Austern categorized different strategies applied in rationalization including fabrication-aware design, optimization, and transition within the temporal definition of pre-, post- and co-rationalization (Austern et al., 2018) (Figure 17).

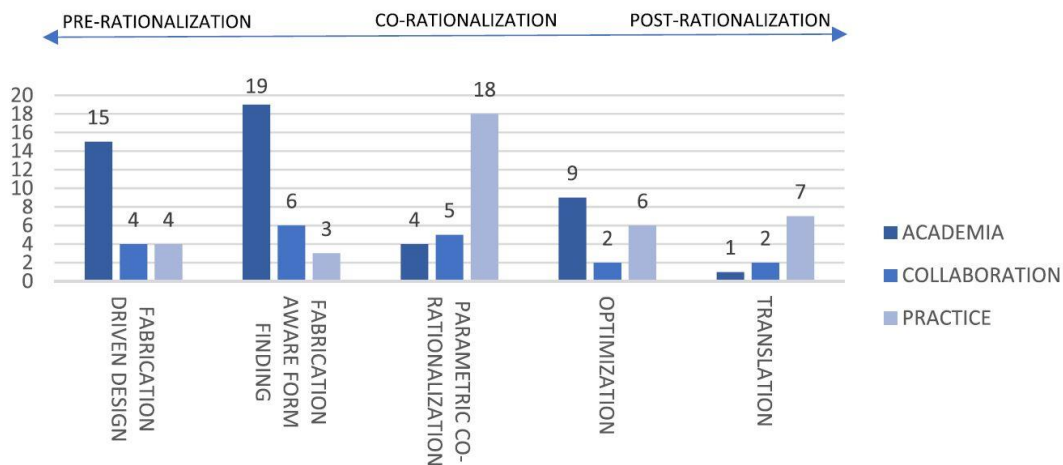


Figure 17_Types of rationalization strategies within temporal categories of rationalization (Austern et al., 2018).

Based on the results shown in Figure 17, the temporal category of pre-rationalization is divided in two different design strategies. The first strategy is the fabrication driven design where the

designer actively uses family of geometries which are known to be buildable with a specific fabrication process (Attar et al., 2010; Mostafavi et al., 2016). Therefore, the knowledge of a specific fabrication method and the properties of the corresponding geometry become the main design drivers. A classic example of this strategy is the application of hyperbolic paraboloids by Felix Candela as doubly curved concrete systems and using wooden form work for construction (Pedreschi, 2008). Another example of this strategy regarding robotic fabrication is designing geometries to be cut using robotic hot blade (Brander et al., 2016). In the industry these strategies are mainly used in constructable façade glazing systems through the introduction of geometric modellings such as Face-Edge offset meshes (Ross et al., 2016), Marionette meshes (Mesnil et al., 2016), and isogonal modelling surfaces (Mesnil et al., 2015).

The other design strategy in pre-rationalization is fabrication-aware form-finding. This method is different from the previous one, as the designer does not actively steer the design to any specific shape. Instead, using computational design and constraint-based modeling techniques the fabrication constraints are implemented in the computational model, creating a virtual space of solutions. This is what Menges and Schwin refer to as the Machinic Morphospace (Menges et al., 2012), where an algorithm resolves the design constraints towards buildable design solutions (Austern et al., 2018). Numerous computational techniques have been developed for resolution of fabrication constraints regarding specific fabrication methods, structural requirements, or material properties. The application of physics-based modeling techniques for fabrication constraint resolution, mesh relaxation methods to rationalize mesh geometry, and simulation-based modelling of material behavior are good examples of these strategies (Pedersen et al., 2014; Schwinn et al., 2015; Fornes, 2016; Senatore and Piker, 2015). As depicted by the data in (Figure 17), these strategies are mainly used in academic researcher (Bechert et al., 2016;

Georgiou et al., 2014). Figure 18-10 show some examples of the application of this method in research projects.



Figure 18_ICD/ITKE Research Pavilion 2010 and application of bending active simulation using FEM to find the global geometry of the interconnected system based on the material behavior under large deformations with predefined connection points (Fleischmann and Menges, 2011).

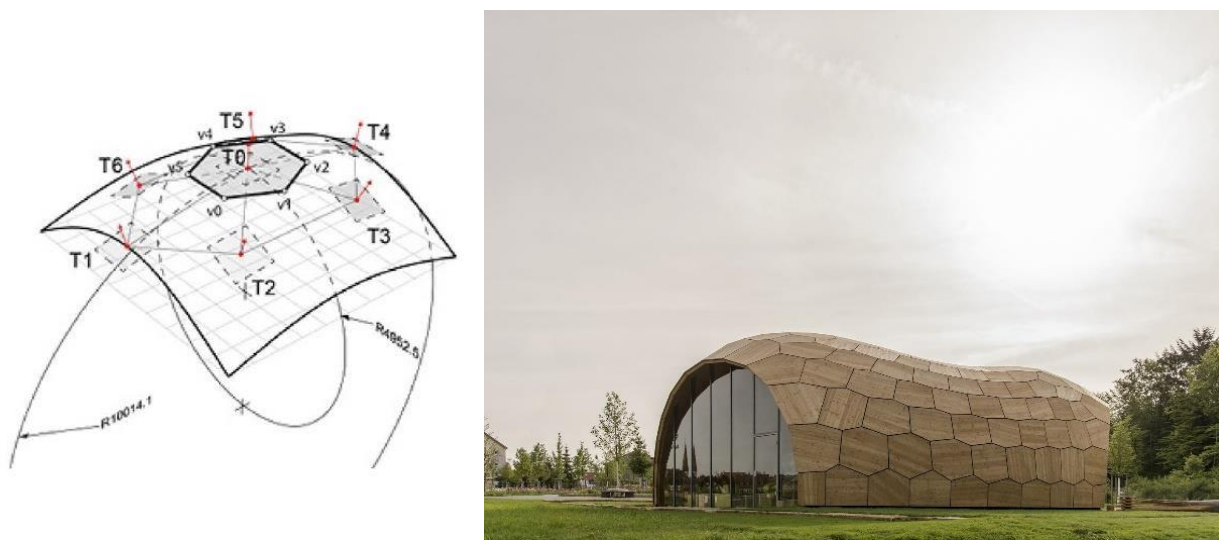


Figure 19_Computational design and robotic fabrication of thin timber plate shell. ICD/ITKE/IIGS Landesgartenschau exhibition hall. Application of packing algorithm with a novel integrated edge connection detailing to inform the paneling patterns and fabrication process for a timber plate shell (Schwinn and Menges, 2015).

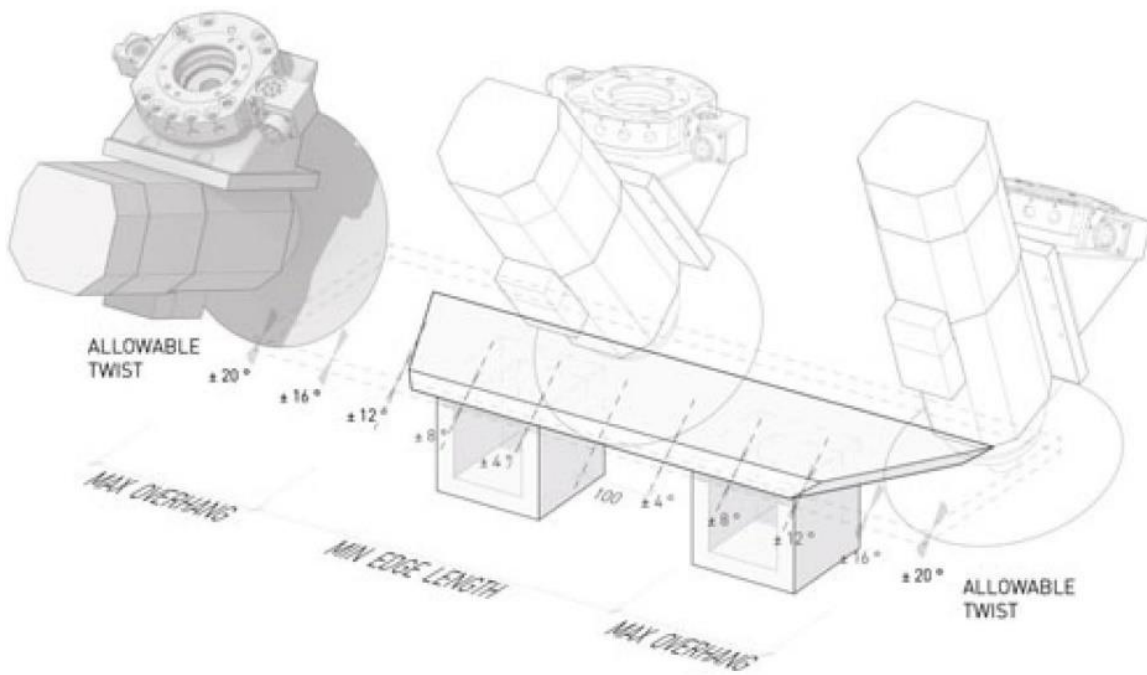
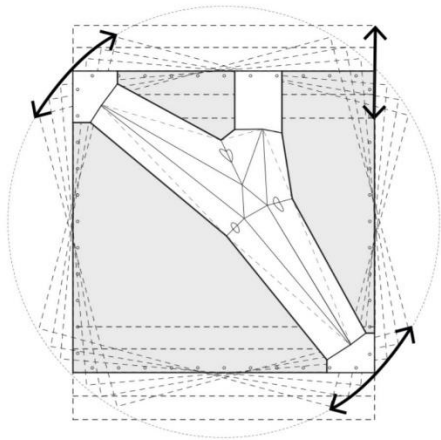


Figure 20_Quasi-reciprocal timber and discontinuous post-tensioned concrete structure and fabrication constraints. Completed Utzon 40 Pavilion (Maxwell et al., 2014).

Austern et al. propose the term parametric “co-rationalization”, based on the original term coined by Whitehead, to reflect the role of parametric modeling in design and engineering (Austern et al., 2018). This strategy uses the inherent flexibility of parametric tools to calibrate the design as

different fabrication constraints are discovered. As depicted in Figure 17 this is a hybrid strategy often mixing pre-rationalization assumptions of constraint modelling with post-evaluated efficiency measures, allowing for manual or automatic optimization processes. This strategy is the most commonly used strategy in architectural projects, especially in industry (Clifford and McGee, 2011; Pedersen et al., 2014; Harding et al., 2015; Musil et al., 2016; Agkathidis and Brown, 2013; Williams et al., 2013; Clifford and McGee, 2014; Dillenburger and Hansmeyer, 2014; Peters, 2007; Schlueter and Tobias, 2008). Some academic design-build examples of this method is shown in Figure 21 and Figure 22.

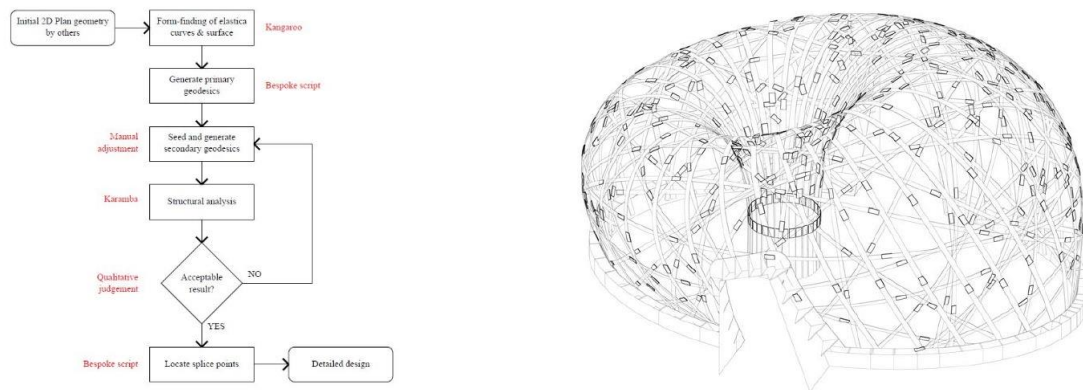


Figure 21_ The Ongreening Pavilion, Schematic diagram showing the overall process of form generation and co-rationalization of interweaving members and their structural performance. (Harding et al., 2015).

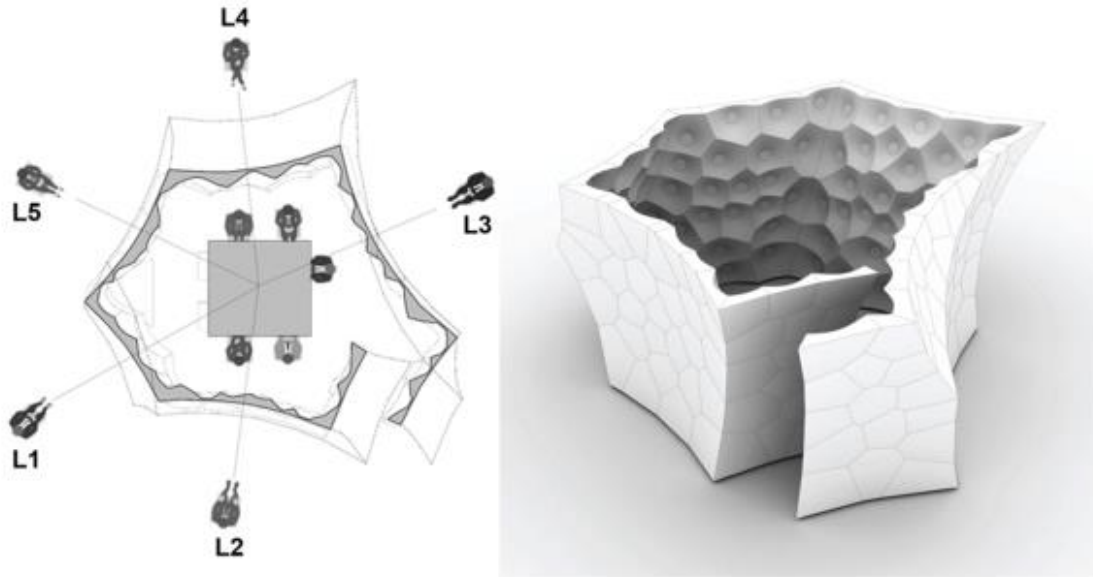


Figure 22_ FABPOD: A design-to-fabrication system integrating early sound performance prediction and fabrication constraints in a co-rationalization process. (Williams et al., 2015).

The two main strategies in the post-rationalization method are optimization and translation. In the context of architectural discourse optimization refers to a repetitive process in which designs are generated using a parametric definition, numerically evaluated using simulation models and improved using a mathematical algorithm to search within the possible solution space (Bradner et al., 2014; Holzer et al., 2007; Adriaenssens et al., 2014; Austern et al., 2018). In the context of fabrication, optimization refers to a post-rationalized process in which the geometry is first designed free from constraints of fabrication and then adapted based on constructability considerations by computational procedures (Attar et al., 2010; Schiffner et al., 2012; Crolla, 2012; Vazquez et al., 2014; Mollica, 2016). Translation strategies in post-rationalization refer to methods that usually fabricators or fabrication specialists use in the fabrication process of the project. In this strategy the design model is usually transferred to a different computational medium that is better suited for fabrication setup. The design intent plays a crucial role in the creation of the new model and due to reconstruction of the model the tolerance between the two

models can be considerable. This transition from design to fabrication instructions naturally falls into the domain of industry related projects performed by fabricators or design-assist companies (Scheurer, 2010). While post-rationalization might be preferred by many designers who argue that the formal constraints will limit their creativity in the conceptual design phase. However, the approximation resulting from rationalization can deviate considerably and uncontrollably from the unconstrained input model, and this can distance the realized project from the designed form. In contrast, pre-rationalization is a process that directly integrates fabrication-awareness and lets the designer explore and choose a final model in a more informed manner throughout the design process (Deuss, 2015). In the application of computational design in research and academic projects, rationalization methods are either pre-rationalized, where the computational process is the primary tool for form generation, or post-rationalized, where the computational process takes account of fabrication constraints to guarantee the constructability of the design (Austern et al., 2018). These methods ignore the complexity of design process between the conceptual phase and fabrication phase. To create a more informed design process the feedback from the design constraints needs to be addressed through all the design stages. This requires a more flexible computational design process which is continuously informed by different types of design constraints including performance constraints (material, structural, environmental) and fabrication constraints (construction and assembly) as proposed by (Pottmann et al., 2015). Achieving such integrative computational processes requires the development of real-time feedback systems which can respond to design changes in real-time to inform the design process with quantitative and qualitative feedback in both pre- and post-rationalization (Pigram et al., 2016; Attar et al., 2010; Jiang et al., 2014; Yong et al., 2012; Tang et al., 2015).

2.5 Performance-based and fabrication-aware design process for reciprocal systems

In this section, we propose the structure for an integrative performance-based and fabrication-aware design process aimed at the design to construction of reciprocal systems. This process integrates modelling, form-finding, analysis and fabrication data generation in a comprehensive computational design process in four steps.

1_ The modelling process uses a novel generative formulation for reciprocal pattern design, this formulation uses the quadrilateral mesh data derived from the rationalization of the design geometry to generate the reciprocal patterning on the design geometry. The proposed formulation additionally generates geometric and connectivity data to formulate the mathematical fabrication constraints for each member to member connection based on the connection design constraints.

2_ The form-finding process uses dynamic relaxation to solve the constraint-based model, which iteratively and simultaneously minimizes the eccentricities between the members to generate the proper geometric model for analysis and fabrication of 2-D and 3-D reciprocal system. The analysis process uses the output of the form-finding process and generates the analytical model for structural analysis.

3_ A scalable and generalizable analysis method is proposed which takes account of member connectivity conditions and can accommodate design and analysis of free-form geometries.

4_ The modelling and form-finding processes generate the required topological and geometric data for fabrication data generation. This data is then used to create 3-D member geometries and member to member connection cuts integrating the fabrication tolerances from the 5-axis CNC machinery.

5_ The computational design processes provides the medium for integration and management of the dataflow between different design modules and generation of feedback systems for different performance metrics (structural performance, material use, perforation calculations) as well as fabrication data (machine time, connection detailing properties, estimated sheet material use, fabrication tolerances) to inform the design process in multiple steps. The proposed process is an example of a flexible computational design process which provides continuous and real-time feedback throughout the design process regarding performance metrics and fabrication awareness in design to fabrication of reciprocal systems. As a case study this computational method is used in a multi-objective exploration process for design and fabrication of a full-scale prototype located at Matthaei Botanical Gardens in Ann Arbor, Michigan.

2.6 Conclusions

In this chapter some of the main concepts and strategies in the field of computational design were explained, and their scope and applications were explored within academic and industry driven research. Through investigation of qualities and limitations of pre-, post-, and co-rationalization methods, this study explains the necessity for the implementation of flexible computational design processes with capacities for continuous data feedback including performance goals and fabrication constraints. Finally, the structure of the proposed integrative performance-based and fabrication-aware design process for design to construction of reciprocal systems is summarized as a computational design process which integrates modelling, form-finding, analysis, and fabrication data generation.

References

Adriaenssens, Sigrid, Philippe Block, Diederik Veenendaal, and Chris Williams, eds. *Shell structures for architecture: form finding and optimization*. Routledge, 2014.

Agkathidis, Asterios. *Generative Design*. Laurence King Publishing, 2015.

Agkathidis, Asterios, and André Brown. "Tree-structure canopy: a case study in design and fabrication of complex steel structures using digital tools." *International Journal of Architectural Computing* 11, no. 1 (2013): 87-104.

Alexander, Christopher. *Notes on the Synthesis of Form*. Vol. 5. Harvard University Press, 1964.

Attar, Ramtin, Robert Aish, Jos Stam, Duncan Brinsmead, Alex Tessier, Michael Glueck, and Azam Khan. "Embedded rationality: A unified simulation framework for interactive form finding." *International journal of architectural computing* 8, no. 4 (2010): 399-418.

Austern, Guy, Isaac Guedi Capeluto, and Yasha Jacob Grobman. "Rationalization methods in computer aided fabrication: a critical review." *Automation in Construction* 90 (2018): 281-293.

Bechert, Simon, Jan Knippers, Oliver David Krieg, Achim Menges, Tobias Schwinn, and Daniel Sonntag. "Textile fabrication techniques for timber shells." *Advances in architectural geometry* (2016).

Brander, David, Jakob Andreas Bærentzen, Kenn Clausen, Ann-Sofie Fisker, Jens Gravesen, Morten N. Lund, Toke Bjerger Nørbjerg, Kasper Hornbak Steenstrup, and Asbjørn Søndergaard. "Designing for hot-blade cutting: geometric approaches for high-speed manufacturing of doubly-curved architectural surfaces." In *Advances in Architectural Geometry (AAG 2016)*, pp. 306-327. vdf Hochschulverlag AG an der ETH Zürich, 2016.

Bradner, Erin, Francesco Iorio, and Mark Davis. "Parameters tell the design story: ideation and abstraction in design optimization." In *Proceedings of the symposium on simulation for architecture & urban design*, p. 26. *Society for Computer Simulation International*, 2014.

Burry, Mark. *Scripting cultures: Architectural design and programming*. John Wiley & Sons, 2011.

Carpo, Mario. *The alphabet and the algorithm*. MIT Press, 2011.

Clifford, B., and W. McGee. "Matter and making: periscope foam tower." *Fabricate: making digital architecture*. Riverside Architectural Press, London (2011): 76-79.

Clifford, Brandon, and Wes McGee. "La Voûte de LeFevre: a variable-volume compression-only vault." *Fabricate: negotiating design & making* 2 (2014): 146-153.

- Crolla, Kristof. "Building simplicity: golden moon, 2012 mid-autumn festival lantern wonderland." *Fabricate—Negotiating Design & Making*, gta Verlag, Zurich (2014): 22-29.
- Deuss, Mario Moacir. *Computational Methods for Fabrication-aware Modeling, Rationalization and Assembly of Architectural Structures*. No. THESIS. EPFL, 2015.
- Helmut Pottmann, Michael Eigensatz, Amir Vaxman, and Johannes Wallner. Architectural geometry. *Computers & Graphics*, 47(0):145 – 164, 2015.
- Dieste, Eladio. "Some reflections on architecture and construction." *Perspecta* (1992): 187-203.
- Dillenburger, Benjamin, and Michael Hansmeyer. "Printing architecture: castles made of sand." Gramazio, F. Kohler, M. and Langenberg, S.(eds) *Fabricate: negotiating design & making*. Eidgenössische Technische Hochschule Zürich (2014).
- Dritsas, Stylianos. "Design-built rationalization strategies and applications." *International Journal of Architectural Computing* 10, no. 4 (2012): 575-593.
- Fischer, Thomas. "Rationalizing bubble trusses for batch production." *Automation in construction* 16, no. 1 (2007): 45-53.
- Fischer, Thomas. "Geometry rationalization for non-standard architecture." *Architecture Science* 5 (2012): 25-47.
- Fleischmann, Moritz, and Achim Menges. "Icd/itke research pavilion: A case study of multi-disciplinary collaborative computational design." In *Computational Design Modelling*, pp. 239-248. Springer, Berlin, Heidelberg, 2011.
- Fornes, Mark. "The Art of the Prototypical." *Architectural Design* 86, no. 2 (2016): 60-67.
- Georgiou, M., O. Georgiou, and T. Kwok. "Form complexity—Rewind|‘God’s Eye’Sukkahville 2013." In *Proceedings of the 34th annual conference of the association for computer aided design in architecture (ACADIA)*, Los Angeles. 2014.
- Glymph, James, Dennis Shelden, Cristiano Ceccato, Judith Mussel, and Hans Schober. "A parametric strategy for free-form glass structures using quadrilateral planar facets." *Automation in construction* 13, no. 2 (2004): 187-202.
- Harding, John, Will Pearson, Harri Lewis, and Stephen Melville. "The ongreening pavilion." In *Advances in architectural geometry* 2014, pp. 295-308. Springer, Cham, 2015.
- Hensel, Michael, Achim Menges, and Michael Weinstock. "Techniques and Technologies in Morphogenetic Design (*Architectural Design* March April 2006 Vol. 76 No. 2)." (2006).
- Holzer, Dominik, Richard Hough, and Mark Burry. "Parametric design and structural optimization for early design exploration." *International Journal of Architectural Computing* 5, no. 4 (2007): 625-643.

Hudson, Roland. "Strategies for parametric design in architecture: an application of practice led research." PhD diss. University of Bath, United Kingdom (2010).

Jiang, Caigui, Chengcheng Tang, Marko Tomičić, Johannes Wallner, and Helmut Pottmann. "Interactive modeling of architectural freeform structures: combining geometry with fabrication and statics." In *Advances in architectural geometry* 2014, pp. 95-108. Springer, Cham, 2015.

Jonas, Katrin, Alan Penn, and Paul Shepherd. "Designing with discrete geometry." In *Rethinking Comprehensive Design: Speculative Counterculture-Proceedings of the 19th International Conference on Computer-Aided Architectural Design Research in Asia, CAADRRIA 2014*, pp. 513-522. *The Association for Computer-Aided Architectural Design Research in Asia (CAADRRIA)*, 2014.

Kolarevic, Branko. "Digital production." *Branko Kolarevic, "Architecture in the Digital Age—Design and Manufacturing"*, Taylor & Francis, New York (2003): 31-51.

Kolarevic, Branko. "Information master builders." *Architecture in Architecture in the Digital Age: Design and Manufacturing, Washington, DC: Taylor & Francis* (2005): 56-62.

Lindsey, Bruce, Frank O. Gehry, and A. Saggio. Digital Gehry. Englische Ausgabe.: *Material Resistance Digital Construction*. Springer Science & Business Media, 2001.

Menges, Achim, and Tobias Schwinn. "Manufacturing reciprocities." *Architectural Design* 82, no. 2 (2012): 118-125.

Maxwell, Iain, David Pigram, and Ole Egholm-Pedersen. "Fabrication Aware Form-Finding: A Combined Quasi-Reciprocal Timber and Discontinous Post-tensioned Concrete Structure." (2014).

Mesnil, Romain, Cyril Douthe, Olivier Baverel, Bruno Léger, and Jean-François Caron. "Isogonal moulding surfaces: a family of shapes for high node congruence in free-form structures." *Automation in Construction* 59 (2015): 38-47.

Mesnil, R., C. Douthe, O. Baverel, and B. Léger. "Marionette mesh: from descriptive geometry to fabrication-aware design, advances in *architectural geometry 2016*, vdf Hochschulverlag AG, Zurich." (2016).

Mogas-Soldevila, Laia, Jorge Duro-Royo, Daniel Lizardo, Markus Kayser, William Patrick, Sunanda Sharma, Steven Keating, John Klein, Chikara Inamura, and Neri Oxman. "Designing the ocean pavilion: Biomaterial templating of structural, manufacturing, and environmental performance." In *Proceedings of IASS Annual Symposia*, vol. 2015, no. 16, pp. 1-13. International Association for Shell and Spatial Structures (IASS), 2015.

Mollica, Zachary, and Martin Self. "Tree Fork Truss." *Advances in architectural geometry* 2016 (2016): 138-153.

- Mostafavi, Sina, and Henriette Bier. "Materially informed design to robotic production: a robotic 3D printing system for informed material deposition." In *Robotic Fabrication in Architecture, Art and Design 2016*, pp. 338-349. Springer, Cham, 2016.
- Musil, Josef, Darron Haylock, Matthew Hayhurst, Samuel Wilkinson, Xavier De Kestelier, and Eilon Vaadia. "Safra Neuron Screen." *Advances in architectural geometry* (2016).
- Oxman, Rivka, and Robert Oxman. *Theories of the Digital in Architecture*. Routledge, 2014.
- Pedersen, Ole Egholm, Niels Martin Larsen, Dave Pigram, and Iain Maxwell. "Fabrication Aware Form-finding: A combined quasi-reciprocal timber and discontinuous post-tensioned concrete structure." In *Acadia 2014: Design Agency*, pp. 375-384. Riverside Architectural Press, 2014.
- Pedreschi, Remo. "Form, force and structure: a brief history." *Architectural Design* 78, no. 2 (2008): 12-19.
- Peters, Brady. "The Smithsonian Courtyard Enclosure: A case-study of digital design processes." In *Expanding Bodies: Art-Cities-Environment: Proceedings of the 27th Annual Conference of the Association for Computer Aided Design in Architecture (ACADIA)*, pp. 74-83. 2007.
- Pigram, Dave, Iain Maxwell, and Wes McGee. "Towards Real-Time Adaptive Fabrication-Aware Form Finding in Architecture." In *Robotic Fabrication in Architecture, Art and Design 2016*, pp. 426-437. Springer, Cham, 2016.
- Pottmann, Helmut. "Architectural geometry as design knowledge." *Architectural Design* 80, no. 4 (2010): 72-77.
- Pottmann, Helmut, Andreas Asperl, Michael Hofer, Axel Kilian, and D. Bentley. *Architectural geometry*. Vol. 724. Exton, PA: Bentley Institute Press, 2007.
- Pottmann, Helmut, Michael Eigensatz, Amir Vaxman, and Johannes Wallner. "Architectural geometry." *Computers & graphics* 47 (2015): 145-164.
- Ross, Elissa, Daniel Hambleton, and Robert Aish. "Face-offsetting polygon meshes with variable offset rates." *Advances in Architectural Geometry 2016* (2016): 40-61.
- Scheurer, Fabian. "Materialising complexity." *Architectural Design* 80, no. 4 (2010): 86-93.
- Schiftner, Alexander, Nicolas Leduc, Philippe Bompas, Niccolo Baldassini, and Michael Eigensatz. "Architectural geometry from research to practice: the eiffel tower pavilions." In *Advances in Architectural Geometry 2012*, pp. 213-228. Springer, Vienna, 2013.
- Schlueter, Arno, and Tobias Bonwetsch. "Design rationalization of irregular cellular structures." *International journal of architectural computing* 6, no. 2 (2008): 197-211.

Schodek, Daniel L., Martin Bechthold, Kimo Griggs, Kenneth Martin Kao, and Marco Steinberg. *Digital design and manufacturing: CAD/CAM applications in architecture and design*. New Jersey: John Wiley & Sons, 2005.

Schwinn, Tobias, and Achim Menges. "Fabrication agency: Landesgartenschau exhibition hall." *Architectural Design* 85, no. 5 (2015): 92-99.

Senatore, Gennaro, and Daniel Piker. "Interactive real-time physics: an intuitive approach to form-finding and structural analysis for design and education." *Computer-Aided Design* 61 (2015): 32-41.

Shelden, Dennis Robert. "Digital surface representation and the constructibility of Gehry's architecture." PhD diss., Massachusetts Institute of Technology, 2002.

Shepherd, Paul, and Paul Richens. "The case for subdivision surfaces in building design." *Journal of the International Association for Shell and Spatial Structures* 53, no. 4 (2012): 237-245.

Soddu, Celestino. "The design of morphogenesis. An experimental research about the logical procedures in design processes." *Demetra Magazine* 1 (1994): 56-64.

Terzidis, Kostas. *Algorithmic architecture*. Routledge, 2006.

Thompson, d'Arcy, W. *On growth and form*. Vol. 1. Cambridge university press, 1952.

Vazquez, Alicia Nahmad, Shajay Bhooshan, Asbjorn Sondergaard, Chikara Inamura, Joshua Zabel, and Mustafa El-sayed. "Design, analysis and fabrication of expressive, efficient shell structures: a prototype exploring synergy between architecture, engineering and manufacture." *In Proceedings of IASS Annual Symposia*, vol. 2014, no. 11, pp. 1-12. International Association for Shell and Spatial Structures (IASS), 2014.

Veltkamp, Martijn. *Free form structural design: Schemes, systems & prototypes of structures for irregular shaped buildings*. IOS Press, 2007.

Whitehead, Hugh. "*Laws of Form in Architecture in the Digital Age: Design and Manufacturing*." Washington, DC: Taylor & Francis (2003): 123.

Williams, Nicholas, Jane Burry, Daniel Davis, Brady Peters, Alexander Pena de Leon, and Mark Burry. "FabPod: Designing with temporal flexibility & relationships to mass-customisation." *Automation in Construction* 51 (2015): 124-131.

Yong, Xin Zhao Cheng-Cheng Tang, Liang Yang Helmut Pottmann, and Niloy J. Mitra. *Intuitive design exploration of constrained meshes*. Springer, 2012.

Tang, Chengcheng, Xiang Sun, Alexandra Gomes, Johannes Wallner, and Helmut Pottmann. "Form-finding with polyhedral meshes made simple." In *ACM SIGGRAPH 2015 Posters*, p. 5. ACM, 2015.

Chapter 3: Generative Design and Form-Finding of Reciprocal Systems

3.1 Introduction

The principle of structural reciprocity is based on the 3-D assembly of loadbearing members that mutually support each other along their span and create a self-supporting spatial configuration without structural hierarchy, which can span multiple times the length of members. In reciprocal frames, elements are geometrically interdependent in that the position of one element depends on the elements it connects to, and these dependencies form a circular graph (Figure 23).

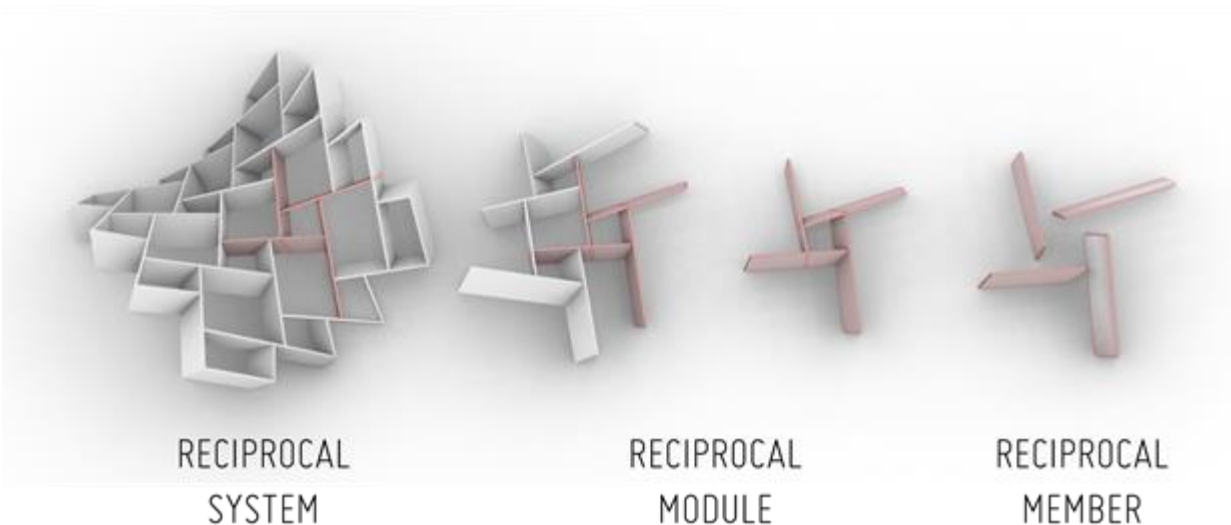


Figure 23_ The interconnected structure of the reciprocal systems.

3.2 Chapter methodology

This chapter studies the importance and the necessity of development and application of interactive design methods to address the complexities of designing reciprocal systems. Using computational design methods, the geometric and fabrication constraints are defined and resolved iteratively in design of free-form reciprocal systems.

The proposed design method consists of two steps, a generative modelling process and a form-finding process. The modelling process uses a generative formulation for reciprocal pattern design, this formulation uses the quadrilateral mesh data derived from the rationalization of the design geometry to generate the reciprocal patterning on the design geometry. The proposed formulation also generates geometric and connectivity data to formulate the mathematical fabrication constraints for each member to member connection based on the connection design constraints. The form-finding process uses the dynamic relaxation method to solve the constraint-based model (this process is explained in details in section 7 of this chapter), which iteratively and simultaneously minimizes the eccentricities between the members to generate the proper geometric model for analysis and fabrication of 2-D and 3-D reciprocal system. Effectiveness and efficiency of the proposed method is studied quantitatively, and visualization techniques are developed for post-processing of the form-finding results.

3.3 General approaches for design and form-finding of reciprocal systems as discrete systems

There are two general approaches for the design of reciprocal structures. The first approach takes the module as a primary building block and the final global form emerges as a result of the module's properties. The second approach results from adjusting the module's properties throughout the surface of the structure to fit its predefined global shape. The first approach

belongs to a family of methods in which the global geometry is generated based on a bottom up logic of the constituent parts (Anastas et al., 2016). The bottom up nature of the process is usually governed by a nonlinear interaction between the constituent parts. This bottom up process is an example of what Hensel referred to as digital morphogenesis (Hensel et al., 2006), which is inspired by the self-organizing process, underlying the growth of living organisms where form is no longer being made, but found, based on a set of rules or algorithms governing the interactions of the constituent parts. In this research the morphogenetic behavior is defined through a definition of a constraint-based model where the topological network information and the fabrication constraints define the rules of interaction between the reciprocal members. Subsequently a dynamic method is used to solve the constraints that generate the final configuration of reciprocal members in the system.

The second method belongs to a family of methods in which the design parameters are optimized for the global geometry to converge to the design geometry (Mesnil et al., 2018). This process belongs to a family of computational methods called post-rationalization where the geometric and fabrication constraints are set in a way to generate the best approximation of the design geometry (Anastas et al., 2016).

The proposed method in this chapter belongs to the bottom up family of methods, in which the reciprocal member is considered as the primary building block of the system and through a series of geometric rules these reciprocal members form a network of interconnected reciprocal modules in a non-hierarchical system. Although the modeling starts with a primitive surface geometry, the emergence of the interconnected system does not necessarily follow the primitive geometry as it responds to the geometrical rules controlling the reciprocal member (primary building block) geometry and the behavioral constraints controlling the interconnection of the

reciprocal members. As will be explained in this section, the geometric rules will be defined through a reciprocal pattern generation formulation. Further, the behavioral constraint system is defined through the constraint-based modeling technique resolved by a dynamic form-finding process through which the final reciprocal geometry emerges.

In summary, the proposed design method in this research consists of two steps, generative modelling process and form-finding process. The modelling process uses a novel generative formulation for reciprocal pattern design, this formulation uses the quadrilateral mesh data derived from the rationalization of the design geometry to generate the reciprocal patterning consisting of 1-D reciprocal members on the design geometry. The proposed formulation generates geometric and member connectivity data to formulate the mathematical fabrication constraints for each member to member connection based on the connection design constraints. The form-finding process uses the dynamic relaxation method to solve the constraint-based model, which iteratively and simultaneously minimizes the eccentricities between the members to keep them below the fabrication tolerances (fabrication tolerances include material dimensional tolerances and digital fabrication tolerances), and to generate the final geometry for analysis and fabrication (Oliyan Torghabehi, 2018).

3.4 Review of modeling methods for generation of reciprocal patterns

From the sketches of Leonardo da Vinci in the Codex Atlanticus to contemporary art works and calligraphy, reciprocal patterns have dwelled for centuries in arts and crafts of artists and designers worldwide as a practical configuration of materials or artistic visual expression (Figure 24).

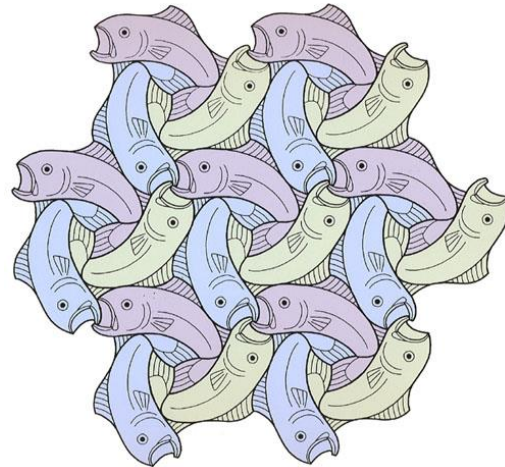
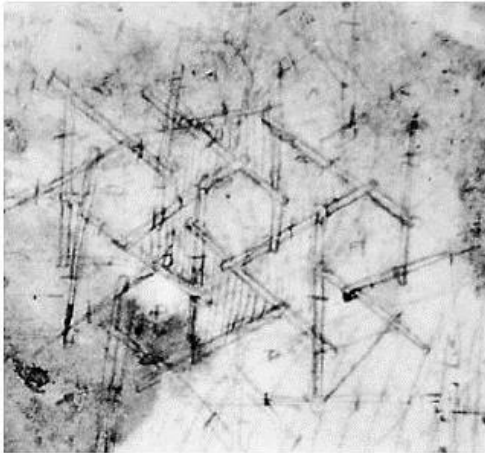


Figure 24_ Sketches of Leonardo da Vinci in sheet 898 of the Codex Atlanticus (1452-1519). Three Fishes tessellation. Robert Fathauer, screen print made in 1994.

However, in terms of architectural design and engineering there are technical complexities that need to be addressed for design and fabrication of free-form reciprocal systems. While there has been significant research on development of practical design methods for these systems, the existing methods usually designed for specific types of reciprocal systems and are not generalizable for design purposes (Figure 11). The goal is to develop a generalizable formulation for designing and form-finding of these systems.

There are multiple methods for pattern generation of reciprocal systems. Most of these methods are based on transforming a standard network of frames through expanding their nodes with different geometric methods (Figure 25) (Douthe and Baverel, 2009, Parigi and Kirkegaard, 2014, Mesnil et al., 2018).

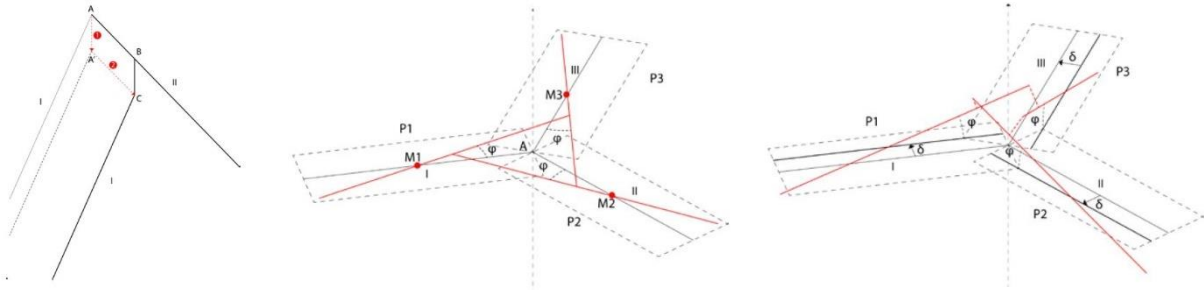


Figure 25_ From the left: Translation method, rotation method, extended translation method.

Other methods use conformal mapping of a 2-D geometry of reciprocal system on the 3-D surface (Figure 26) (Song et al., 2013, Mellado et al., 2015).

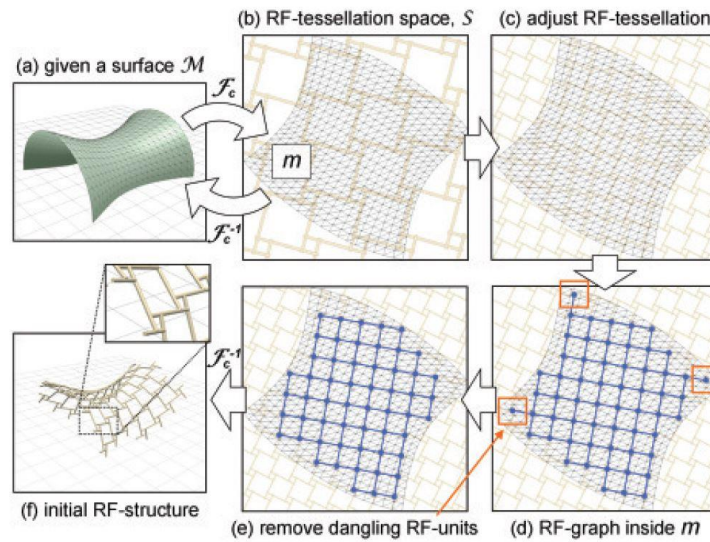


Figure 26_ Mapping procedure for mapping of a 2-D reciprocal pattern to the 3-D space (Song et al., 2013).

A different approach is to use the mesh data to generate the reciprocal pattern based on the rationalized definition of the free-form geometry (Figure 27) (Anastas et al., 2016).

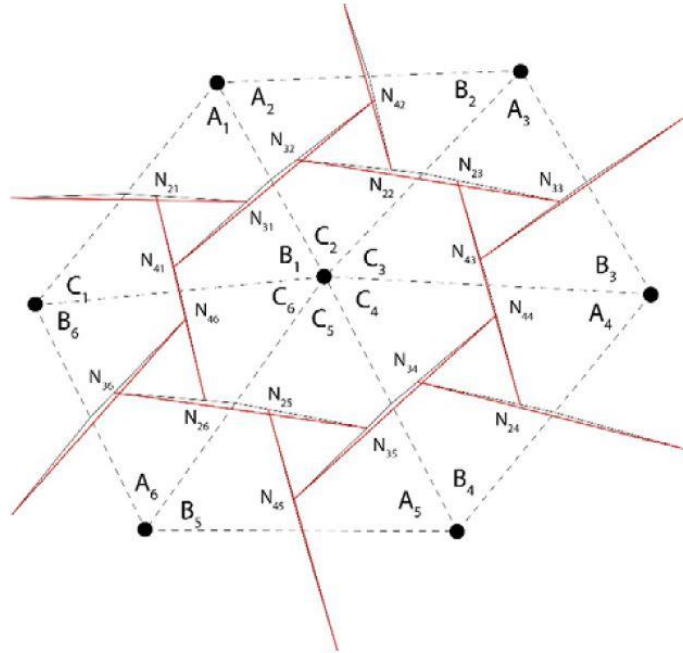


Figure 27_ Mesh based tessellation method for generation of reciprocal patterns on a 3-d surface (Anastas et al., 2016).

In this research, an extended version of cell-based formulation for reciprocal pattern generation first developed by Anastas et al. is proposed, which uses mesh data from the rationalization of the free-form surface geometry (Anastas et al., 2016). This means the generation of the reciprocal pattern is based on the rationalized mesh surface generated from the desirable global geometry. The proposed formulation generates geometric and member connectivity data (network topological data) to formulate the fabrication constraints for each member to member connection based on the connection design constraints. This data is necessary for mathematical formulation of fabrication constraints in the form-finding process.

Unlike the method proposed by Anastas, this method identifies the neighboring reciprocal modules and generates a data structure based on the interconnections of these modules (Anastas et al., 2016). This will eliminate the need for renumbering the mesh faces and also provides a generalizable formulation for free form design.

Moreover, this method proposes an optimal geometric data structure which provides the necessary geometric data for analytical model development for analysis as well as necessary data for detailed generation of 2-D and 3-D member geometry for connection design as well as generation of fabrication data for digital fabrication. This method is significantly robust and flexible for design purposes and can be applied to free-form designs with varying curvature.

3.5 Proposed mesh-based generative formulation for reciprocal pattern generation

As mentioned earlier, the proposed design method in this research consists of two steps, generative modelling process and form-finding process. In this section we explain the generative modeling process.

The proposed method populates the free-form design surface with interconnected reciprocal modules. The algorithm for generation of reciprocal systems uses a discretized mesh geometry which approximates the surface geometry. This parametric algorithm uses mesh data (topology data, vertices, edges, faces) and generates the reciprocal structure based on the reciprocal system parameters (discretization size and engagement length).

Step_1: The process starts with discretization of the design geometry. For this matter we use quadrilateral mesh to discretize the continuous surface geometry into a collection of quadrilateral surfaces with the topological mesh data. These geometric and topological data will be used in the proposed algorithm to populate the surface with reciprocal modules (Figure 28).

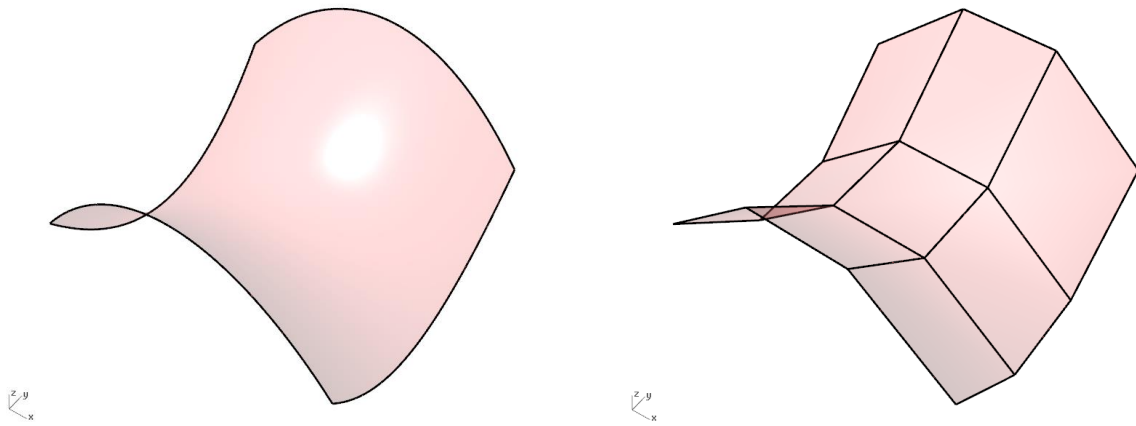


Figure 28_ Sample discretization of a doubly curve surface using quadrilateral meshes.

Step_2: The mesh topological data is used to generate the required data for modelling. In this process, using the mesh faces, mesh vertices, and mesh edges, the half-edge data is generated which will be used later to identify the neighboring cells (mesh faces) to interconnect the neighboring reciprocal modules (Figure 29).

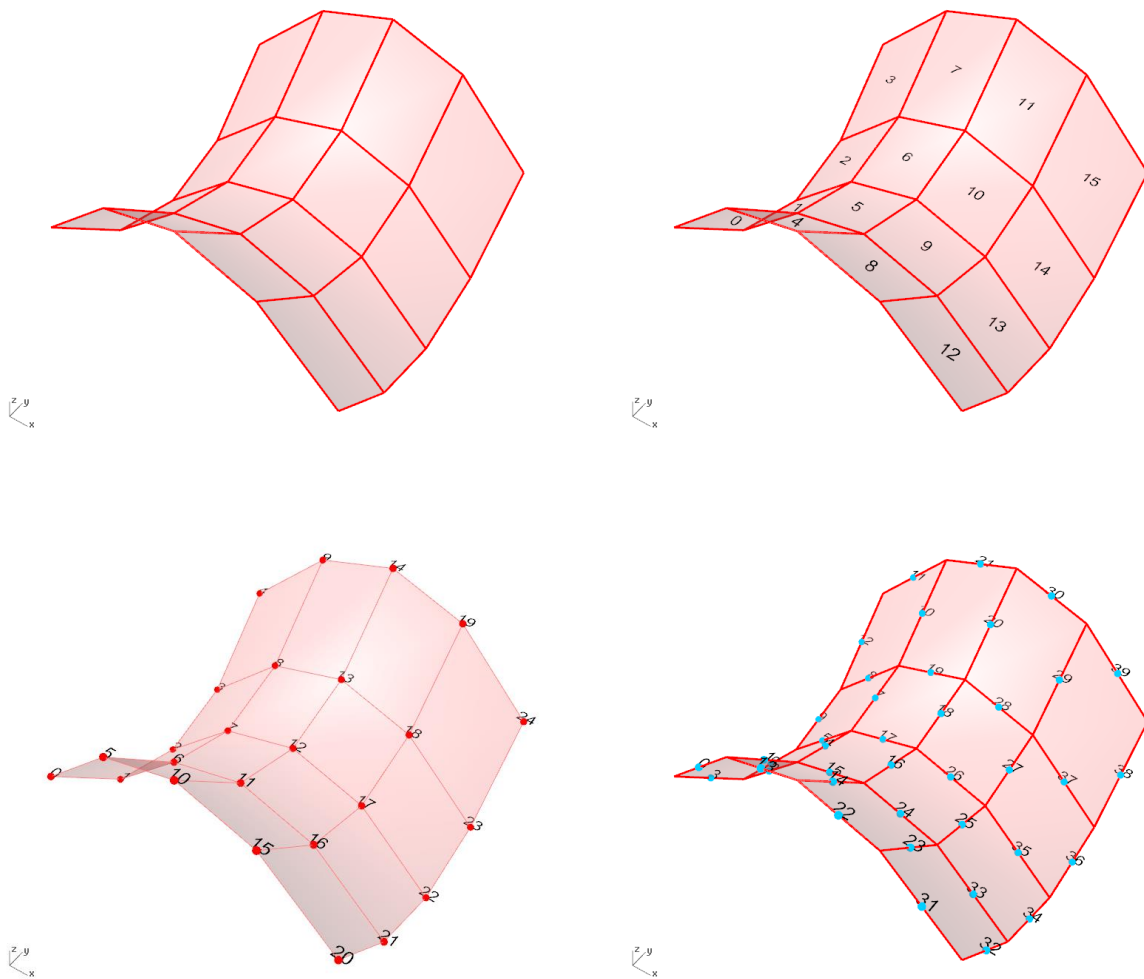


Figure 29_ Numbering mesh faces, mesh vertices and generating mesh half-edge data.

Step_3: The mesh data is used to generate the reciprocal modules. A homogeneous dilation is required for the generation of the modules on the designed surface. The homogeneous dilation is a homothetic transformation of an affine space determined by a center point and a nonzero scale factor (Pottmann et al., 2007). In this study, the transformation for each cell is determined by its centroid using a user-defined scale factor. This scale factor controls the engagement length in reciprocal modules (Figure 30).

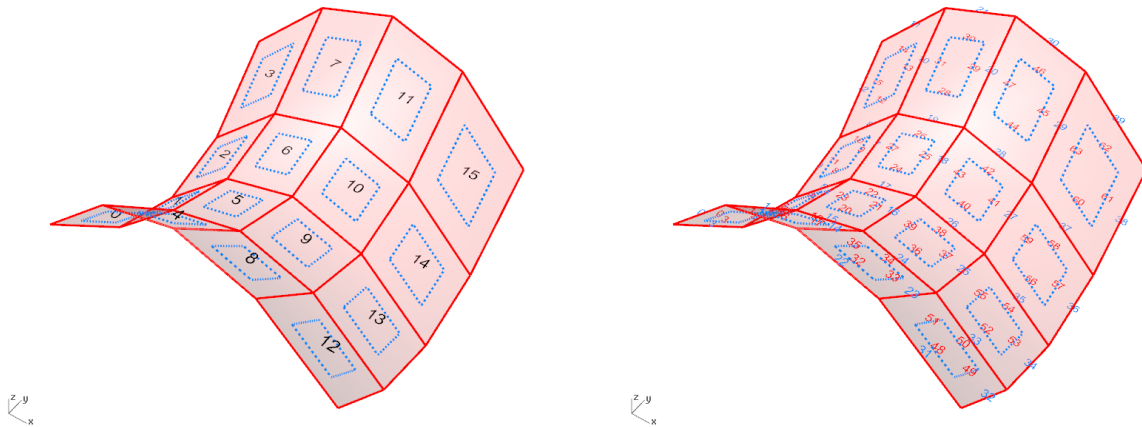


Figure 30_ Application of homogeneous dilation and generation of scaled quadrilateral cells.

Step_4: The homogeneous dilation transforms the initial quadrilateral cell $ABCD$ to a scaled quadrilateral cell $A'B'C'D'$. The reciprocal modules are generated based on the scaled cells. To generate the reciprocal patterns the mid-points of the edges of the quadrilateral cells $ABCD$ and $A'B'C'D'$ are connected following a rotational order. $MP_1, MP_2, MP_3,$ and MP_4 are the midpoints of the edges of the original (unscaled) quadrilateral cell $ABCD$ while $MP_1', MP_2', MP_3',$ and MP_4' are the midpoints of the edges of the scaled quadrilateral cell $A'B'C'D'$. Midpoints are connected following a rotational order as: MP_1 to MP_4', MP_2 to MP_1', MP_3 to $MP_2',$ and MP_4 to MP_3' .

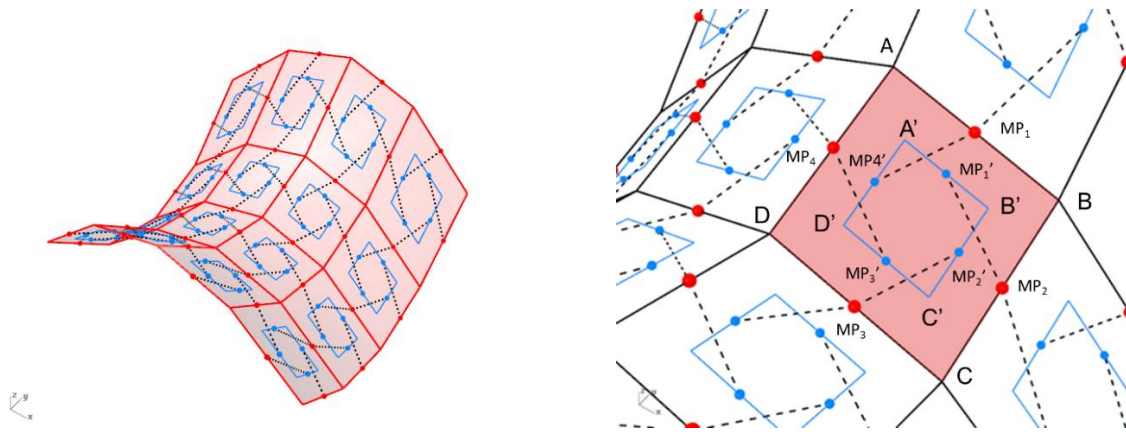


Figure 31_ Generating reciprocal patterns on each cell based on the scaled cells. Notations of the geometric entities on a cell.

To complete the reciprocal module intersections are found between the four elements (1).

$$(MP_i MP'_{i+1}) \cap (MP_{i+1} MP'_{i+2}) = N_{i+1} \quad (1)$$

The geometry of the reciprocal module on each cell is composed of line segments connecting $MP_i N_{i+1}$, $MP_{i+1} N_{i+2}$, $MP_{i+2} N_{i+3}$, and $MP_{i+3} N_{i+4}$ (Figure 32).

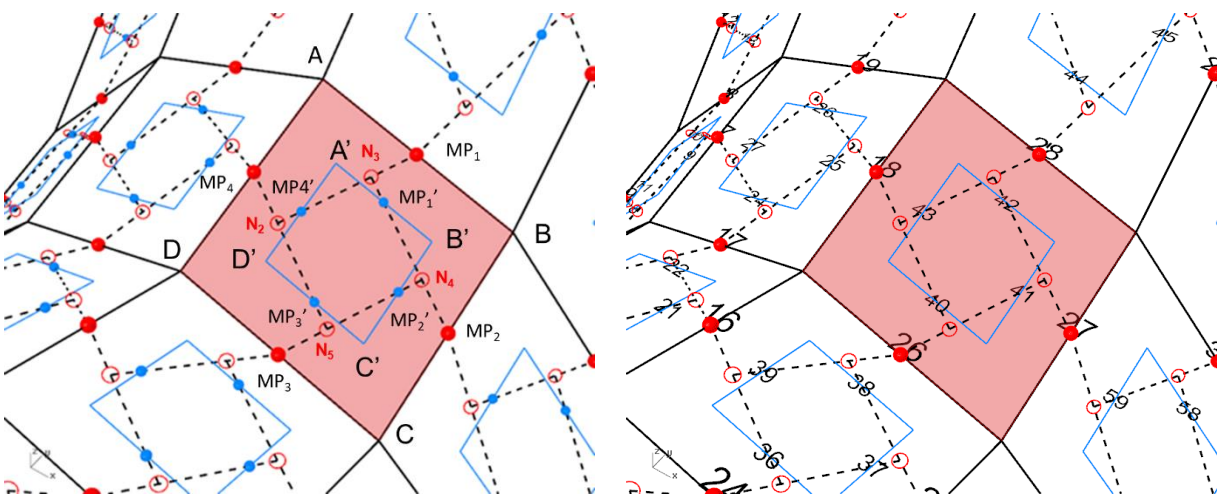


Figure 32_ Intersections between the four elements are found and used to generate the segmented reciprocal modules. Left: notations of the geometric entities on a cell, right: numbering of the intersection points after pattern generation.

Step 5: This process results in a set of independent modules with each module being in the pseudo-plane defined by its corresponding quadrilateral cell. However, to obtain a continuous network of reciprocal modules (Figure 33), continuous reciprocal members need to be generated between the neighboring cells which creates an interconnected network of reciprocal modules throughout the predefined surface. This process induces eccentricities between the intersecting reciprocal members. Eccentricities are induced connecting the intersection points N_i between the elements i of a module j with the intersection points of its adjacent cell. For instance, if $N_{i,j}$ is the i^{th} element of the j^{th} cell: $N_{i,j}$ will be connected to points $N_{i,j \neq i}$ (Figure 33 and Figure 34). As a result, the elements in a module no longer intersect as they now lay on different planes.

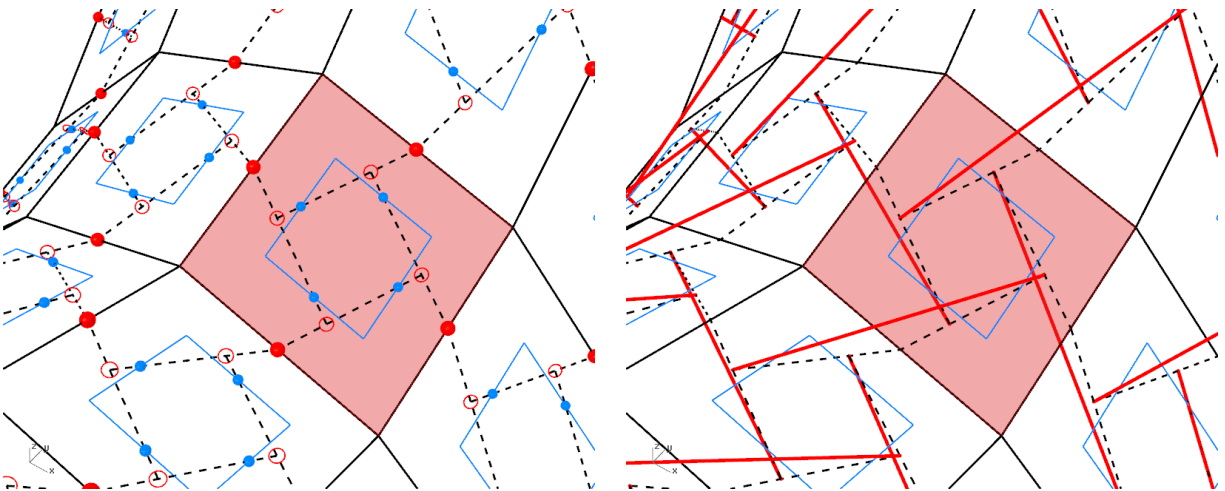


Figure 33_ Left: independent modules on the pseudo-plane of cells, right: continuous network of interconnected reciprocal members with eccentricities.

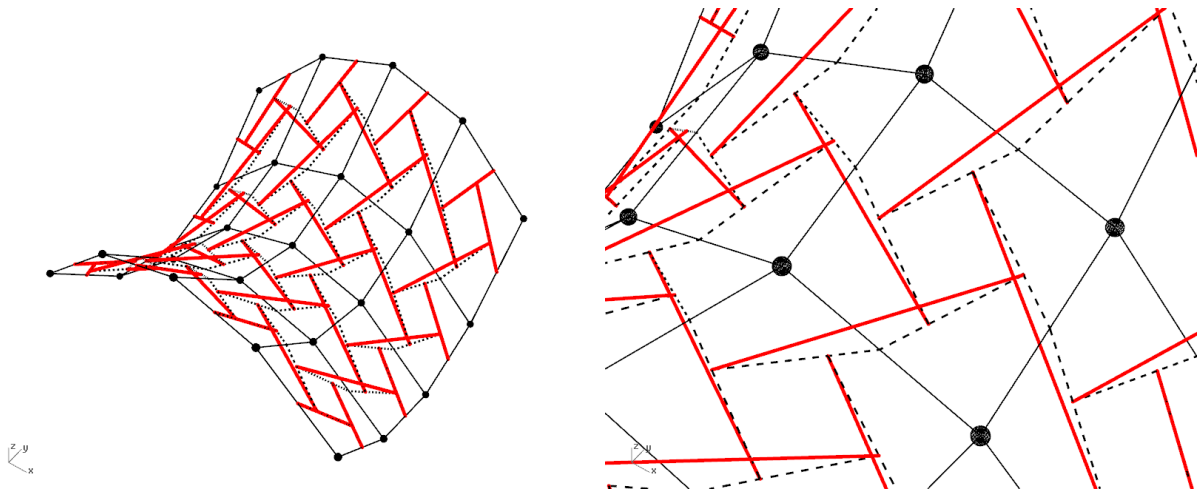


Figure 34_Generation of continuous network of reciprocal modules on the predefined surface and introduction of eccentricities between the elements.

Figure 34 shows the calculation and distribution of the eccentricities on the doubly curved surface. Eccentricities are calculated as the shortest distance between the intersecting reciprocal members. The eccentricities are visualized numerically at the member to member connection point (Figure 35).

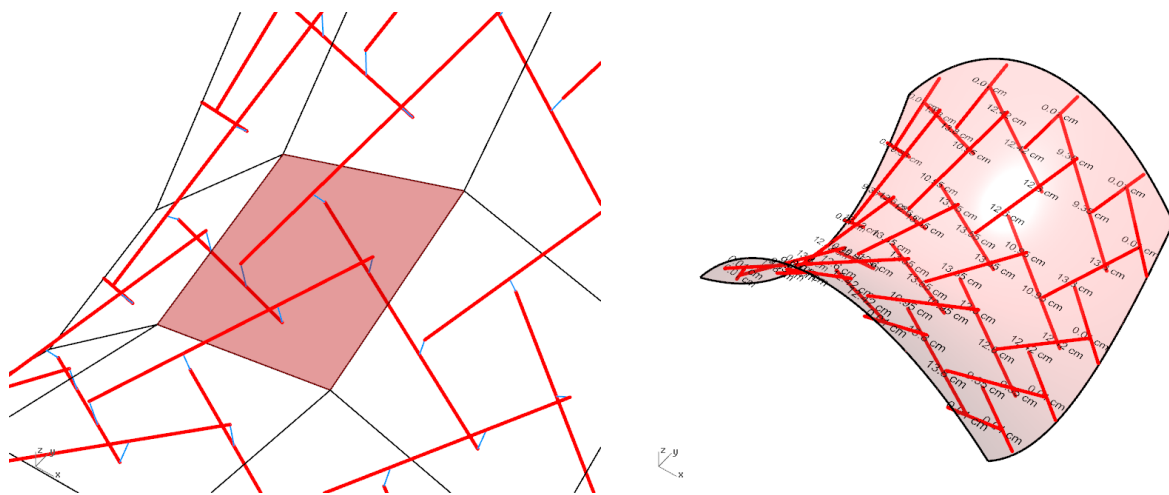


Figure 35_ Calculation of member eccentricities in the reciprocal system.

Using false color visualization, we can see how surface curvature effects the eccentricities between the intersecting reciprocal members. Figure 36 show the Gaussian curvature of the doubly curved surface at any point on the surface with false color visualization. Figure 36 also shows the false color visualization of eccentricities with spheres where the size and color of the sphere shows the normalized size of the eccentricity at any connection point.

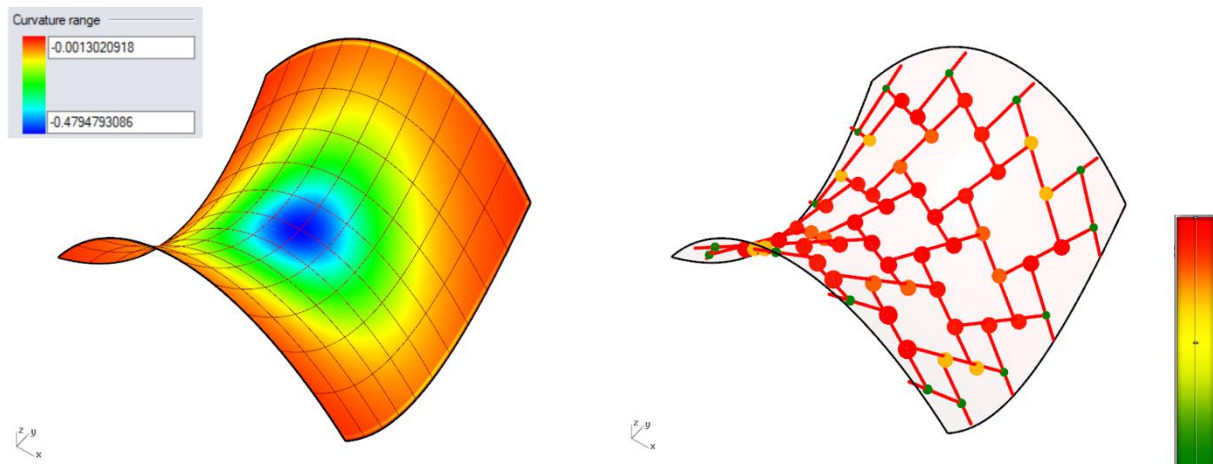


Figure 36_ Left: False color visualization of Gaussian surface curvature. Right: False color visualization of the eccentricities size and distribution.

Figure 36 shows direct relation between eccentricities and surface curvature. As the surface curvature increases towards the center of the surface member eccentricities increase accordingly. This behavior has a geometric explanation, as through the process of approximation of the surface by quadrilateral meshes, the angle between the neighboring mesh faces increases with increase in curvature. Bigger angles between the neighboring mesh faces (cells) cause bigger eccentricities as reciprocal modules are generated between the neighboring cells (Figure 37).

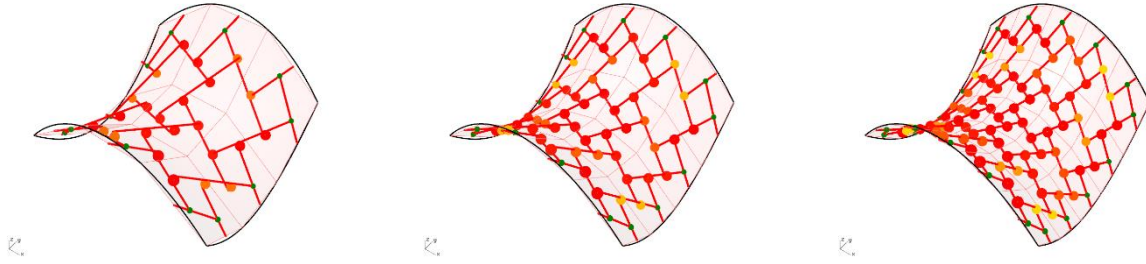


Figure 37_ Refining the mesh density and distribution of eccentricities on the doubly curve surface.

The form-finding process will address the eccentricities between the reciprocal members based on fabrication constraints.

3.6 Review of form-finding methods for reciprocal systems

To investigate the family of structures that can be built with so many geometrical constraints, different form-finding methods were developed. These form-finding methods usually operate on constraint-based models which define the geometric constraints in the reciprocal system.

Depending on the type of mathematical formulation of the reciprocal constraints, these form-finding methods usually employ optimization methods to find the optimal condition of constraints within the system. In the case of reciprocal systems with 2-D and 3-D members the constraints are eccentricities between the intersecting members and the optimal condition is a system with the minimum eccentricities.

Baverel et al. proposed a numerical method based on a genetic algorithm, (Baverel et al., 2007, Baverel, 2000, Mesnil et al., 2018). Douthe et al. proposed an adaptation of dynamic relaxation method and a fictitious dynamic behavior to define the suitable geometrical parameters and also investigated some potentials of this method for double layer systems (Douthe and Baverel, 2014). Parigi and Kirkegaard also implemented a similar interactive form-finding method for

design and form-finding of reciprocal systems with 1-D elements (Parigi and Kieckergard, 2014). A similar method is now implemented in some physics-based modelling tools for modelling and simulation of dynamic constrained systems (Senatore and Piker, 2015).

Some research has been carried out on the development of analytical solutions for the form-finding problem of reciprocal structures. Senechal et al. studied the transformation of regular polyhedra by the rotation method and solved the resulting system of constraints analytically (Sénéchal et al., 2011). Alternatively, Baverel studied the transformation of regular polyhedra by the translation method (Figure 38) (Baverel and Nooshin, 2007).



Figure 38_ Reciprocal polyhedra generated by expanding the vertices. Variation in a dodeca-icosahedron for rotation angles 5, 10, and 20 degrees (Sénéchal et al., 2011).

Finally, in their research, Song et al. used conformal mapping for geometry generation and used iterative least-square optimization for minimization of eccentricities in the reciprocal structure with 1-D members (Figure 39) (Song et al., 2013, Mellado et al., 2015).

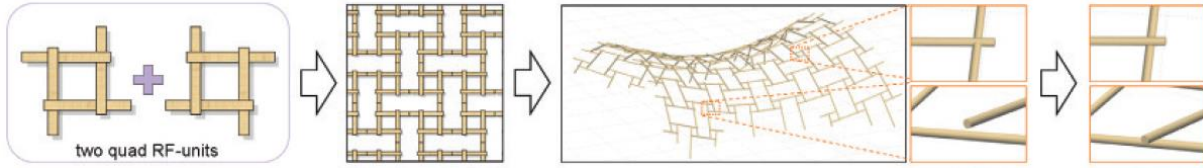


Figure 39_ mapping a 2-D pattern to 3-D space and least-square optimization for 1-D members. (Song et al., 2013).

Each of these methods has specific benefits in terms of accuracy and speed, ease of implementation and application. However, for design purposes, a fast and interactive system can provide better feedback during the design process. In this regard, the dynamic relaxation method can provide an interactive feedback from the form-finding process numerically and visually. Moreover, different constraints can be implemented as geometrical constraints in the form-finding process to address specific behavior between the reciprocal members. Importantly, knowing that numerical methods like dynamic relaxation can only converge to a local minimum, is important in the formulation of the problem so that the residual eccentricities after the form-finding process can be addressed both in analytical model developed for the analysis and also in the fabrication models for digital fabrication.

3.7 Proposed method for form-finding of reciprocal systems

3.7.1 Methodology

The proposed process of reciprocal pattern generation results in a continuous network of reciprocal modules that approximate the design geometry based on the density of the underlying mesh. The finer the initial mesh the closer the reciprocal network to the design geometry. However, it is important to take into account that the process of pattern generation on free-form geometries induces varying amounts of eccentricities between the intersecting reciprocal members in the modules. These eccentricities need to be addressed in order to create analytical

models for analysis or fabrication models for digital fabrication. In the case of reciprocal systems with 1-D elements where the elements have the same circular cross-sections, eccentricities should be equal to the diameter of the circular cross-section and the connection is fabricated with ties or clamps. In the case of reciprocal systems with 2-D and 3-D members the optimal condition is a reciprocal system with the minimum eccentricities between the intersecting members so that the connection detailing can be appropriately defined as T-joints , notched connections or custom 3-D connections (Figure 40). The connection constraints are the main factors in the definition of the constraint-based model in the form-finding process of reciprocal systems.



Figure 40_ Fabrication of reciprocal connections. From the left: clamped connection, notched connection, T-joint connection.

In this section we describe the form-finding process for reciprocal systems. The form-finding process is defined through a constraint-based model. As was explained in Chapter 2, constraint-based modeling refers to modelling approaches which directly integrate the design constraints in the design process, leading to a bottom-up generation of form based on the generative rules and design constraints (Deuss, 2015). The power of constraint-based modelling depends on the mathematical definition of design constraints and the efficiency and efficacy of the constraint resolution process. In our research we use dynamic relaxation as the constraint resolution method in the form-finding process. This method is a generalized formulation for calculation of

equilibrium using the dynamic relaxation formulation developed by Piker (Senatore and Piker, 2015).

In this process eccentricity is considered as the objective function of the constraint resolution process (form-finding), and is therefore not treated as a hard constraint, but rather as a soft constraint. This means that these constraints will be resolved to the desired tolerance and not necessarily resolved completely. This is contrary to the point of view of Baverel and Nooshin who considered that eccentricity was a technological constraint (Baverel et al., 2004). Also, this is different from the point of view of (Mesnil et al., 2018) who defined the form-finding process to optimize the engagement length of members towards a constant length for all reciprocal modules. In the proposed method the target is to limit the eccentricities within the constructible fabrication tolerances (material dimensional tolerances and digital fabrication tolerances).

The residual eccentricities are addressed within the detailing and fabrication strategy so that they are accommodated along with the fabrication tolerances of the digital fabrication machinery.

This process requires determination of the type of connections and assembly process as well as fabrication method prior to the form-finding process. This means that residual eccentricities need to be targeted to be consistent with the digital fabrication tolerances. In another way, this fabrication-aware method does not eliminate the fabrication tolerances but rather accommodates them within an acceptable margin in the process of fabrication. This method offers a more flexible design to fabrication process where the form-finding process can accommodate different scenarios based on the requirements of different reciprocal connection design. Moreover, this method provides controllable margins of error which can be accommodated along with the tolerances of the digital fabrication machinery.

The mathematical formulation of the constrain-based model is defined using four main geometrical constraints. The dynamic relaxation method is used to iteratively and simultaneously reduce the eccentricities throughout the structure to keep them within the acceptable margins. The results show that dynamic relaxation is an effective method for the form-finding process and can minimize the eccentricities within the system in a real-time fashion. Moreover, the dynamic process of form-finding can be visualized which can provide better understanding of the form-finding process for design purposes.

In the following section the formulation of the constraint-based model is defined and the application of the dynamic relaxation method for constraint resolution is explained.

Subsequently, this method is used for design and form-finding of a doubly curved reciprocal system, and the convergence and efficiency of the method is studied quantitatively.

3.7.2 Constraint-based modelling formulation

As has been explained in section 3.5, the proposed process of reciprocal pattern generation results in a continuous and nonhierarchical network of interlocking lines which do not necessarily intersect in the design of free-form geometries. Each line in the network is considered as a centerline of an element. Eccentricities are defined as the shortest distance between the pairs of centerlines. The constraint-based model is defined base on the eccentricities and other behavioral constraints and then a dynamic method is used to iteratively and simultaneously reduce the eccentricities throughout the structure to keep them below the fabrication tolerances and also to generate the final geometrical configuration of the reciprocal systems.

The constraint-based model is defined base using four main constraints as follows:

1_ Each eccentricity constraint is defined by a pair of intersecting reciprocal members (Figure 41).

2_ To maintain the size of the reciprocal members we define them as springs with rest length equal to their original length.

3_ To accommodate free movement for each reciprocal member during the form-finding process, all the members are considered rigid bodies which have translational and rotational movements under the application of the form-finding loads.

4_ Boundary conditions are defined by clamping certain reciprocal member's end nodes which will not move during the form-finding process. These boundary conditions define the space in which the reciprocal members will find their final configuration in the reciprocal structure.

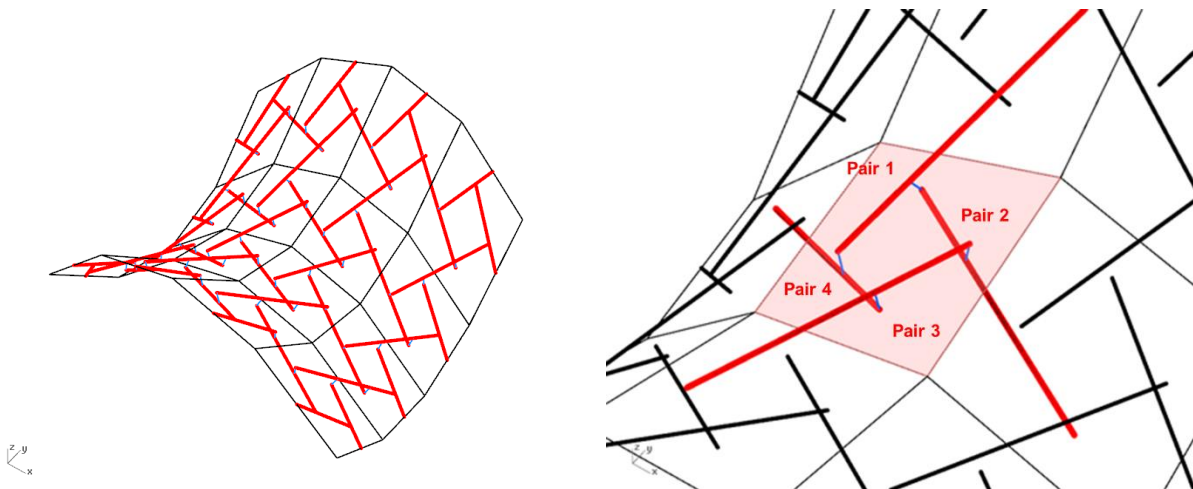


Figure 41_ Pair assignment in a reciprocal module. Each module will have four pairing constraints.

3.7.3 The dynamic relaxation method for constraint resolution

Dynamic relaxation is based on the discretization of the continuum into a set of concentrated masses (called particles or nodes) linked by elements (which can be one, two or three dimensional). Dynamic relaxation uses the concept of forces applied to particles for approximating the physical behavior of rigid and non-rigid objects and defines how forces propagate through the system and how the stability is reached through reconfiguration of the nodes and elements. Just as in traditional Finite Element Methods (FEM), the use of a local element stiffness matrix is retained. However, unlike FEM routines forces, and inertia are appropriately lumped at nodes following the dynamic relaxation method. Information regarding position, velocity and acceleration of each node is computed iteratively. A semi-implicit time integration scheme updates linear and angular momentum, and subsequently the local coordinate frames of the nodes. The main idea is to “follow” the movements of the nodes caused by the out of balance forces (Senatore and Piker, 2015). With the capability of application of different force systems including gravity (constant forces), different force fields (position or time dependent force systems), drag and damping (velocity dependent forces) and the most common form, spring forces (stiffness and elasticity based forces), this method has significant flexibility to simulate the interactions between the components of modular systems in the form-finding process. These interactions can be defined as geometrical constraints in the mathematical model, which is then resolved iteratively using dynamic relaxation method. Constraint-based modelling helps us to define new logics between the system components in the form of design and fabrication constraints and control the behavior of the modular system to respond to a specific design or fabrication requirements. Moreover, due to the dynamic nature of the method, the updates in the system configuration can be visualized at each step of the simulation. This provides the designer

with deeper insight about the form-finding process and also simplifies the debugging of the system definition should there be a fault in the constraints definition.

For some optimization and analysis purposes it is only the final equilibrium result which is desired, and the intermediate steps are not needed to be visualize. In these cases, the damping and mass coefficients may be chosen purely for the sake of convergence. A kinetic damping scheme (Barnes, 1999) may also be used, which zeros the velocities whenever kinetic energy peaks are reached, achieving faster convergence. However, if appropriate damping and mass values are set, the same system can also be used to model realistic dynamics (Ambrósio and Neto, 2013). In our work, the fast convergence to the final equilibrium stage is important when we work with fabrication processes or optimization of reciprocal systems as the final solution for the geometry is the preliminary step in the development of analytical model for performance evaluation or generation of the fabrication data for fabrication purposes. Both of these capabilities are implemented in the formulation developed by (Senatore and Piker, 2015).

Generally, dynamic relaxation is a nonlinear method which can converge to a local minima but does not systematically converge to the global minimum. In the case of reciprocal systems this means there will be residual eccentricities between the members in the system after the form-finding process which is an important factor in development of analytical models for structural analysis and also for development of fabrication models for digital fabrication.

3.7.4 Numerical formulation of dynamic relaxation method

In this section, we will discuss the dynamic relaxation scheme adopted for calculating a particle's positions in space in the state of equilibrium. One particle is defined as an object with its own data structure mainly consisting of a fictitious scalar mass M and a set of 3-D vectors representing position δ , velocity v and acceleration a . The motion of any particle i at time t is governed by Newton's second law of motion (Suzuki and Knippers, 2017).

In this section the formulation for the dynamic relaxation method proposed by Piker is explained (Senatore and Piker, 2015). For the discretized system the equation of motion can be written as (2).

$$M_{ij}a_{ij}^t + Cv_{ij}^t + K_{ij}\delta_{ij}^t = P_{ij} \quad (2)$$

$$j = (x, y, z); \quad v = \dot{\delta}; \quad a = \ddot{a}$$

defining the force residuals as out of balance forces F_{ij}^t resulting from the difference between the internal forces $K_{ij}\delta_{ij}^t$ and the external applied load vector P_{ij} , Equation (3) can be rewritten as:

$$F_{ij}^t = M_{ij}a_{ij}^t + Cv_{ij}^t \quad (3)$$

Using Newton's 2nd law and a simple modification of the forward Euler integration scheme, it is possible to obtain a simple 1st order accurate integration scheme called semi-implicit or symplectic Euler (Equation (4)).

$$v_{ij}^{t+\Delta t} = v_{ij}^t + \Delta t \frac{F_{ij}^t}{M_i} \quad (4)$$

$$r_{ij}^{t+\Delta t} = r_{ij}^t + \Delta t v_{ij}^{t+\Delta t}$$

Where Δt is the time step and r_{ij}^t is the j^{th} coordinate position of the i^{th} node. The integration scheme is semi-implicit because it uses the forward Euler to compute the velocity but the backward Euler to obtain the position using the velocity at $t + \Delta t$ (Senatore and Piker, 2015). The equilibrium of forces is achieved in an iterative fashion as the nodes oscillate around the minimum kinetic energy configuration and eventually settles when the out of balance forces become very small. Using the four-step formulation for a constraint-based model (explained in part 7 of this section), the proposed form-finding process for reciprocal structures is used for design and the form-finding of a doubly curved reciprocal system. Additionally, the convergence and efficiency of the method is studied quantitatively. Figure 42 shows the reciprocal pattern generation on a four by four mesh discretization of the doubly curve surface. Figure 42 also shows the constrained model containing, pairs of reciprocals defining eccentricities, rigid body reciprocal members and boundary conditions defined by the boundary nodes.

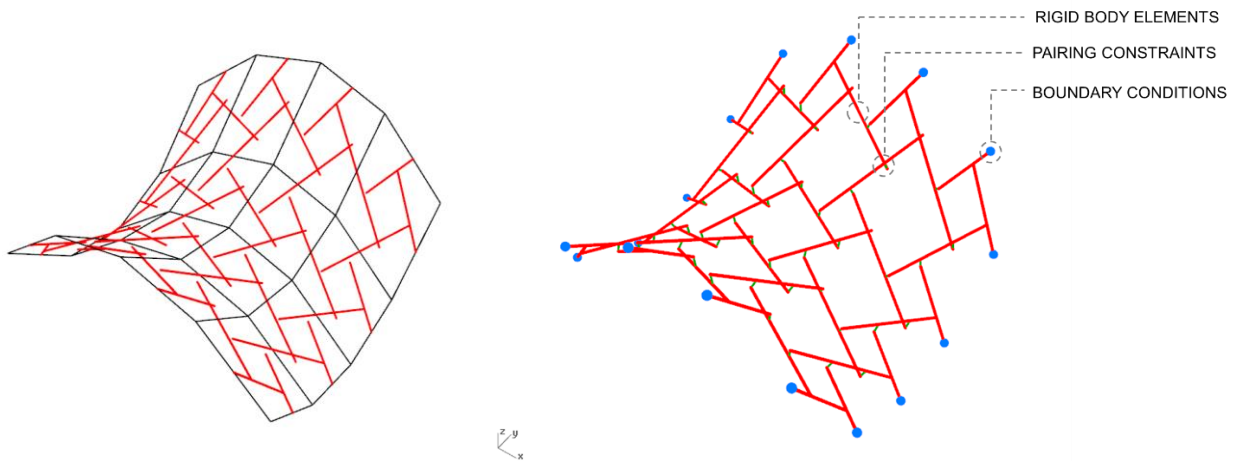


Figure 42_ Figure a: Reciprocal pattern generation. Figure b: Definition of the constrained model, boundary conditions, member pairings and rigid body definition.

The form-finding process minimizes the member to member eccentricities iteratively and simultaneously. During the form-finding process reciprocal members move and slide on each other as rigid bodies to minimize the eccentricity constraints. This freedom of movement will allow the interconnected network of reciprocal members to reconfigure into a new reciprocal configuration with the same topology but with minimum eccentricities. Consequently, through this process, as the members slide on each other the location of member to member connections will change. Although, the size of the members will stay intact (due to the member size constraint) but the process does not guarantee for the member ends to intersect at their extremes anymore. These members will be cut at their intersection at both ends and the hanging part will be eliminated to develop analytical models for analysis and fabrication models for digital fabrication.

This form-finding process is significantly efficient and can be used in real-time. Figure 43 shows the reciprocal eccentricities before and after the form-finding process.

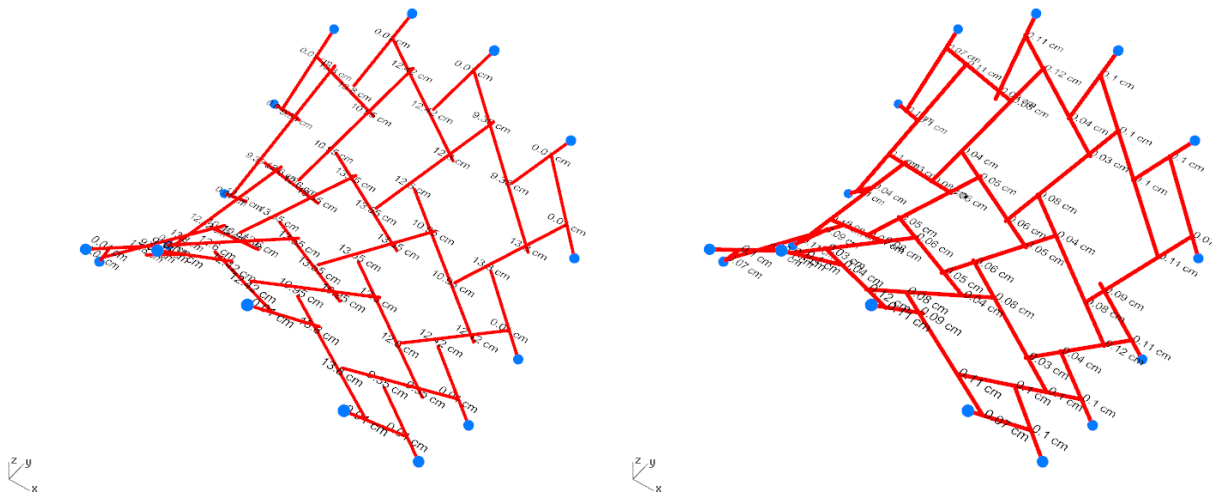


Figure 43_ Member to member eccentricities in reciprocal systems before (on the left) and after (on the right) the form-finding process.

3.8 Quantitative study of the results for the proposed form-finding method

The process of minimization of the reciprocal eccentricities is shown in the graphs below.

Maximum reciprocal eccentricity and average reciprocal eccentricity are used as the measures to study the process. The graphs show fast convergence of the system under 50 iterations (Figure 44).

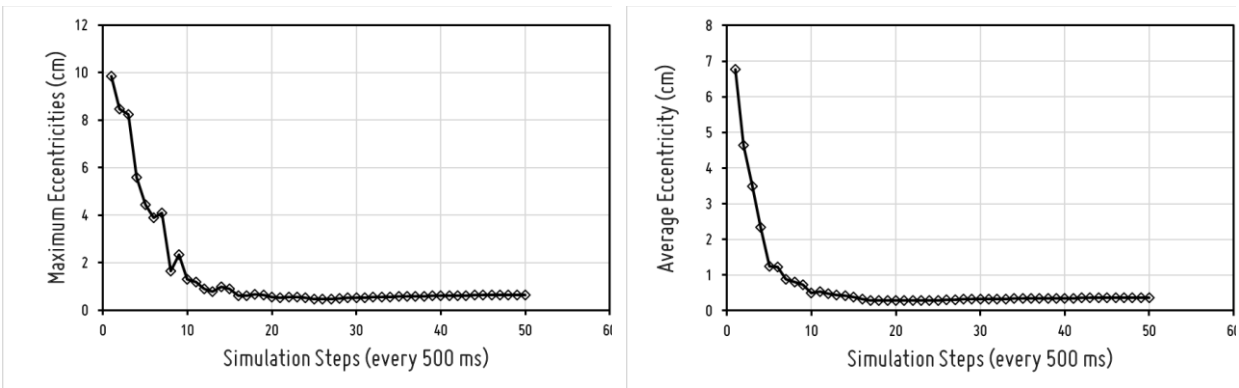


Figure 44_ Variation in eccentricities during the form-finding process in a four by four reciprocal grid. Left: minimization of the maximum eccentricity. Right: minimization of the average eccentricity.

The graph below shows an overlay of maximum and average eccentricities during the form finding process (Figure 45).

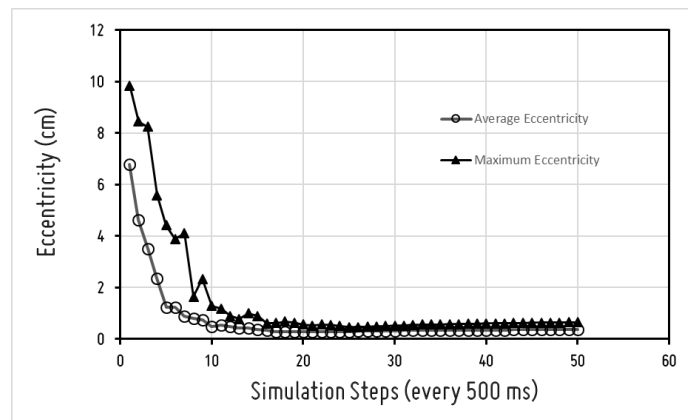
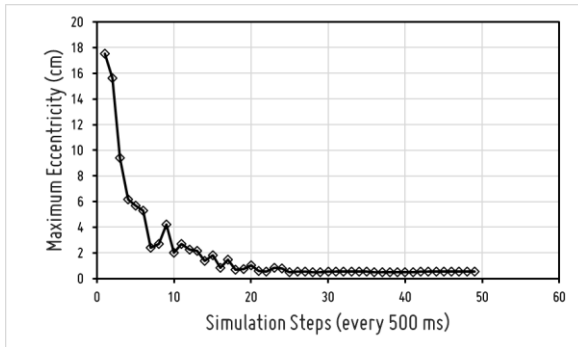
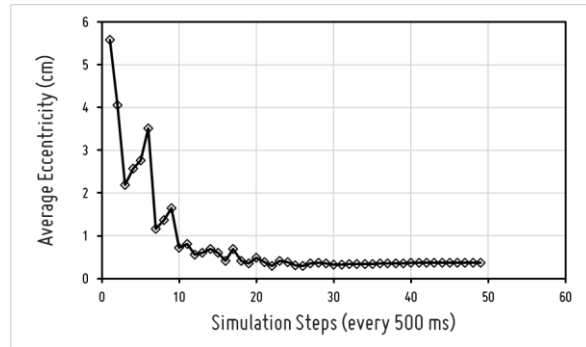


Figure 45_ The overlay of maximum and average eccentricities.

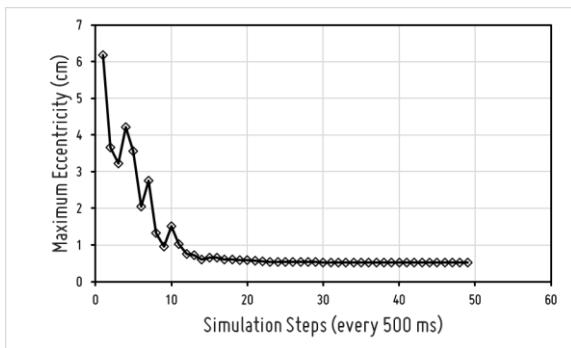
In this section we study the effect of mesh density on the form-finding process. The number of reciprocal modules increase with refinement of mesh density as each reciprocal module introduces four eccentricity constraints to the model. Figure 46 shows the results for the form-finding process with two different mesh densities of 3 by 3, and 5 by 5 grids.



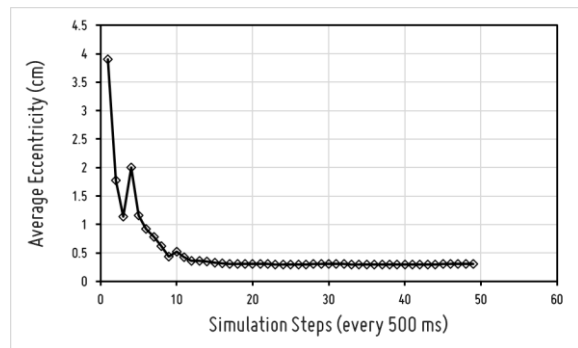
3X3 grid



3X3 grid



5X5 grid



5X5 grid

Figure 46_ Figure 27_ Variation in eccentricities during the form-finding process for different grid densities. Top: Minimization of maximum and average eccentricity in a three by three grid. Bottom: Minimization of maximum and average eccentricity in a five by five.

Figure 47 and Figure 48 show the results of the form-finding process for different grid densities in one graph. As depicted in Figure 47 the maximum eccentricity is higher in the lower mesh density. This is due to the rough approximation of the geometry by a course mesh which lead to

reciprocal patterns with bigger eccentricities. Moreover, there are more fluctuations in the maximum eccentricity of the system in the coarse mesh discretization which is due to the bigger movements of reciprocal members during the form-fining process in a coarse grid. However, all the three systems converge under 30 iterations with the proposed method.

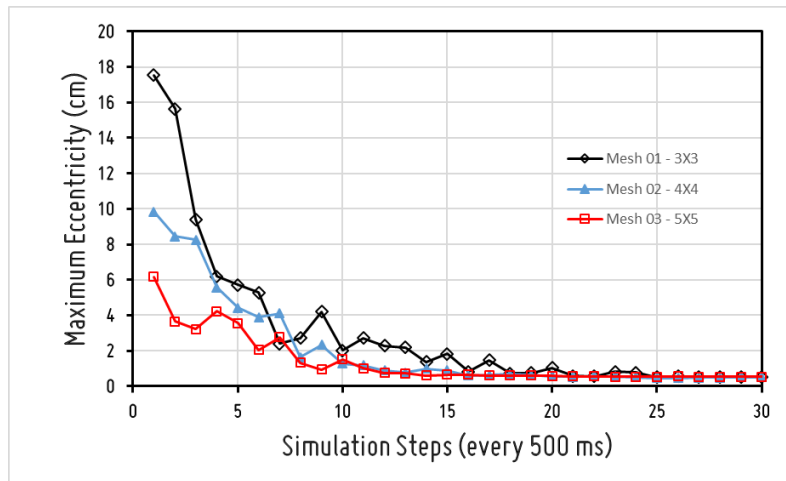


Figure 47_ Variation in maximum eccentricities during the form-finding process for different grid densities.

Figure 48 shows the average eccentricities in the form-finding process. The main difference between Figure 47 and Figure 48 is that the average eccentricities are not necessarily lower in grids with higher mesh density. As shown in Figure 48 the average eccentricity is higher in a four by four mesh density in comparison to three by three grid system. However, the convergence patterns are similar to the convergence patterns of maximum eccentricity graphs in Figure 47. The numerical study of the form-fining process shows the effectiveness and the speed of the convergence of the proposed form-finding method for reciprocal systems (convergence under 15 seconds).

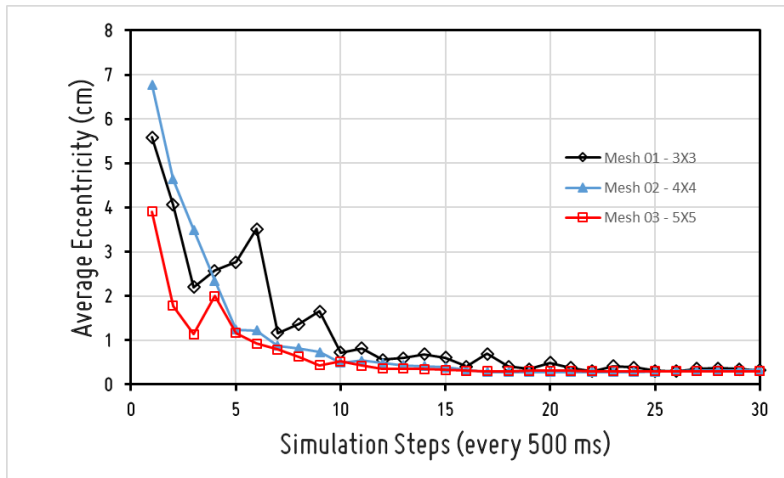


Figure 48_ Variation in average eccentricities during the form-finding process for different grid densities.

The goal of the form-finding process is to define the local and global geometry of the system. After all the results of the proposed pattern generation and form-finding process manifest themselves in an interlocking network of members that approximate the designed surface geometry. However, the goal of form-finding is not to best approximate the designed surface geometry, as it is often the case with paneling systems for surface rationalization. In the proposed method the goal of pattern generation formulation is to generate the nonhierarchical interlocking network of reciprocal modules, and the goal of form-finding is to resolve the configuration of these members based on the member to member fabrication constraints. As a result the global geometry may diverge from the designed surface geometry in the form-finding process based on the constraints that control the interactions between the reciprocal members, as shown in Figure 49. In a bottom up process of form-finding the local interactions between the system components propagate through the system which generates the final global geometry. The distance of the reciprocal member center points from the surface geometry is used to

visualize the divergence of the reciprocal system from the designed geometry as shown in the Figure 49.

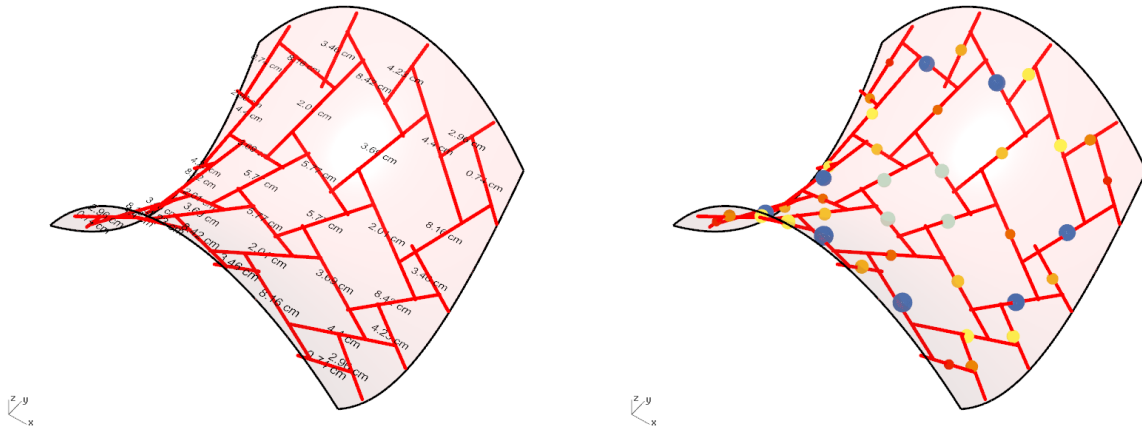


Figure 49_ Distribution of the divergence of the reciprocal system from the designed geometry after the form-finding process.

In this section we study the effect of form-finding on the distribution of eccentricities as well as divergence from the designed surface geometry in a doubly curved surface.

Figure 50 shows the distribution of eccentricities before and after the form-finding process. In the previous section we discussed how eccentricities increase with the increase in the curvature of the surface geometry. As shown in Figure 50 as Gaussian curvature of the surface increases towards the center of the surface, member eccentricities increase accordingly. However, as shown in Figure 50, after the form-finding process the distribution of eccentricities reverses. The form-finding process produces members in the center of the surface that are the ones with minimum eccentricities. This observation shows how the process of form-finding changes the configuration of the reciprocal structure to respond to the form-finding goal. The reason that members in the center of the structure reach the minimum eccentricity in the process of form-

finding is due to the higher degree of freedom they have in the constrained model which is controlled by the definition of the boundary conditions for the system (Figure 42 and Figure 50). Since the boundary conditions restrict the reciprocal member's end points from moving in the boundary of the reciprocal structure, these members have less freedom to move and resolve the eccentricities. However, the farther the members get from the boundary the system becomes more flexible and the members can move and slide on each other more freely to minimize the eccentricity between the reciprocal pairs.

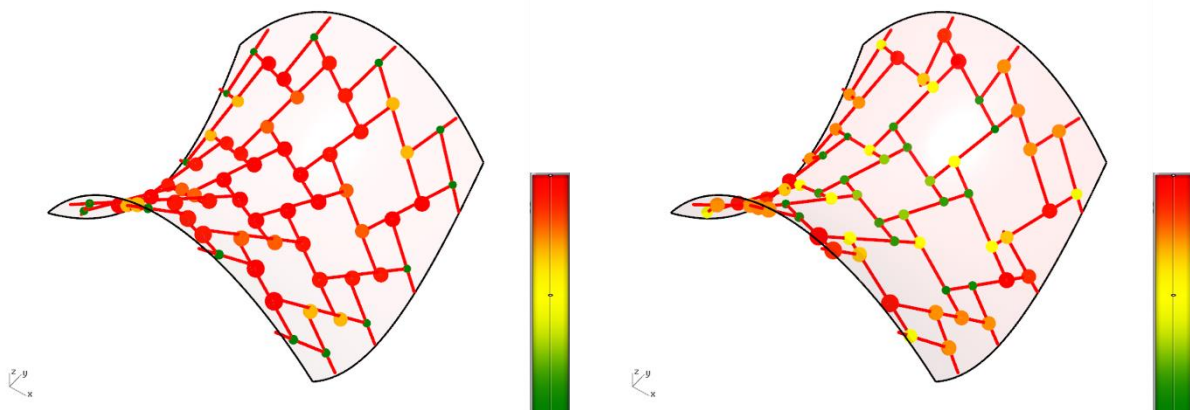


Figure 50_ Comparison of distribution of eccentricities before (on the left) and after (on the right) the form-finding process.

These results show the nonlinear nature of form-finding process with so many design constraints.

Despite the fact that the form-finding result is guided by a constraint definition, prediction of the final state for all of the constraints is difficult. This shows the importance and necessity of the development and application of interactive form-finding methods.

Understanding the size and distribution of eccentricities is crucial in fabrication of reciprocal members. It is important where the biggest residual eccentricities occur in the reciprocal system

to consider an appropriate measure and tolerances in the fabrication of connection detailing which informs the assembly process. Visualization of the distribution of the eccentricities is a very useful approach for an immediate assessment of the design options for fabrication. On the other hand, understanding and controlling the divergence of the reciprocal system from the designed geometry is important in assessing the acceptability of the design solution based on design aesthetics.

3.9 Conclusions

Reciprocal structures are considered as a practical way to reduce the complexity of member connections. Moreover, reciprocal systems produce efficient and low-cost modular systems for assembly. By definition, connections in reciprocal systems are two-valent, meaning that only two members meet at a connection, thereby reducing the complexity of the connection which can be designed for minimal material use and also can expedite the assembly process. However, this reduction in construction complexity is replaced with geometrical complexity due to numerous compatibility constraints which requires an effective design method which can address these complexities in the design process.

Lack of generalizability and significant limitations of the existing design methods for reciprocal systems makes these methods unsuitable for design purposes. Moreover, as these methods do not accommodate integration of fabrication requirements of these systems in the process of design, this causes a disconnection in the design-build process. In this chapter a generalizable and scalable fabrication-aware design method is proposed for design and form-finding of reciprocal systems which accommodates varying degrees of formal complexity.

The proposed design method consists of two steps, a generative modelling process and a real-time form-finding process. The modelling process uses a novel generative formulation for reciprocal pattern design which uses the quadrilateral mesh data derived from the rationalization of the design geometry to generate the reciprocal patterning on the design geometry. Also, the proposed formulation generates geometric and connectivity data to formulate the geometric and fabrication constraints based on the connection design requirements. The mathematical formulation of the constraint-based model is defined using four main design constraints. The form-finding process uses dynamic relaxation method to solve the constraint-based model, which iteratively and simultaneously minimizes the eccentricities between the members to generate the proper geometric model for analysis and fabrication of 2-D and 3-D reciprocal system. Effectiveness and efficiency of the proposed method are studied quantitatively, and visualization techniques are developed for post-processing of the form-finding results.

References

- Ambrósio, J., and M. Augusta Neto. "Dynamics of structural components subjected to large rotations using a flexible multibody approach." In *Research and Applications in Structural Engineering, Mechanics and Computation*, pp. 91-92. CRC Press, 2013.
- Anastas, Youssef, Landolf Rhode-Barbarigos, and Sigrid Adriaenssens. "Design-to-construction workflow for cell-based pattern reciprocal free-form structures." *Journal of the International Association for Shell and Spatial Structures* 57, no. 2 (2016): 159-176.
- Apolinarska, Aleksandra A. "Complex Timber Structures from Simple Elements: Computational Design of Novel Bar Structures for Robotic Fabrication and Assembly." PhD diss., ETH Zurich, 2018.
- Barnes, Michael R. "Form finding and analysis of tension structures by dynamic relaxation." *International journal of space structures* 14, no. 2 (1999): 89-104.
- Baverel, Olivier, and Hoshyar Nooshin. "Nexorades based on regular polyhedra." In *Nexus Network Journal*, pp. 281-297. Birkhäuser Basel, 2007.

- Baverel, O., H. Nooshin, Y. Kuroiwa, and G. A. R. Parke. "Nexorades." *International Journal of Space Structures* 15, no. 2 (2000): 155-159.
- Baverel, Olivier, Hoshyar Nooshin, and Yoshihiko Kuroiwa. "Configuration processing of nexorades using genetic algorithms." *Journal of the International Association for Shell and Spatial Structures* 45, no. 2 (2004): 99-108.
- Baverel, Olivier LS. "Nexorades: a family of interwoven space structures." PhD diss., University of Surrey, 2000.
- Danz, Calder. "Reciprocal Frames, Nexorades and Lamellae: An Investigation into Mutually Supporting Structural Forms." *University of Washington* (2014).
- Deuss, Mario Moacir. *Computational Methods for Fabrication-aware Modeling, Rationalization and Assembly of Architectural Structures*. No. THESIS. EPFL, 2015.
- Douthe, Cyril, and Olivier Baverel. "Design of nexorades or reciprocal frame systems with the dynamic relaxation method." *Computers & Structures* 87, no. 21-22 (2009): 1296-1307.
- Douthe, Cyril, and Olivier Baverel. "Morphological and mechanical investigation of double-layer reciprocal structures." *Nexus Network Journal* 16, no. 1 (2014): 191-206.
- Hensel, Michael, Achim Menges, and Michael Weinstock. "Techniques and Technologies in Morphogenetic Design (*Architectural Design* March April 2006 Vol. 76 No. 2)." (2006).
- Larsen, Olga Popovic. *Reciprocal frame architecture*. Routledge, 2008.
- McQuaid, Matilda, and Frei Otto. "The Japanese pavilion." *Phaedon* (2006): 60-67.
- Mellado, Nicolas, Peng Song, Xiaoqi Yan, Chi-Wing Fu, and Niloy J. Mitra. "Computational design and construction of notch-free reciprocal frame structures." In *Advances in Architectural Geometry 2014*, pp. 181-197. Springer, Cham, 2015.
- Mesnil, Romain, Cyril Douthe, Olivier Baverel, and Tristan Gobin. "Form finding of nexorades using the translations method." *Automation in Construction* 95 (2018): 142-154.
- Oliyan Torghabehi, Omid. "Reciprocal Shades: A computational workflow for knowledge-based design and fabrication of multi-performance reciprocal systems." In *Proceedings of IASS Annual Symposia*, vol. 2018, no. 11, pp. 1-8. International Association for Shell and Spatial Structures (IASS), 2018.
- Parigi, Dario, and Poul Henning Kirkegaard. "The Reciprocalizer: an agile design tool for reciprocal structures." *Nexus Network Journal* 16, no. 1 (2014): 61-68.
- Pottmann, Helmut, Andreas Asperl, Michael Hofer, Axel Kilian, and D. Bentley. *Architectural geometry*. Vol. 724. Exton, PA: Bentley Institute Press, 2007.

Roelofs, Rinus. "Three-dimensional and dynamic constructions based on Leonardo grids." *International Journal of Space Structures* 22, no. 3 (2007): 191-200.

Schlaich, Jörg, Hans Schober, and Kai Kürschner. "New trade fair in Milan—grid topology and structural behaviour of a free-formed glass-covered surface." *International Journal of Space Structures* 20, no. 1 (2005): 1-14.

Senatore, Gennaro, and Daniel Piker. "Interactive real-time physics: an intuitive approach to form-finding and structural analysis for design and education." *Computer-Aided Design* 61 (2015): 32-41.

Sénéchal, B., Cyril Douthe, and Olivier Baverel. "Analytical investigations on elementary nexorades." *International Journal of Space Structures* 26, no. 4 (2011): 313-320.

Song, Peng, Chi-Wing Fu, Prashant Goswami, Jianmin Zheng, Niloy J. Mitra, and Daniel Cohen-Or. "Reciprocal frame structures made easy." *ACM Transactions on Graphics (TOG)* 32, no. 4 (2013): 94.

Suzuki, Seiichi, and Jan Knippers. "ElasticSpace: A computational framework for interactive form-finding of textile hybrid structures through evolving topology networks." *International Journal of Parallel, Emergent and Distributed Systems* 32, no. sup1 (2017): S4-S14.

Chapter 4: Design Parameters, Simulation and Structural Behavior

This chapter is dedicated to the comprehensive study and understanding of the structural behavior of reciprocal systems. To this end, a flexible and scalable analysis method is proposed and implemented to study the effect of design parameters on the structural behavior and flexibility of the systems. Due to the geometric complexity of these systems and the inherent eccentricities between their members, the geometry cannot be directly translated to an analytical structural model. Thus, a geometric method is proposed to generate an analytical model that can be analyzed using a finite element method.

The first section of this chapter reviews different analysis methods for reciprocal systems and their limitations, then describes the proposed new analytical method. Then, a comprehensive parametric study of the reciprocal systems and quantitation of the effect of different design parameters are described. These investigations reveal multiple levels of interconnection between structural performance, constructability, and the assembly process. The ways in which these issues affect the efficiency of the reciprocal systems and introduce new potentials for design are examined and discussed. It becomes clear that the implementation of a fabrication-aware process is necessary to address these issues starting at the conceptual design phase.

4.1 Reciprocal structures as discrete systems: Introduction to analytical study of reciprocal behavior

Reciprocal structures are comprised of relatively short members that support each other in a non-hierarchical system. The simplicity of connection detailing and use of relatively short members to cover a large area are some of the construction benefits of these systems. For that matter, such systems have been used since medieval architecture.

Although, in the medieval times these systems were mainly invented and were built out of round timber due to the need for spanning distances larger than the size of available timbers, however, the contemporary examples of reciprocal systems are designed using new materials and fabrication technologies, both for inherent aesthetic features as well as the practical capacities these systems offer. Their practical features include self-supporting assemblies with simplified connection detailing, modular fabrication and assembly, inherent three dimensionality, capacity for local variation to modulate light and sound, and practical pre-rationalization for free-form design. These capacities qualify reciprocal systems as sources of ideation for innovative assembly design and performance integration in the context of contemporary architectural design.

Reciprocal systems are highly complex, as are their mechanics. There is no clear understanding of the effect of geometric parameters, such as engagement length or mesh density, on structural behavior. However, such an understanding is a necessary step for design and construction of efficient reciprocal structures.

The choice of connection detailing in these systems depends on fabrication and assembly (Mesnil and Beverel, 2018). This choice directly affects the performance and flexibility of the

structure and requires an analytical model that can account for the member connection effect. This shows how design, constructability and performance are interconnected in designing reciprocal systems and must be addressed by a fabrication-aware design process (Douthe et al., 2018).

Another issue that complicates analysis of curved reciprocal systems is the inherent eccentricities between the center line of connecting reciprocal members, as shown in Figure 51 and discussed in Chapter 3 (which described a study of such eccentricities and implemented a form-finding process to minimize them in reciprocal systems). However, even after optimization of the eccentricities, a minimal amount of eccentricity will still exist between the center lines of the reciprocal members. These discontinuities emerge in curved geometries due to the variation in curvature in relation to discretization of smooth surface with a faceted reciprocal pattern. A compatible analytical model is needed to account for these discontinuities in the structure, which affect mechanical behavior.

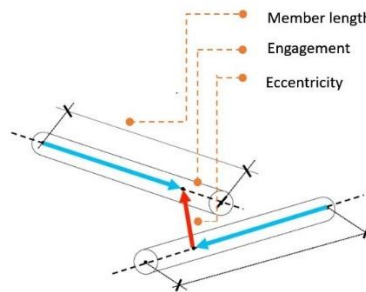


Figure 51. Eccentricities between the centerline of concurrent members in reciprocal structures.

Classic reciprocal structures (flat reciprocal systems under perpendicular loading) are made of bars and have pin-jointed member connections (friction-only connections using tied members).

In these systems, each reciprocal member acts as a simple beam, which results in a statically determinate structure. Due to the nature of the structural determinacy, the internal forces are only associated with geometrical and topological relationships within the structure, free-from material properties and member cross-section properties (Parigi et al., 2013, Zou and Xiao 2017). The same behavior can be observed in non-conventional reciprocal structures with 2-D or 3-D members (depending on the member connection detailing and type of loading). Moreover, in the geometrical analysis, reciprocal structures can be decomposed into basic units (reciprocal modules, three-membered, or four-membered fans) consisting of single bars (reciprocal members), as shown in Figure 52. In other words, three levels of composition for reciprocal structures can be identified: whole system, reciprocal module, and reciprocal member.

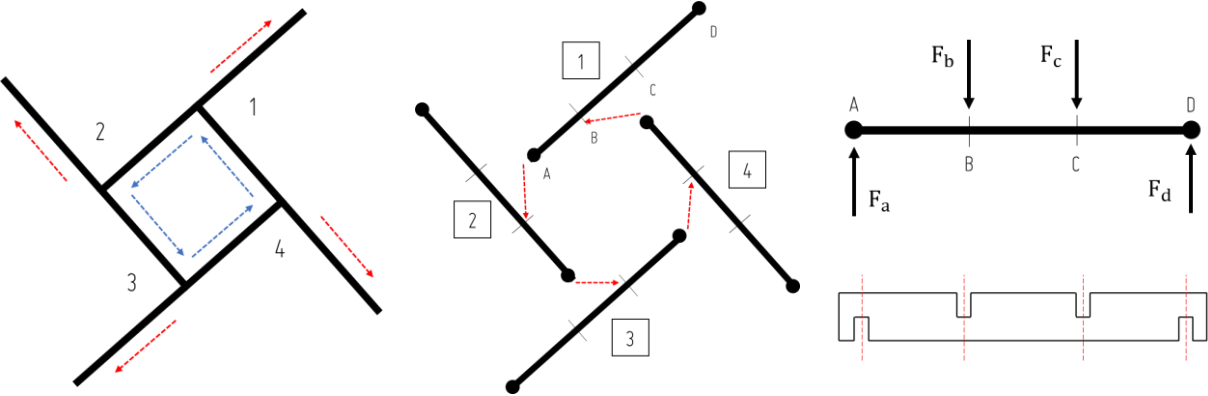


Figure 52_Decomposition of a reciprocal module. From left: load transmission within the unit, unit assembly, force diagram of reciprocal member with corresponding fabrication cuts.

When a joint load is applied at a node on the reciprocal member, the load distributes along the bar in two opposing directions, to the internal bearing and to the outer bearing that connects to the neighboring reciprocal module. The value of each portion depends on the engagement length of the reciprocal module, which defines the distances of load application on the member.

Depending on the number of participating bars in the reciprocal module (in the case of, four-member reciprocal modules) the load distributes throughout the structure in one of two ways: circulation within the unit or transmission between neighboring units, the latter spreads the load outward. The interdependency of the members in the reciprocal modules, and the interdependency of reciprocal modules with neighboring modules through the shared members, makes reciprocal systems structurally non-hierarchical (Zou and Xiao 2017).

To address these issues, two steps are required. Firstly, a flexible and scalable analysis model must be developed, one which can accommodate the effects of connection detailing, member connectivity issues, and member orientation issues. Secondly, the effect of controlling design parameters must be studied parametrically to understand the effect of these parameters and their interaction in relation to the structural behavior of reciprocal structures.

4.2 Methodology

The approach in this chapter is to use numerical and analytical methods to study and understand the structural behavior of reciprocal systems. A simplified analytical method using a finite element method is proposed for fast and interactive analysis of the reciprocal system. The proposed method is flexible and accommodates the effects of different member connectivity conditions, and is also scalable to facilitate analysis of non-planar and complex reciprocal geometries.

First, through a series of parametric studies of the reciprocal systems, controlling parameters are defined and their quantitative effects on the loadbearing capacity and flexibility of the system examined. To understand the differences between the behavior of a discrete reciprocal geometry and its continuous grid shell counterpart, the structural performance of these two systems are compared for different mesh densities. While these parametric studies show the effect of a singular parameter on the structural performance of the reciprocal systems, it does not capture the simultaneous effect of all design parameters. To address this issue, the optimal design process for a flat reciprocal system is studied through optimization of the structure using all the controlling design parameters. Toward this goal, a full 3-D finite element model of the structure is developed and optimized using a simulated annealing method.

4.3 Simulating the reciprocal behavior

To understand the structural behavior of reciprocal structures, this research will first focus on structural behavior of flat reciprocal systems and the development of a consistent simulation model. Through a parametric study of flat reciprocal structures, the governing design parameters are defined and their effect in the structural performance quantitatively analyzed.

The simulation starts with flat systems because in the flat reciprocal frames, the system can be directly defined by generation of reciprocal pattern. Since the curvature of the surface is zero the center line of concurrent reciprocal elements will have no eccentricity. In the design of free forms (any curved form) the center line of members will not coincide at the intersection and the center lines can have significant eccentricities (depending on the curvature of the surface and density of reciprocal modules), as shown in Figure 53. In that case, form-finding methods are needed to minimize the eccentricities before we develop an analytical model for simulation or fabrication model for digital fabrication.

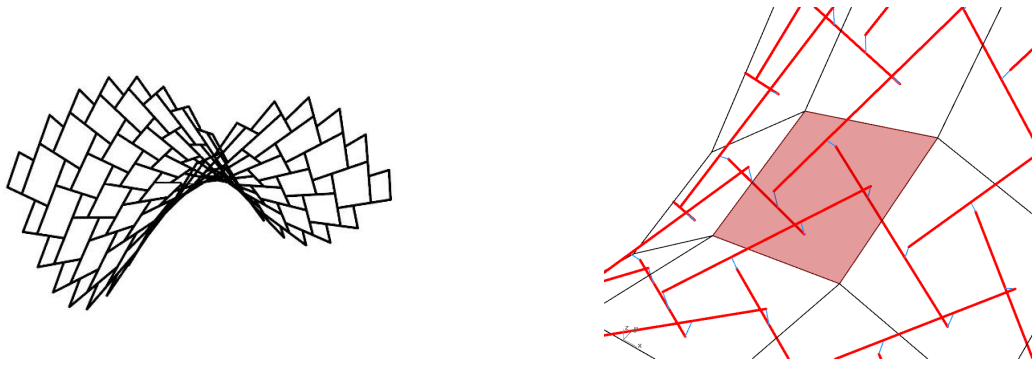


Figure 53_ Examples of a non-flat reciprocal structure and the inherent eccentricities between members.

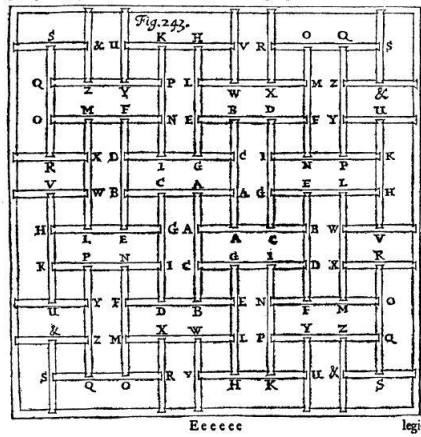
There have been multiple research studies on the mechanical behavior of these systems, and both analytical and numerical models have been developed for their analysis. A review of these methods is provided in this section.

In his 1669 *Opera Mathematica*, John Wallis (Professor of Geometry at the University of Oxford) published a method to calculate the internal forces for a planar reciprocal grillage system. The structure was an extended version of aligned axis floor system designed by Sebastiano Serlio in 1545. The brilliance of Wallis's work is that he developed the first mathematical method to calculate the internal forces of the structure induced by the self-weight of the beams. The core of his method is similar to the essential approach of the finite element method in modern structural analysis (Houlsby, 2014). In his analysis, Wallis systematically solved 25 simultaneous equations to obtain the required forces (Figure 54). However, his calculations only account for self-weight of the structure and ignore the external loading (live load), calculating the internal member forces and not structural deformations.

P R O P. X.
 Contignationem planam ex Tignis multo Brevioribus quam fit Areae
 Latitudo invicem conjunctis construere: Et computo aestimare,
 Quantum cuique juncturae Onus incumbat.

Contignationis seu Tabulati Constructio.

Potesť quidem hoc variis modis fieri. Eam vero formam prae ceteris seligendam
 putavi, quam jam olim Anno 1644. Cantabrigiae primum delineabam, in Col. Fig. 143.



Calculi Synopsis.

1	A = T + A + C.	14	O = T + M + F.
2	B = T + C + A.	15	P = T + Y + Z.
3	C = T + G + I.	16	Q = T + Z + Y.
4	D = T + I + G.	17	R = T + O + Q.
5	E = T + B + D.	18	S = T + O + Q.
6	F = T + D + B.	19	V = T + H + K.
7	G = T + E + L.	20	U = T + K + H.
8	H = T + L + E.	21	W = T + V.
9	I = T + N + P.	22	X = T + R.
10	K = T + P + N.	23	Y = T + U.
11	L = T + W + X.	24	Z = T + &.
12	M = T + X + W.	25	& = T + S.
13	N = T + F + M.		

Per Prop. 5. vel 7. hujus Cap.

Figure 54_ The extended structure by John Wallis. Wallis’s 25 simultaneous equations. Detail from Opera Mathematica.

The significance of Wallis’s work is evident, as it is possible that this analysis represents the first recorded example of a comprehensive structural analysis of a non-trivial structure (Houlsby, 2014). (Kohlhammer, 2014) proposes a similar method for systematic analysis of plane reciprocal structures. His approach is based on decomposing the reciprocal system to basic systems (modules) and decomposing the modules to elements in the process of analysis. It is an iterative process, one which analyses the supporting forces of reciprocal members based on their engagement with neighboring modules one at a time. This method converges as all the modules are observed and the effect of neighboring modules have been dissipated. Later on Zou and Xiao used Kohlhammer’s concept to develop a systematic matrix format that is generalizable and efficient to scale up for large scale flat structures, as shown in Figure 55 (Zou and Xiao, 2017).

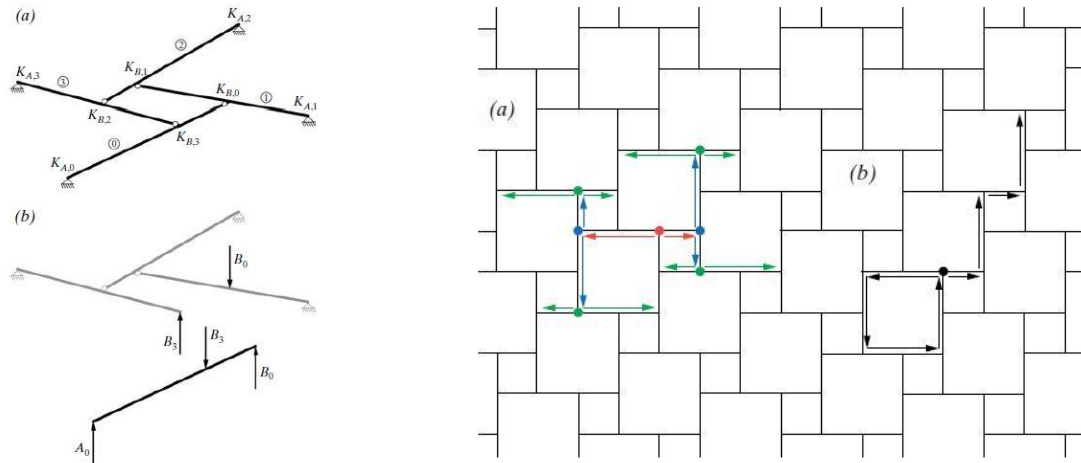


Figure 55_Example of a basic system ($n = 4$). (a) statics system; (b) sub-system. Example of three iterative steps: first red, second blue, third green; (b) right: Example of a cyclical and a diffused iteration step progression.

This method shows the load distribution in flat reciprocal systems in a systematic way and gives a better understanding of the overall structural action of these systems. But as the author states, it is not meant to be useful for practical design. This is especially evident since this method is only applicable to flat reciprocal systems of bars with friction-only connections—and this method can only consider the effect of perpendicular external forces, which is a critical limitation for practical purposes, where multiple load combinations, including lateral and perpendicular forces, are required for a safe structural design.

In a more practical effort toward understanding the mechanical behavior of reciprocal structures, (Gelez et al., 2011) analyzed the behavior of planar reciprocal structures with four-member fans. Baverel proposed a finite element method for analysis of reciprocal systems built of circular cross-sections (Baverel, 2005). The proposed method used short, rigid connection members to account for the eccentricities between the connecting reciprocal members and ignored the pinned

connection of reciprocal members, which causes unrealistic extra stiffness in the analytical model, as shown in Figure 56.

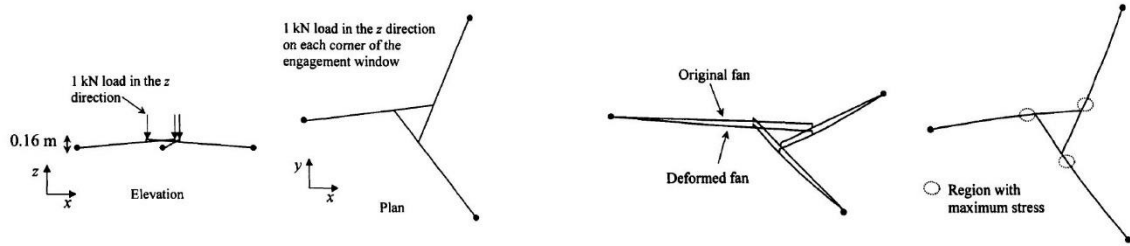


Figure 56_Finite element analysis of reciprocal module with four members.

Douthe and Baverel proposed an analytical method for form finding and analysis of reciprocal structures based on dynamic relaxation (Figure 57) (Douthe and Baverel, 2009). The proposed method takes account of minimizing eccentricities between the members in curved structures and calculation of internal (axial and bending) forces at the same time. However, the proposed method was only applied to reciprocal members with circular cross-sections, which are traditionally tied together.

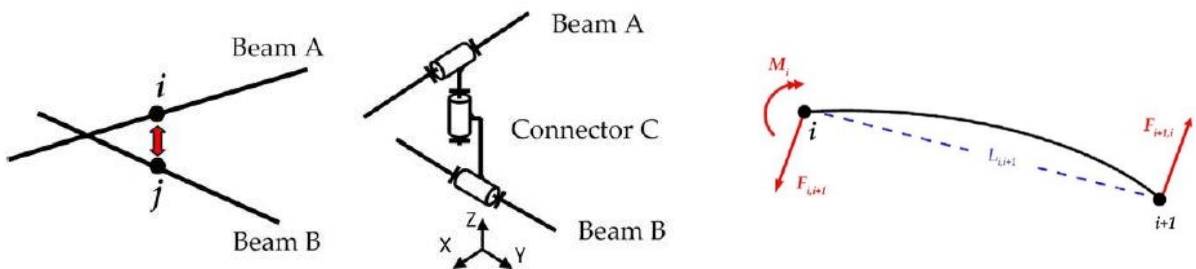


Figure 57_Kinematic scheme of connectors accounting for eccentricities. Local equilibrium of the reciprocal member subjected to bending.

Gelez et al. proposed a numerical analysis for flat, rectangular reciprocal systems with zero eccentricities between the members and a constant 50% engagement length. Although his method was highly constrained in terms of geometry and design parameters, his comparative quantitative study of structural performance and connectivity conditions between members is useful to understand some aspects of the complexity of reciprocal behavior in terms of load distribution and sensitivity to scale (Gelez et al., 2013). Moreover, it shows the inherent potentials of reciprocal systems for efficient fabrication and assembly.

Most of these methods have been developed to study the structural behavior of conventional reciprocal systems with tubular elements. For reciprocal systems comprised of 2-D elements or non-conventional reciprocal systems, the analytical method must take account of members' geometry and orientation for accurate analysis. Moreover, the method should have the flexibility to accommodate definition of different member connectivity conditions (e.g., pinned, fixed, and partially fixed), which is defined based on the fabrication detailing.

The analytical model we propose here can be used to analyze both flat and non-flat reciprocal systems. The difference is that for non-flat systems, series of geometrical manipulations are required before the analytical model is applied. These geometrical manipulations are specifically important in the sense that they take account of tolerances created as the result of the form-finding (eccentricity minimization) process. Moreover, different member connectivity conditions can be defined in the analytical model to account for those effects.

In this work, a finite element method is used to analyze reciprocal systems. Unlike the method proposed by Baverel, this method does not develop a custom reciprocal element; instead each

reciprocal element is discretized into three beam elements, each with 12 degrees of freedom (Figure 58).

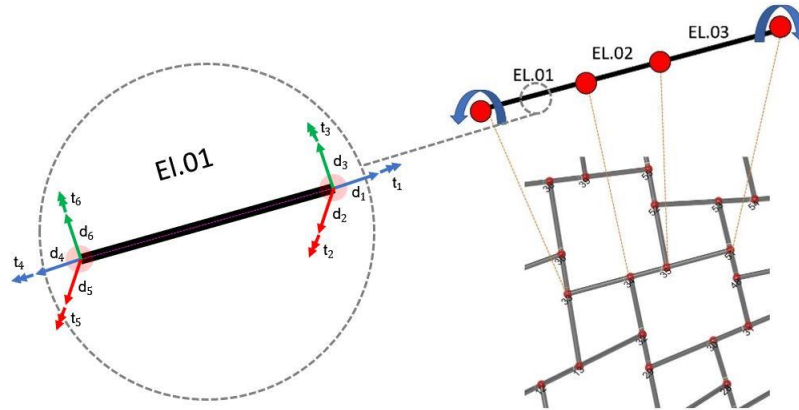


Figure 58_Structural reciprocal element discretized to three beam elements with 12 degrees of freedom in each element six displacement and six rotation degrees of freedom.

The main advantage of this method is that it is fast and can be used for analysis of reciprocal systems using existing commercial software. Moreover, it is generalizable and can be applied to non-flat reciprocal systems with drastic curvature changes. Another advantage of this method is that since we are treating each reciprocal element as three beam elements, we have much more control of the boundary condition of the elements at the connecting points. This is specifically important since the degree of rigidity at the connection condition is defined based on the connectivity method and the fabrication detailing (Oliyan Torgahbehi and von Buelow, 2018). Anastas et al. proposed similar method; however, they had to use short connector members to take account of eccentricities between the concurrent members (Anastas et al., 2016).

The connectivity of the reciprocal elements will significantly affect the structural performance of the reciprocal systems. The three-beam method will allow us to analytically model the boundary condition based on the connection detailing. This can be done by restraining the degrees of

freedom for the two side beams in each element through definition of fixed, pinned, or semi-fixed conditions for each connection. For the purpose of this section we consider two structural conditions—pinned and fixed—for the connection and compare their effect on structural behavior (Figure 59).

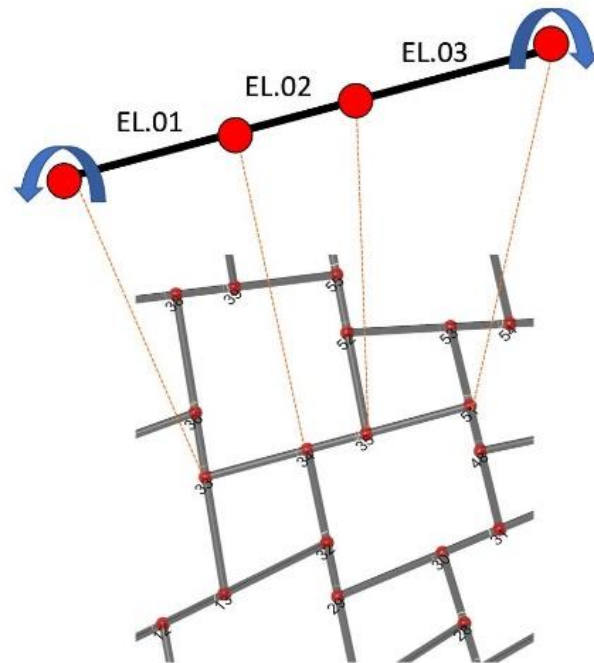


Figure 59_ The side beams can be restrained to define the connection behavior.

As mentioned above, element connection type can significantly affect the structural behavior and rigidity of reciprocal systems, which shows the direct connection between fabrication constraints and structural performance in these systems. There are multiple levels of interconnection between structural performance, fabricability, and assembly processes, which necessitate an integrative process to address them in the design process. The implemented method is generalizable and can accommodate any level of formal complexity in the design of reciprocal systems.

In this chapter, we show how these considerations are implemented in the analytical model for structural performance evaluation and design. In the Chapter 6, we will show how this numerical simulation module will be integrated into the computational design process to provide structural performance feedback as well as information about material use.

4.3.1 Module analysis

In this section, we use the three-beam formulation to study the structural analysis of one reciprocal module and study the connection between geometric parameters and the structural behavior. Rectangular cross-sections are used for modelling and simulation. Rotation angle is implemented to control the depth and size of the reciprocal geometry. We will study the effect of connection detailing and geometric parameters on the performance of the reciprocal module. The goal of this study is to understand the force distributions as well as connections between geometric parameters and member connection, detailing their effects on the structural behavior of reciprocal structures. The results are intended to define the main design parameters and factors affecting the performance of such structures.

The analysis starts with modelling and simulation of a reciprocal module to understand its mechanical behavior. Consequently, the model is used to parametrically study module behavior in relation to controlling geometric parameters. Then, this process is extended to a flat reciprocal system to study the overall behavior of reciprocal systems with multiple reciprocal modules and verify the applicability of the proposed method for large-scale analysis and design.

The structural analysis is first conducted on a single reciprocal module. Towards this goal, a four-membered reciprocal module is modelled on a flat 3 ft. by 3 ft. (0.91 m by 0.91 m) surface.

We use the same pattern formulation developed in Chapter 3, where reciprocal pattern generation was defined (Figure 60).

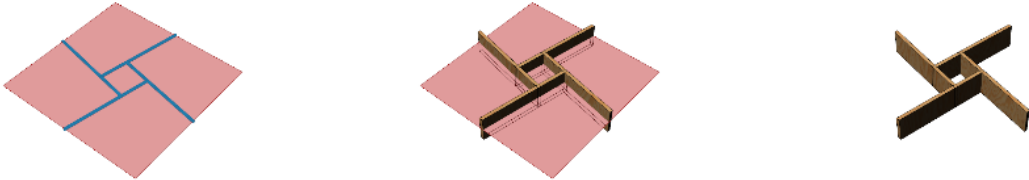


Figure 60_From left: Fat surface and reciprocal pattern, reciprocal module with 2-D elements in relation to the mesh geometry, reciprocal module.

The controlling parameters are engagement length, which is controlled based on the mesh scaling factor, rotation angle between -40° and 40° , member depth and member thickness, as shown in Figure 61.

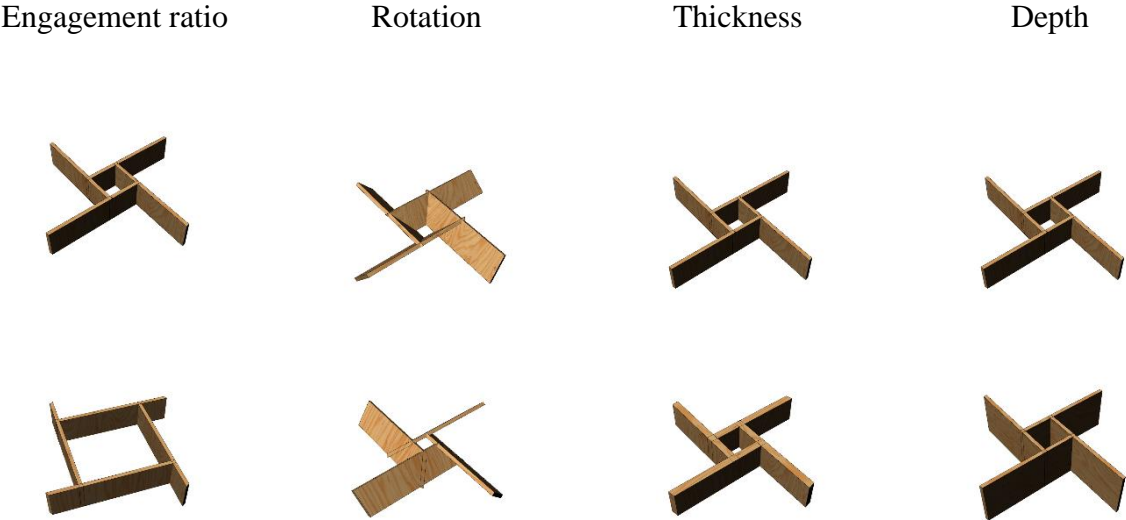


Figure 61_Controlling parameters. From left: Engagement ratio, rotation angle, member thickness, and member depth.

Since the reciprocal module is flat (created on a flat surface), the reciprocal members' center lines intersect and there are no eccentricities, as described in Figure 51. These member center lines are used to create the analytical model for structural analysis. Since we have only one module, the reciprocal members have only two connection points at one end. In this case when we discretize the members each will be discretized into two beam members (Figure 62). It is clear that in reciprocal systems with more than one module, each member has four connection points, as seen in Figure 52.

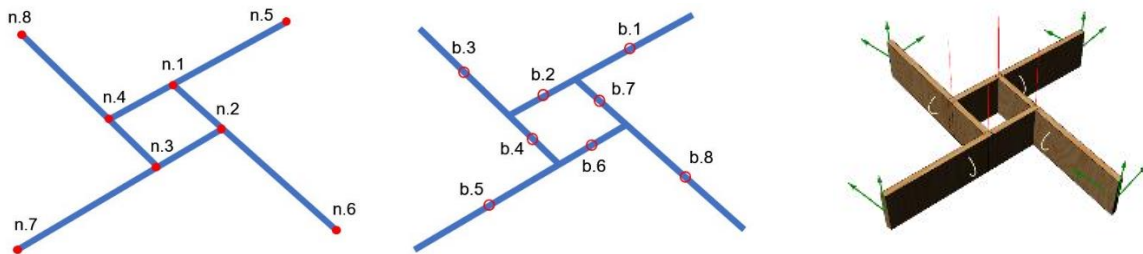


Figure 62_Structural model: reciprocal member discretization, structural nodes numbering, beam numbering, structural model with external loads and supports.

Cross-sections of rectangular members are used for modeling and analysis. The material properties of plywood based on Engineered Wood Association (APA) specifications for plywood material are used for these members. The wood type is assumed to be Douglas fir, which is categorized as Group 1 based on Table 1.5 of the APA specification (Figure 64). The APA is a nonprofit trade association of the United States and Canadian engineered wood products industry which represents manufacturers of engineered wood, mandate quality testing, and supports product research.

TABLE 1.5

CLASSIFICATION OF SPECIES

Group 1	Group 2	Group 3	Group 4	Group 5(a)	
Aptiong ^{(b)(c)}	Cedar, Port Orford	Maple, Black	Alder, Red	Aspen	Basswood
Beech, American	Cypress	Mengkulang ^(b)	Birch, Paper	Bigtooth Quaking	Poplar, Balsam
Birch	Douglas-Fir 2 ^(d)	Meranti, Red ^{(b)(e)}	Cedar, Alaska	Cativo	
Sweet Yellow	Fir	Mersawa ^(b)	Fir, Subalpine	Cedar	
Douglas-Fir 1 ^(d)	Balsam	Pine Pond	Hemlock, Eastern	Incense Western Red	
Kapur ^(b)	California Red	Red	Maple, Bigleaf	Cottonwood	
Keruing ^{(b)(c)}	Grand Noble	Virginia Western White	Pine Jack	Eastern Black (Western Poplar)	
Larch, Western	Pacific Silver White	Spruce Black	Lodgepole	Pine Eastern White	
Maple, Sugar	Hemlock, Western	Red	Ponderosa Spruce	Redwood	
Pine	Lauan	Sitka	Spruce	Sugar	
Caribbean	Almon	Sweetgum	Redwood		
Ocote	Bagtikan	Tamarack	Spruce Engelmann		
Pine, Southern	Mayapis	Yellow-poplar	White		
Loblolly	Red Lauan				
Longleaf	Tangile				
Shortleaf	White Lauan				
Slash					
Tanoak					

(a) Design stresses for Group 5 not assigned.

(b) Each of these names represents a trade group of woods consisting of a number of closely related species.

(c) Species from the genus *Dipterocarpus* are marketed collectively: Aptiong if originating in the Philippines; Keruing if originating in Malaysia or Indonesia.

(d) Douglas-fir from trees grown in the states of Washington, Oregon, California, Idaho, Montana, Wyoming, and the Canadian Provinces of Alberta and British Columbia shall be classed as Douglas-fir No. 1. Douglas-fir from trees grown in the states of Nevada, Utah, Colorado, Arizona and New Mexico shall be classed as Douglas-fir No. 2.

(e) Red Meranti shall be limited to species having a specific gravity of 0.41 or more based on green volume and oven dry weight.

Figure 63_ APA specification for classification of species.

GUIDE TO USE OF ALLOWABLE STRESS AND SECTION PROPERTIES TABLES

EXTERIOR APPLICATIONS

Plywood Grade	Description and Use	Typical Trademarks	Veneer Grade			Common Thicknesses	Grade Stress Level (Table 3)	Species Group	Section Property Table
			Face	Back	Inner				
APA RATED SHEATHING EXT ⁽³⁾	Unsanded sheathing grade with waterproof glue bond for wall, roof, subfloor and industrial applications such as pallet bins.		C	C	C	5/16, 3/8, 15/32, 1/2, 19/32, 5/8, 23/32, 3/4	S-1 ⁽⁶⁾	See "Key to Span Rating"	Table 1 (unsanded)
APA STRUCTURAL I RATED SHEATHING EXT ⁽³⁾	"Structural I" is a modifier for this unsanded sheathing grade. For engineered applications in construction and industry where full Exterior-type panels are required. Structural I is made from Group 1 woods only.		C	C	C	5/16, 3/8, 15/32, 1/2, 19/32, 5/8, 23/32, 3/4	S-1 ⁽⁶⁾	Group 1	Table 2 (unsanded)
APA RATED STURD-I-FLOOR EXT ⁽³⁾	For combination subfloor-underlayment where severe moisture conditions may be present, as in balcony docks. Possesses high concentrated and impact load resistance during construction and occupancy. Touch-sanded. (4) Available with tongue-and-groove edges. (5)		C plugged	C	C	19/32, 5/8, 23/32, 3/4	S-2	See "Key to Span Rating"	Table 1 (touch-sanded)
APA UNDERLAYMENT EXT and APA C-C-PLUGGED EXT	Underlayment for floor where severe moisture conditions may exist. Also for controlled atmosphere rooms and many industrial applications. Touch-sanded. Available with tongue-and-groove edges. (5)		C plugged	C	C	1/2, 19/32, 5/8, 23/32, 3/4	S-2	As Specified	Table 1 (touch-sanded)
APA B-B PLYFORM CLASS I or II ⁽²⁾	Concrete-form grade with high reuse factor. Sanded both sides, mill-oiled unless otherwise specified. Available in HDO. For refined design information on this special-use panel see APA Design/Construction Guide: Concrete Forming, Form No. V345. Design using values from this specification will result in a conservative design. (5)		B	B	C	19/32, 5/8, 23/32, 3/4	S-2	Class I use Group 1; Class II use Group 3	Table 1 (sanded)
APA MARINE EXT	Superior Exterior-type plywood made only with Douglas-fir or Western Larch. Special solid-core construction. Available with MDO or HDO face. Ideal for boat hull construction.		A or B	A or B	B	1/4, 3/8, 1/2, 5/8, 3/4	A face & back use S-1 B face or back use S-2	Group 1	Table 2 (sanded)
APA APPEARANCE GRADES EXT	Generally applied where a high quality surface is required. Includes APA A-A, A-B, A-C, B-B, B-C, HDO and MDO EXT ⁽⁵⁾		B or better	C or better	C	1/4, 11/32, 3/8, 15/32, 1/2, 19/32, 5/8, 23/32, 3/4	A or C face & back use S-1 ⁽⁶⁾ B face or back use S-2	As Specified	Table 1 (sanded)

- (1) When exterior glue is specified, i.e. Exposure 1, stress level 2 (S-2) should be used.
 (2) Check local suppliers for availability before specifying Plyform Class II grade, as it is rarely manufactured.
 (3) Properties and stresses apply only to APA RATED STURD-I-FLOOR and APA RATED SHEATHING manufactured entirely with veneers.
 (4) APA RATED STURD-I-FLOOR 2-4-1 may be produced unsanded.
 (5) May be available as Structural I. For such designation use Group 1 stresses and Table 2 section properties.
 (6) C face and back must be natural unrepaired; if repaired, use stress level 2 (S-2).

Figure 64_ APA specification for allowable stress and section properties.

Table 1 shows the material properties used for the analysis of the reciprocal module.

Property	Design Value
Specific Gravity	560 kg/m ³
Elastic Modulus	93000 kg/cm ²
Shear Modulus	46500 kg/cm ²
Tensile Strength	62 kg/cm ²
Compressive Strength	80 kg/cm ²
Bending Strength	62 kg/cm ²

Table 1_Material properties of plywood based on the Engineered Wood Association standard.

Now we can study the behavior of the reciprocal module under point loads. The boundary condition is the presence of a pinned connection at the free end of each member. Also, since the member connections are assumed to be notched, we must consider a rotation release around the y-axis of the members at the connection (strong axis of the cross-section).

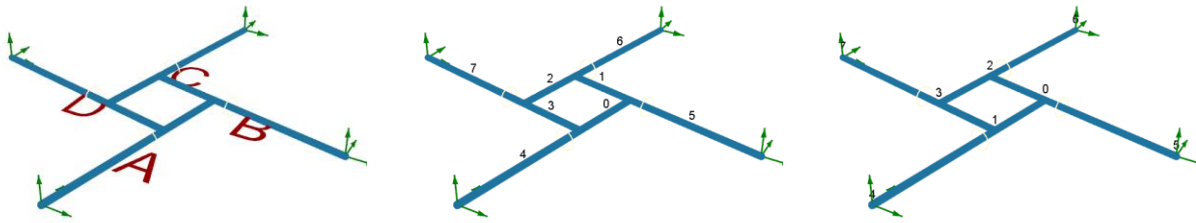


Figure 65_Member numbering, beam element numbering, node numbering.

The first image in Figure 65 is showing the labeling of the four reciprocal members as A, B, C, and D. The second image shows how each reciprocal member is discretized into two beam elements. For example, member A is discretized to beam number 4 and beam number 0. The third image shows the numbering of the member nodes.

Using these labeling and numbering data we can generate our analytical model by defining the equivalent reciprocal beam elements and boundary conditions. For example, reciprocal member A comprises two beam elements, 4 and 0; this member is supported by a pinned connection at one end defined by node number 4 and is connected to member B by a notch defined by node number 0. We can apply a pinned connection at node 4 and a moment release around the Y local axis of member A at node number 0, as shown in Figure 66. This moment release is caused by the notch fabrication properties, which let the connecting member rotate in its X–Z plane, which reduces the stiffness of the structure in comparison to a fixed connection. However, due to tight fabrication tolerances, there will be moment transfer around the X and Z axes. In general, there will be N releases per module in a reciprocal system with modules comprising N members (local axis is color coded as red is X axis, green is Y axis and blue is Z axis of the member).

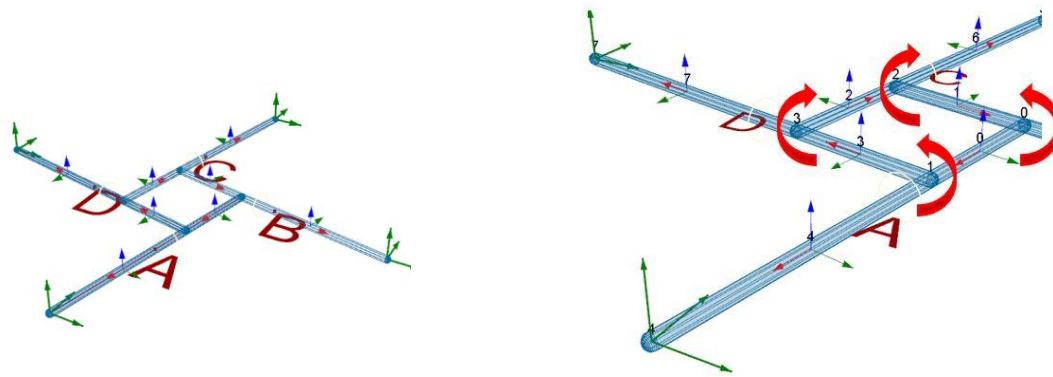


Figure 66_Local member axis and moment releases around the y-axis of members in a reciprocal module.

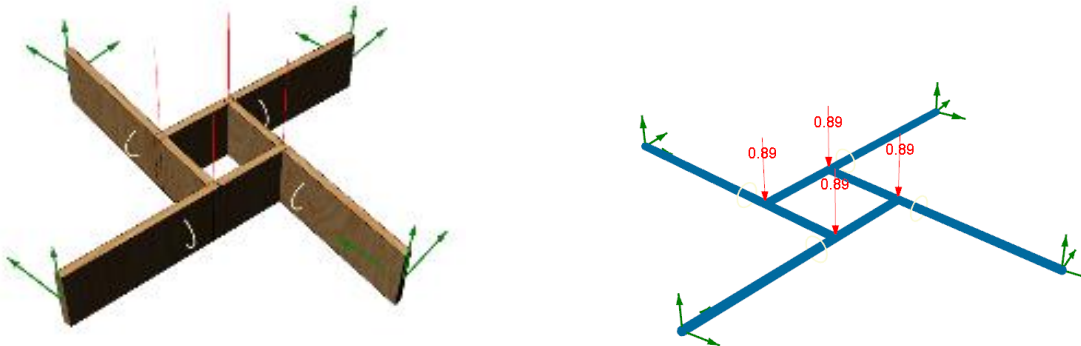


Figure 67_Structural model, boundary conditions, and the external loading used in analysis of a reciprocal module.

Karamba (a structural analysis plugin for McNeel Grasshopper) is used for analysis. Beam element discretization is used to analyze the reciprocal module. Using static linear elastic finite element analysis, the module is analyzed under 0.89 kN point loading on the four central nodes where the reciprocal elements connect, as shown in Figure 67.

The results of the static analysis are shown in Figure 68. The internal forces are shown along the reciprocal members; the main internal forces of interest are the dominant moments around the y-axis, shear forces, and torsional moments around the neutral axis of the members.

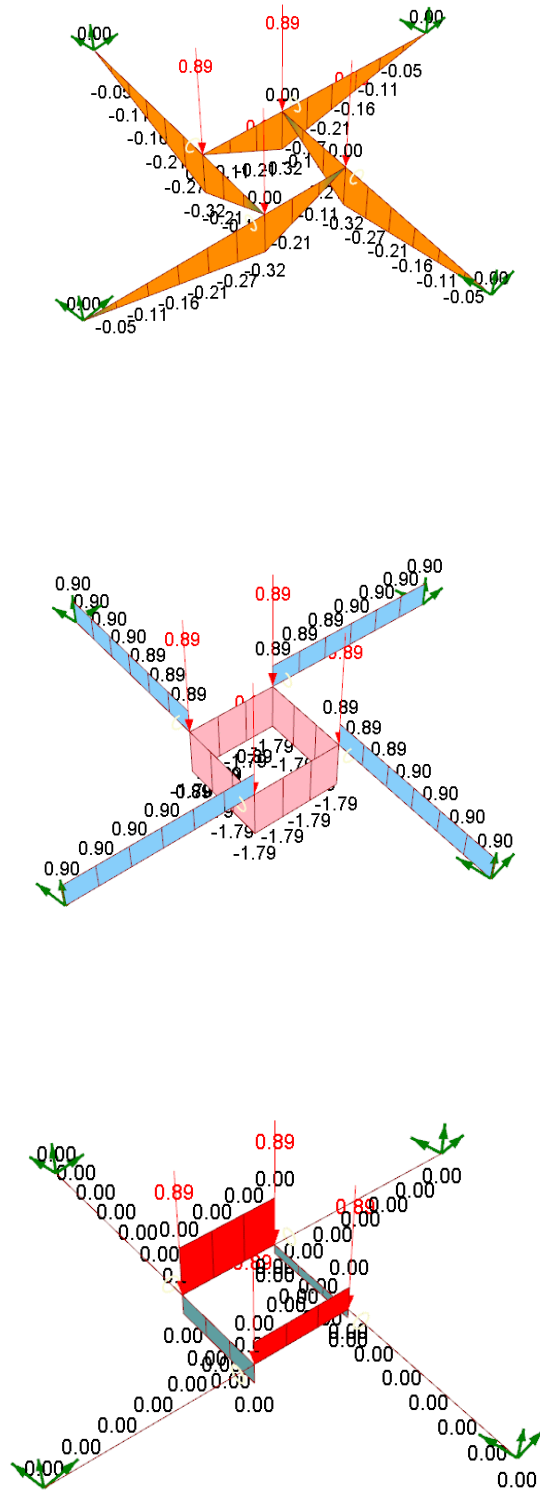


Figure 68_Internal force distribution. From the top: moment distribution, shear force distribution, torsional moment distribution.

Internal moment distribution is important because it defines the connection cuts in 2-D and 3-D reciprocal members. As shown in Figure 68, the maximum moment occurs under the member's connections, which is a critical location.

Torsion is especially important in designing reciprocal configurations. Due to inherent asymmetry of the reciprocal modules any external loading can cause torsional forces in the members, although these forces are below the capacity of the members, nonetheless they can aggravate lateral torsional buckling in reciprocal members (based on the Wood Council Association National Design Specification for Wood Construction).

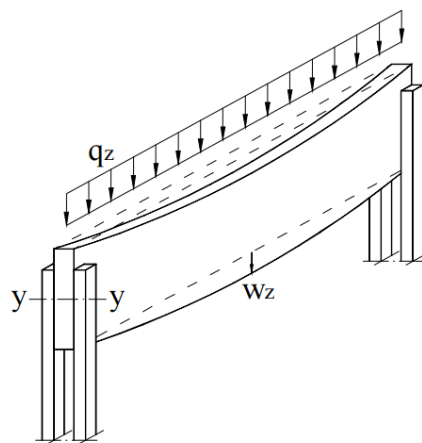


Figure 69_ Lateral torsional buckling based on the Wood Council Association's National Design Specification.

Lateral torsional buckling is a limit state where in-plane beam loading causes out-of-plane deformation in unbraced beams, as shown in Figure 69. Using internal forces, we can calculate the utilization factor for these members based on the bi-axial bending formulation.

Calculation of the loadbearing capacity of the members and overall structural design is based on the Eurocode5 specification for design of timber structures. The Eurocodes are limit-state design codes, which means requirements concerning structural reliability are linked to defined states beyond which the structure no longer satisfies specified performance criteria. There are two types: ultimate and serviceability limit states.

In order to design safe structures, all ultimate limit state criteria should be met. The main variables used in the design are actions, material properties and geological data. Actions are obtained from relevant parts of EN 1991, and include self-weight, snow and wind loads, etc. The duration of the load and its moisture content affect the strength and stiffness properties of timber and wood-based elements and must be considered in the design to ensure mechanical resistance and serviceability.

Reciprocal members are under bi-axial bending and axial loading. To take account of combined forces on the capacity of the reciprocal members we use the combined bi-axial bending and axial force formulation for utilization factor calculation as described in Equation (5). This formulation is extracted from Section 6.2 of EN 1991, which is applicable to straight solid timber, glued laminated timber, and wood-based structural products of constant cross-section whose grain runs essentially parallel to the length of the member. The member is assumed to be subjected to stresses from combined actions or to stresses acting along two or three of its principal axes.

combined biaxial bending and compression

$$\left(\frac{\sigma_c}{F_c}\right)^2 + \left(\frac{f_{bx}}{F_{bx}}\right) + k_m \left(\frac{f_{by}}{F_{by}}\right) \leq 1.0 \quad (5)$$

$$\left(\frac{\sigma_c}{F_c}\right)^2 + k_m \left(\frac{f_{bx}}{F_{bx}}\right) + \left(\frac{f_{by}}{F_{by}}\right) \leq 1.0$$

combined biaxial bending and tension

$$\left(\frac{\sigma_t}{F_t}\right) + \left(\frac{f_{bx}}{F_{bx}}\right) + k_m \left(\frac{f_{by}}{F_{by}}\right) \leq 1.0 \quad (6)$$

$$\left(\frac{\sigma_t}{F_t}\right) + k_m \left(\frac{f_{bx}}{F_{bx}}\right) + \left(\frac{f_{by}}{F_{by}}\right) \leq 1.0$$

σ_c compressive stress

F_c allowable compressive stress

σ_t tensile stress

F_t allowable tensile stress

f_b bending stress (f_{bx} and f_{by} bending stresses around X and Y axis)

F_b allowable bending stress

k_m shape factor, equal to 0.7 for rectangular cross-sections

To calculate the maximum utilization factor in the reciprocal members, maximum bending moments and axial loads are extracted from the analyzed model for each reciprocal member and the utilization factor calculated using Equations 1 and 2. The utilization factor is a good criterion to study the effect of the main geometric parameters on the behavior of the reciprocal module. The results are shown in Figure 70 and Figure 71.

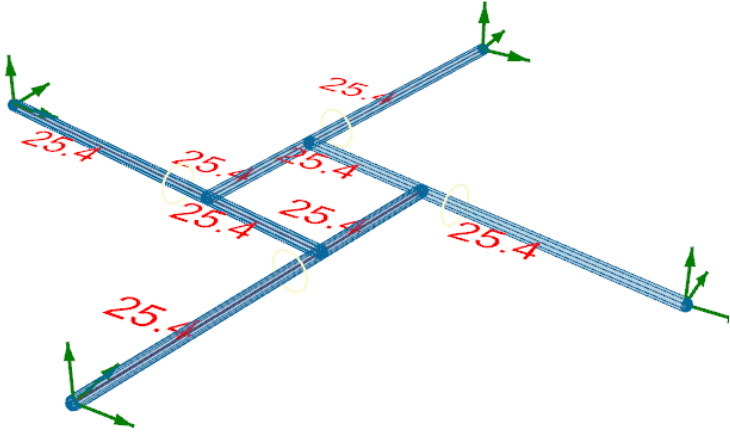


Figure 70_ Utilization calculation in reciprocal members under combined forces.

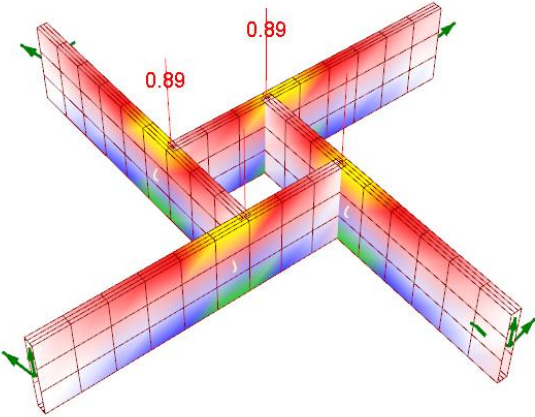


Figure 71_ Stress distribution in reciprocal members under combined forces.

4.3.2 Parametric study of the structural behavior of the reciprocal module

The parametric study of a singular reciprocal module provides interesting information about the geometric parameters and mechanical behavior of the reciprocal configuration. By focusing on structural capacity and deformation of the module, the relationship and sensitivity of the reciprocal module to variation of these parameters can be studied quantitatively. Using the proposed analytical model, we can perform a parametric study of the mechanical behavior of the reciprocal module for each of the four geometric parameters.

Firstly, this section studies the structural performance of the reciprocal module based on the variation in engagement length. Based on the formulation developed in Chapter 3 (where the process of reciprocal pattern generation is explained) engagement length is calculated based on the scale factor of mesh edges. The variation for our study is in a scale factor range of 0.2 to 0.6. The other parameters are kept constant: rotation angle zero, member depth 8 inch, and member thickness 0.75 Inch (Figure 72).

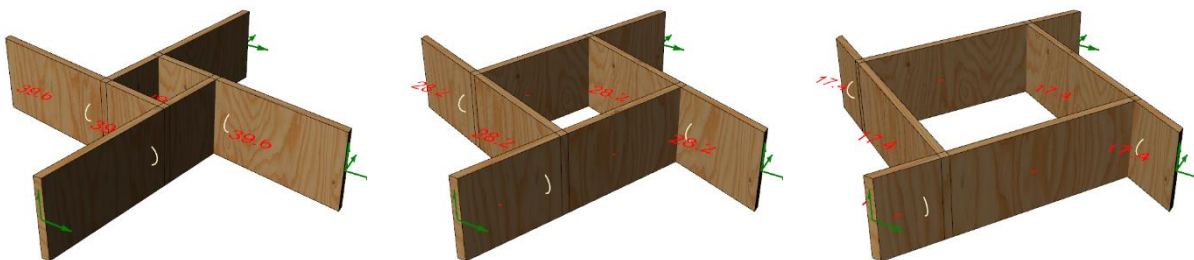


Figure 72_ Variation in reciprocal module geometry based on variation in engagement length. From left: EL=0.2, EL=0.4, EL=0.6.

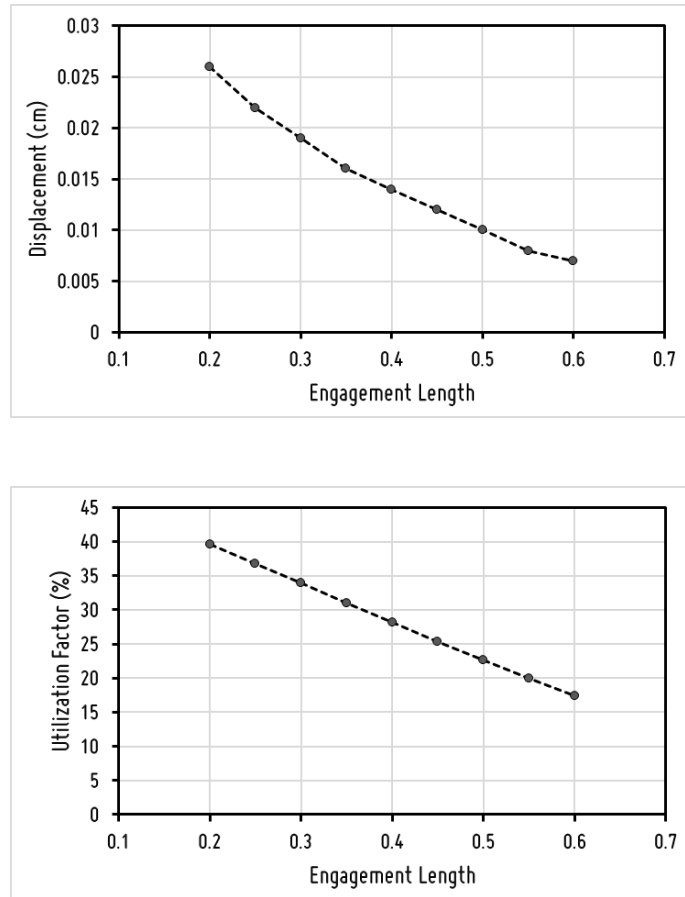


Figure 73_ Parametric study of the effect of engagement length on the structural behavior of a single reciprocal module.

The results of a parametric study of the effect of engagement length on the structural behavior of a single reciprocal module under four-point loads applied at the member connections are shown in Figure 73. The top graph shows how increase in engagement length causes reduction in the maximum displacement in the module in a nonlinear fashion and an almost linear reduction in the maximum utilization factor. These results show the different connection between stiffness and strength metrics in relation to engagement length of reciprocal modules. However, more than it being some inherent behavior of the reciprocal module, this response comes from the boundary conditions of the single module. As shown in Figure 72, increasing the engagement length causes the loading points to approach the supports, which creates a shortcut load path from the member

to the supports and reduces the bending arm on the reciprocal members, which in turn reduces the displacement and utilization factor. Therefore, it is important to study the effect of geometric parameters on the full reciprocal structure, where the effect of boundary condition is dissipated through the interconnection of reciprocal modules.

The next parameter to study is the rotation angle of reciprocal members. We study the structural performance of the reciprocal module based on variation in rotation angle between -40 to 40 degrees. The other parameters are kept constant: engagement length 0.3, member depth 8 inches and member thickness 0.75 inches. Studying the rotation angle in reciprocal members is not conventional, since the angle affects the structural behavior. However, it is of great interest in our research, since it provides design capacities beyond structural performance. Rotation angle causes variations in module perforation that can control the penetration of light, air, and affect other environmental conditions, thus allowing modules to be designed for a passive responsive effect based on the climate and context.

Structurally speaking the rotation in the members changes the local axis orientation and alignment with the perpendicular loading (Figure 74). For analysis, each member orientation should be defined based on the rotation angle in the analytical model.

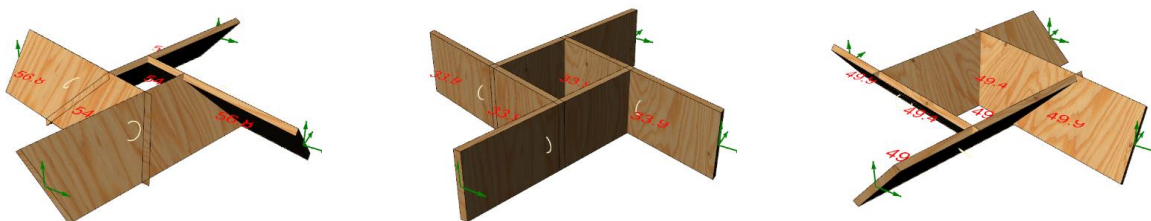


Figure 74_ Variation in the reciprocal module geometry based on variation in rotation angle (RA) From left: RA=-40, RA=0, EL=40.

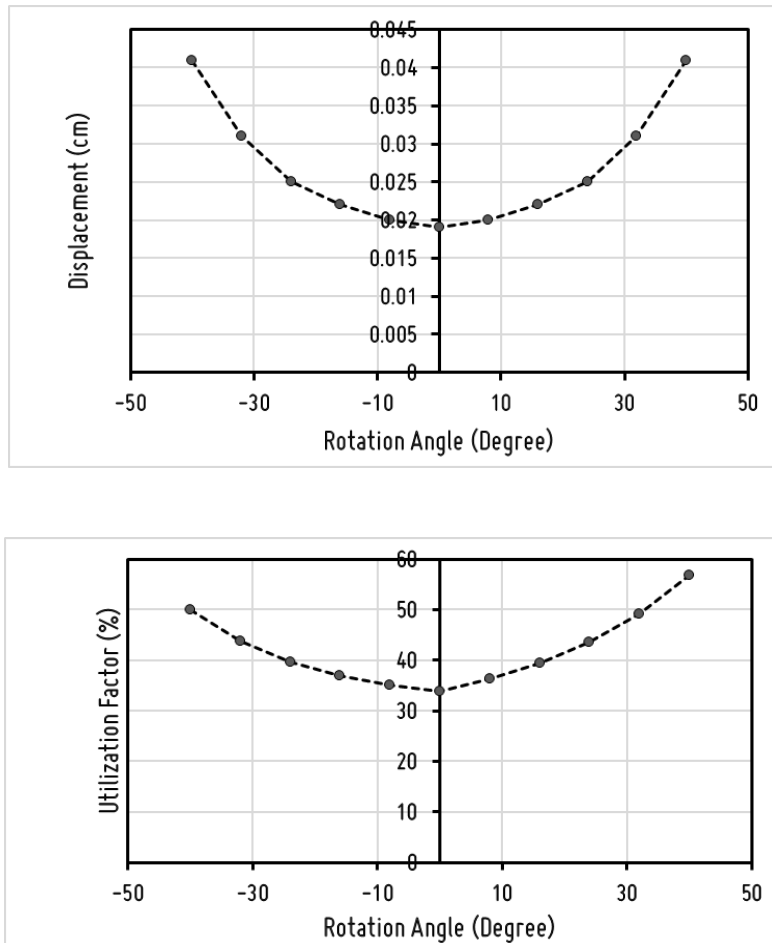


Figure 75_ Parametric study of the effect of the rotation angle on the structural behavior of a single reciprocal module.

A parametric study of the effect of the rotation angle on the structural behavior of a single reciprocal module is shown in Figure 75. The displacement graph (top) shows a symmetric response of the reciprocal module to positive and negative (far left and far right pictures in Figure 74, respectively) rotation angles, which indicates the module has the same stiffness in positive and negative rotation configurations. However, as the bottom graph in Figure 75 shows, the member utilization is not symmetrical. As the graph depicts, member utilization is larger for a positive rotation of the same degree than the identical negative rotation. Although the size and distribution of internal moment are the same for both rotations, negative rotations cause compressive forces in the members, while positive rotations put the members in tension.

Although the size of the axial load is the same, the calculation of the utilization factor will be different based on the Equation (5) and Equation (6). Thus, positive rotations produce bigger utilization factors for the same geometry. These differences in behavior caused by the rotation angle can play an interesting role in the stability and load distribution of reciprocal structures with multiple reciprocal modules.

However, it is important to understand that, based on the results from calculation of the utilization factor for tension and compression members, it is clear that bending action is the dominant factor in the structural behavior of the reciprocal structures. Bending action should be considered the main design criteria both for structural design as well as fabrication of connection detailing.

The next parameter to study is the member depth of reciprocal members. This section shows the results for parametric study of the structural performance of the reciprocal module based on the variation in the member depth of between 5 to 10 inches. The other parameters are kept constant: rotation angle zero, engagement length 0.3, and member thickness 0.75 inches (Figure 76).

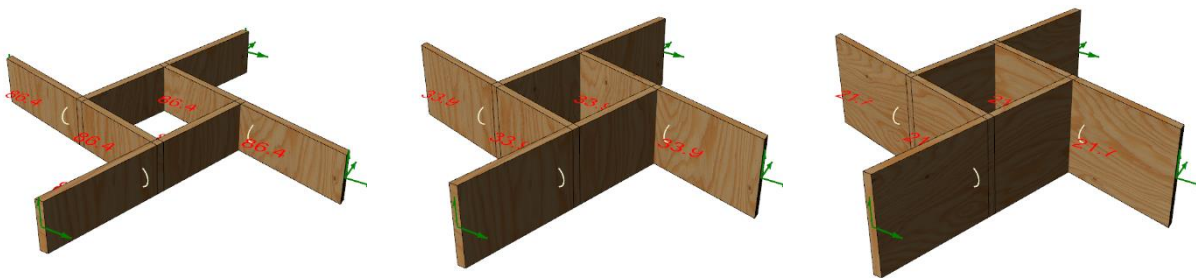


Figure 76_ Variation in reciprocal module geometry based on variation in member depth. From left: D=5 in, D=7.5 in, D=10 in.

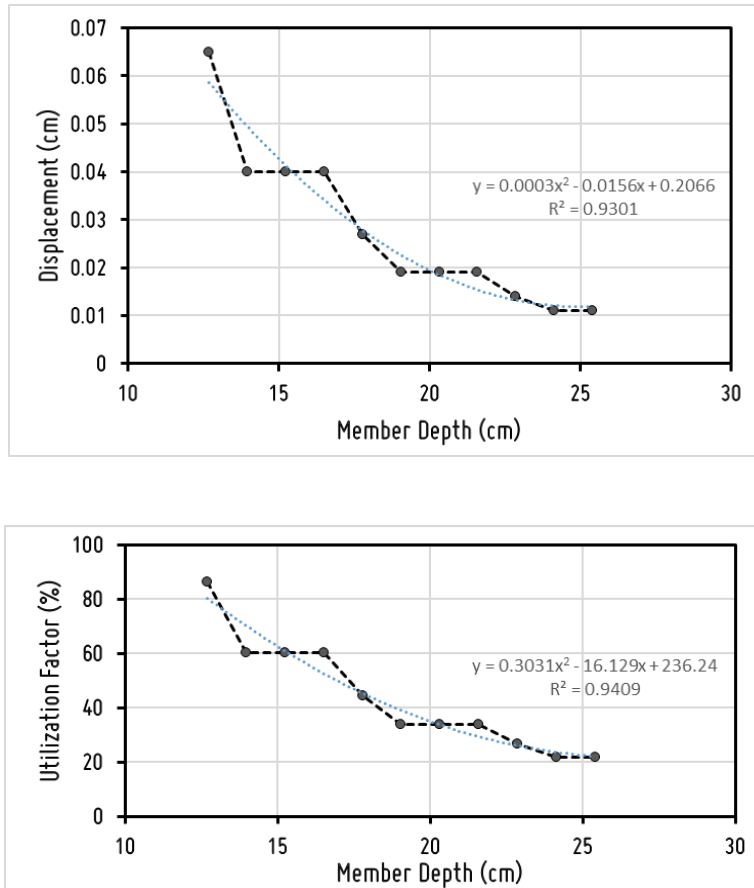


Figure 77_ Parametric study of the effect of the member depth on the structural behavior of a single reciprocal module.

The deformation and utilization factor have a nonlinear (second order relationship) with the member depth, as depicted in Figure 77. This is expected based on the effect of the moment of inertia.

4.3.3 Parametric study of the structural behavior of flat reciprocal systems

Parametric study of the reciprocal module provides a quantitative understanding of relationships between the geometric parameters and the structural behavior of reciprocal modules. This study also provides insight about the governing parameters and their effects in the behavior of the reciprocal systems with multiple modules.

However, to understand the overall behavior of reciprocal systems we must analyze them as a system of interconnected modules, not a single module. As previously discussed, in some cases, the results from the parametric study of a single module are not generalizable to reciprocal systems. Therefore, in this section, we will do a comprehensive parametric study of flat reciprocal systems based on their dominant geometric parameters, derived from the previous study of single reciprocal modules.

For this, we need a better measure for parametric study of the system. Since the parametric model is constituted of several interconnected reciprocal modules, we will have several utilization factors equal to the number of beam members in the analytical model—three times the number of reciprocal members, as depicted in Figure 59. Therefore, we cannot use the utilization factor as a metric in our study. Instead, we will use the results of the structural analysis to design the size of the members based on the EN 1993, Eurocode 3 building code. This process will determine the minimum size of each member based on the building design code for a safe loadbearing system. Consequently, the total weight of the system can be used as the metric for parametric study.

The two other geometric parameters, thickness and member depth, are not controlling parameters, as they are defined automatically in the structural design process. A repetitive algorithm chooses the smallest dimensions for each member as needed to safely bear the external loads.

However, another important parameter exists when analyzing reciprocal systems: the density of the reciprocal modules in the system. The density parameter controls the number of modules in the reciprocal system. Based on the modelling formulation explained in Chapter 3, this

generative capacity of the model is controlled by the mesh-based tessellation of the primitive surface, as each quadrilateral mesh face leads to a reciprocal module in the interconnected system. In this section, we will also study the effect of the density on the structural behavior of the reciprocal system. Moreover, we show that density is an effective parameter in controlling the perforation size and shading capacity of reciprocal systems.

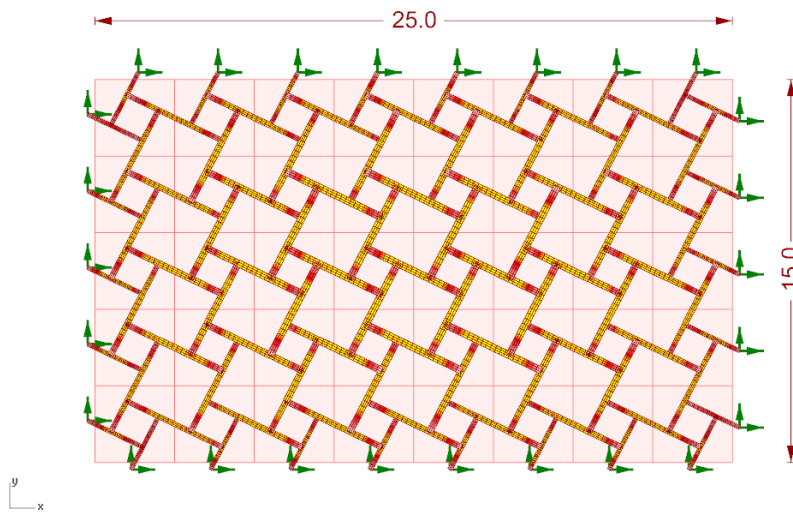


Figure 78_ Sample flat reciprocal system as a roof system.

Figure 78 shows the geometry of the case study structure which is a flat reciprocal system considered as a roof structure. The reciprocal roof covers a rectangular area of 15 ft. by 25 ft. We will use this model to study the effect of engagement length, and rotation angle on the structural performance of the system.

The sample structure is comprised of 40 interconnected reciprocal modules in a 5 by 8 grid. We use the proposed formulation to create the analytical model based on the discretization of reciprocal members to three beam elements. The assembly of the beam elements generates the structural model. We use joint releases at the two ends of each reciprocal member to

accommodate the effect of connection detailing and to control the rigidity of the connections. This is carried out by identification of beam elements at the two ends of each reciprocal member and the generation of a structural joint at one end of the beam to release rotations around Y axis (strong axis of the cross-section) of the reciprocal member (Figure 79).

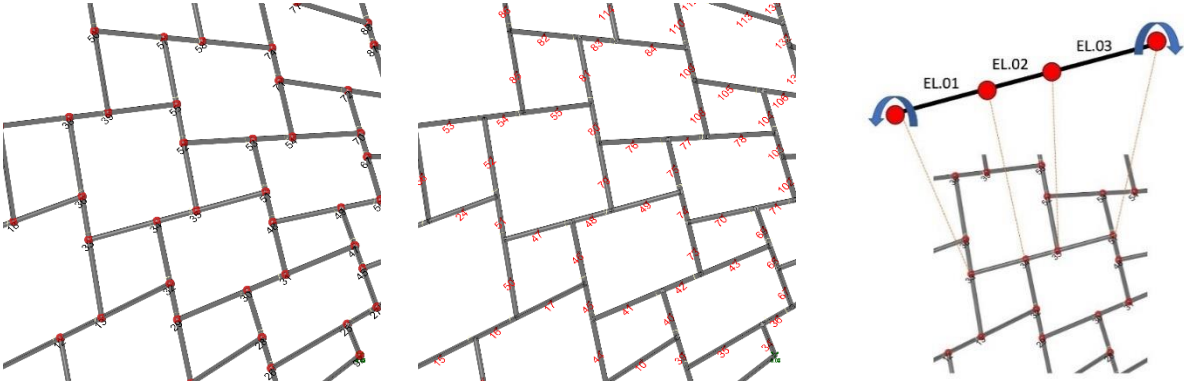


Figure 79_ Generation of analytical model. From left: structural node numbering, beam elements numbering, joint release definition.

In this example, the perimeter of the structure is supported by pinned supports. This is the condition considered for a roof structure sitting on a set of walls, or with pinned connections to a set of columns. To define this condition in the analytical model, we restrain the end of reciprocal members on the perimeter, as shown in Figure 80.

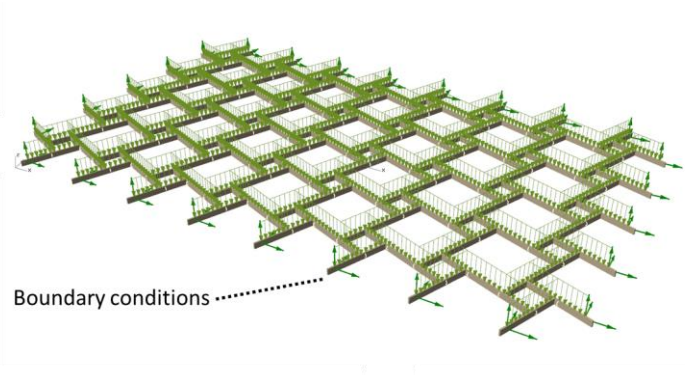


Figure 80_ Distributed loading and boundary conditions for a flat reciprocal system.

For structural analysis of the system, we consider a snow and cladding load of 200 psf plus the dead weight of the structure. Considering steel as the structural material, we use this model to analyze the reciprocal system using a linear elastic analysis method and calculate the internal forces in each beam element. Figure 81 shows the internal forces in the flat reciprocal system.

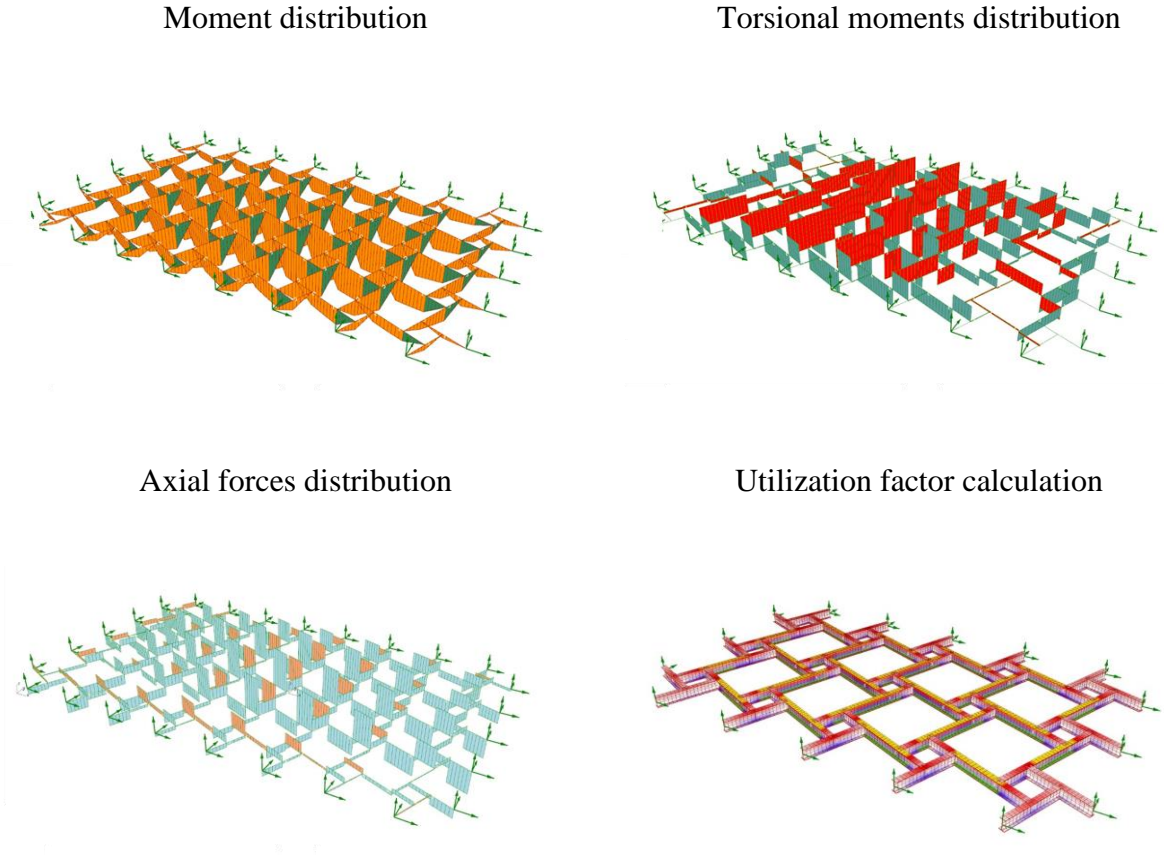


Figure 81_ Visualization of the internal forces in the flat reciprocal system.

The calculated internal forces are then used to design the size of the members based on EN 1993, Eurocode 3 for the design of buildings in steel. We use Karamba’s 3-D Optimize Cross Section function to iteratively check each beam member for the smallest cross-section that will safely bear the external loads based on the design code provisions (Figure 82). This process considers axial loading, biaxial bending, torsion and shear, and also accounts for capacity reduction due to

axial and lateral torsional buckling of the members. The design process is illustrated in Figure 83.

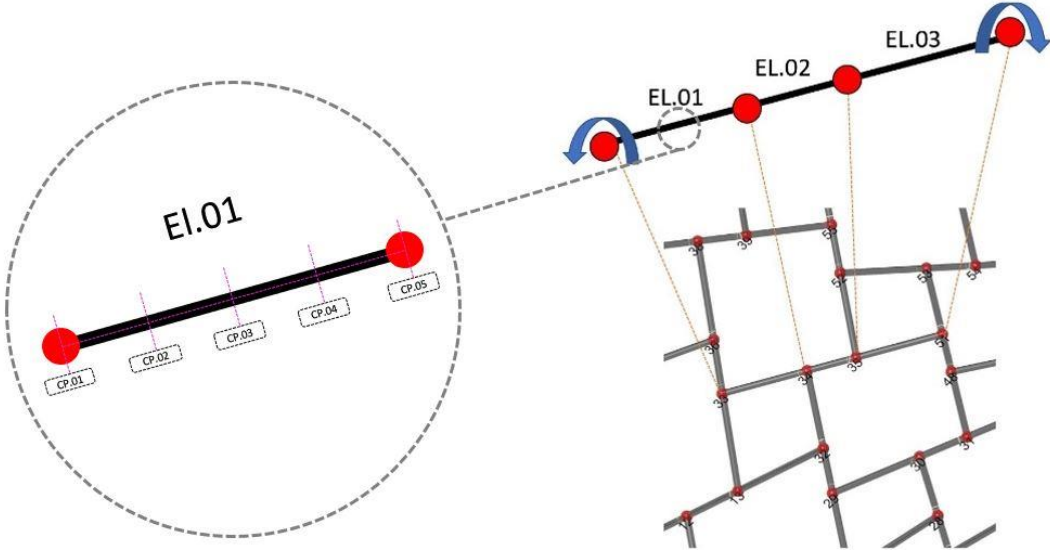


Figure 82_ Discretization of reciprocal member to three beams and creating five design check points on each beam.

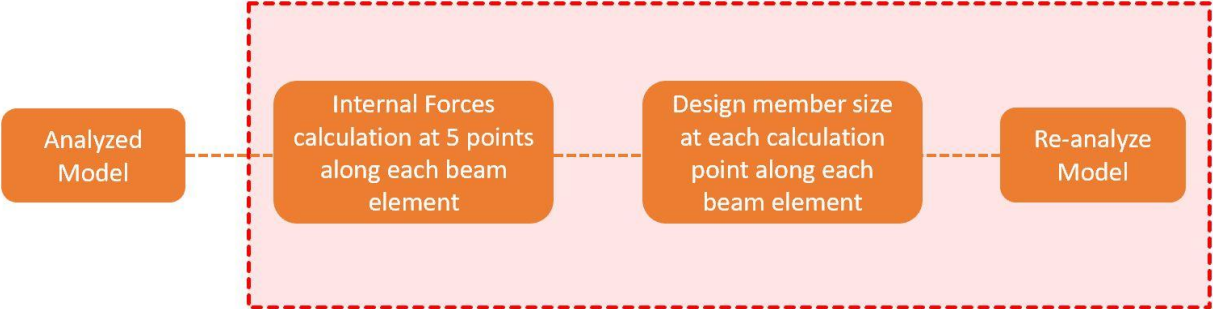
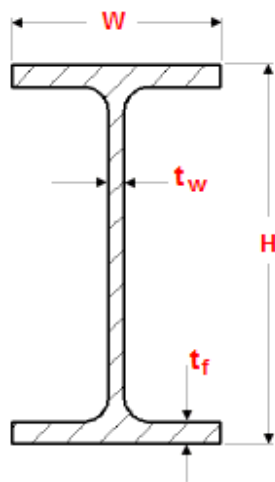


Figure 83_ Iterative structural design process to find the minimum weight cross-section for each beam element.

For this example, steel IPE cross-section family I is considered as the design family for the beam elements. The beams are allowed to take variable cross-sections along the reciprocal members for more accurate minimization of structural weight. Figure 86 shows a sample design for a flat reciprocal system where member sizes are designed from IPE cross-section family based on the minimum required capacity to carry the external loading (Figure 84).



European standard beams IPE					
Designation	Unit Weight	Depth of Section	Width of Section	Thickness of	
	kg/m	mm	mm	Web mm	Flange mm
IPE 80	6.00	80	46	3.80	5.20
IPE 100	8.10	100	55	4.10	5.70
IPE 120	10.40	120	64	4.40	6.30
IPE 140	12.90	140	73	4.70	6.90
IPE 160	15.80	160	82	5.00	7.40
IPE 180	18.80	180	91	5.30	8.00
IPE 200	22.40	200	100	5.60	8.50
IPE 220	26.20	220	110	5.90	9.20
IPE 240	30.70	240	120	6.20	9.80
IPE 270	36.10	270	135	6.60	10.20
IPE 300	42.20	300	150	7.10	10.70
IPE 330	49.10	330	160	7.50	11.50
IPE 360	57.10	360	170	8.00	12.70
IPE 400	66.30	400	180	8.60	13.50
IPE 450	77.60	450	190	9.40	14.60
IPE 500	90.70	500	200	10.20	16.00
IPE 550	106.00	550	210	11.10	17.20
IPE 600	122.00	600	220	12.00	19.00
IPE 750 x 137	137.00	753	263	11.50	17.00
IPE 750 x 147	147.00	753	265	13.20	17.00
IPE 750 x 173	173.00	762	267	14.40	21.60
IPE 750 x 196	196.00	770	268	15.60	25.40

Figure 84_ Cross-section geometric information of IPE; table of design properties for flanged steel profiles.

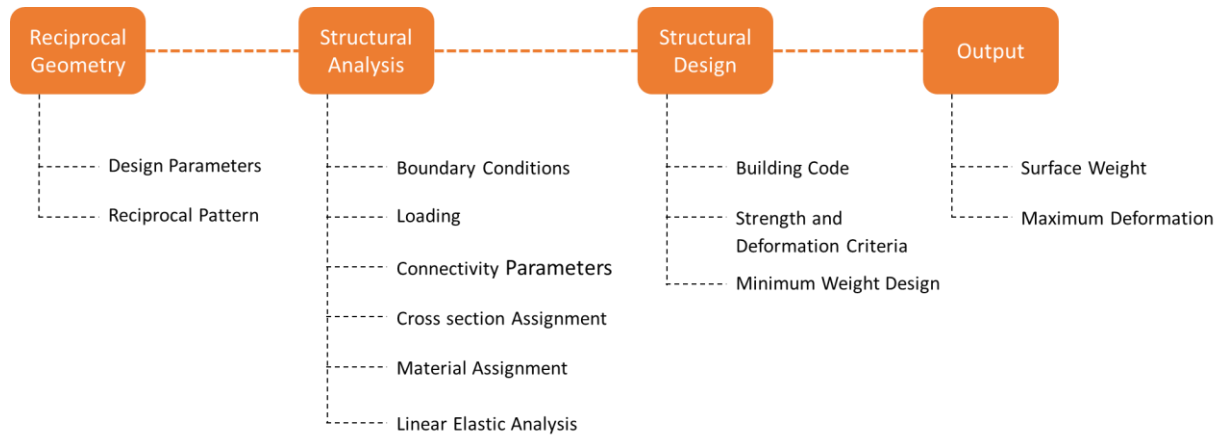


Figure 85_ Structural analysis and member design process.

The structural analysis and member design process for the reciprocal structures is shown in Figure 85. It comprises the generation of analytical model, analysis and calculation of internal forces, member design process, and calculation of minimum total weight and maximum structural deformation. These metrics are used for the parametric study of the reciprocal system.

The utilization factor for the reciprocal structure after designing members for minimum weight based on the building code provisions is shown in Figure 86, and can be compared with Figure 81, from before the design process.

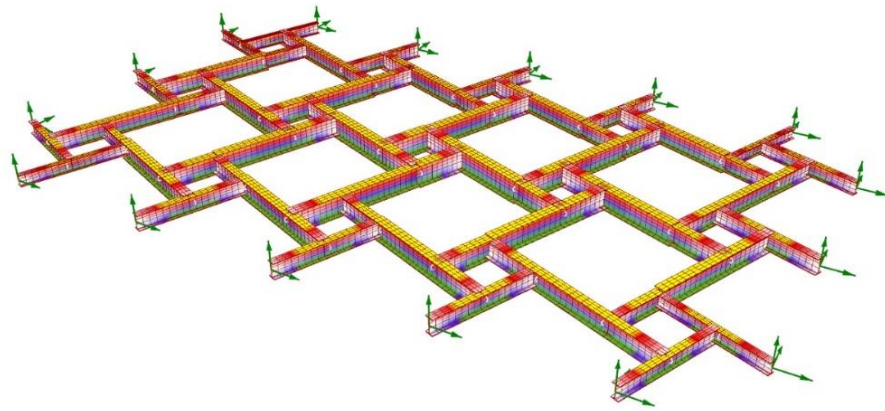


Figure 86_ Visualizing utilization factor after member sizing.

The proposed flat reciprocal structure can now be used for parametric study of structural behavior. The first and the most important parameter to study is the effect of engagement length on the structural performance of the flat structure. To study this effect, the structure is analyzed and designed for variation in a scale factor range of 0.1 to 0.9, which defined the engagement length for the reciprocal structure, as shown in for three samples in Figure 87.

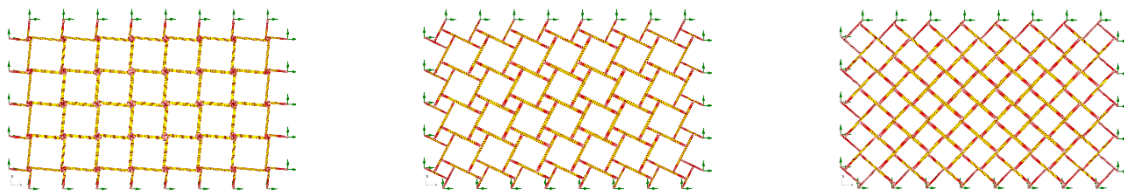


Figure 87_ Variation in reciprocal geometry based on variation in engagement length (EL). From left: EL=0.1, EL=0.5, EL=0.9.

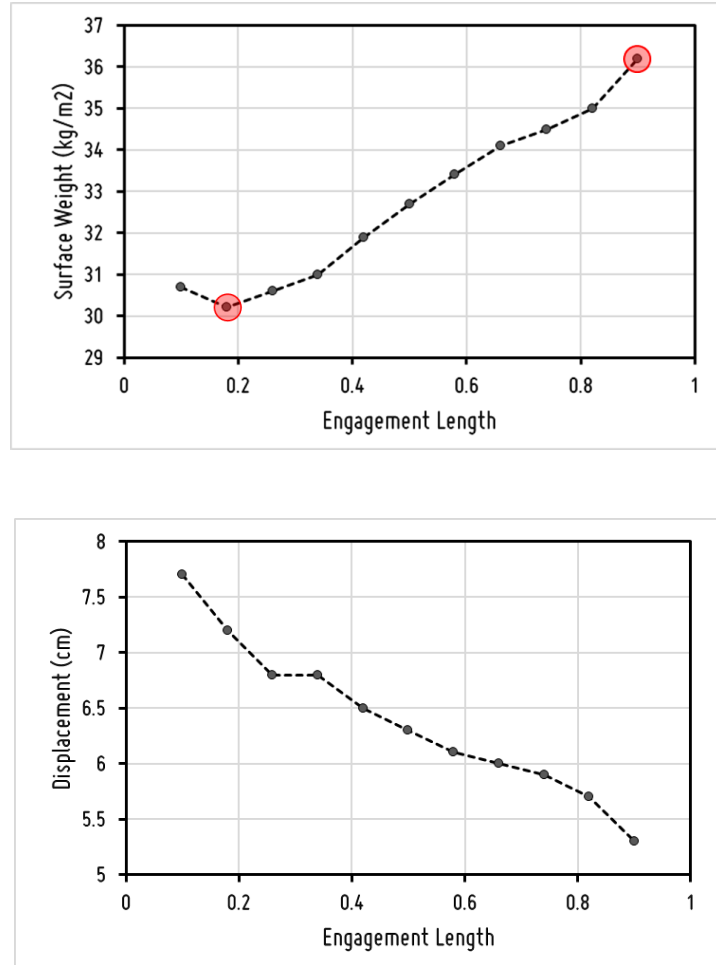


Figure 88_ Parametric study of the reciprocal system's behavior based on the variations in the engagement length.

The results from this analysis are shown in Figure 88, and reveal an important relation between the efficiency and stiffness of reciprocal systems. The first graph shows how an increase in the engagement length affects the efficiency (the total weight of the structure) of the system drops. It is intuitive that with a smaller engagement length the geometry of the reciprocal system approaches the continuous geometry of a grid shell, which offers more efficient loadbearing. However, the most lightweight design does not correspond with the smallest engagement length. Observations of the geometry with a very small engagement length shows that the shear forces increase significantly in the connection areas, and becomes dominant in the design of the

member sizing, dictating bigger member cross-sections at the connections (Figure 89). As a result, maximal system efficiency occurs when these local shear forces dissipate.

A design approach purely driven by structural response would result in reducing the engagement length; however, in reality, the fabrication and assembly process plays a significant role in the design process, which must be addressed. As an example, if the engagement length becomes too small, access to the connection locations will be difficult, which will cause problem in the assembly process. It becomes clear, then, that the design process for these systems cannot be done based solely on structural optimality, and that the constructability of the design must be integrated in the process. It becomes crucial to integrate these constructability considerations as design constraints in the fabrication-aware design process, and to address these issues in the early stages of design for an optimal and practical result.

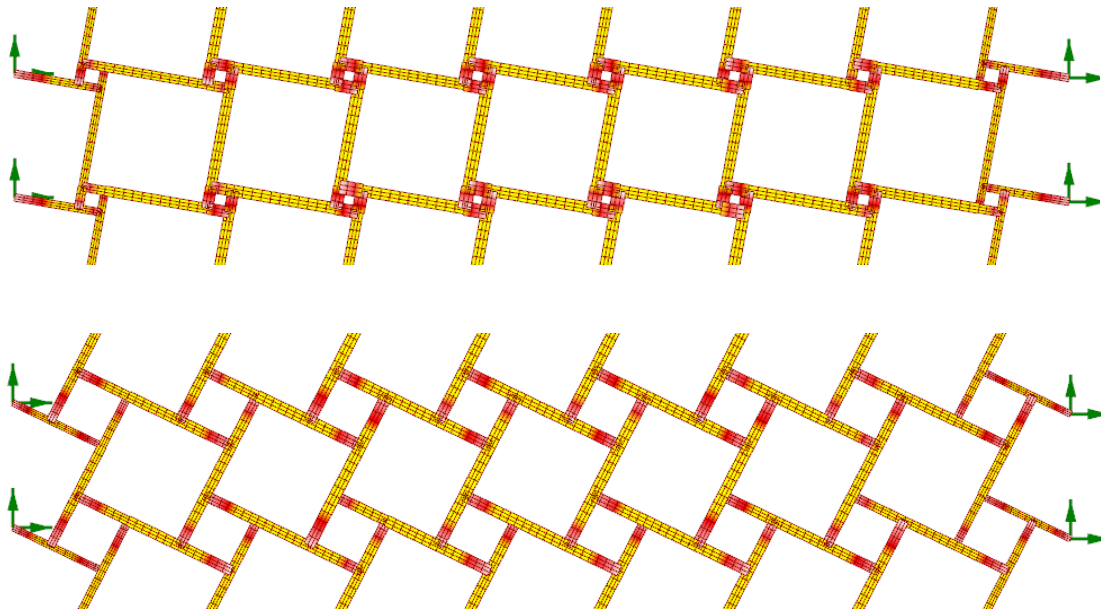


Figure 89_ Increase in member sizing due to local shear forces in reciprocal systems with very small engagement length. Top: reciprocal system with 0.1, bottom: reciprocal system with 0.5.

4.3.4 Comparative study of the determinacy and member connectivity conditions

Using the same process, we study the effect of connection detailing on the performance of the reciprocal systems. If the connection detailing is designed so that it brings the minimal amount of constraints to the structure to obtain stability, it results in a determinate system where the intensity of internal forces does not depend on the cross-sectional properties or material behavior. Lower rigidity of the connection means the connection detailing can be built more easily and cheaply. Determinate systems also show minimal sensitivity to settlement and thermal loads, which is a beneficial characteristic of such systems in designing shelters that are prone to settlement or large roofs that are subject to thermal gradients. Fabrication-wise, it means if a reciprocal member is designed or fabricated with a larger dimensional tolerance (or applying a positive thermal load) it can fit into the system with minimal effect on the load distribution in the system (Gelez, 2011).

However, determinate systems do not have redundancy and so the result lacks robustness, which can lead to progressive collapse in failure. As a result, understanding the conditions of determinacy and redundancy of reciprocal systems is an important issue that varies based on the design's purpose. In this section we use the analysis model to do a comparative study of the structural behavior of the flat reciprocal system in relation to member connectivity conditions.

As described in Section 4.3, in the analytical model, partial rigidity was considered at the connections of reciprocal members, which is implemented in the model by rotational release around the y-axis of reciprocal members. To study the effect of member connectivity on the flexibility and performance of reciprocal systems, we use our simulation model to quantitatively compare the effect of moment releases at the connections on the structural behavior of the systems. The comparative system is geometrically and topologically the same in geometry.

However, all of the member connections are defined as fixed. The results are shown in Figure 90, Figure 91 and Figure 92.

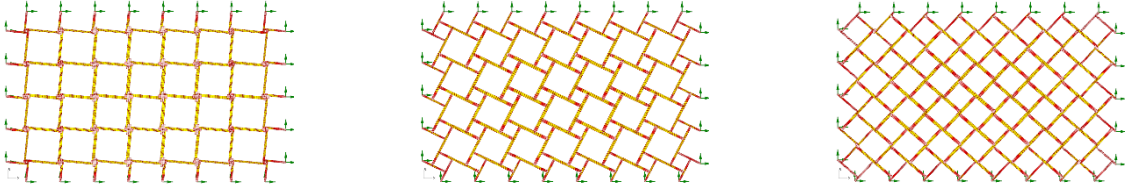


Figure 90_ Variation in reciprocal geometry based on variation in engagement length (EL). From left: EL=0.1, EL=0.5, EL=0.9.

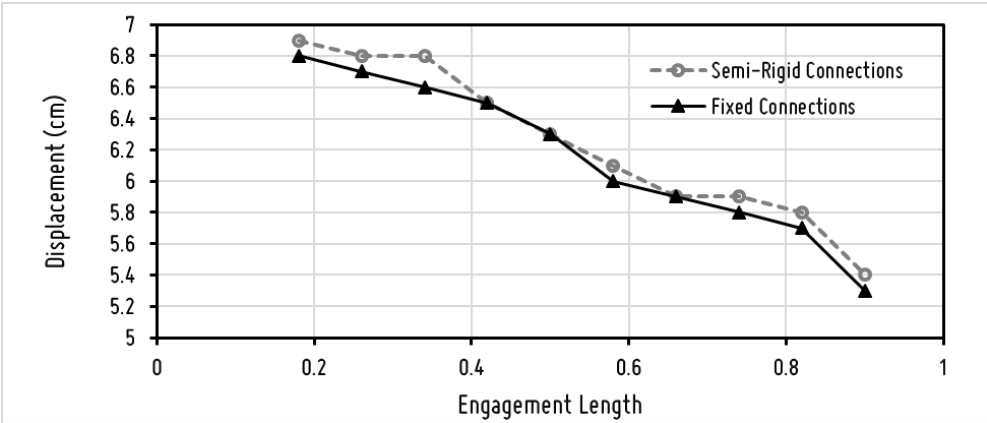


Figure 91_ Comparative study of a structural behavior of the reciprocal systems with semi-rigid and rigid connections.

As expected, the reciprocal system with rigid connections is stiffer, and experiences smaller deformations, which is consistent with results for systems with different engagement lengths.

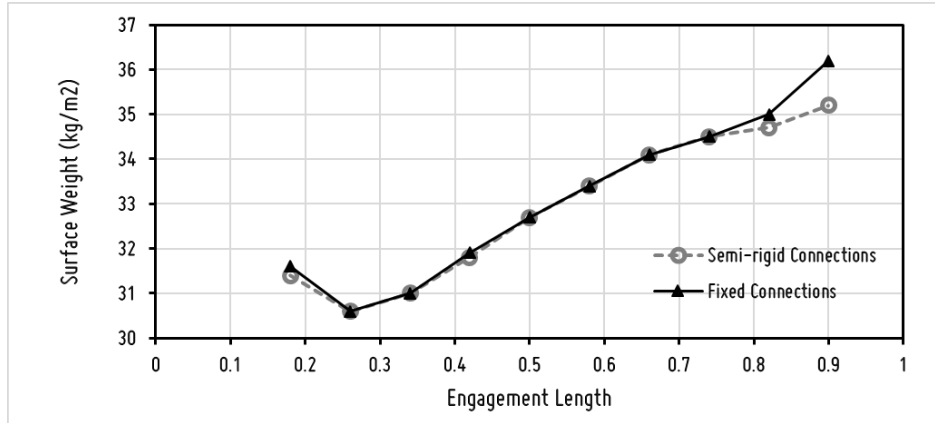


Figure 92_ Comparative study of structural behavior of reciprocal systems with semi-rigid and rigid connections.

The result from the comparative study of the two systems is rather unexpected. As shown in Figure 92, the total weight of the system is almost the same for systems with engagement lengths between 0.2 and 75, but for very large engagement lengths (> 0.75), the rigid system is less efficient. The reason is that because fixing the reciprocal member connections causes negative bending moments to develop at these connections, which affect the design process for member sizing. By increasing the engagement length, these negative bending moments increase substantially and will lead to bigger cross-sections in reciprocal members.

To study the effect of mesh density on the structural behavior of the flat reciprocal system we analyze the same model with different mesh densities. The dual effect of engagement length and mesh density can be studied by comparing the results of variations in mesh density for each engagement length. Variation in mesh density with constant engagement length and a 0.4 scale factor is shown in Figure 93.

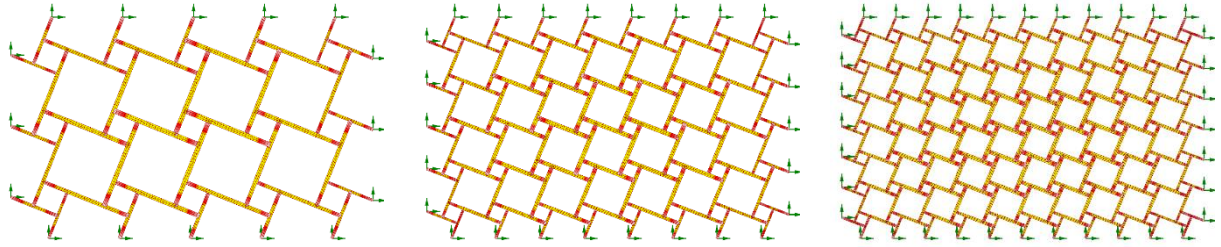


Figure 93_ Variation in mesh density with constant engagement length and a 0.4 scale factor.

We use this model to analyze and design the reciprocal system under loads of 100 psf of snow and cladding. To compare realistic structural weights, we limit the maximum deformation of the structure based on the Eurocode 93 design code. Therefore, in the process of member design, the maximum deformation of the structure is checked after the member sizes are designed in each iteration until the maximum deformation is lower than the maximum allowable deformation. This forces the lower mesh densities to accommodate the allowable elastic deformations, which leads to bigger cross-sections to compensate for a less-dense mesh and provides a more accurate metric to understand the effect of mesh density on the structural performance.

The reciprocal system is designed, generated, and analyzed for progressively denser mesh, which means smaller cell sizes but more reciprocal members. The trade-off between the number of reciprocal members and their size is an important question to be considered in the design process of reciprocal systems. Moreover, mesh density affects the perforation of reciprocal systems, which offers the design potential to integrate effects like light modulation, shading capacities, or ventilation. Understanding the effect of mesh density can provide insight into the overall behavior of these systems and guide the design process.

Figure 94 shows the results for parametric study of the effect of mesh density on the structural behavior of flat reciprocal systems with constant engagement length relative to a 0.4 scale factor.

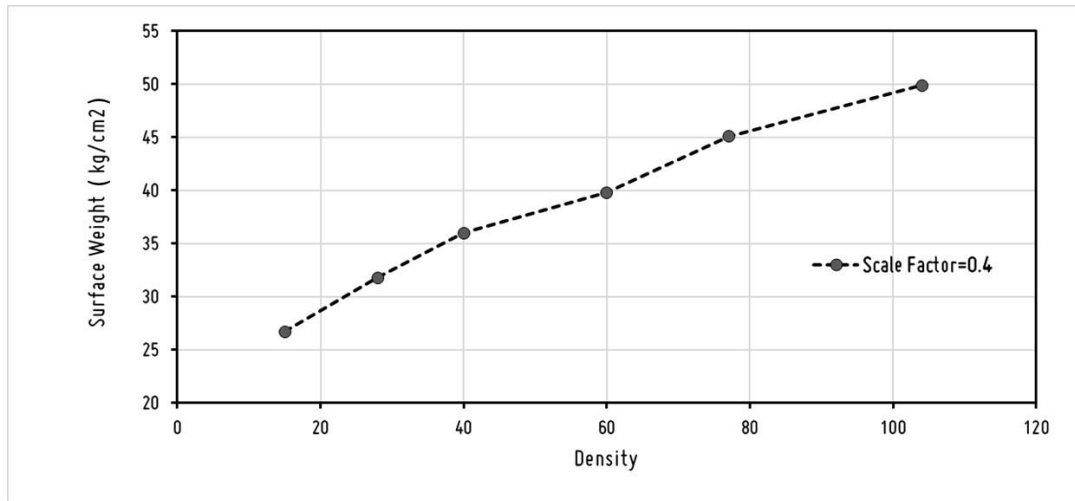


Figure 94_ Parametric study of the effect of mesh density on the structural behavior of flat reciprocal systems. Reciprocal system with engagement length of 0.4.

The results show an increase in the weight of the reciprocal structure with an increase in its density. This effect is due to the exponential increase in the number of reciprocal members, which increases the self-weight that the structure must resist. Moreover, since member sizing is based on the standard list of structural members, some members will be assigned the smallest cross section regardless of the internal forces. The result is that in reciprocal systems with a highly dense mesh the number of over-sized members increases, leading to an increase in the total structural weight.

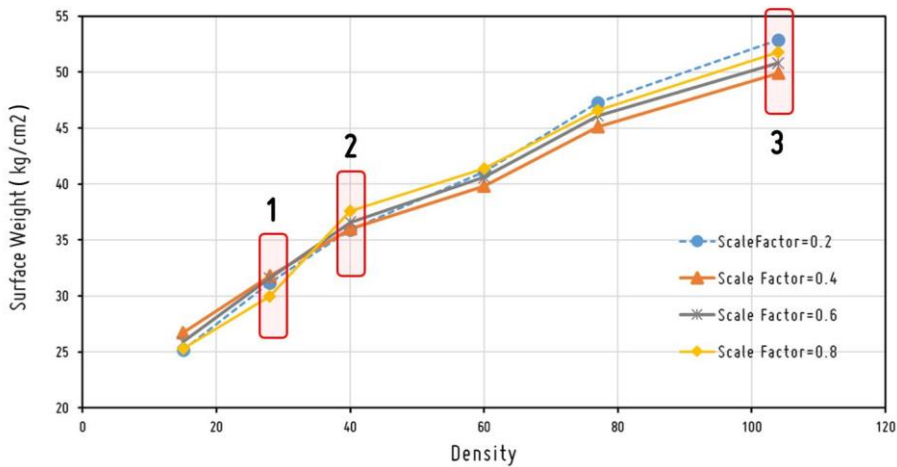
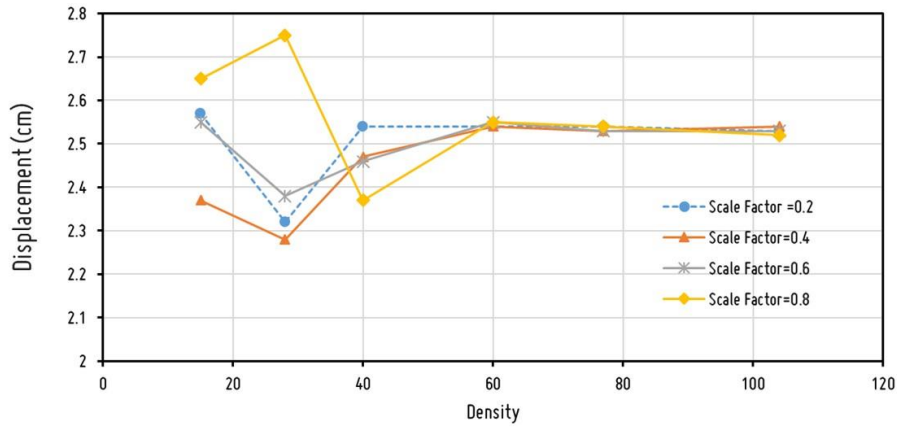


Figure 95_ Parametric study of the effect of mesh density on the structural behavior of flat reciprocal systems. Reciprocal systems with engagement lengths of 0.2, 0.4, 0.6, and 0.8.

The results from the combined parametric study of the effects of density and engagement length provides interesting insight about the complicated behavior of reciprocal systems. Earlier, when we studied the effect of engagement length (Figure 88), we concluded that for the specific mesh density under study (5 by 8), the efficiency of the reciprocal system decreases with an increase in the engagement length (also confirmed by the results in Figure 95 box number two). As depicted in the figure for density 40, the total weight of the structure increases with an increase in engagement length. However, this pattern is not consistent with other mesh densities. As we can

see in the graph in the structures with lower mesh densities (box number one), the most efficient system has the largest engagement length, and the heaviest system has an average engagement length of 0.4. In the structures with higher mesh densities (box number three), though, the least efficient structure has the lowest engagement length while the most efficient one has an average engagement length of 0.4. Figure 96 shows the mesh density and engagement lengths for the three boxes in the graph.

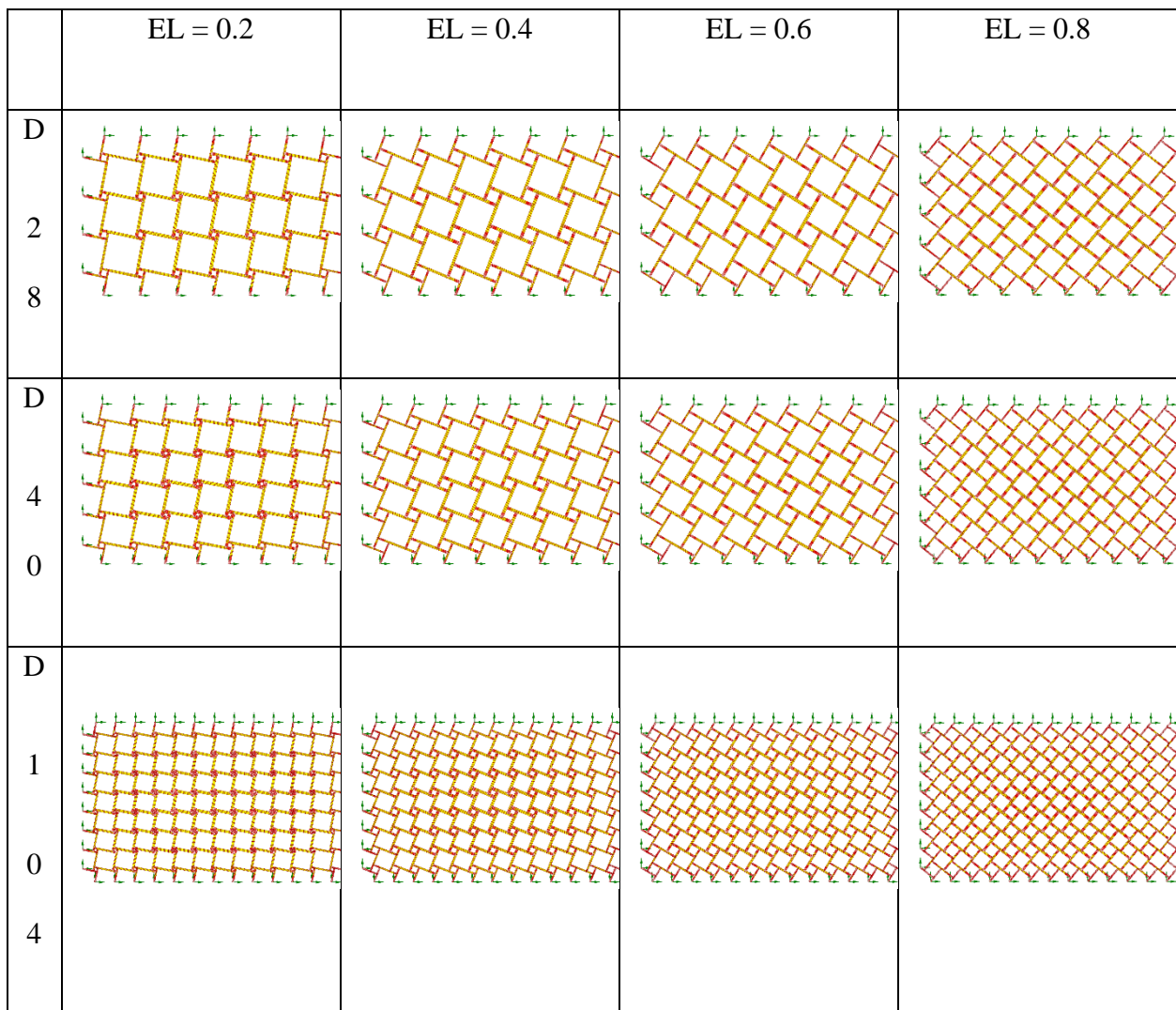


Figure 96_ Reciprocal system with variations in mesh density (D) and engagement length (EL).

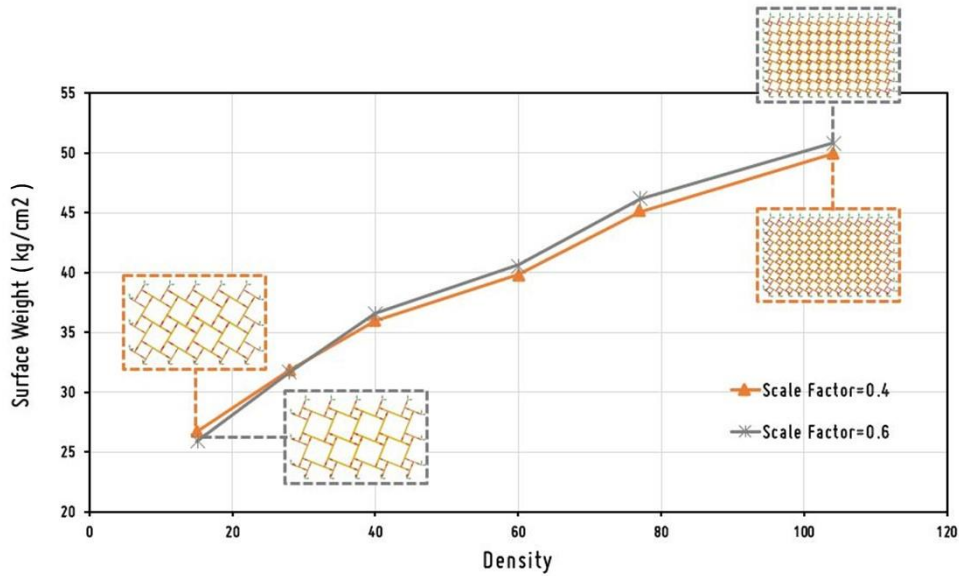


Figure 97_ Parametric study of the effect of mesh density on the structural behavior of flat reciprocal systems with engagement lengths of 0.4 and 0.6.

Based on the result shown in Figure 95, two efficient systems provide consistent behavior with variations in the mesh density (depicted in Figure 97). The most efficient system is that with an engagement length of 0.4. In the same sense, reciprocal systems with too-small of an engagement lengths will produce significant shear forces at the connections, leading to bigger member sizing and hence to heavier structures. The bigger the engagement length, the more the reciprocal action moves away from that of its efficient grid shell counterpart and toward a less efficient structure. Therefore, as a rule of thumb, the sweet spot for the engagement length in designing structurally efficient reciprocal system is somewhere less than half. As discussed earlier, these integrated systems cannot be designed solely based on their structural performance. Not only does the constructability of these systems have a direct effect on their structural performance, but the fabrication and assembly of these systems also requires specific considerations to be integrated in the design process.

4.4 Comparative study of reciprocal systems and grid shells

Grid shells, referred to in academia as “reticulated” or “lattice” shells, are a family of long-span space structures comprising a lattice of single-layer members, usually forming a curved surface. Grid shells can be made of a wide range of materials, from steel to wood, and can cross large spans efficiently (Douth et al., 2006). Depending on the material and construction method, a grid shell is defined either by its structural action or by its construction process. As an example, grid shells made from wood are formed by laying a wooden grid flat and pushing the surface up to create the final form in a bending active state, as was done in Mannheim Multihalle (Happold and Liddell, 1975), or steel grid shells optimized based on their performance, like the great court grid shell at the British Museum (Figure 98).

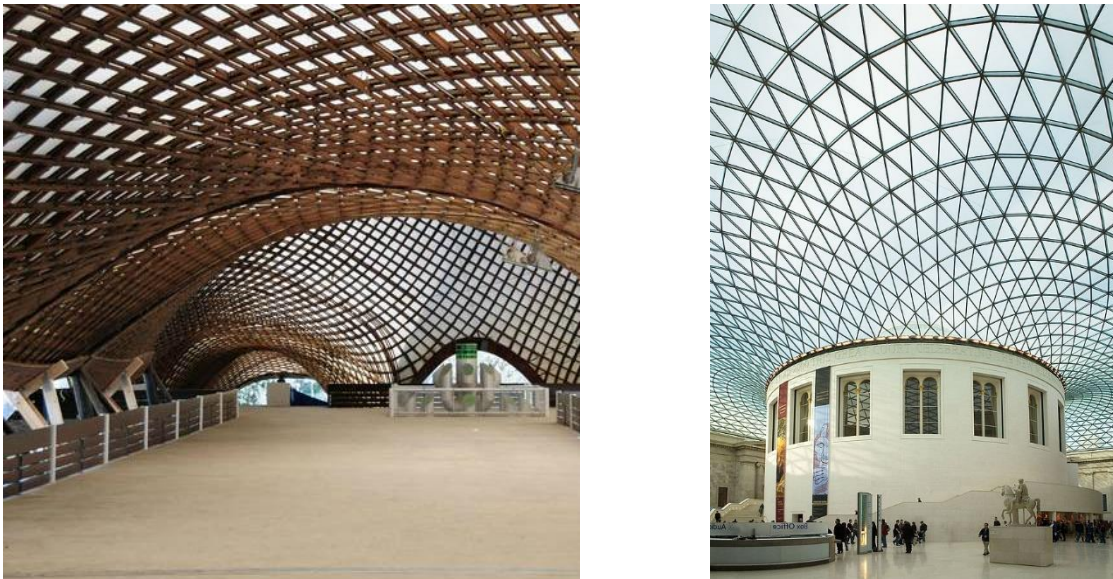


Figure 98_ Left: Mannheim Multihalle (Happold and Liddell, 1975), Right: The great court grid shell at the British Museum.

The excellent performance of grid shells come from the continuity and rigidity of the lattice, though this comes with the requirement for more elaborate and expensive connection detailing. In contrast, reciprocal systems require simple connection detailing with a modular fabrication

and assembly process that also accommodates customized variation in the geometry for modulation of lighting and shading. However, these flexibilities come with the price of lower efficiency in load bearing. Therefore, it is useful to compare the structural performance of reciprocal systems with their equivalent grid shell structures.

In this section we compare the performance of a flat reciprocal system with its flat grid shell counterpart and study the effect of density on the structural performance. Later in this chapter we show how a structurally efficient reciprocal system converges to its grid shell counterpart.

The grid shell equivalent of the reciprocal system under study is a flat grid of beams, which can be modeled directly from the underlying mesh discretization. Using the mesh edges, the grid shell members are generated and used as beam members to create a model for analysis. The boundary condition and loading are kept the same as those of the reciprocal counterpart. Figure 99 shows the reciprocal geometry and the grid shell counterpart based on a 5 by 8 mesh.

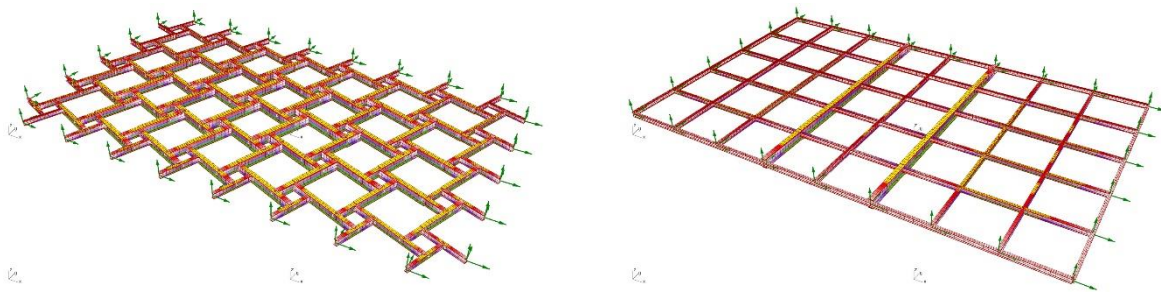


Figure 99_ Geometry and structural design of the model reciprocal system and its grid shell counterpart.

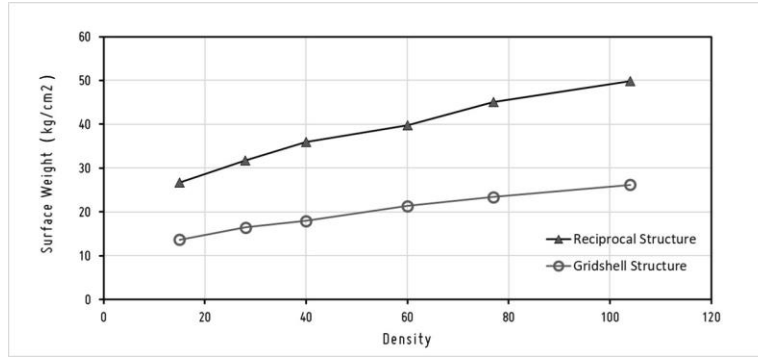


Figure 100_ Comparing the efficiency of reciprocal geometry and grid shell counterpart.

Before comparing the two system it is important to point out the similarity of the results in terms of variation in efficiency of each system with increase in structural member density. As discussed in the previous section, the efficiency of reciprocal structures decreases with an increase in member density, mainly due to the increase in the number of reciprocal members and resulting increase in self-weight that the structure. This effect is the same for grid shell geometry, as depicted in Figure 100.

The comparative study shows that, regardless of structural member density, the grid shell structure is almost twice as efficient as its reciprocal counterpart. The efficiency of the grid shell structure mainly comes from the rigidity of the connections and continuity of load path in these systems. Although the capacities of grid shells are better explored in non-planar geometries (mainly domes), the rigidity of the system is still considerable in comparison to its reciprocal counterpart. Although grid shells are usually designed in funicular shapes to reduce the bending moments in the structure toward compression-dominated system, the dominant behavior in reciprocal system is bending action (Mesnil and Baverel, 2018) which leads to an increase in the size of structural members and reduces efficiency.

4.5 Optimization of flat reciprocal systems

To this point, we have studied the effect of different geometric and analytical parameters on the structural behavior of reciprocal systems. However, up to this point we have only studied the effects of these parameters separately. Although this type parametric study offers significant insight into the behavior of the reciprocal system in relation to each parameter, it is crucial to study the cumulative effects of the design parameters to support a practical design process.

Toward this goal, two practical reciprocal design problems are proposed and solved for optimal structural performance. They are formulated as optimization problems with design constraints on stress level and deformation, then solved using a stochastic optimization method. Data from the optimization are then post-processed to study the simultaneous effect of design parameters (Oliyan Torghabehi et al., 2017).

4.5.1 Methodology

This method integrates parametric assembly design with FE analysis and a structural performance feedback loop in a process that explores the design space while minimizing the total weight of the structure (Figure 101).

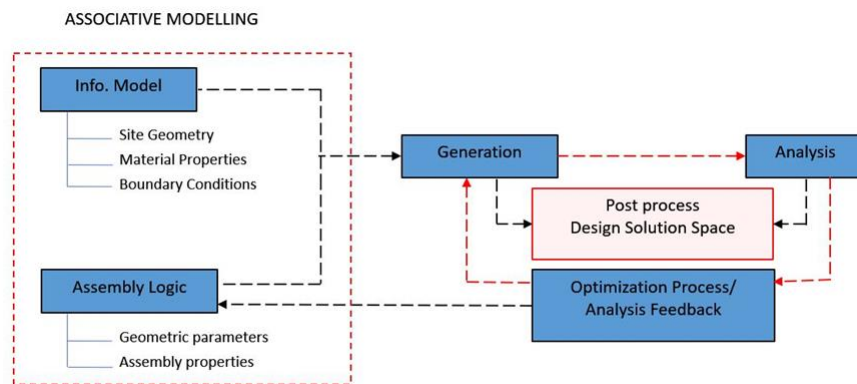


Figure 101_ Form exploration workflow and design considerations.

4.5.2 Geometry definition and parametric modeling

The first case study is a flat reciprocal structure with a structural depth in the mid-span comprising four membered reciprocal modules (Figure 102).

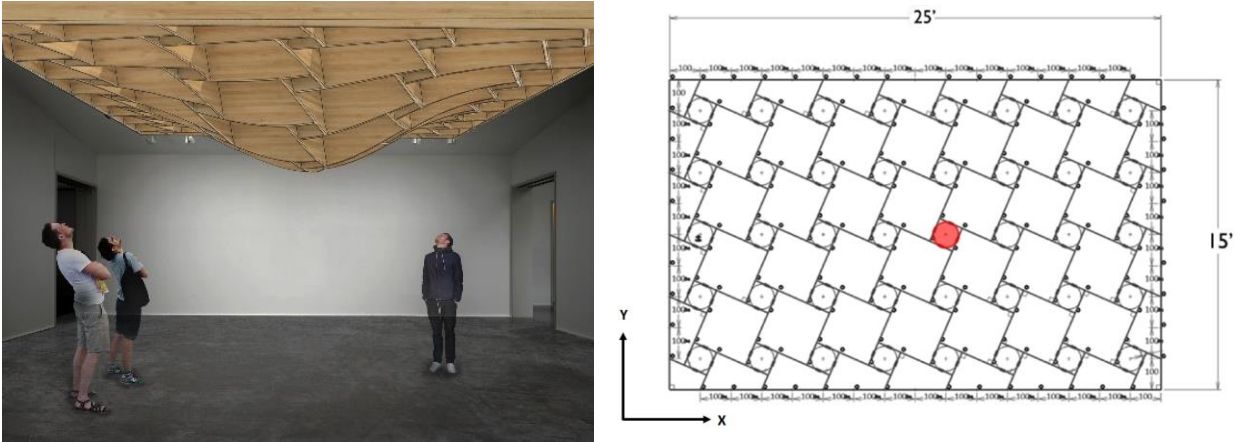


Figure 102_ First case study, 2-D parametric pattern.

The 2-D pattern mapping method for reciprocal systems with 1-D elements is used to model the associative parametric geometry. A 2-D parametric pattern of the structure was created in the XY plane and this pattern was mapped on a surface with a parametric depth in the mid span. Subsequently, the mapped members were extruded in the z direction to create the 2-D planar elements, as shown in Figure 103.

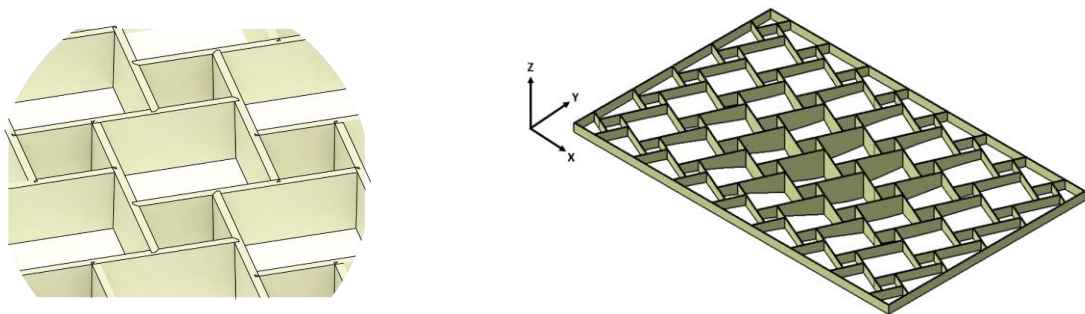


Figure 103_ Reciprocal module and the global geometry.

This parametric model has four controlling parameters: a) the reciprocal parameter, which controls the opening of the reciprocal modules based on their engagement length; b) the thickness parameter, which controls the thickness of the elements; c) the structural depth parameter, which controls the depth of the members by controlling the mid-span depth; and d) the depth on the edge (Figure 104). This parametric model is used to study the variation of form and performance metrics in the flat reciprocal structure.

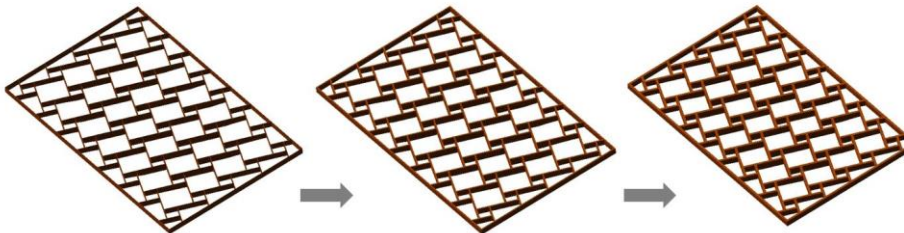
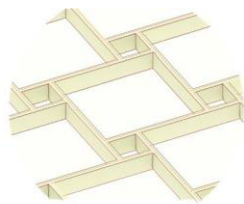
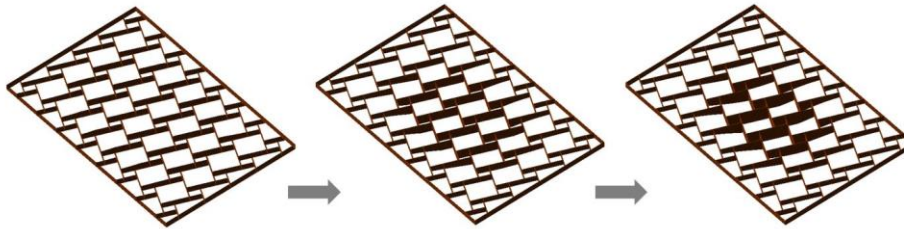
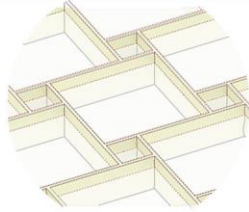
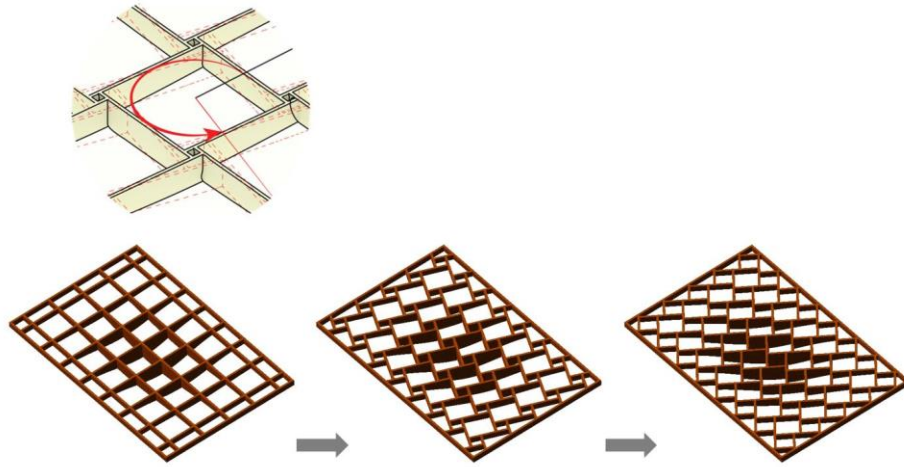


Figure 104_ Design parameters: reciprocal parameter (left), depth parameter (middle), thickness parameter (right), geometric variations based on the reciprocal changes (bottom).

The second case study uses the same 2-D pattern with uniform structural depth, in this case a rotational parameter is introduced to the model where planar elements rotate around their longitudinal axis based on an angular parameter. This angular parameter is an important agent which transforms the reciprocal geometry, allowing the assessment of non-orthogonal typologies of modules and their effect on the structural performance (Figure 105).

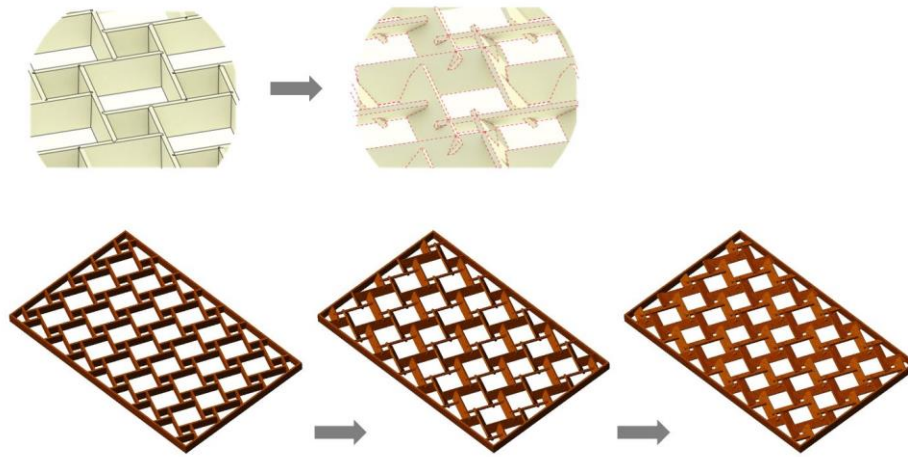


Figure 105_ Rotational parameter and transformation of the reciprocal system to a non-orthogonal configuration.

4.5.3 Simulation model

Structural models for the two case studies are created with fixed boundary conditions on four edges. A 30 psf snow load and a 15 psf cladding load are applied to the structures in addition to self-weight. The material properties of Northern Red Oak wood are used for both case studies (Figure 107).

Instead of the simplified method for the analysis of flat reciprocal structures using simplified 1-D elements, in this study a 3-D finite element analysis is applied for structural analysis. A fine 3-D finite element mesh describes the 3-D geometry of the rotated connections and correct

representation of stress concentrations and guarantees a more accurate structural analysis of the structure (Figure 106).

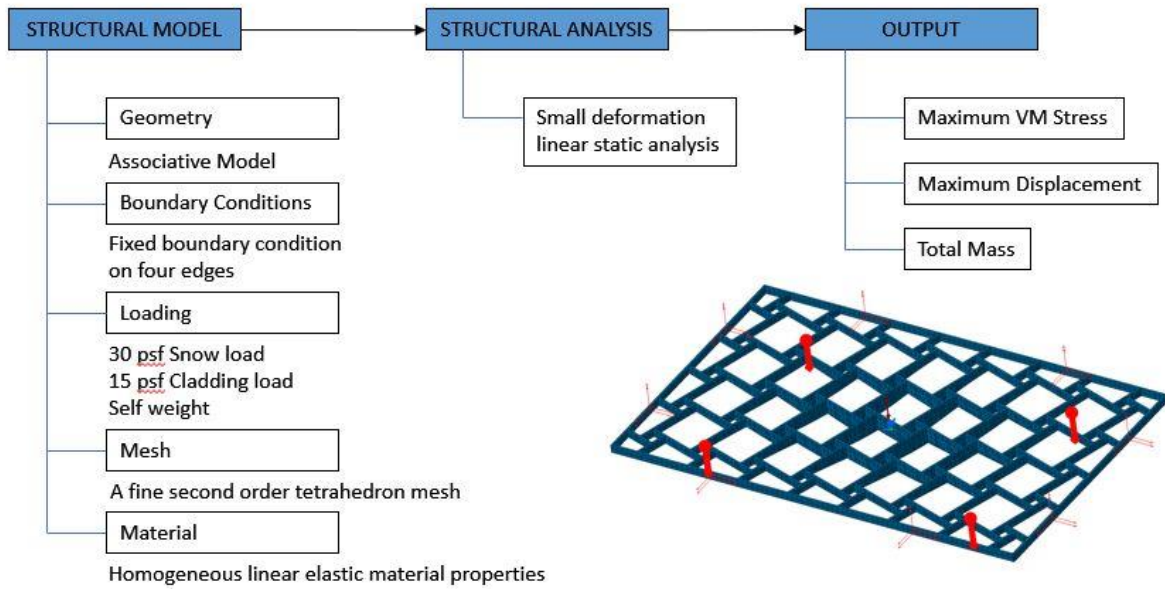


Figure 106_ Analytical model.

The results of analysis (maximum stress and maximum deflection) are fed back into the optimization process, which informs the design parameter changes for the next iteration (Figure 108).

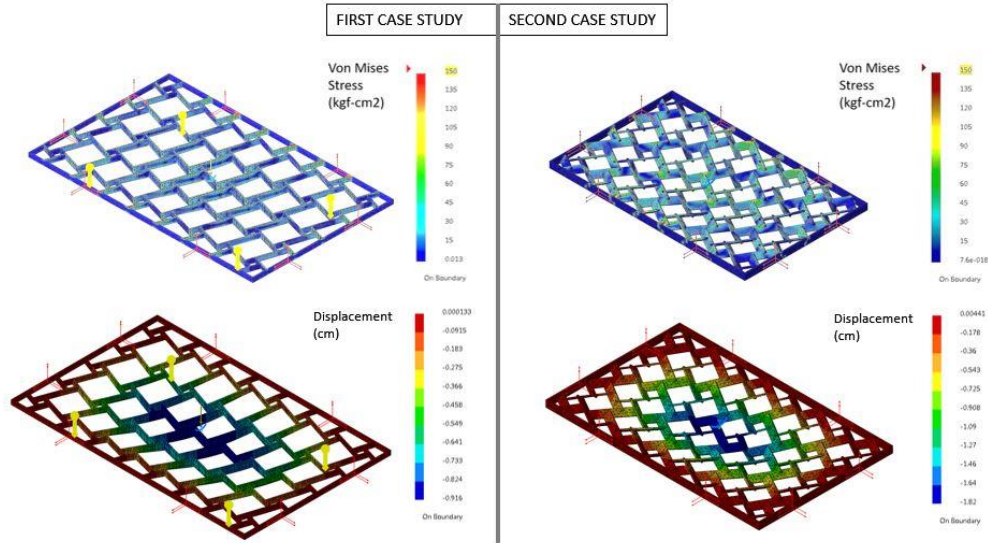


Figure 107_ Structural model and FE analysis results.

4.5.4 Form exploration

Computational optimization methods for form exploration are primarily suited for well-defined design problems, and the choice of the method is often a trade-off between computing time and the nature of the solution space. However, in design, the definition of a parametric model, boundary conditions, and solution domains, together with the understanding of how the optimization project actually performs the search for the suitable shape, is more important than reaching an optimal result (Gerber, 2007). Thus, population-based form exploration methods that incorporate a database of solutions have become popular in the form exploration processes.

In the current study, CATIA (a software package developed by Dassault Systems for CAD, CAM and CAE) has been used for the analysis and optimization process. The Product Engineering Optimizer (PEO) workbench is used to integrate parametric modeling and FE simulation with feedback of results into the optimization process. The optimization algorithm changes the design parameters stochastically toward convergence to the optimal solution.

Moreover, the simulation data from each step of the optimization process is stored for post-processing and exploration of the design space.

Simulated Annealing (SA) is chosen among the available optimization algorithms in the PEO workbench. The stochastic nature of SA can accommodate the nonlinearity of the proposed optimization problem and improve the exploration of the design space. The results of the form exploration for 400 iterations are stored in a database for post processing. The optimization formulation for the case studies are given in Table 2 and Table 3.

Minimization Target Function	Total Mass (kg)
Constraints	Max Von Mises < 300 (kg/cm ²) Max Displacement < 2 (cm)
Variable Bounds	0.5 (cm) < Reciprocal < 70 (cm) 1 (cm) < Mid-span depth < 20 (cm) 5 (cm) < Edge Thickness < 30 (cm) 1 (cm) < Thickness < 8 (cm)

Table 2_ Optimization formulation definition for the first case study.

Minimization Target Function	Total Mass (kg)
Constraints	Max. von Mises < 300 kg/cm ² Max. Displacement < 2 cm
Variable Bounds	0.5 cm < Reciprocal < 70 cm 5 cm < depth < 50 cm 1 cm < Thickness < 8 cm 1 deg. < Rotation < 70 deg.

Table 3_ Optimization formulation definition for the second case study.

Through the iterative optimization process design parameters are changed based on performance feedback toward minimization of the total mass of the structure. A range of design solutions are explored and stored for post processing towards the further study of geometric configurations with corresponding structural and geometric performances (Figure 108).

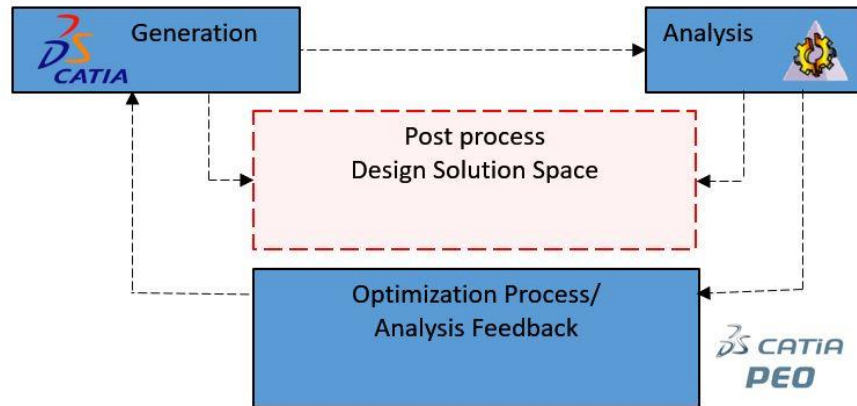


Figure 108_ Iterative optimization process toward minimization of the total mass based on performance feedback.

4.5.5 Optimization results and post processing

In this section, we study the numerical results of the optimization with a focus on the geometric variations and changes in the design parameters of the reciprocal assembly for each case study. The results of the optimization process for the first case study are shown in Figure 109. The minimization process converges at around 400 iterations. Some of the critical design solutions found in the process of form exploration are shown to demonstrate the geometric variations.

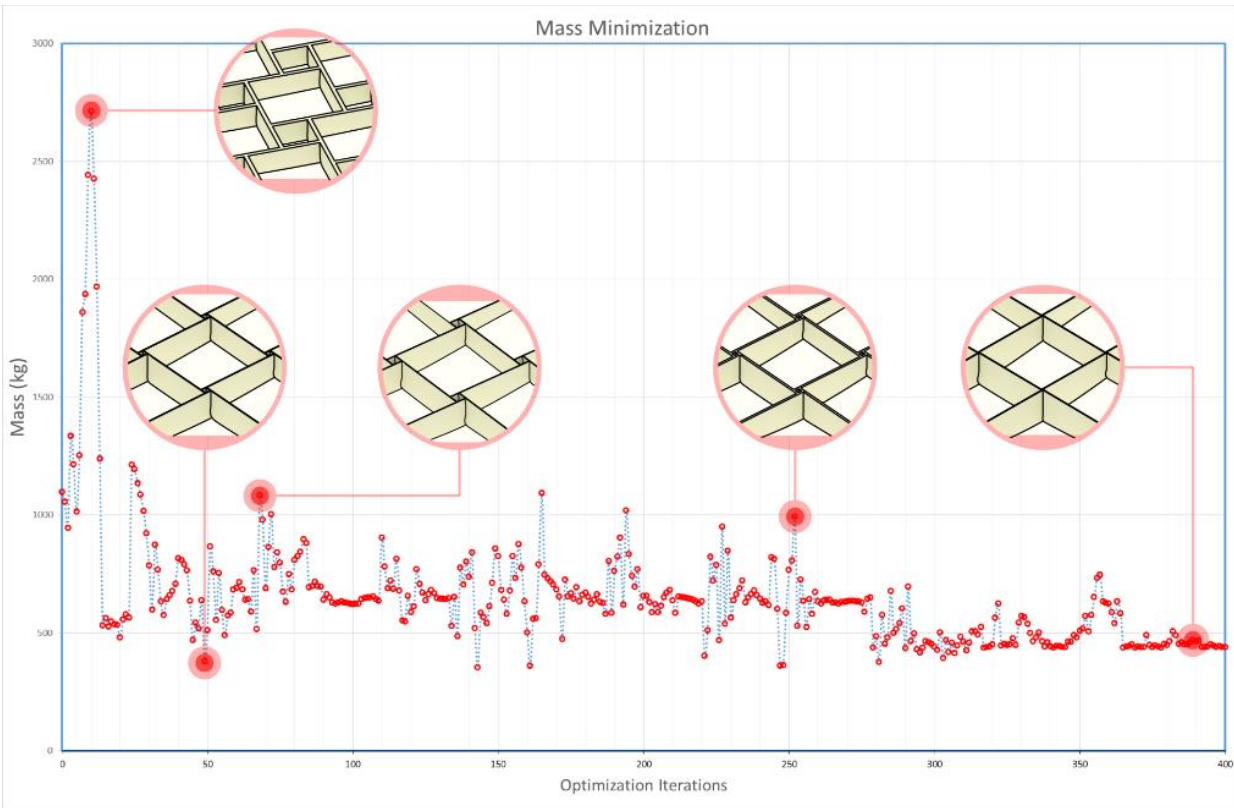


Figure 109_ Optimization results for the first case study.

In this case study, the numerical results indicate that the local optimum solution has the minimum engagement length (Figure 109). This specific case study is interesting as it demonstrates the transition of the discrete reciprocal geometry with larger engagement lengths to a more continuous configuration, close to a grid shell, as the engagement length decreases toward zero in the process of optimization. This transition shows the behavioral connection between these two types of structural systems, Moreover, theoretically, this transition from a discrete geometry of a reciprocal system to a continuous geometry of a grid shell is a proof of convergence to the global minimum for the optimization process, as the existence of a more continuous load path in the geometry increases the loadbearing efficiency of the system. These

results were also validated by the parametric study of the effect of engagement length on loadbearing efficiency in Figure 88.

Figure 110 to Figure 113 show variation of the design variables through the process of optimization and the interaction of depth, thickness and reciprocal parameters toward an optimal combination.

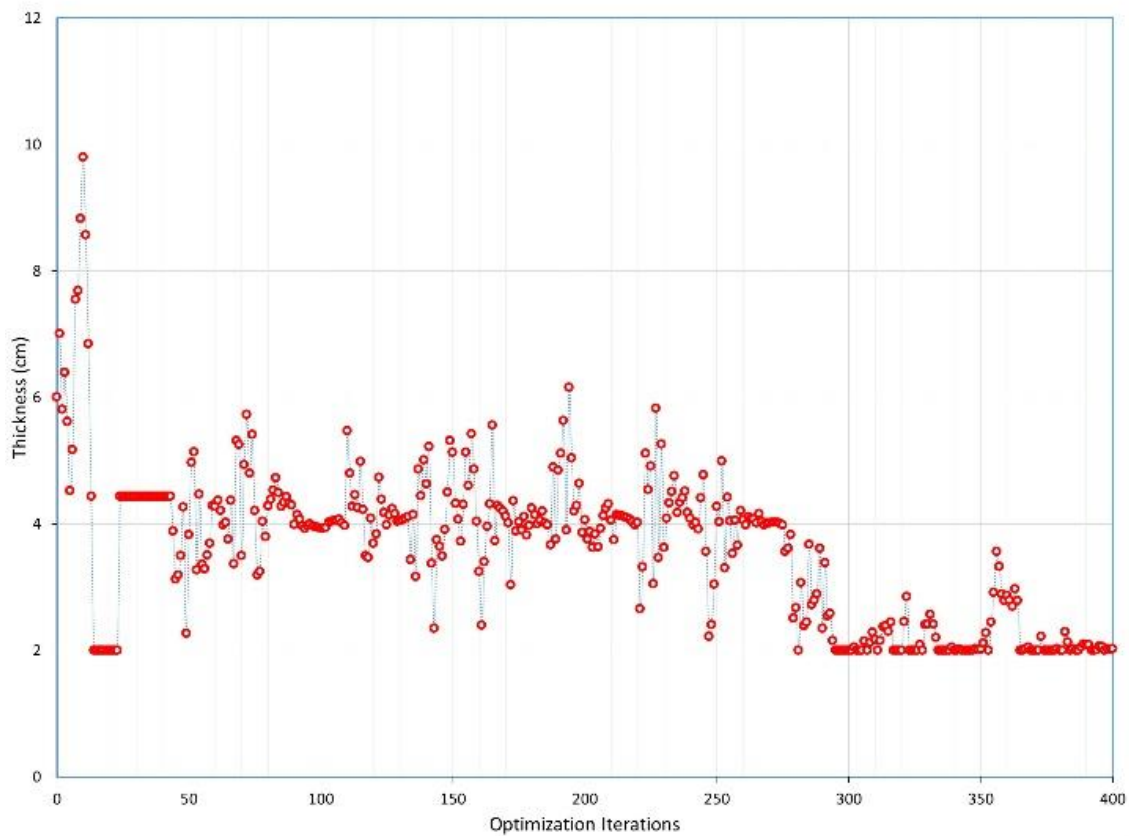


Figure 110_ Variation of member thickness through the optimization process.

The graph in Figure 110 shows the variation in member thickness through the optimization process. The member thickness converges to the minimum thickness to reduce the total weight.

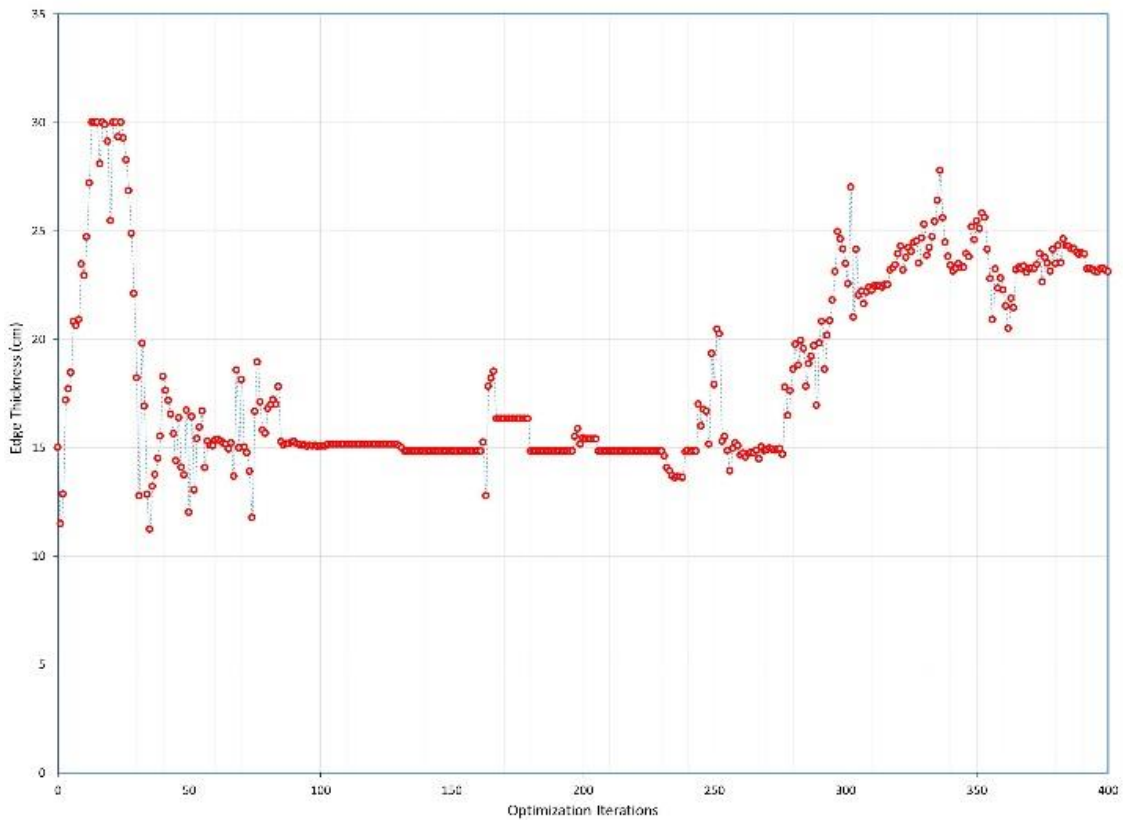


Figure 111_ Variation of the edge depth through the optimization process.

Figure 111 shows the variation of the edge depth through the optimization process. It is interesting that in the final stages of the optimization the edge depth increases to 24 cm. This increase results from the boundary conditions at the borders of the structure. Due to the application of fixed supports, negative moments emerge at the borders, and the structure tends to become thicker to reduce the bending stresses.

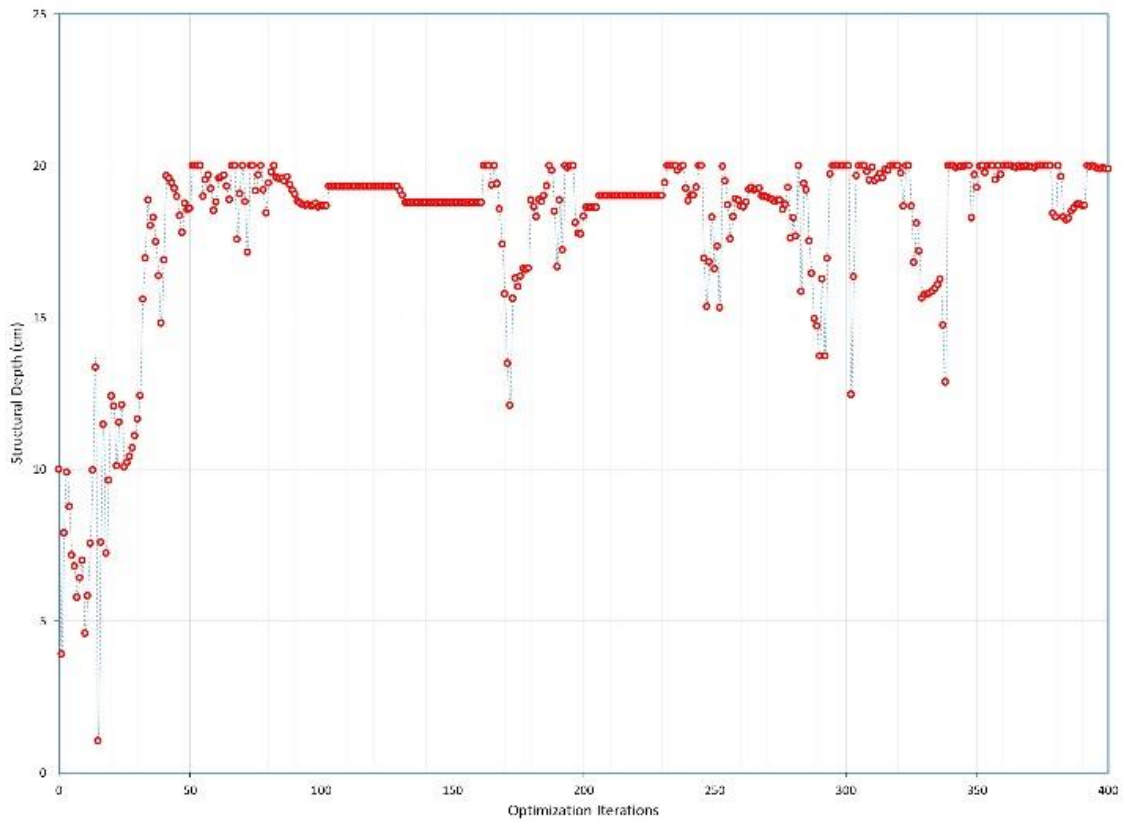


Figure 112_ Variation of structural depth through the optimization process.

The variation of the structural depth of the structure through the optimization process is shown in Figure 112. Interestingly, it shows that the structural depth approaches its maximum in the optimization process to reduce maximum deformation to keep it within the limits. The increase in structural depth helps reduce the bending stresses in the middle of the structure.

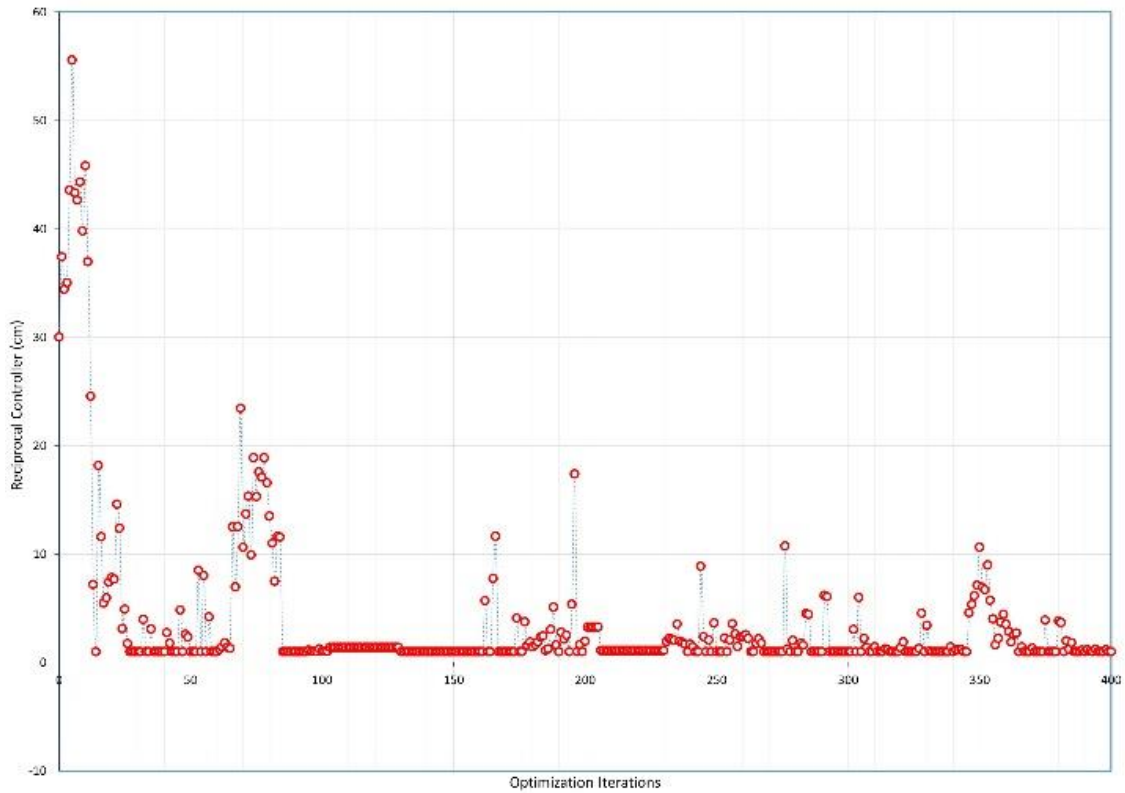


Figure 113_Variation of the engagement length through the optimization process.

Figure 113 shows the result for the variation of engagement length in the reciprocal structure under study. The results show how the search algorithm jumps to the minimum engagement length in the search for the optimal design. This result was expected, as we previously studied the effect of engagement length on the optimal design of reciprocal systems (previous section, Figure 88) and the reason, as explained earlier, is related to the convergence of a reciprocal structure to its optimal grid shell configuration, with zero engagement length.

However, there is a difference between the results in Figure 88 and Figure 113 that arises from differences in the simulation model. First of all, the simulation model used to produce Figure 88 uses a 1-D beam equivalent analytical model for FE analysis to calculate the results, and does not

have the capacity to reduce the engagement length to zero due to the type of geometric modelling. More importantly, the graph results show that as the engagement length falls below 0.2, the efficiency of the reciprocal structure decreases. As was explained earlier, with very small engagement length the shear forces increase significantly in the connection areas and becomes dominant in the design of the member sizing, which will dictate bigger member cross-sections at the connections and increase the overall weight of the structure. However, Figure 113 shows the results for solid geometry modelling and 3-D FE analysis of the reciprocal structure to calculate stresses in the structure. This model has the capacity to reduce the engagement length to a theoretical zero and calculate the stresses in the 3-D members. Since this simulation model calculates the stresses in the members, the acceptance criterion is the allowable stress level, and the model does not design the member cross-section. So, the combined stresses do not change the member cross-section size proportionately. As a result, the optimal reciprocal geometry can converge to the theoretical optimal grid shell geometry. This is vital, since, although the 3-D FE analysis model can provide a detailed result for the stress distribution, a 1-D beam equivalent analysis will provide more practical results if the structure is designed based on the building code.

The same optimization process is used to incorporate a rotational parameter that transforms the modular assembly of the reciprocal system. The transformation of the geometry and evolution to the optimal geometry can be studied through the optimization process, as shown in Figure 114.

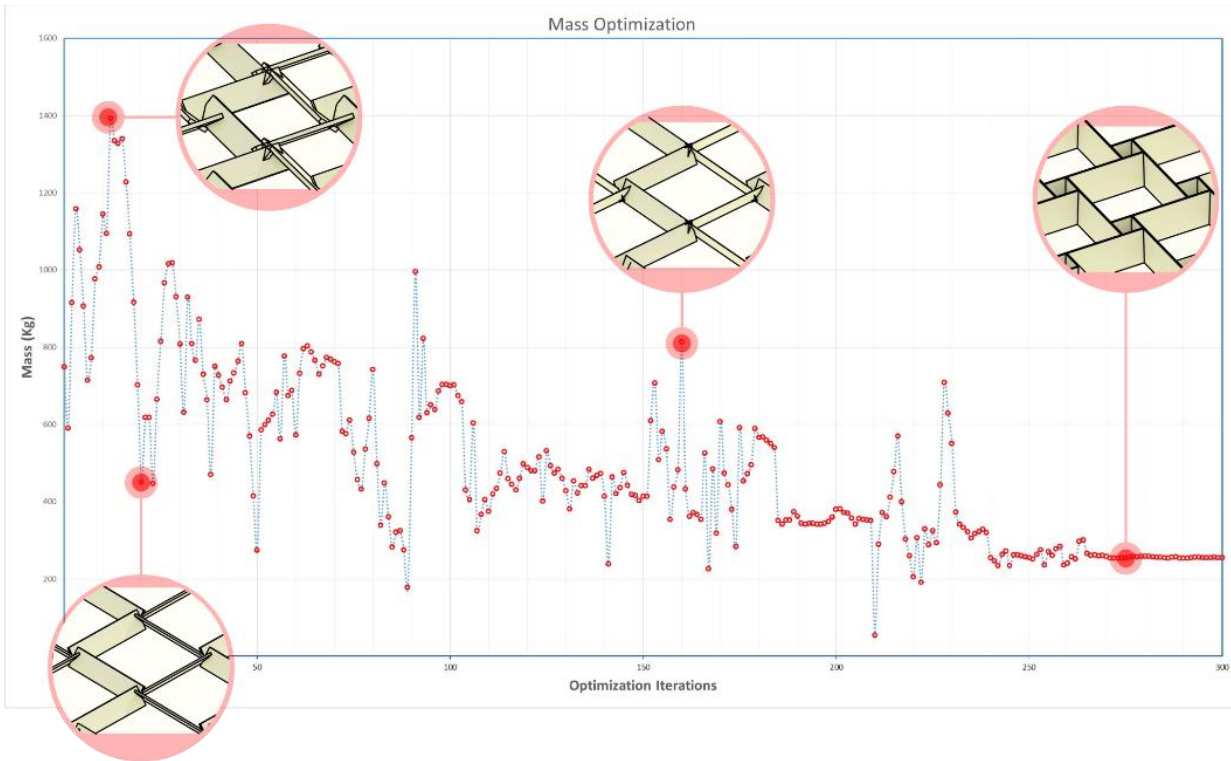


Figure 114_ Optimization results for the second case study and geometric transformation.

As stated earlier, the focus of the second case study is to change the standard assembly of reciprocal systems. This change has been implemented through the introduction of a new geometric parameter that rotates the reciprocal elements around their longitudinal axis. The rotational parameter changes the orthogonal configuration as well as the aperture of each cell, which affects the structural performance of the system as well as the openness of its geometry.

The numerical results show that the optimization process converges to an orthogonal reciprocal configuration as the rotation parameter approaches zero, which corresponds to the fact that larger rotation angles decrease the structural depth, and consequently the loadbearing capacity of reciprocal systems. However, this rotational parameter controls the aperture of the reciprocal cells, which can be used, for example, as a design parameter for the shading performance of the

structure. These results correspond with the result of the parametric study of the rotational angle in a reciprocal module shown in Figure 72.

4.6 Discussion

This chapter attempts to provide an overall understanding of the structural behavior of reciprocal systems with respects to constructability and assembly considerations. Using a parametric approach, this chapter shows the use of simulation to quantitatively study the effects of different design parameters on structural behavior. The parametric study is carried out on different scales of reciprocal member, reciprocal module, and reciprocal structure.

A flexible and scalable analysis method is proposed and implemented to study the effect of design parameters on the structural behavior and flexibility of reciprocal systems. The geometric complexity of these systems and the inherent eccentricities between the members lead to complications in translation of the geometric model to the analytical model. Multiple methods have been proposed for this purpose, and each have their own limitations in application or compromise in the accuracy of results. In this chapter, we proposed a geometric method which translates the reciprocal geometry into a simplified structural model. This model can be analyzed using commercial structural analysis software while maintaining the accuracy of performance evaluation for large-scale design purposes. Moreover, the proposed analytical model can accommodate the effect of different member connections, including the rigidity and load bearing capacity of the structure.

Focusing on the four-membered reciprocal modules, the main design parameters, including mesh density, engagement length, rotation angle, member depth and member thickness, are

determined, and their effect on the loadbearing capacity and flexibility of the reciprocal system studied. This study provides practical insights about the structural performance of these systems.

Based on the behavior of reciprocal systems, bending is dominant even in funicular shapes, so real-time feedback from FE analysis is necessary to design the optimal structural shape. The main advantages of the proposed method are that it is fast and can be used for analysis of reciprocal systems using existing commercial software. In addition, this method is generalizable and can be applied to non-flat reciprocal systems with drastic curvature changes. Another advantage of this method is increased control on the boundary condition of the elements at the connecting points, since we are treating each reciprocal element as an assembly of three beam elements. This is important, since the degree of rigidity at the connection condition is defined based on the connectivity method and the fabrication detailing.

In this chapter, the analysis starts with modelling and simulation of a single reciprocal module to determine the main design parameters and understand the mechanical behavior of the module, then the model is used to parametrically study the module behavior in relation to controlling geometric parameters. This process is then extended to a flat reciprocal system to study the overall behavior of the reciprocal systems with multiple reciprocal modules and verify the applicability of the proposed method for large-scale analysis and design.

The results show that the effect of engagement length on the loadbearing capacity cannot be studied using a single module and must be addressed in a multi-module reciprocal structure. The results also show that an increase in rotation angle and reduction in member depth substantially reduce the efficiency of the reciprocal module (via a second-order relationship).

After analysis of a single reciprocal module, the method is applied to a sample flat reciprocal system. However, for analysis of the reciprocal system a member design procedure is integrated into the performance evaluation to choose member sizes based on the results of analysis. This allows the surface weight of the structure to be used as the optimality criteria for the parametric study.

The results show that the efficiency of the reciprocal system decreases with an increase in the engagement length, as with the smaller engagement length the geometry of the reciprocal system approaches the continuous geometry of a grid shell, which is more efficient in loadbearing. However, the most lightweight design does not correspond with the smallest engagement length, since the shear forces increase at the connections, which require bigger member sizes. As a result, the maximum efficiency of the system occurs when these local shear forces dissipate.

A design approach purely driven by structural response would result in reducing the engagement length; however, the fabrication and assembly process plays a significant role in constructability of the structure, and must be addressed for a practical design process. As an example, if the engagement length is too small, access to the connection locations will be difficult, causing problems in the assembly process. It becomes clear that the design process for these systems cannot be done based solely on structural optimality, and the constructability of the design must be integrated in the process.

Understanding the conditions of determinacy and redundancy of reciprocal systems is an important issue based on the design purpose. If the connection detailing is designed to bring the minimal number of constraints to the structure necessary to obtain stability, it results in a determinate system where the size of internal forces does not depend on cross-sectional

properties or material behavior. A less rigid connection means the connection detailing can be built more easily and cost effectively.

The determinate system also shows minimal sensitivity to settlement and thermal loads; fabrication-wise, if a reciprocal member is designed or fabricated with a larger dimensional tolerance, it can fit into the system with minimal effect on the load distribution in the system. However determinate systems do not have extra redundancy and as a result lack robustness, which may lead to progressive collapse in failure. As a result, the conditions of determinacy and redundancy of reciprocal systems is an important issue based on the design purpose.

This effect was studied for different engagement lengths, and the results show that the reciprocal system with rigid connections is a stiffer system that goes through smaller deformations, a finding which is consistent through variations in the engagement length. However, the total weight of the system (optimality criterion) is almost the same for determinate and indeterminate systems but with very large engagement lengths (>0.75) the rigid system will be less efficient due to the development of negative moments at the member connections.

The proposed method has also been used to compare the behavior of a reciprocal system and its grid shell counterpart. The results show that, regardless of the structural member density, the grid shell structure is almost twice as efficient (50 percent less weight) as its reciprocal counterpart. The efficiency of the grid shell structure mainly comes from the rigidity of the connections and continuity of load path in these systems. This efficiency comes with the price of more elaborate and expensive connection detailing. In contrast, reciprocal systems require simple connection detailing with a modular fabrication and assembly process, which can also accommodate

customized variation in the geometry for modulation of lighting and shading; however, this flexibility comes with the price of lower efficiency in load bearing.

One of the most important design parameters in reciprocal structures is the mesh density of the structure which defines the number of reciprocal modules, and consequently, reciprocal members in the structure. The trade-off between the number of reciprocal members and their size is an important question to be considered in the design of reciprocal systems. Moreover, mesh density affects the perforation of reciprocal systems, which is an important design potential to integrate other performances considerations into the system.

To study the effects of mesh density on the behavior of reciprocal systems, a combined parametric study of the effects of density and engagement length has been carried out. The results provide an interesting insight about the complicated behavior of reciprocal systems: among structures with lower mesh densities, the most efficient system has the largest engagement length, and the heaviest system has an average engagement length of 0.4. In the structures with higher mesh densities, the least efficient structure has the lowest engagement length, while the most efficient has an average engagement length of 0.4. In the same sense, reciprocal systems with too-small engagement lengths will produce significant shear forces at their connections which lead to bigger member sizing, and hence to a heavier structure. At the same time, the larger the engagement length, the more the reciprocal action moves away from its efficient grid shell counterpart, leading to a less efficient structure. Therefore, as a rule of thumb, the sweet spot for designing a structurally efficient reciprocal system is an engagement length of less than half (engagement length equal to the scale factor of 0.5). As discussed earlier, these integrated systems cannot be designed solely based on their structural performance. Not only does the connection detailing in these systems have a direct effect on structural performance, but

the construction and assembly of these systems also requires specific considerations, which must be integrated in the design process.

However, the unique benefits of reciprocal systems come from their discrete geometry, which simplifies the connection detailing and provides freedom for local variations in the system. These local variations can control the openings, offering the potential for modulation of light, shading, and ventilation design to be integrated in the design process. The goal of this work is to study and activate these capacities and develop an integrative design process which informs design decisions based on the comprehensive capacities of reciprocal systems, including their structural performance, shading, material use, fabrication process, aesthetics, and expression.

References

APA – The Engineered Wood Association. <https://www.apawood.org/plywood>

Anastas, Youssef, Landolf Rhode-Barbarigos, and Sigrid Adriaenssens. "Design-to-construction workflow for cell-based pattern reciprocal free-form structures." *Journal of the International Association for Shell and Spatial Structures* 57, no. 2 (2016): 159-176.

Ding Zou and Nan Xiao. "A Standard Matrix Assembly Approach for Static Analysis of Planar Reciprocal Structures." *International Journal of Engineering and Technology* 9, no. 4 (2017).

Douthe, Cyril, Romain Mesnil, Olivier Baverel, Tristan Gobin, Xavier Tellier, Nicolas Ducoulombier, and Nicolas Montagne. "Design and construction of a shell-nexorade hybrid timber structure." In *Proceedings of IASS Annual Symposia*, vol. 2018, no. 20, pp. 1-8. International Association for Shell and Spatial Structures (IASS), 2018.

Douthe, Cyril, and Olivier Baverel. "Design of nexorades or reciprocal frame systems with the dynamic relaxation method." *Computers & Structures* 87, no. 21-22 (2009): 1296-1307.

Houlsby, Guy T. "John Wallis and the numerical analysis of structures." *Nexus Network Journal* 16, no. 1 (2014): 207-217.

Gelez, Simon, Simon Aubry, and Bernard Vaudeville. "Behavior of a simple nexorade or reciprocal frame system." *International Journal of Space Structures* 26, no. 4 (2011): 331-342.

Garavaglia1a, Elsa, Attilio Pizzigoni2b, and Luca Sgambi. "Collapse behaviour in reciprocal frame structures." *Structural Engineering and Mechanics* 46, no. 4 (2013): 533-547.

Ip, Gerry, and Corentin Fivet. "Geometric Optimization of a Reciprocal Floor-Framing System with Self-Weight and Area-Loading Considerations." In *Proceedings of IASS Annual Symposia*, vol. 2017, no. 16, pp. 1-9. International Association for Shell and Spatial Structures (IASS), 2017.

Kohlhammer, Thomas, and Toni Kotnik. "Systemic behaviour of plane reciprocal frame structures." *Structural Engineering International* 21, no. 1 (2011): 80-86.

Mesnil, Romain, Cyril Douthe, Tristan Gobin, and Olivier Baverel. "Form finding and design of a timber shell-nexorade hybrid." 2018.

McNeel, R., Rhinoceros: NURBS modeling for Windows, Computer software, 2010, available at: <http://www.rhino3d.com>

Oliyan Torghabehi, Omid. "Reciprocal Shades: A computational workflow for knowledge-based design and fabrication of multi-performance reciprocal systems." In *Proceedings of IASS Annual Symposia*, vol. 2018, no. 11, pp. 1-8. International Association for Shell and Spatial Structures (IASS), 2018.

Oliyan Torghabehi, Omid, Peter von Buelow, and Alireza Seyedahmadian. "A performance based computational method for assembly design of reciprocal architectural systems with 2D elements." In *Proceedings of the Symposium on Simulation for Architecture and Urban Design*, p. 14. Society for Computer Simulation International, 2017.

Parigi, Dario, Mario Sassone, Poul Henning Kirkegaard, and Paolo Napoli. "Static and kinematic formulation of planar reciprocal assemblies." *Nexus Network Journal* 16, no. 1 (2014): 37-59. .
Preisinger, C., Karamba: parametric structural modeling, Computer software, 2011, available at: <http://www.karamba3d.com>

Preisinger, Clemens, and Moritz Heimrath. "Karamba—A toolkit for parametric structural design." *Structural Engineering International* 24, no. 2 (2014): 217-221.

Rutten, D., Grasshopper: generative modeling for Rhino, Computer software, 2012, available at: <http://www.grasshopper3d.com>

Chapter 5: Physical Prototyping, Destructive Structural Tests, and Scaled Model Fabrication

5.1 Introduction

In the traditional sense, reciprocal structures combine the advantages of timber as a renewable source of construction material, with carbon-dioxide storage, low-energy production and favorable weight-to-strength ratio, with the modular fabrication, fabrication efficiency and structural efficiency and elegance of reciprocal interconnection of members. However, reciprocal assemblies are by no means necessarily bound to be built with wood material. These systems can be designed for range of construction materials including composites, recycled materials, steel and even concrete and masonry.

Reciprocal structures are systems comprised of relatively short members which support each other in a self-supporting, non-hierarchical and interconnected network. Baverel and Popovic situated the reciprocal systems in the context of woven structures and classify them according to their characteristics and the mechanical behavior of each system (Figure 115) (Baverel and Popovic, 2011).

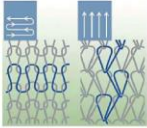
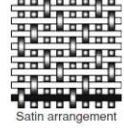

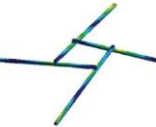
Woven structures				
Type	Knitting	Woven fabrics	Basket work	Reciprocal structures or Nexorades
Characteristics	Continuous elements Linked only with adjacent elements	Continuous elements Crossing with other elements	Continuous and discontinuous elements	Discontinuous elements
Example		 Satin arrangement		
Bending Stiffness of the elements	Very low	Very low	Medium	Medium to large

Figure 115_ Classification of woven structures based on their characteristics and bending stiffness. (Baverel and Popovic, 2011).

As a discrete system, reciprocal members are connected with joints, and the behavior of these joints has significant effect on the structural performance as well as the fabrication and assembly of these systems. Moreover, the nonhierarchical nature of these systems and lack of redundancy (the stability of the system is sensitive to stability of all of the members which means, in case of few members failure a progressive collapse of the structure may happen) requires development of a practical design for the member joinery. On the one hand a good connection design can guarantee the structural integrity and on the other hand it can facilitate the fabrication and assembly process of prefabricated reciprocal systems. Other factors in design and fabrication of reciprocal members joinery system include precision, affordability, rapidity and guides for the assembly, especially in fabrication of nonstandard reciprocal systems. As a result connection detailing is an important design parameter in reciprocal systems which directly effects the structural performance and more importantly defines the constructability and reliability of the assembly process.

The interconnection between, form, mechanical behavior and fabrication process in reciprocal structures requires an integrative design process that integrates fabrication parameters and

performance feedbacks into the design process. This chapter studies the fabrication and assembly process for reciprocal systems through investigation of different joinery systems and their design parameters, their fabrication properties, their mechanical properties and their assembly process. The generalizability and scalability of the proposed method is tested through design and fabrication of a scaled half-arch reciprocal geometry.

5.2 Fabrication data generation and analytical model development

As was explained in Chapter 3 the non-hierarchical and interconnected nature of a reciprocal structure's network requires a form-finding process for free-form reciprocal systems design. The proposed design and form-finding process generates the wireframe geometry of the reciprocal structure. The proposed method effectively reduces the eccentricities between the reciprocal members. However there might be minimal residual eccentricities between some of the members after the form-finding process. These residual eccentricities should be addressed in both developing the analytical models for structural analysis as well as fabrication models for digital fabrication. This section explains the 3-D fabrication data generation as well as analytical model generation for structural performance simulation.

5.2.1 Generating 3-D reciprocal member geometry

The proposed reciprocal pattern generation formulation introduced in Chapter 3 generates the required geometrical and topological data for definition of the reciprocal structure. Moreover, the formulation generates a series of structured data which is required to design the fabrication detailing including 3-D member geometry and connection detailing. The first data set identifies the reciprocal members in each reciprocal module of the reciprocal system. This data is specifically important since due to the interconnected nature of the reciprocal network every

reciprocal member is shared with two reciprocal modules, as a result any variation (variation in member rotation or perforation depth) will propagate in the system through the shared members. The second data set identifies the four intersecting members to each reciprocal member, this data is required to firstly calculate each intersection point based on the existing residual eccentricities and then generate a new wireframe member for analysis purposes based on the calculated intersection points. Secondly, these intersection points are needed to generate connection detailing data (Figure 116).

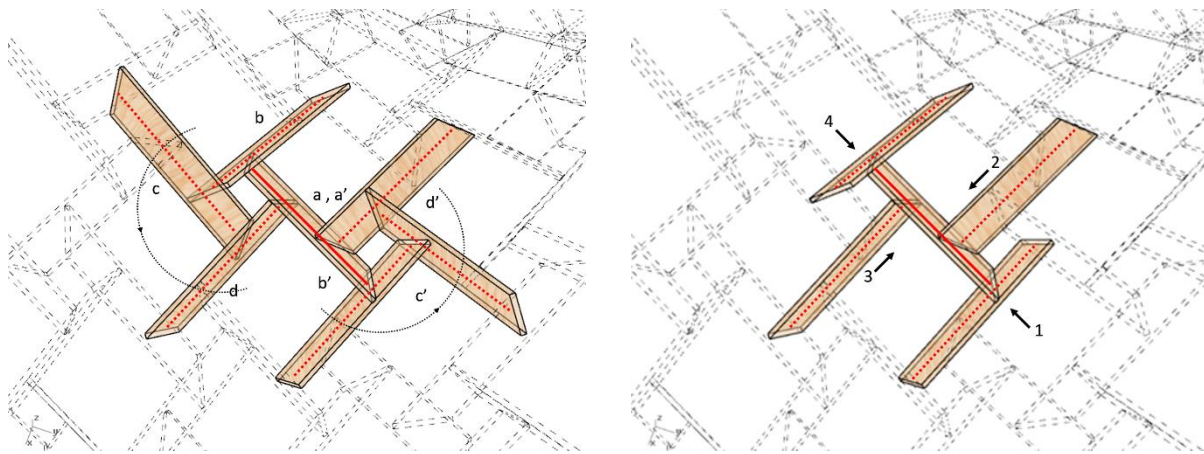


Figure 116_ Left: Generating reference and storage data for the reciprocal members in each reciprocal module of the reciprocal system. Right: Generating reference and storage data for the four intersecting members to each reciprocal member for fabrication purposes.

The wireframe geometry is basically the center line of the reciprocal members. In this research rectangular member cross-sections with large height to width ratio (bigger than 4) are considered to generate the reciprocal member geometry. These considerations relate to the construction considerations and efficiency of using flat sheet materials for fabrication. Also, a large height to width ratio guarantees construction of reciprocal systems with perforation depth which has

applications in modulating light and generating shades. However, the parametric process can be modified to accommodate any cross-section types: circular, rectangular, or irregular.

Cross-sections are oriented along each element following the Darboux-frame convention (Figure 117). Where the expansion of the reciprocal member is defined by the normal of the underlying mesh face geometry (Figure 117). Once the orientation is determined, the surface geometry of the member is generated based on the depth parameter. Once the surface geometries of the members are generated, they are cut by the intersecting members at the two ends.

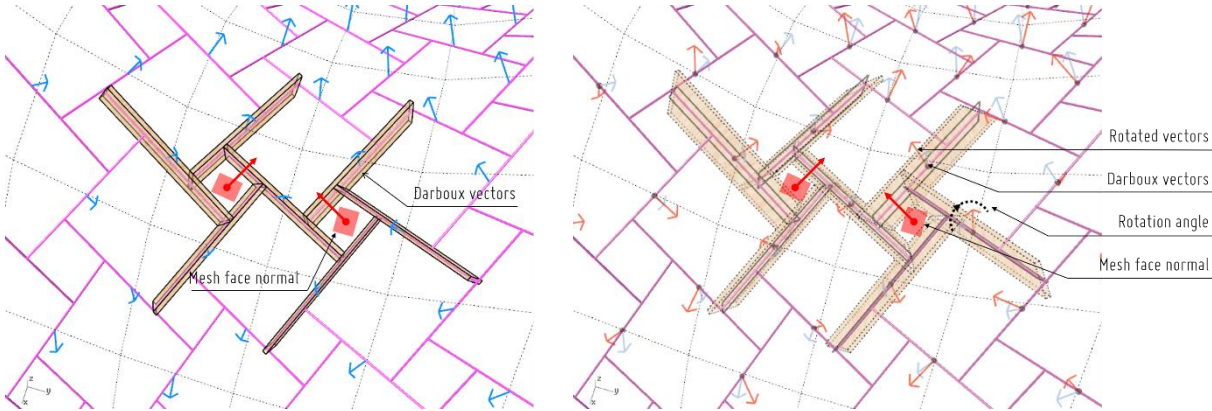


Figure 117_ Left. Member orientation is generated based on the Darboux-frame convention. Right Rotation parameter controls the angle between the Darboux-frame vector and the member orientation.

These trimmed surfaces are used to generate the 3-D solid geometry of the members based on the member thickness parameter or the calculated member thickness based on the structural requirements (Figure 118).

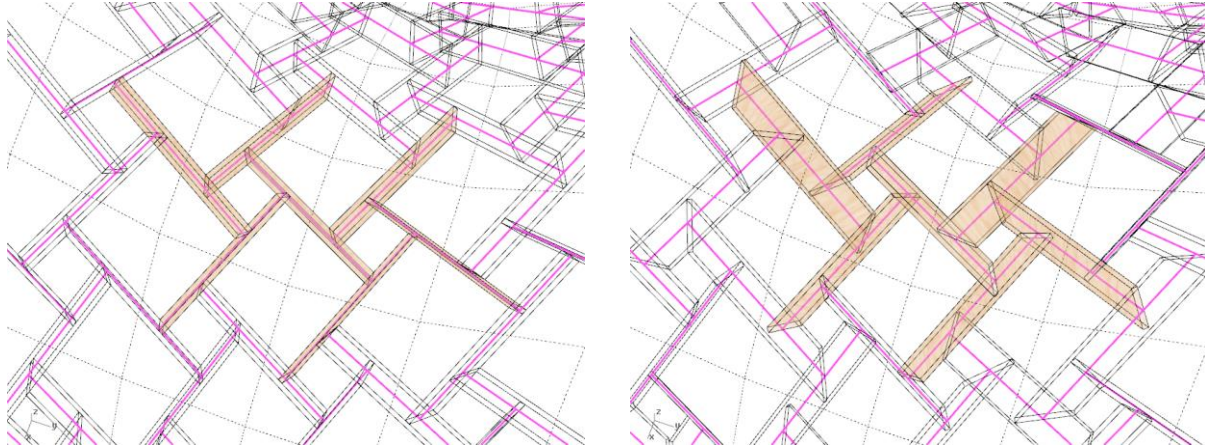


Figure 118_ Solid geometry of the reciprocal members. Left: Members following the Darboux-frame convention, right: application of the rotation parameter.

5.2.2 Generating analytical model from the wireframe geometry

As was mentioned earlier, the form-finding process will minimize the eccentricities but will not eliminate them for all members, however for development of the analytical model these eccentricities need to be addressed either by generation of highly rigid linking members or by eliminating the eccentricities by regeneration of reciprocal members based on the calculated connection points. As was investigated in Chapter 3, the residual eccentricities are negligible. As the result it is accurate enough to regenerate each reciprocal member from the calculated intersection points from four intersecting members. These new members are used to generate the analytical model where each reciprocal element is discretized into three beam elements each with 12 degrees of freedom (Figure 119).

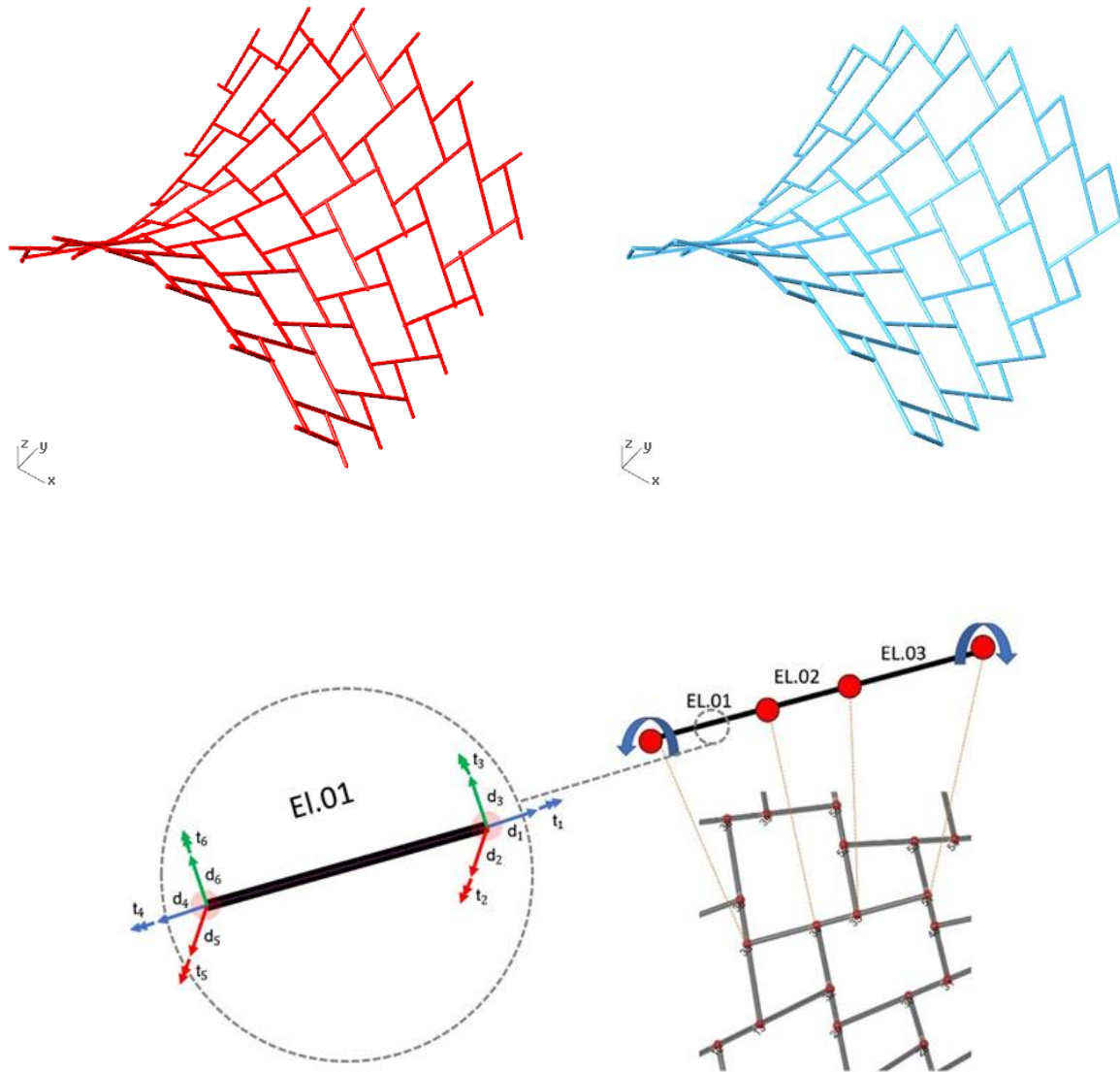


Figure 119_ Regeneration of reciprocal members based on the calculated connection points. And generation of three beam elements for structural analysis.

5.3 Reciprocal connections

5.3.1 Design parameters and types of reciprocal connections

In design and fabrication of discrete systems connections are one of the most important aspects of design. On the one hand, in the structural systems connections are usually the weak points of the structure in the loadbearing process, hence they should be designed to guarantee the structural integrity. On the other hand, the connection detailing directly effects their assembly process, especially in the interconnected systems such as reciprocal systems.

In the past, joining was often an afterthought, even though the need was obvious. Instead of joining being a secondary process, in the material synthesis common to most manufacturing or construction methods of the past, it will increasingly become a primary process that occurs at the same time as other steps in the design process (Messler, 2004).

Messler's vision for the future of design to construction is reflected in the contemporary fabrication-aware design processes. Where constraints of fabrication and constructability are directly integrated in the design process. In this regard, there are different fabrication parameters (tolerances of the digital fabrication machinery, material dimensional tolerances, geometric modeling and form-finding tolerances) that can be addressed in the design process of joints.

Figure 120 shows different types of wood joinery through application of digital fabrication. The flexibility and accuracy of digital fabrication enables designers to design and build more complex joinery systems which are more responsive to the design needs or more aesthetically pleasing. More importantly, availability of digital fabrication for design purposes opens up new opportunities for design and fabrication of systems which would not be constructible or cost effective otherwise.

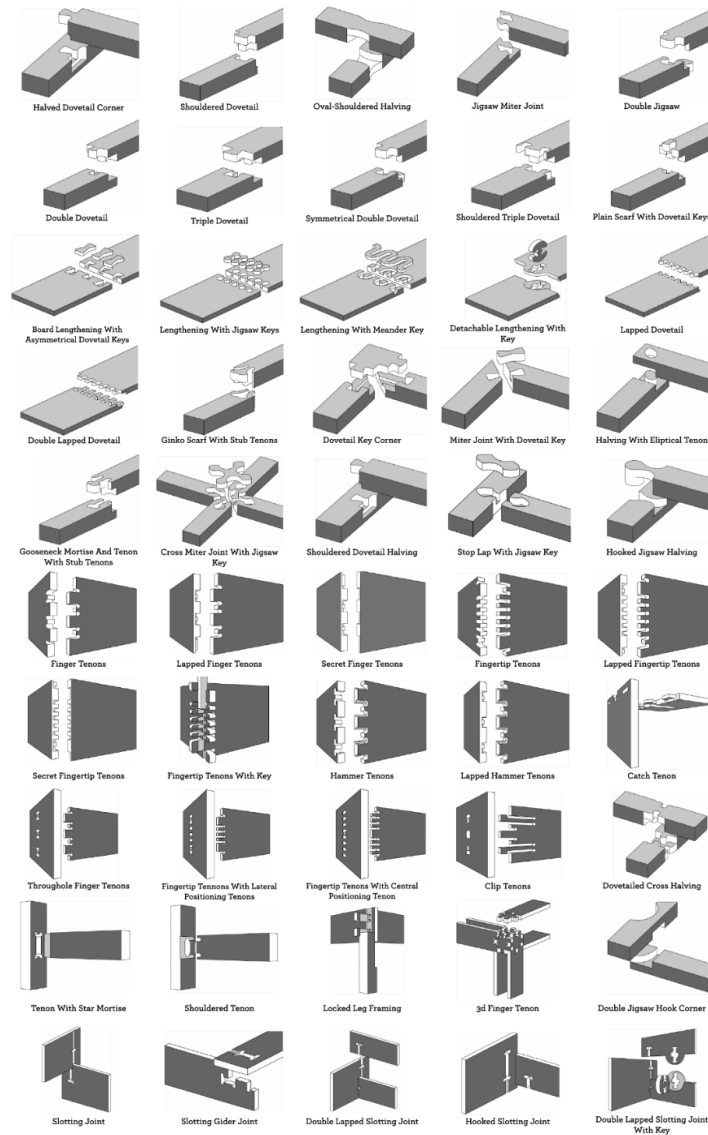


Figure 120_ 50 digital wood joints project by Jochen Gros. www.flexiblestream.org

As was explained in Chapter 3, one effective way to design safer and more cost-effective connections is to reduce the complexity of connections through reducing the number of members connecting at each node. This is one of the benefits of reciprocal systems, as by definition, connections in reciprocal systems are 2-valent, meaning that only two members meet at a connection this reduces the complexity of the connection which can be designed for minimal

material use and also can expedite the assembly process (Mesnil et al., 2018). Reciprocal structures are considered as a practical way to reduce the complexity of member connections, however, this reduction in construction complexity is replaced with geometrical complexity due to numerous compatibility constraints in the form-finding process.

Conventional reciprocal structures were comprised of rod like members with circular cross-sections. The tubular geometry of members creates minimal connection area between the members in these systems. The members were usually attached to each other with ties or clamps.

Application of 2-D and 3-D member geometries as reciprocal members significantly changes the design of the member connections. Moreover, the connection detailing and fabrication significantly effects both the mechanical behavior of the connection and the assembly process of these systems. Therefore, to design a practical connection detailing for reciprocal systems with 2-D and 3D member geometries it is crucial to understand the mechanical behavior of the connection including the fabrication detailing and fasteners as well as assembly constraints including member placement and alignment and connection accessibility.

Different connection methods have been designed for contemporary reciprocal member connections. The application of these connection types depends on the digital fabrication process, structural requirements, the properties of construction materials, cost and aesthetics.

In recent years, reciprocal structures have been a popular topic in design build projects with timber structures (Figure 121). Most of these projects focus on application of digital and robotic fabrication or robotic assembly in design build projects using reciprocal network of timber elements. Using robotic fabrication most of these projects have T-joint with an end grain screw connections.



Figure 121_ A. single-layer reciprocal frame, Gramazio Kohler Research, ETH, Zurich, 2018.

B. double-layer reciprocal structure, Gramazio Kohler Research, ETH, Zurich, 2018.

C. KREOD Pavillion Chun Li architects, Ramboll Engineering 2015.

D. Quasi-reciprocal timber and discontinuous post-tensioned concrete structure and fabrication constraints. Utzon 40 Pavilion, 2015.

E. Timber Shell-Nexorade Hybrid pavilion, Ecole des Ponts Paris Tech, 2018.

F. Robotically produced reciprocal wooden pavilion, 100 years Bauhaus, Sina Mostafavi, 2019.

In this research the focus is on application of planar members in the design and fabrication of reciprocal systems from sheet materials using 3-axis and 5-axis CNC routers. The goal is to design low cost reciprocal systems which can accommodate rotation of reciprocal members to control the perforation size. The connection detailing should enhance the structural integrity and also provide guides to align the members and facilitate the assembly process.

Considering the design requirements for the connection detailing, four types of connection detailing applicable to 2-D and 3-D reciprocal members are proposed and illustrated in Figure 122.

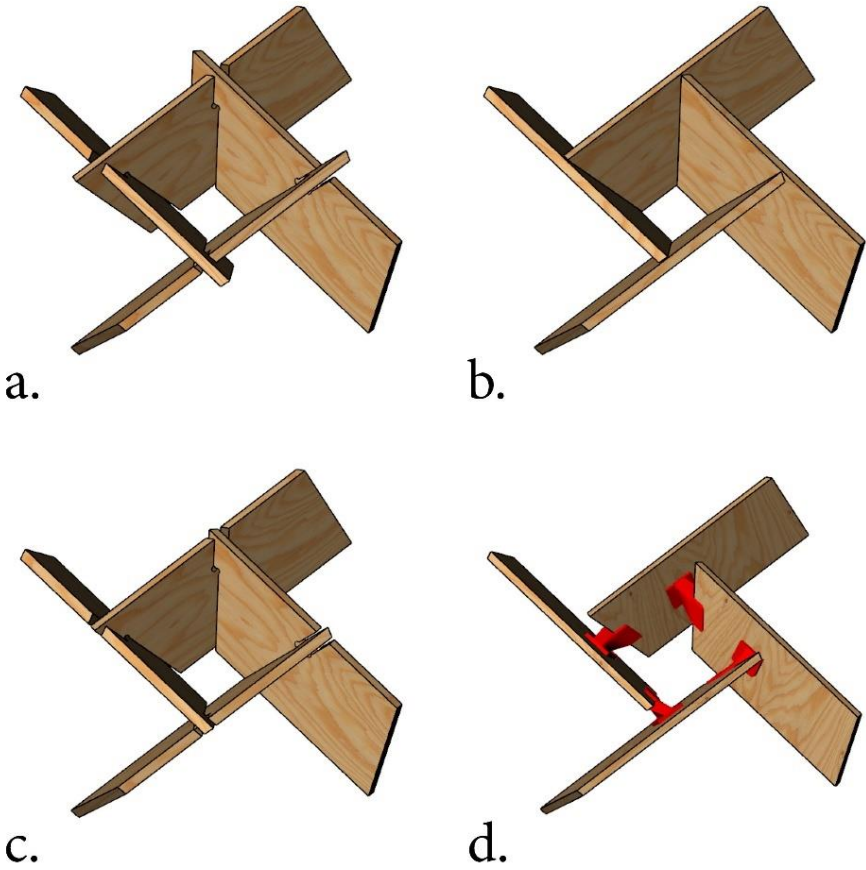


Figure 122_ A. Conventional reciprocal connection adapted for rotated reciprocal members, b. T-joint member connection, c. modified conventional connection, d. 3-D printed connection.

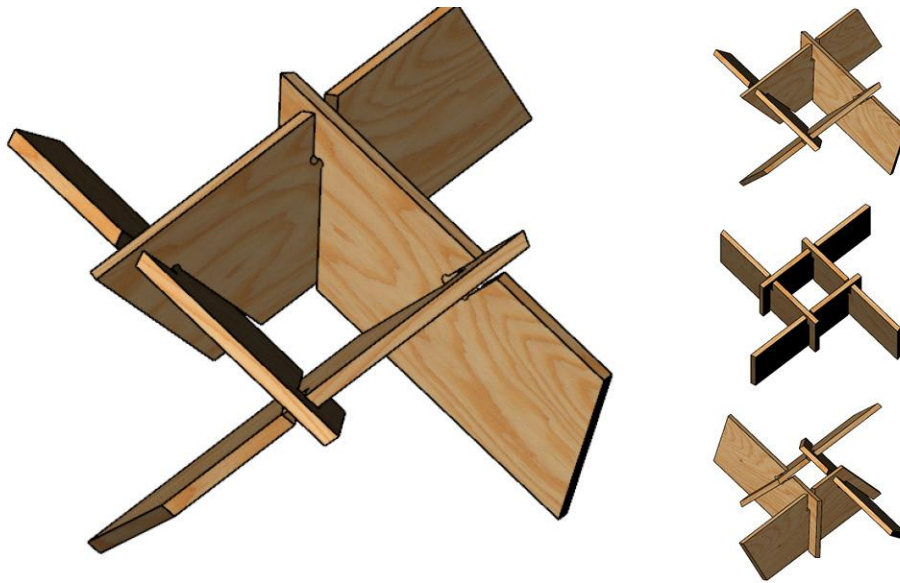


Figure 123_ Conventional reciprocal connection adapted for rotated reciprocal members.

The design above is basically an adapted variation of the conventional reciprocal connection which was used for timber structures (Figure 123). Oblique notches define the connection surfaces of the intersecting members. This section explains the design requirements and limitations for this type of connection. These connections need to be fabricated with oversized cuts for assembly purposes. The notch geometry provides assembly guides for the crossing member's alignment. The notch slot provides enough support and the connection can be designed without extra fasteners. The connection detailing transfers shear forces, however, does not provide any moment stiffness around the strong axis of the member. This connection can be fabricated from sheet material with fast machine feed rates using 5-axis CNC routers. However, there is a limitation on the tool inclination which depends on multiple parameters including the angle of oblique cuts controlled by the rotation angle of members, specific geometry of the tool, tool-holder and the spindle used for the joint fabrication. Different types of materials can be used for reciprocal members including wood, composite and metal.

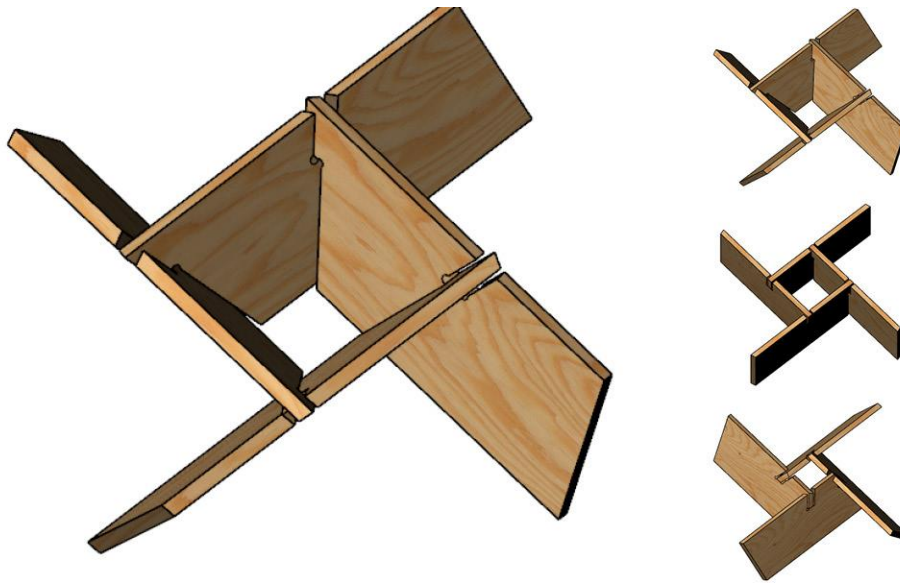


Figure 124_ modified conventional connection adapted for rotated reciprocal members.

Figure 124 shows an adapted version of the conventional reciprocal connection. As demonstrated in Figure 124, the extension of the member is trimmed in this variation. This simple change in the connection design can significantly enhance the connection performance and facilitate the assembly process. As a result, these connections can be built with minimum fabrication tolerances (1/16 in. or less) depending on the CNC tolerances and dimensional stability of sheet materials. However, extra fasteners are required to secure these connections. This connection detailing transfers shear forces and can provide minimal moment stiffness around the strong axis depending on the type of fasteners. This connection detailing can be fabricated from sheet material with fast machine feed rates using 5-axis CNC routers.

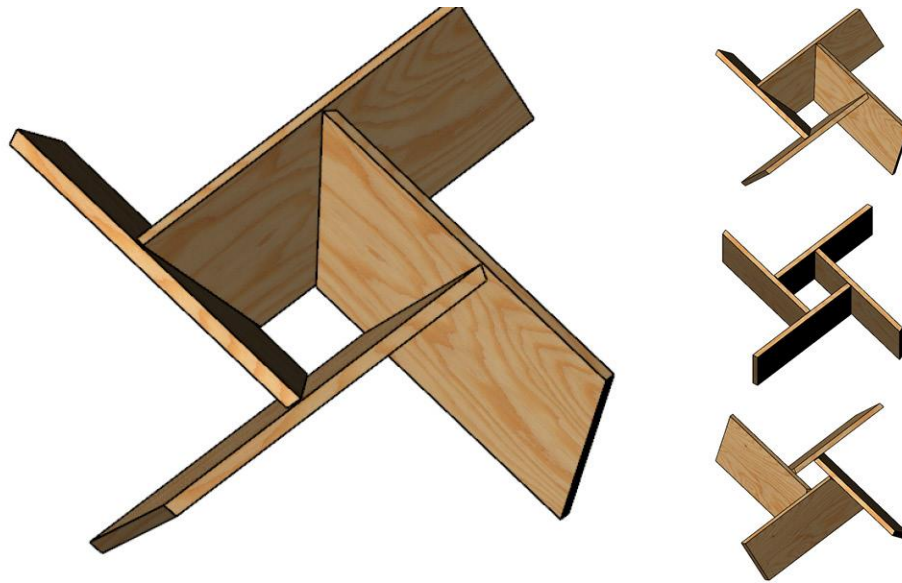


Figure 125_ T-joint member connection.

T-joint member connections are the most popular connections, especially for robotic assisted fabrication projects (Figure 121). However, manual assembly of these connections is difficult when working with planar elements with variation in their alignment since there are no guides to determine the exact orientation of the connecting members. To solve this problem there needs to be hatching or a shallow slot routing on the side of the members at the point of connection to correctly align the rotational orientation of the reciprocal member. These connections can be built with minimum fabrication tolerances (close to zero) using 5 axis routers or robotic fabrication. The connection needs external fasteners such as end grain screws or clamping fasteners for stability. Depending on the type of connection fasteners this connection can provide variable degrees of stiffness and can transfer shear forces as well as bending moments. The members need to be elevated for fabrication and usually robotic fabrication is needed for generation of end grain holes and guide hatches or slots on both sides of the members or alternatively using robotic assisted assembly for construction (Figure 126). Since the CNC cuts

are single oblique planes and both ends, members can be fabricated from sheet material with fast machine feed rates. Different types of materials can be used for reciprocal members including wood, composite, metal and masonry.

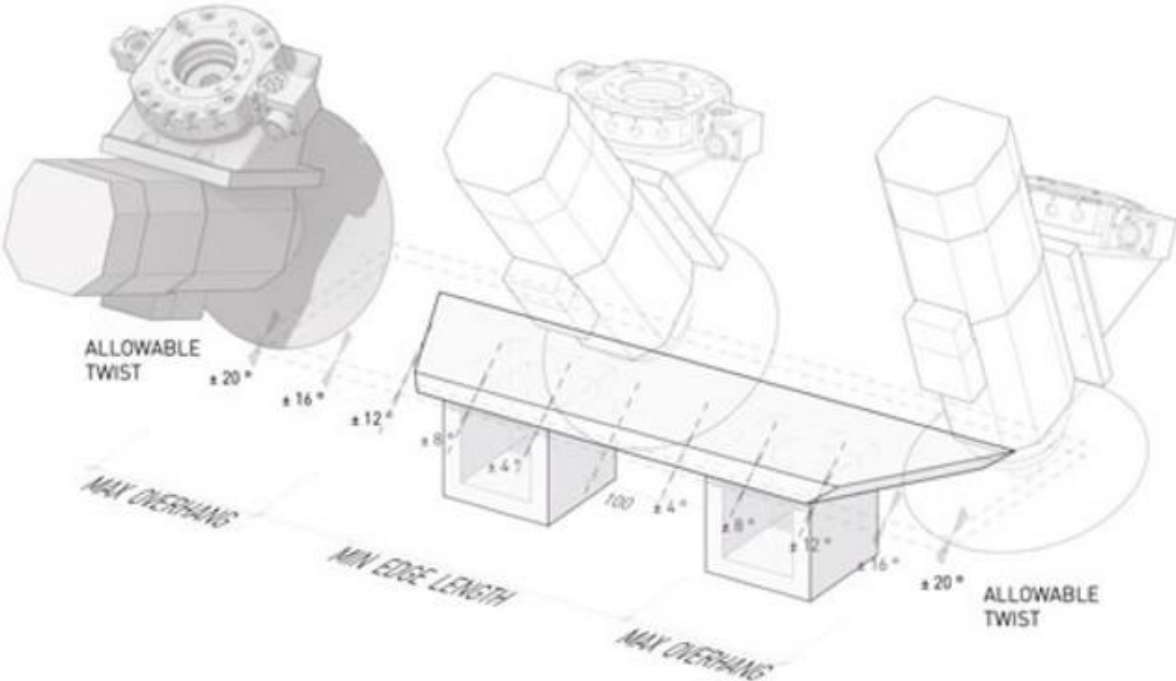


Figure 126_ Robotic fabrication with elevated members for Utzon 40 Pavilion.

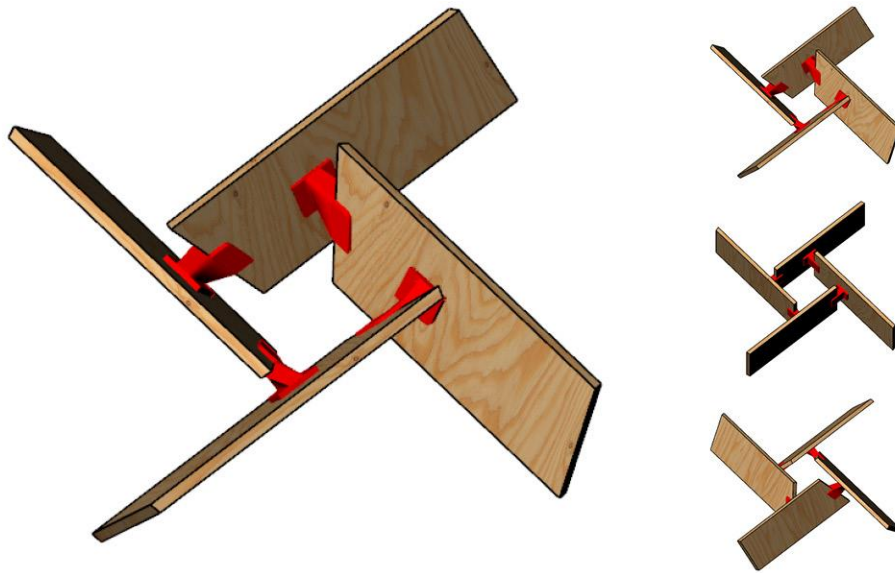


Figure 127_ 3-D printed connection.

Figure 127 shows an example of the application of custom connections using metal fasteners or 3-D printed connections. These connections are highly adaptive and can be designed and optimized based on the required stiffness and strength at the connection nodes or assembly requirements. However, this type of connection requires 3-D printing or custom fabrication techniques to fabricate the connection detailing for each joint which can be costly depending on the method of fabrication. Taking advantage of the accuracy of additive manufacturing these connections provide exact alignments for the members. Depending on the type of connection detailing this type of connection can provide variable degrees of stiffness and can transfer shear forces as well as bending moments. Since the CNC cuts are single oblique planes at both ends, members can be fabricated from sheet material with fast machine feed rates. Also, there will be less limitations on the tool inclination for fabrication since the oblique cutting planes do not necessarily need to follow the plane of the crossing members. Different types of materials can be used for reciprocal members including wood, composite, and metal. There are potentials for

optimization of the connection detailing based on the internal forces at each node to reduce weight and material use (Figure 128).



Figure 128_ Topology optimization of metal connection for optimal distribution of material and weight reduction (Galjaard et al., 2014).

5.3.2 Physical prototyping of the reciprocal modules

To understand the fabrication constraints and parameters for the connection detailing multiple tests have been carried out. These tests include:

- Physical prototyping of reciprocal modules with variable fabrication tolerances.
- Destructive structural testing of the modules for qualitative and quantitative study of the mechanical behavior of the reciprocal modules.
- Detailed finite element analysis of modules to understand stress concentrations and mechanical behavior.
- Finally, the results of these tests are used to design and fabricate a scaled prototype in the form of a half-arch geometry to test the design to fabrication process and also study different scenarios for assembly.

Figure 129 and Figure 130 show physical prototypes of reciprocal module with orthogonal connections and conventional notched connection detailing. MDF sheet material with $\frac{3}{4}$ inch thickness is used for fabrication of the prototypes. Samples are 3-inch wide and 13-inch long and each member has four connection notches. These four connection notches define four different engagement lengths for the reciprocal module. Each connection notch is fabricated with different fabrication tolerance ($\frac{1}{8}$ inch, $\frac{1}{16}$ inch, $\frac{1}{32}$ inch, $\frac{1}{64}$ inch). These tolerances are supposed to account for tolerances of the CNC machinery, material dimensional tolerances and tolerances needed for assembly.



Figure 129_ Conventional reciprocal connection for orthogonal flat members with four different engagement lengths (EL) with different fabrication tolerances (TL).

Physical testing of the prototype with the conventional connection detailing shows that the assembly process for this system is very difficult for small engagement lengths. It is important to understand that these tests are done on reciprocal modules where the number of crossing members for each reciprocal member is just two. As a result, the assembly process for a reciprocal system with multiple reciprocal modules will be much more difficult since in a multi-module system the number of crossing members for each reciprocal member is four and the system is completely interconnected with shared members between the modules (Figure 118).

Moreover, the rotational parameter creates an extra level of complexity in the assembly process and as a result the connection detailing should be flexible enough to facilitate the assembly process in the reciprocal systems. Also it should accommodate low fabrication tolerances. Figure 130 shows a reciprocal module with modified notched connection

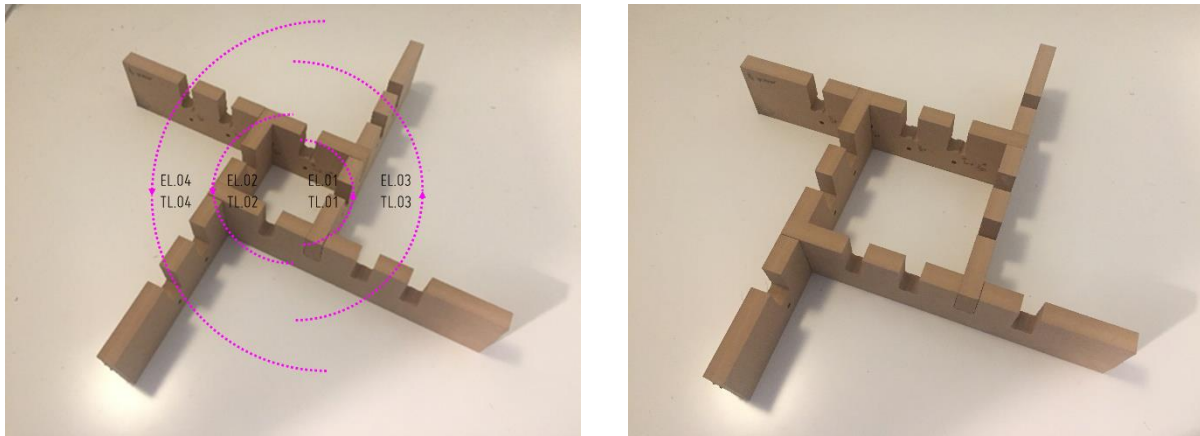


Figure 130_ Modified connection detailing for orthogonal flat members with four different engagement lengths with different fabrication tolerances.

Figure 131 shows a physical prototype of a reciprocal module with rotated members and 3-D connection detailing. The physical prototyping shows how modified connection detailing can easily accommodate rotated member connections with fabrication tolerances, unlike traditional connection detailing which makes the assembly impossible for this type of reciprocal system.

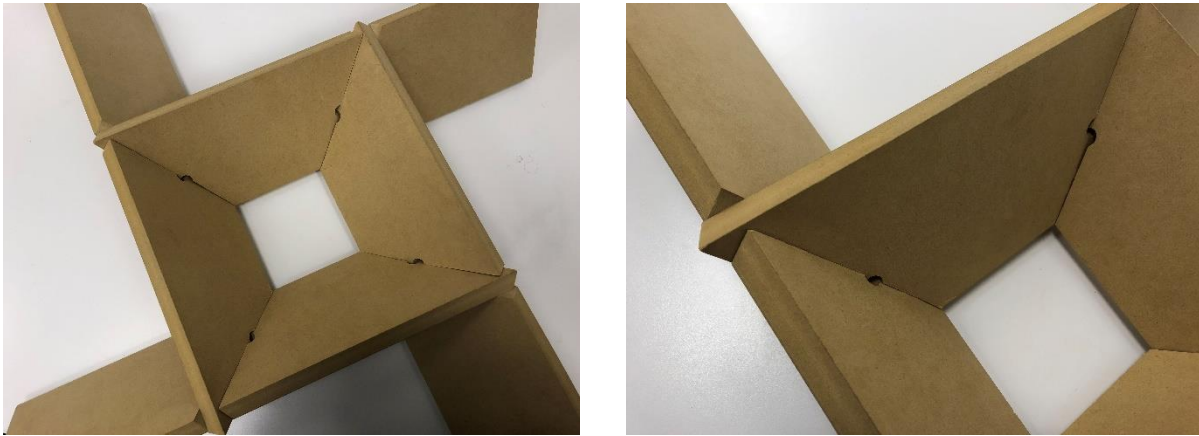


Figure 131_ Modified connection detailing for rotated flat members.

5.3.3 Application and types of connection fasteners

As was mentioned in the previous section, the modified connection detailing requires extra fasteners to secure the connection. For this purpose, end grain metal screws are used to connect the crossing members at the connection (Figure 132).

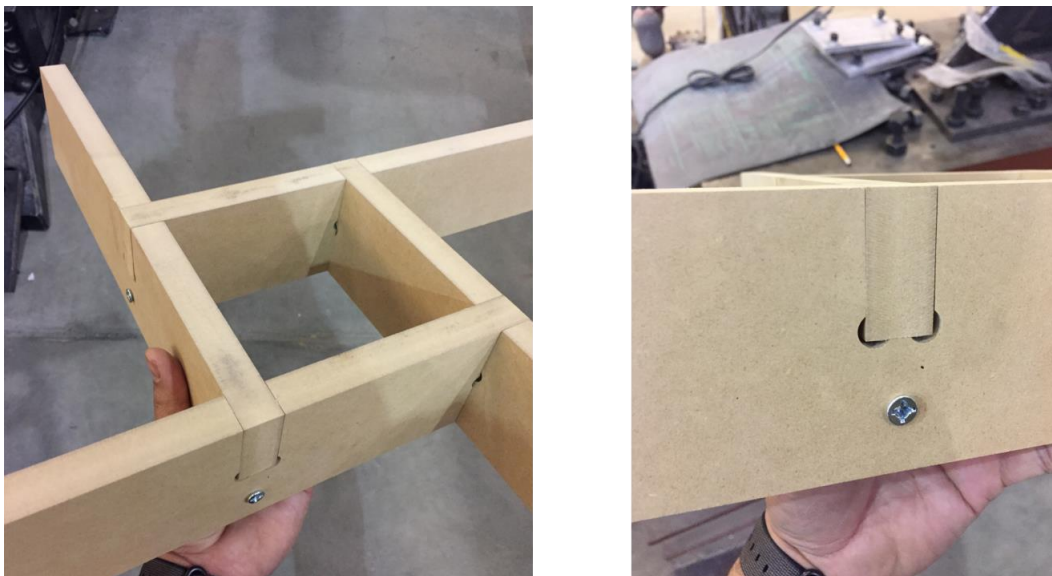


Figure 132_ Initial detailing for orthogonal connection with end grain screws.

Although this screw connection would work well for planar orthogonal connections, it would not be practical for three dimensional rotated members due to difficult accessibility for drilling during the assembly process.

The proposed connection uses side screw holes across the grain using a Kreg jig instead of screw wholes parallel to the wood grain (Figure 133, Figure 134). The screw hole can be either drilled with extension bits using 5 Axis or can be created manually using Kreg jig (Figure 134). The aesthetic benefit of the proposed connection detailing is also important since it creates hidden screw holes on the side instead of exposed screw head on the edge.

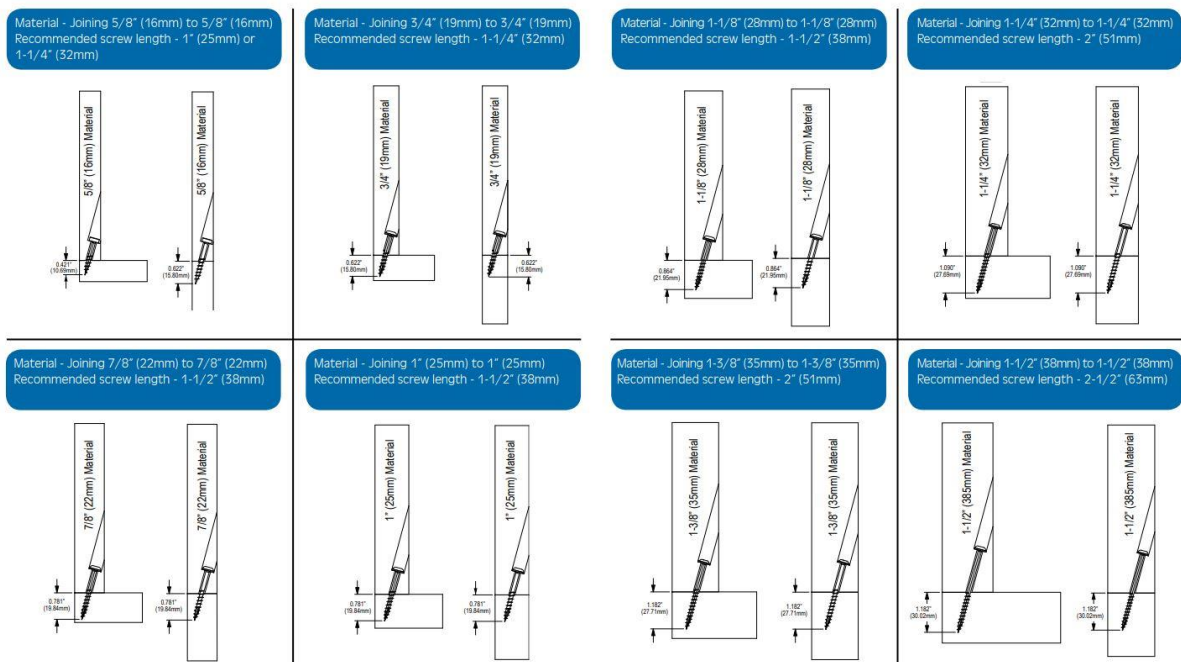


Figure 133_ Standard guidelines for screw penetration based on the material thickness.
 (<https://www.kregtool.com/files/newsletters/kregplus/Images/february12/selecting-the-correct-screw>)

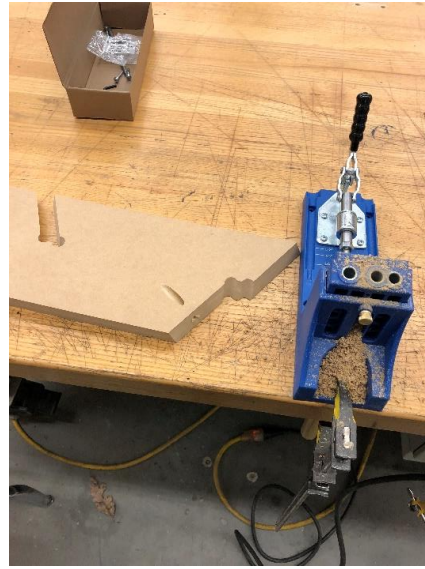


Figure 134_ Application of Kreg jig to drill the connection holes.

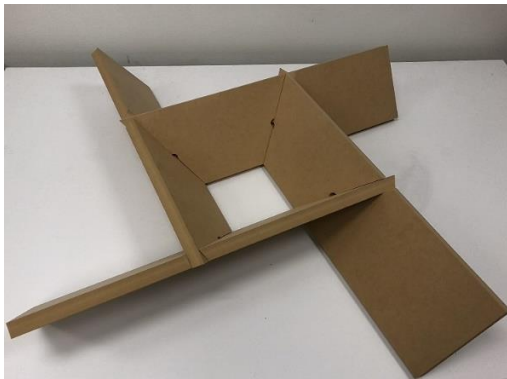


Figure 135_ Modified connection detailing for rotated flat members with Kreg screws.

5.4 Destructive structural tests

5.4.1 Fabrication of test samples

This section explains the destructive structural testing undertaken for the reciprocal modules. These tests are necessary to understand the warping behavior of reciprocal members due to the intrinsic asymmetry in the reciprocal module geometry. More importantly, the tests show different modes of failure and how the combination of shear forces and bending moments are affecting the failure of the reciprocal members and the connection detailing. Moreover, detailed measurements of force-displacement will demonstrate nonlinear behavior of the connections with regard to the fabrication tolerances. Towards this goal a destructive structural test has been devised to study the failure behavior of reciprocal modules and the connection behavior. Additionally, a detailed 3-D finite element simulation of the reciprocal module is carried out to study the stress concentrations quantitatively in the member and connection region. Fifteen reciprocal modules are fabricated using 3-axis CNC machine. Relatively small fabrication tolerance (1/32 in.) is used for connection cuts and end grain screws are used at each connection (Figure 136 and Figure 137).

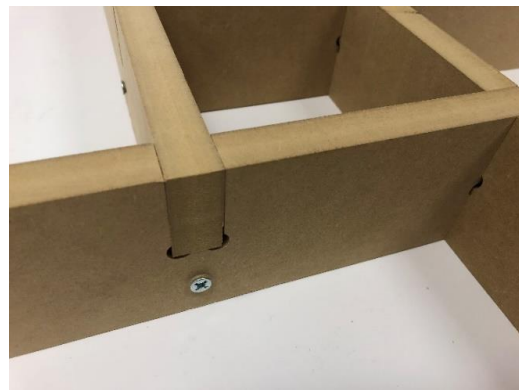


Figure 136_ Modified connection detailing for orthogonal flat members with end grain screw fasteners.

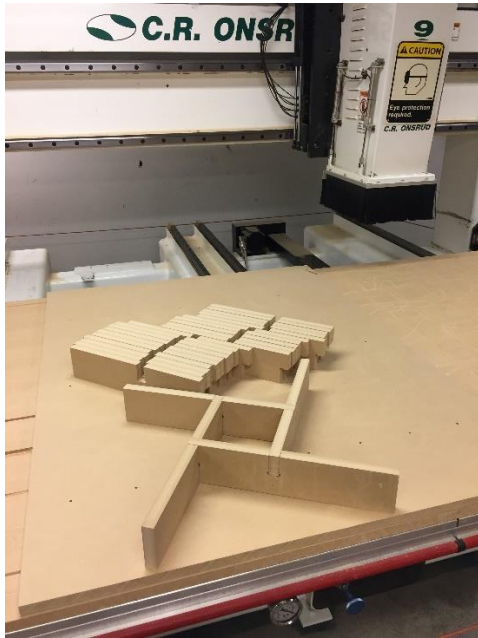


Figure 137_ reciprocal modules are fabricated for structural testing using 3-Axis CNC machine.

5.4.2 Structural setup and results

Testing the reciprocal modules requires custom set up to address the boundary conditions appropriately. The two main concerns are the support and the loading condition. The supports are designed to accommodate the slight rotation of the whole module under loading, which happens due to the intrinsic asymmetry of the reciprocal module for this purpose each leg of the reciprocal module is sitting on a slider pad which allows movement on top of a rigid steel block. The loading surface is covered by a rigid steel plate fitting the engagement area of the reciprocal module. Under the displacement control loading the rigid plate applies uniform displacement to the loading area. Using the displacement control loading (0.2 in/min) the specimens are loaded until fracture. The load and displacement values are recorded by the system for the post processing.

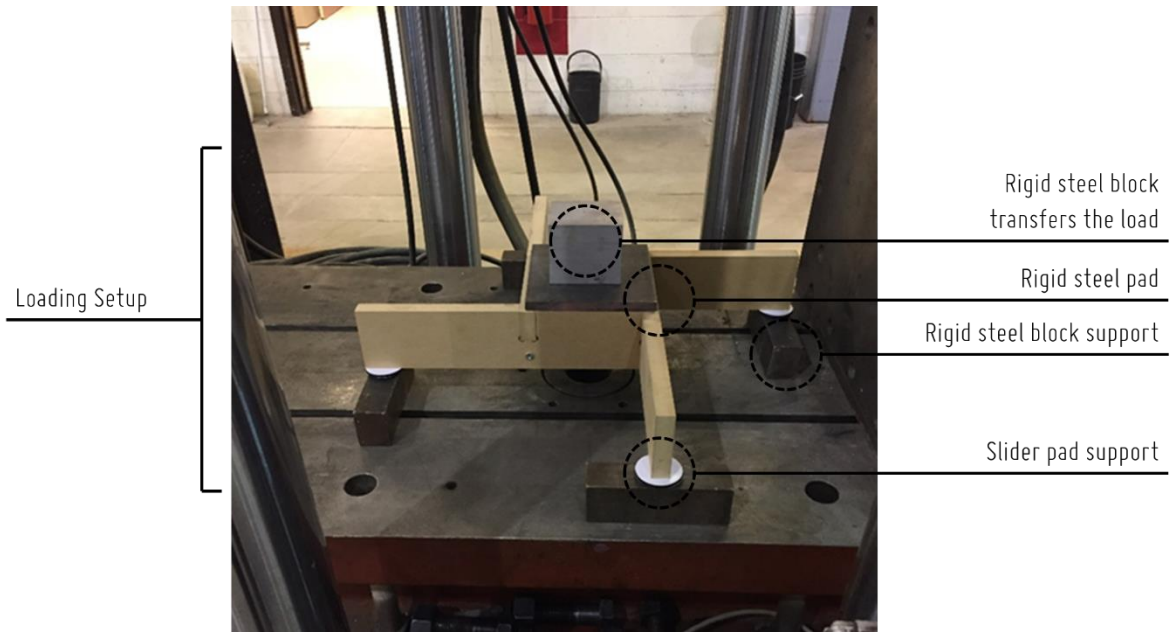


Figure 138_ Test setup for the destructive structural test.

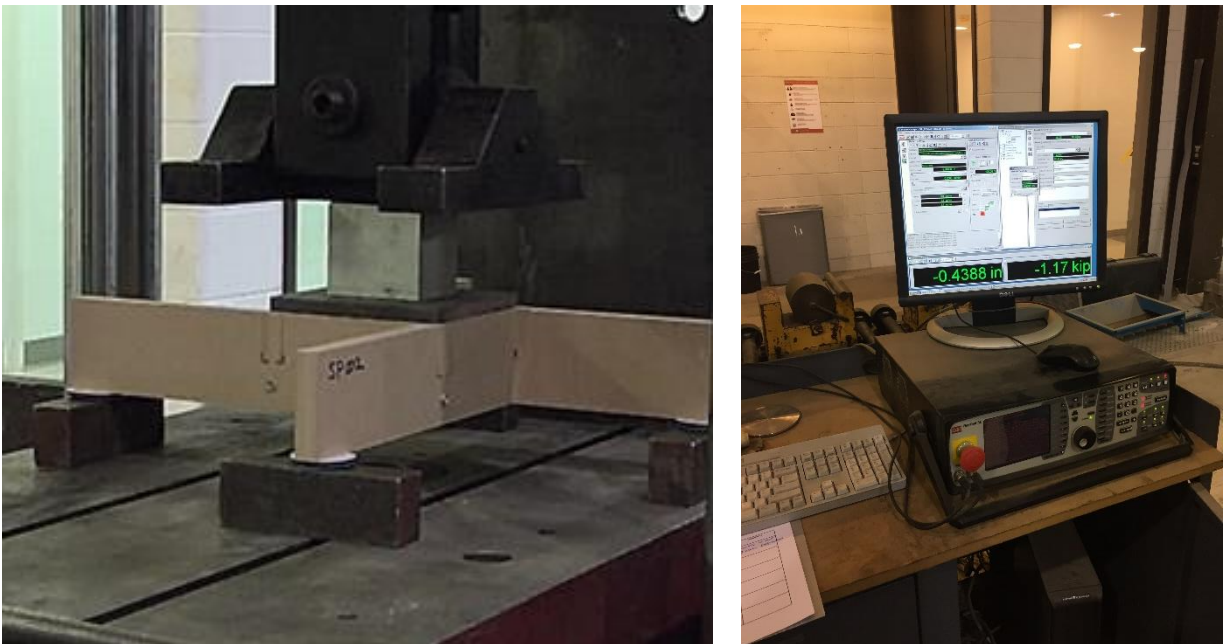


Figure 139_ Destructive structural testing using displacement control with Universal machine.



Figure 140_ Failure of test samples under displacement control loading. Left: 13-layer Birch plywood material, right: MDF material.

Qualitative study of the test results shows the failure mode of the reciprocal modules (Figure 140). One of the characteristic behaviors of the reciprocal module is the warping deformations caused by the geometric asymmetry of these structures. These warping deformations are observable during the structural test and also are simulated with a detailed finite element simulation as shown in Figure 141. The test results show that these warping deformations can cause delamination failure in the members in the connection region as was observed in the form of a vertical fracture through the member in one of the test samples made from MDF material. However, this delamination was not observed in the main test samples which were made from Birch plywood material. The dominant failure mode in all the MDF samples was a bending failure at the connection region in the crossing member. The failure was sudden, and the crack propagated through the screw hole. As the analysis results show, maximum bending moments

happen under the connection region of the reciprocal module and since this region is weakened by the fabrication cuts and the screw hole the failure is guaranteed at this region.

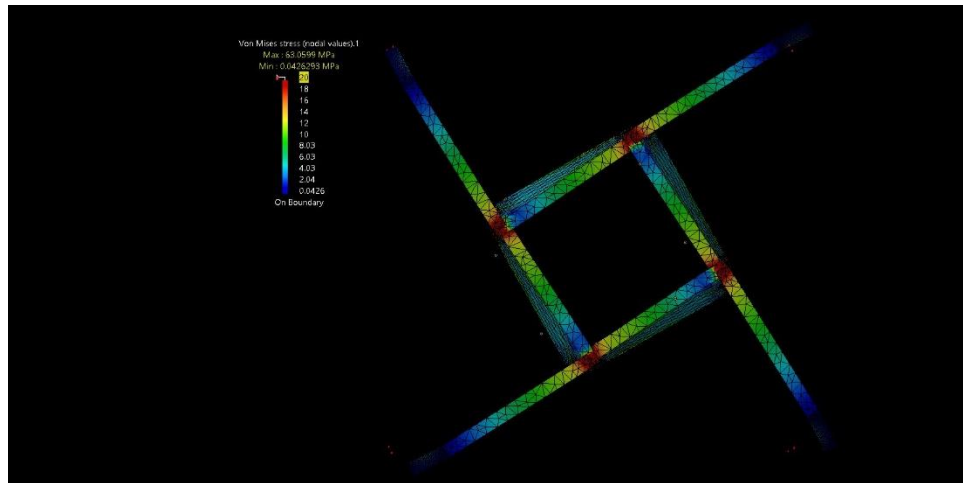


Figure 141_ Slight rotation of the reciprocal module and warping of the reciprocal members under symmetric loading.

The load-displacement data from the tests is shown for eight test samples in Figure 142 and Figure 143. It is important to consider that due to flexibility of the sliding pad at the supports the total deformation includes the deformation of the slider pad.

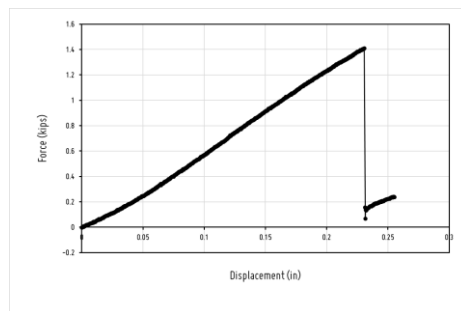
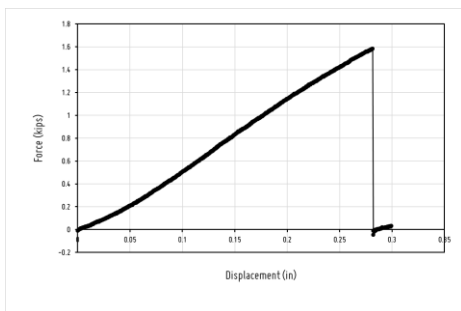
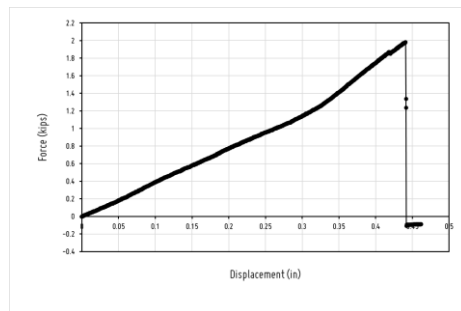
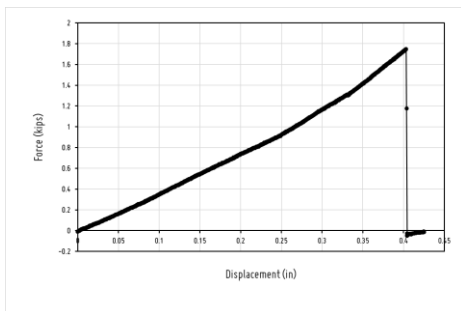
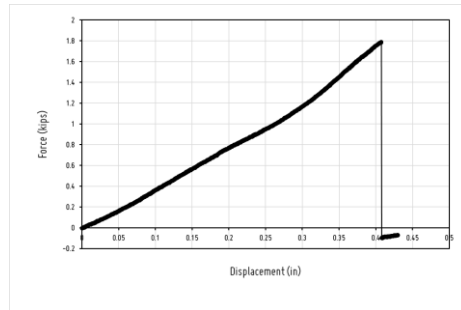
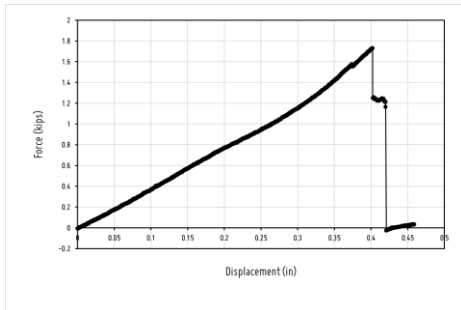
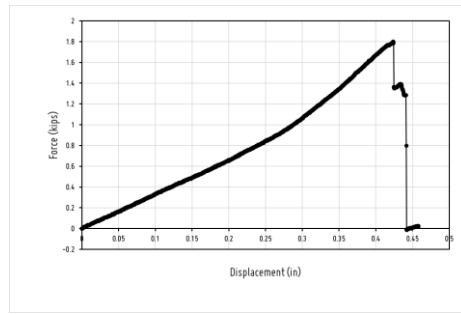
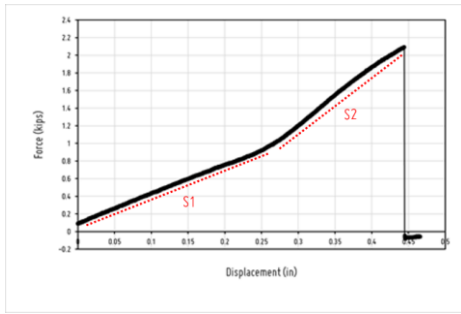


Figure 142_ Load-displacement graph for 8 sample tests with bilinear slopes.

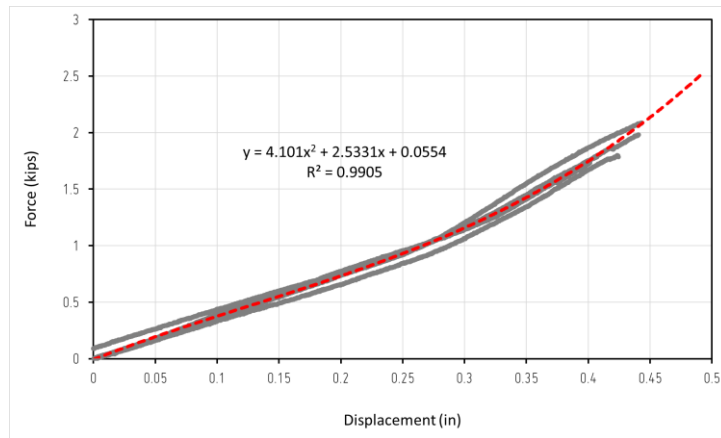
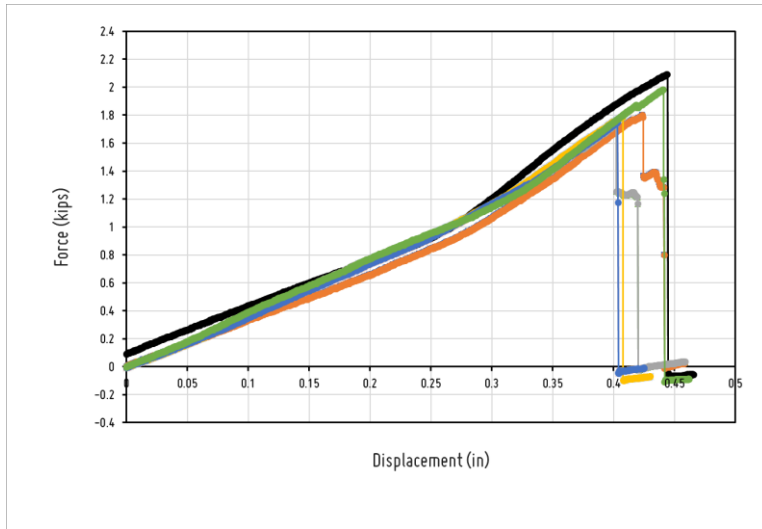


Figure 143_ Top: force deformation graphs for six test samples with maximum ultimate force and deformation. Bottom: Cumulative regression model for the force-displacement data.

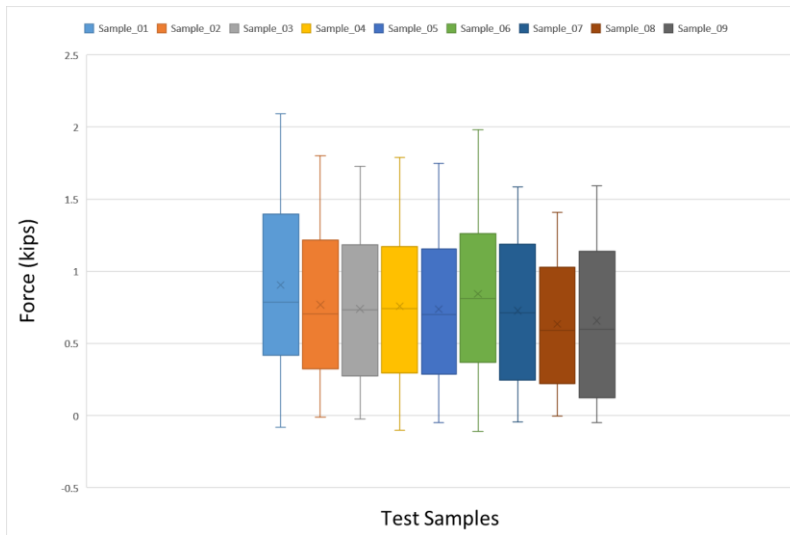


Figure 144_ Box plot of the loading data for 9 test samples.

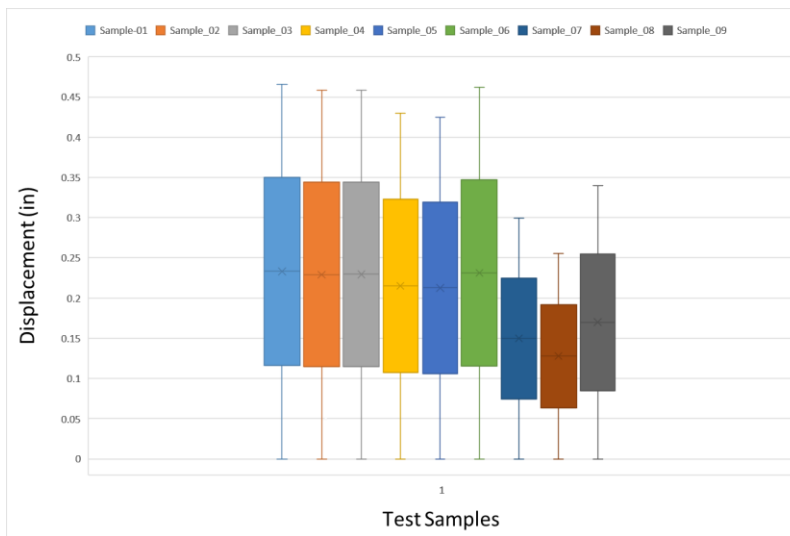


Figure 145_ Box plot of the displacement data for 9 test samples.

However, the important information that is derived from the graph is the trend of load deformation which is a bi-linear curve (Figure 142). The change in the graph slope shows that

under small deformations the reciprocal module shows more flexible behavior and the stiffness of the system almost doubles as the maximum deformation exceeds 1/4 inch (Figure 143).

This change in the stiffness is directly related to the fabrication tolerances of the connection. The test observations and the finite element simulation results show that with increase in the loading the gap at the notch location of the connection decreases until the notch completely closes against the crossing member, at that moment the full depth of the member participates in the loadbearing at the connection region which increases the stiffness of the system. This observation has an important implication, firstly it is important to reduce the depth of the notch cuts to keep the structural depth as much as possible, secondly it is structurally beneficial to fabricate the connection cuts with minimum tolerances. As was observed during the loading test, if the fabrication tolerances are small enough, they will be eliminated by the elastic deformations of the structure and the full capacity of the member cross-section participates in the loadbearing process (Figure 146).

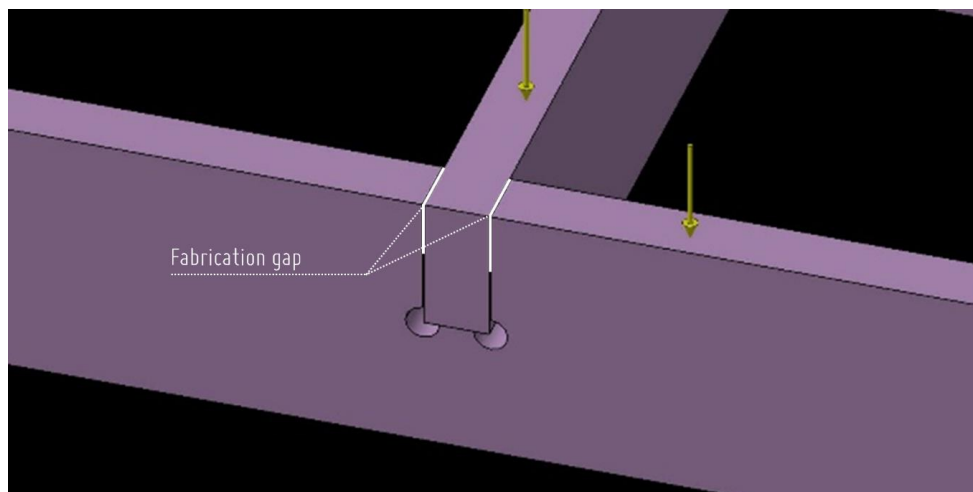


Figure 146_Connection detailing and fabrication tolerances in the reciprocal module before loading.

5.5 Detailed finite elements analysis and results

Understanding the mechanical behavior of reciprocal module and distribution of the forces is crucial for decision making about the specific design of the connection detailing. Connection design always presents a compromise between different design constraints such as fabrication constraints, assembly constraints, and architectural and structural functions. Reliable simulation models are very helpful to study the mechanical behavior of the system in different scenarios and also study the stress distributions and stress concentrations in the system.

Towards this goal a detailed finite element model of the reciprocal module is created. Birch Plywood material properties are used for analysis, and Table 4 shows its material properties. A second order tetrahedron mesh elements are used for analysis. Contact elements are generated at four contact surfaces of each connection as shown in (Figure 147, Figure 148 and Figure 149), this leads to total of sixteen contact surfaces in the reciprocal module (Figure 149 and Figure 150). The contact is modeled with the general contact function of CATIA. The contact elements allow arbitrary movements of the parts relative to each other until the parts come to contact, when they come to contact, they can still slide but they cannot inter-penetrate, and separation after contact is allowed in the model. Attention was paid to refine the mesh at the contact zones (Figure 150). The boundary conditions are defined to model the test condition. The supports are restricted from vertical movement, but they are free to move in the plane of the reciprocal module to accommodate the slight rotation of the module under vertical loading.

Similar to the structural tests these simulations are not aimed for exact prediction of the system which can be very complicated due to all the possible defects and nonlinearities of material behavior and fabrication detailing. They rather provided some fundamental knowledge about the load-bearing capabilities, stress distributions and the possible failure mode of the system (Figure

150 and Figure 151). This information is crucial in decision making about different design and fabrication parameters of reciprocal connections.

Property	Design Value
Specific Gravity	560 kg/ m ³
Elastic Modulus	93000 kg/ cm ²
Shear Modulus	46500 kg/ cm ²
Tensile Strength	62 kg/ cm ²
Compressive Strength	80 kg/ cm ²
Bending Strength	62 kg/ cm ²

Table 4_ Material properties of Plywood based on APA (Engineered Wood Association) standard.

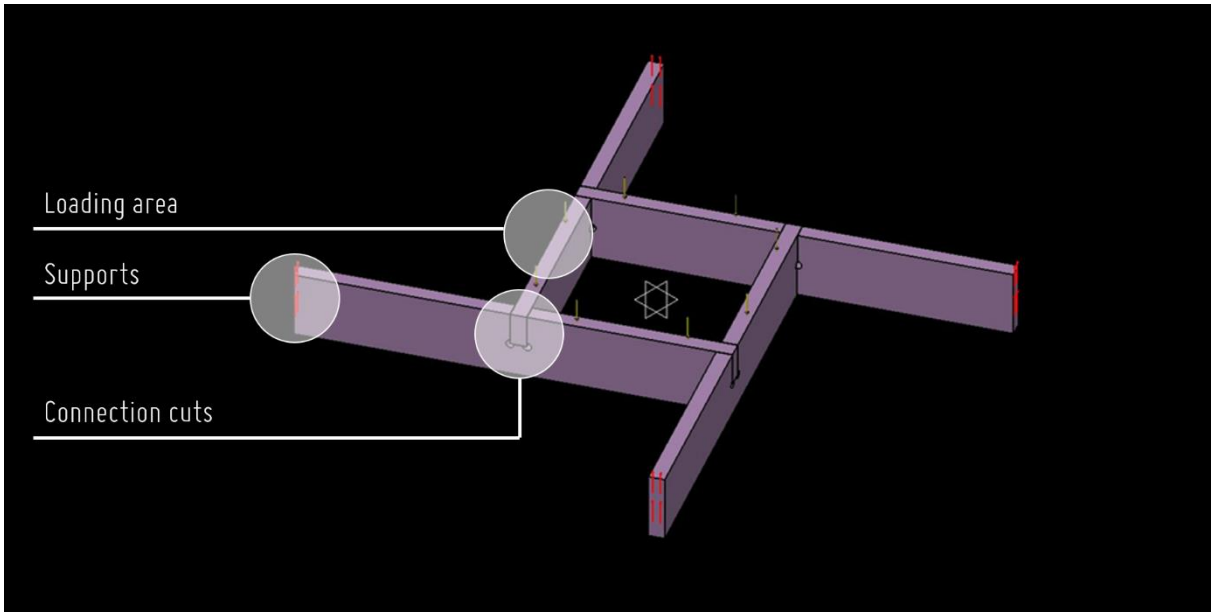


Figure 147_ Solid modelling and assembly of a four membered reciprocal module.

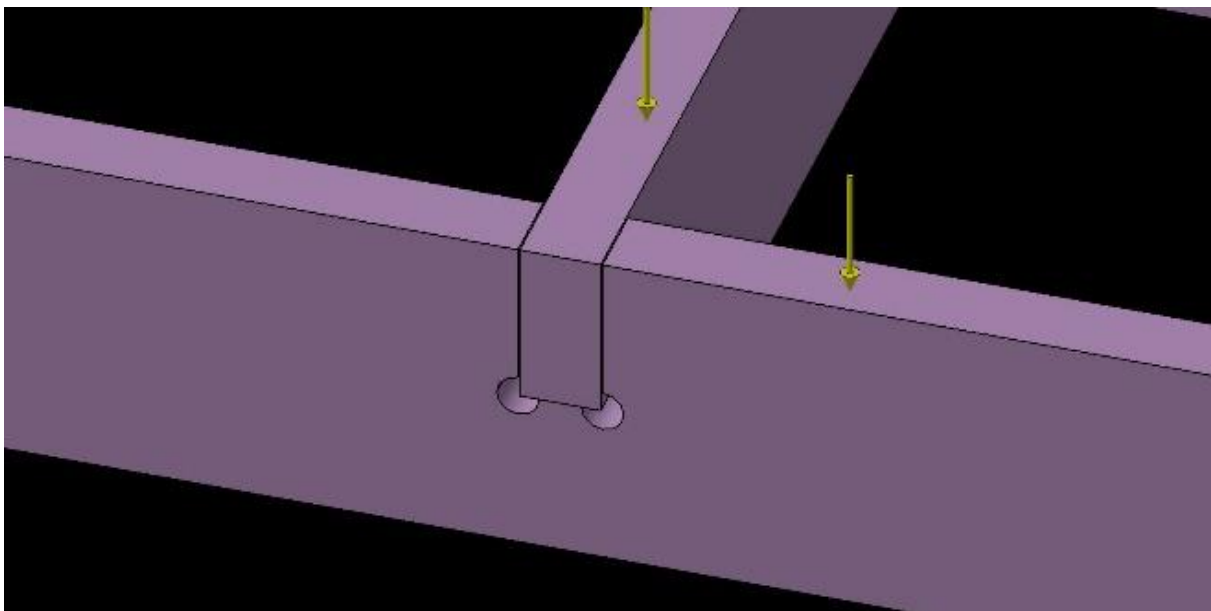


Figure 148_ Solid modelling of the reciprocal connection (member cuts and dog bones) and fabrication tolerances.

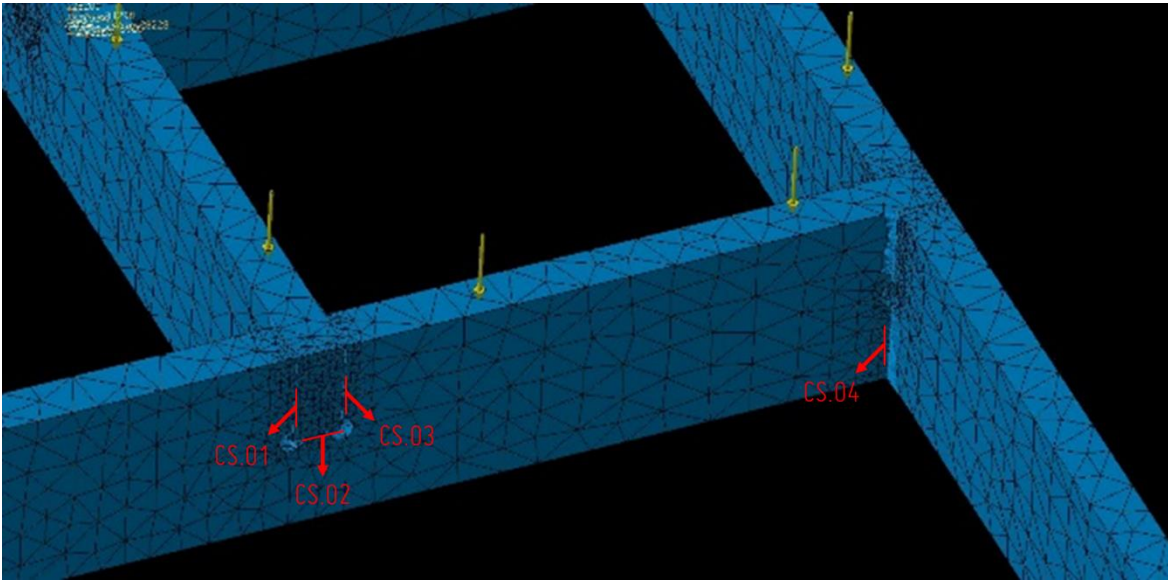


Figure 149_Definition of contact faces for the connecting members and 3-D finite element mesh. Four contact surfaces (CS) are shown in the picture.

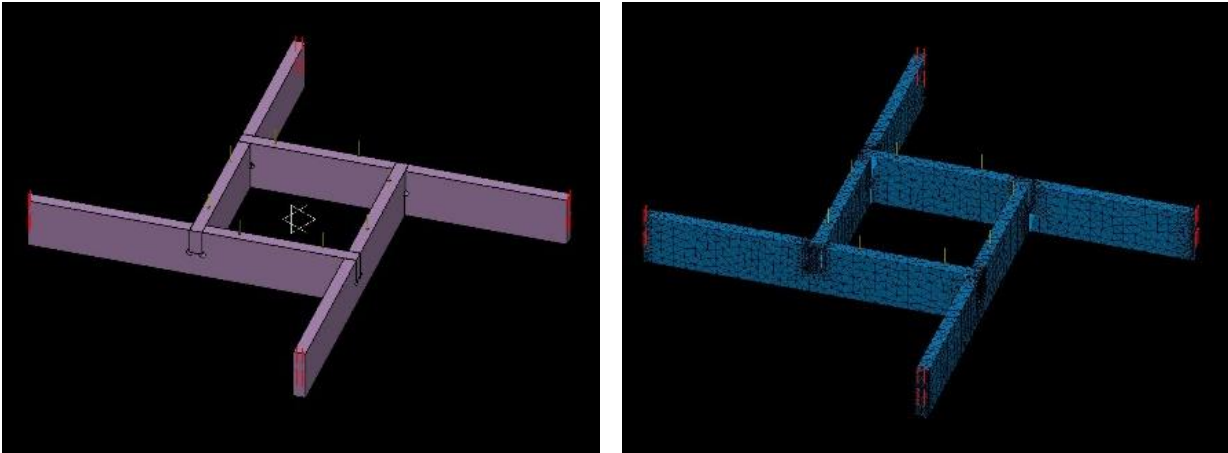


Figure 150_Solid modelling and assembly of a four membered reciprocal module. 3-D Finite Element Mesh of the reciprocal module including contact elements and boundary conditions.

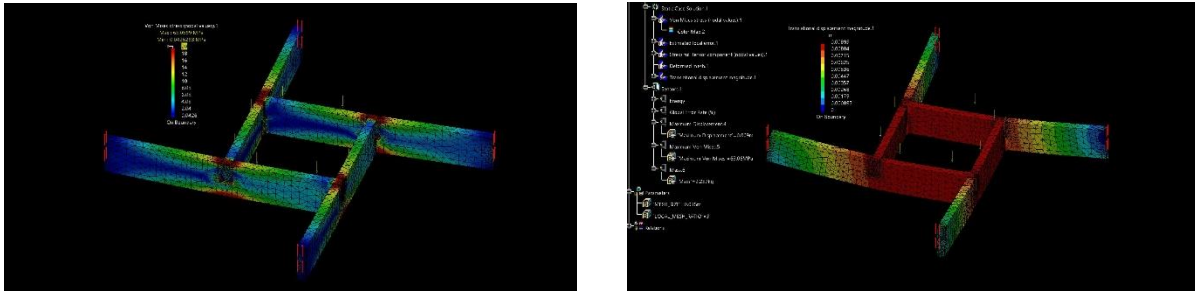


Figure 151_ Finite Element analysis results of the structural module. Left: Von Mises stress distribution, right: Deformations.

Figure 152 shows the Von Mises stress distribution in the reciprocal module. As the stress distribution shows there are three main locations of stress concentration and all of them are located in the connection region. Region one is the top edge of the crossing member in the connection region. In the beginning of the loading and under low load levels this region is stress free until the gap in the connection point is eliminated by the elastic deformations. After that the bending and bearing stresses increase as the loading increases. Region two is the flat contact surface at each joint. Bearing stresses increase as the vertical loading increases. Region three is the bottom edge of the crossing member in the joint. This region is experiencing the maximum tensile stress caused by the bending moments. Combination of the tensile stresses and shear forces is critical at this region and based on the test results the failure initiates from this region.

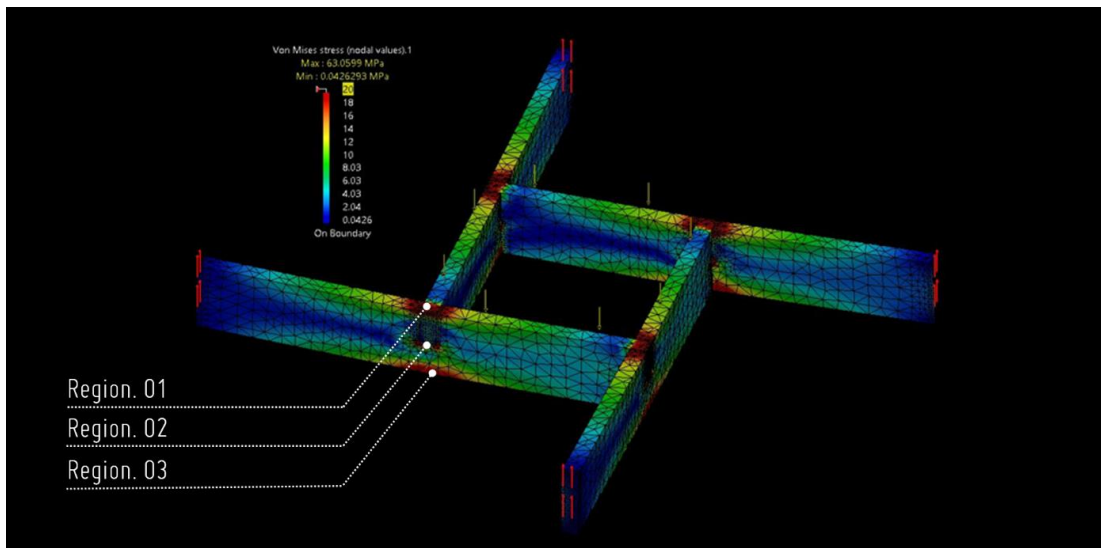


Figure 152_ Finite Element analysis results the structural module under distributed loading on the engagement area. Von Mises stress distribution.

Figure 153 shows Von Mises stress distribution in the reciprocal module for different engagement lengths under the same loading. As shown in Figure 153 stress levels are higher in the reciprocal module with smaller engagement length. These results correspond to the simplified analysis results discussed in Chapter 3 and as was discussed there, this response is not an inherent behavior of the reciprocal systems and rather caused by the boundary conditions of the single module in the simulation. Basically, increasing the engagement length causes the loading surface to approach the supports which creates a shortcut load path from the member to the supports and reduces the bending arm on the reciprocal members.

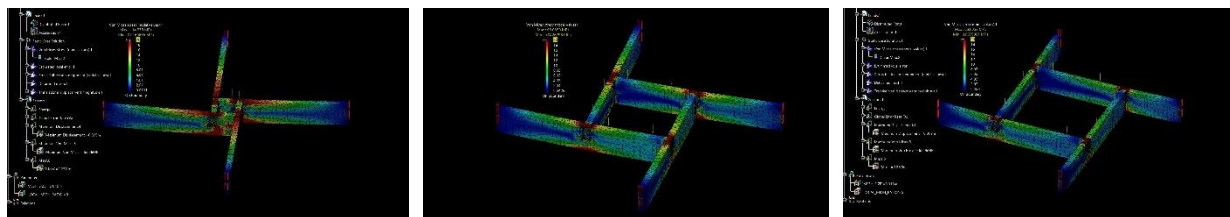


Figure 153_ Detailed 3-D finite element analysis of reciprocal module with three different engagement lengths. Von Mises stress distribution.

Figure 154 shows exaggerated deformations of the module which shows vertical deformation of the module under loading as well as the warping behavior of the members at the connections.

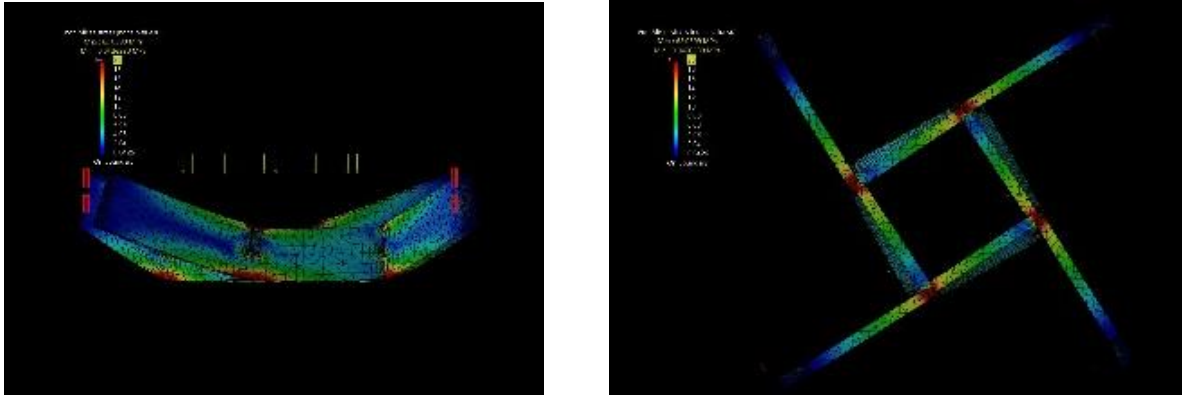


Figure 154_ Detailed 3-D finite element analysis of the reciprocal module with exaggerated deformations.

5.6 Scaled model fabrication

5.6.1 Scaled model definition

Physical prototyping of the reciprocal module provides critical information about the fabrication constraints, connection detailing and the assembly logic. It does not exactly describe the fabrication requirements of the reciprocal systems in relation to the assembly process since the reciprocal module does not reflect the interconnected nature of reciprocal systems. To have a better understanding of the fabrication parameters and assembly logic a scaled model of a reciprocal system is designed and built using the proposed design to construction workflow.

This scale model is designed to test the fabrication process for a half-arch reciprocal system with rotated 4-inch wide planar elements (Figure 155). In this prototype the proposed modified connection detailing is tested, and the required fabrication tolerances are studied for large scale fabrication. Swarf cuts and dog-bone detailing are tested on 13-layer Baltic Birch Plywood

material, the fabrication parameters such as drill bit size, and different speed and feed rates are tested as well. The assembly process is tested to design an appropriate assembly logic for large scale fabrication. Three sets of fabrication tests were carried out to determine the fabrication parameters for the large-scale fabrication of reciprocal systems with 3-D connection detailing using a 5-axis CNC machine.

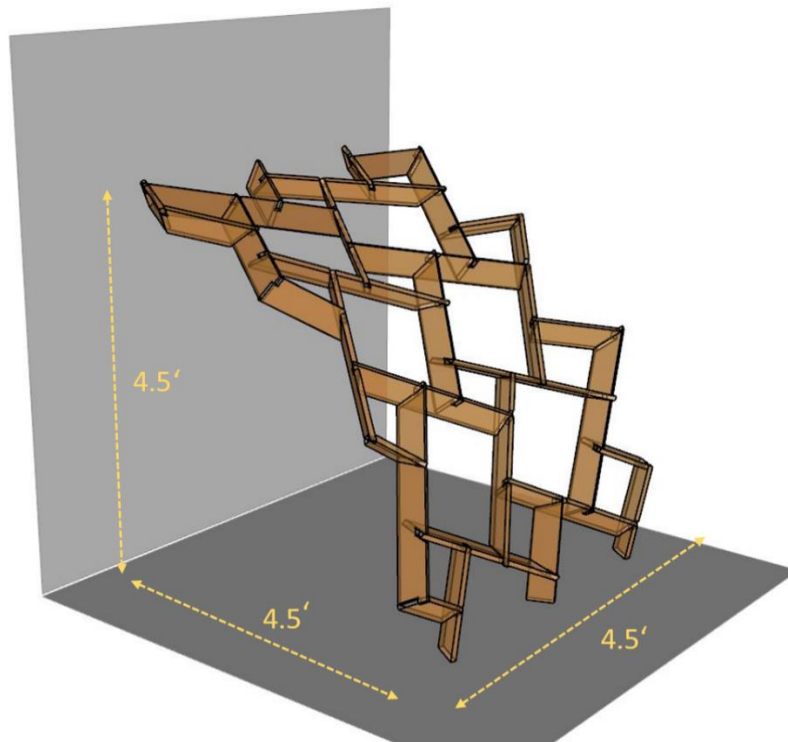


Figure 155_ Scaled prototype. The geometry and measurements of a half arch reciprocal system with rotated planar elements.

5.6.2 Fabrication process_ Test 01

Swarf cuts are used for the fabrication of the connection detailing, using a 1/4 inch down-shear bit with four depth cut tool paths. Swarf cuts use two contours on the lower and upper sides of the cutting surface geometry to define the 3-D cut surfaces (Figure 156). A 3/8 inch compression bit is used for contour cuts. A single toolpath can be defined for compression bit for contour cuts,

thereby speeding up the production process. Tabs were created to hold each piece through the contour cutting (Figure 157 and Figure 158).

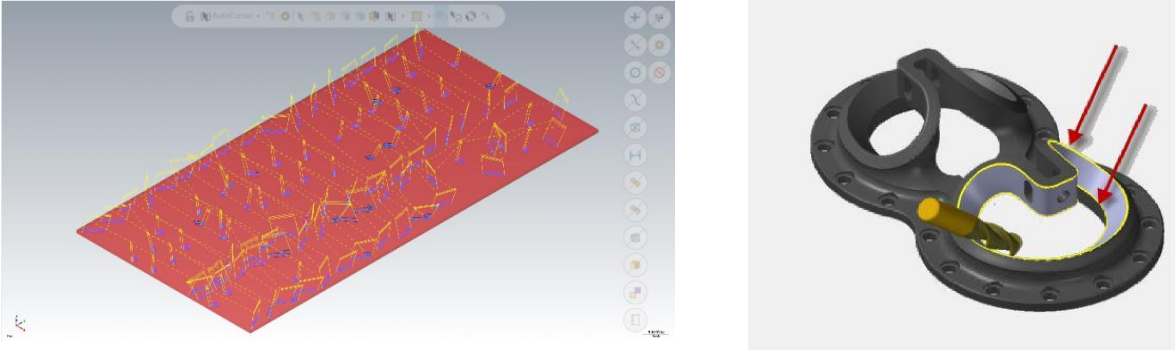


Figure 156_ Swarf cuts tool pathing.

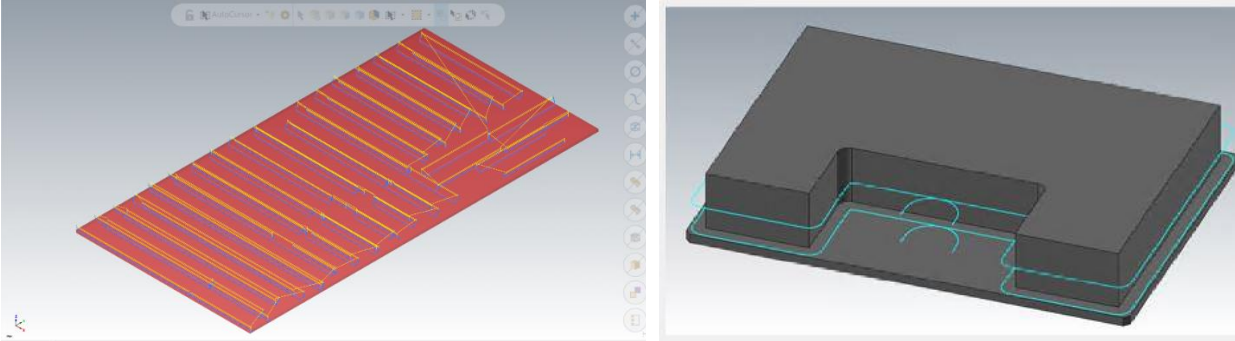


Figure 157_ Contour cuts tool pathing.

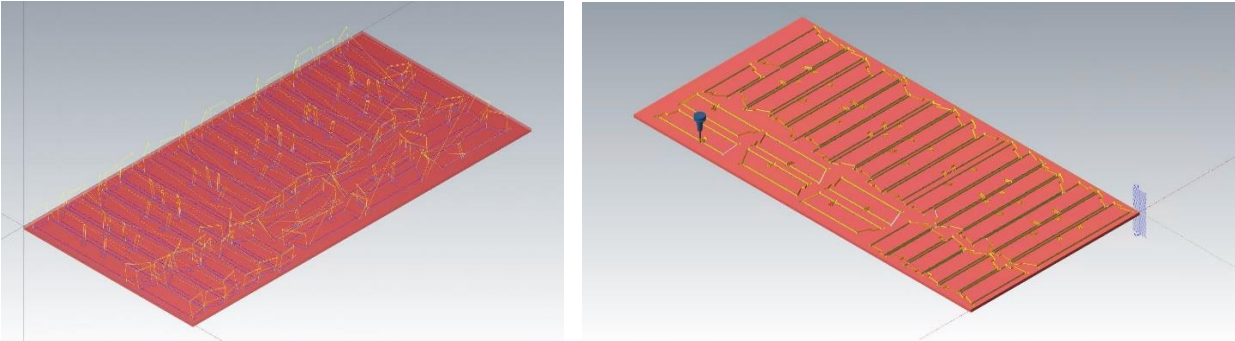


Figure 158_ Full tool pathing for the 5-axis CNC cutting.

For this test 3/4 inch 13-layer Baltic Birch Plywood is used as the fabrication material. 3/4 inch thickness is essential to test the thickness for the full-scale project design. The thickness variation for plywood is considerable and it makes it difficult to work with tight tolerances, so it is important to find a working tolerance to accommodate for the 0.02 inch thickness variation across the sheet (typical dimensional tolerance for the type of plywood used in this research). Considering the modified connection detailing for fabrication, tight connection tolerances can be used. As a result, we used 0.01 inch tolerance on each side of the connection cuts ($0.01 < 1/64$ inch conventional tolerance).

For production purposes the swarf cuts are programmed to be cut first and then followed by the compression cuts. The material is located with a 4-inch offset from the edge of the CNC table to accommodate for the rotation of the 5-Axis in the vicinity of the table edges (Figure 159 and Figure 160).



Figure 159_ 5-axis CNC bed and the test cut results for the fabrication test one.

The speed of the cuts was reduced by 25% to reduce the load on the bit for swarf cuts.

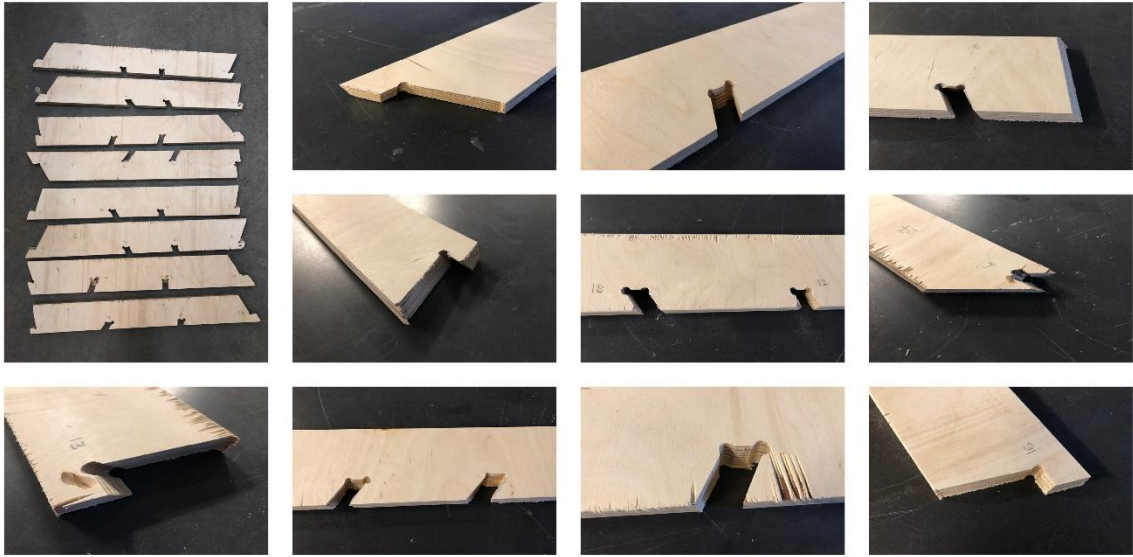


Figure 160_ Fabrication results for the fabrication test one.

A thin spoil board (0.4 inch) was used for test one. The spoil board material burned multiple times due to the heat caused in down-shear swarf cuts (Figure 161).



Figure 161_ Excess heat in swarf cuts: Left, burning in the spoil board. right, successful cuts.

Using down shear bits gives nice edge cuts for the connections, however down shear causes a lot of heat accumulation during the swarf cuts. The speed and feed of the cuts should be reduced manually to 70%, and this should enhance the heat control. Also, the size of the dog-bones (curves around the corner cuts) should be increased in the code which creates smoother movement of the bit around the acute corners.

The drill collet hit the material in multiple occasions where the swarf cuts were too deep. The collision moved the material from the origin which caused miss alignment of cuts after the collision (Figure 162).



Figure 162_ Collision of the drill collet with material.

There are two solutions for this problem. Either to expose more of the drill bit out of the collet or using an extra-long flute bit for swarf cuts. Using a long flute 1/4 inch bit causes more vibration in the bit so the best way around this issue is to expose more of the current bit from the collet. The current bit length can be increased by 3/8 inch which is expected to resolve this problem which is tested in the next test (Figure 163).



Figure 163_ 1/4 inch down shear drill bit extension capacity.

Contour cuts with the compression bit causes a lot of rough edges, the problem was caused by using depth cuts for the contours which engaged the up-shear part of the compression bit with the material which caused rough edges. In the next test single toolpath is used for the contour cuts which is faster and also doesn't engage the up-shear part of the bit with the material.

Below is the list of the considerations for the next test run:

- Using single depth cuts instead of two depth cuts for contour cuts.
- Using longer 1/4 inch down-shear drill bit. 3/8 inch longer to avoid collision with the stock.
- Increasing the size of the dog-bones and create smoother tool-pathing for connection cuts.
- Using thicker spoil board 0.6 inch instead of 0.4 inch.
- Manually decreasing cut speed and feed rate to 75%.
- Moving the material 5 inch away from the edges of the CNC bed accommodate more space for rotation of the 5-Axis in vicinity of the edges.

5.6.3 Fabrication process_ Test 02

For this test all of the considerations from test one are implemented to enhance the fabrication process. A 1/4 inch down-shear drill bit was used for swarf cuts, the exposed length of the bit is extended to avoid the collision with the material. Also, the size of the dog bones was increased to accommodate smoother tool pathing. A 3/8 inch compression bit is used to cut the contour cuts in one toolpath. A single toolpath will avoid engaging the up-shear part of compression bit with the material and gives a smoother edge (Figure 164). The speed and feed rate of the cuts were manually decreased to 75% to avoid the burning of the material in the swarf cuts area. The stock was located five inches away from the edge of the table to accommodate smoother movements of the CNC machine (Figure 164).



Figure 164_ 5-axis CNC bed and the test cut results for the fabrication test two.

The swarf cuts were done very smoothly after implementation of changes. Also reducing the speed and feed rates of the machine was effective in controlling the heat in swarf cuts area. The increase in the size of the doge bones created smoother movement of the bit around the connection cuts and better edge cut results. Also increasing the length of the bit ensured no collision with the stock material.

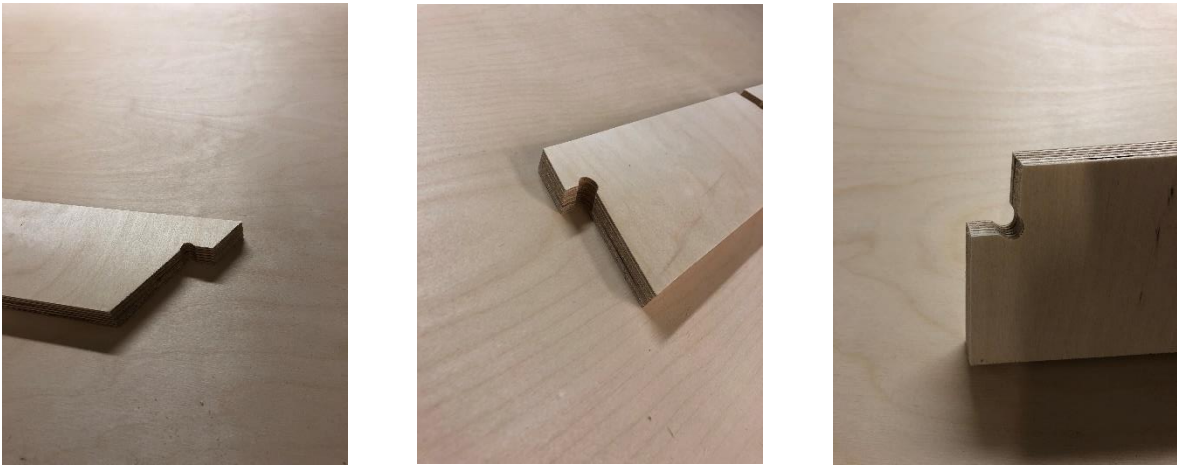


Figure 165_ Fabrication results for the fabrication test two.

Although these changes in the process resulted in clean and smooth cuts, however, the increase in length of the bit increased the bending moments in the bit and the bit broke soon after cutting the second swarf cut (Figure 164 and Figure 166).



Figure 166_ Drill bit failure in swarf cuts in test two.

Since the bit broke we could not finish the cuts and test the assembly process. Moreover, knowing that using the longer 1/4 inch bit will not work for this process we decided to increase the size of the bit to 3/8 inch. Increasing the size of the bit increases the size of the adaptive dog bones in the code which is not applicable since bigger dog bones causes bigger cuts at the base of the connections which will reduce the base size. Reduction in the size of the connection base compromises the structural performance of the connection and is not visually desirable. This issue calls for a change in the fabrication process. A practical option is to remove the dog bones from the code and instead drill the connection corners using a brad drill bit. This process is implemented in the third fabrication test.

5.6.4 Fabrication process_ Test 03

Based on the results of the previous tests some revisions are implemented in the fabrication process as below.

- Dog bones are removed from the fabrication geometry generation code and replaced with drilling for connection corners.
- 3/8 inch down-shear bit is used for swarf cuts
- 3/8 inch compression bit is used for contour cuts
- 3/8 inch brad bit is used to create holes in the connection corners
- 1/2 inch brad bit is used to drill holes at acute angles of the connections

The 4-foot by 8-foot plywood sheet is reused from the previous test.



Figure 167_ 5-axis CNC bed and the test cut results for the fabrication test three.

The Swarf cuts are used for connection cuts. To simultaneously test a different routing process, the last three pieces were programmed to be cut completely using swarf cuts instead of contour

cuts. Three depth cuts were used with 0.25 inch cut for each step. The speed and feed were manually reduced to 75% (Figure 167 and Figure 168).



Figure 168_ Using swarf cuts to test the full member cutting in one toolpath.

These settings for the swarf cuts seem to be working smoothly with a 3/8 inch bit. The edges are clean and smooth and also using swarf cuts to cut the whole piece produces clean pieces and is less time consuming in terms of tool pathing process using Mastercam software (creating 30 toolpaths instead of 120 for this project).

The only consideration is that swarf cuts on the last toolpath cut (non-uniformly) deeper into the spoil board due to the inherent angle that engages the drill bit with the material during the cut. We moved the toolpaths up manually ($0 \text{ inch} < \text{depth} < 0.03 \text{ inch}$) to avoid deep cuts in the spoil board. The down side in this change is that, due to this vertical movement of the tool path some parts of some of the members would not be completely cut in the last tool path (Figure 169).

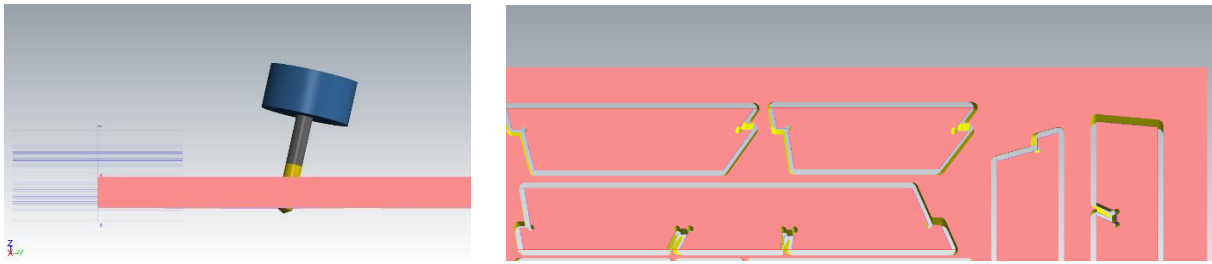


Figure 169_ Swarf cut tool pathing and depth cut consideration.

3/8 inch compression contour cuts were used similar to previous tests to cut the straight part of the pieces. The goal is to compare the compression cuts with the full length down-shear swarf cuts for production. The results show that using the 3/8 inch down-shear swarf cuts can be used to cut all of the edges of the pieces smoothly and without a problem. This actually saves machine time and tool pathing time and creates nicer edges in comparison to using swarf cuts for cuts around the connection edges and compression contouring for straight edges. Moreover, no tabs were needed in this process.

We eliminated the dog bones and used 3/8 inch bit to cut the holes at the corner of the connection cuts. Although dog bones were aesthetically more desirable due to their adaptation to angles of cuts and more effective since the toolpath is cutting out the connection corners with minimal material elimination but it was impossible to use bits bigger than 1/4 inch drill bit to cut them since using 3/4 inch sheet thickness, bigger dog bones would cut most of the connection base and would reduce the effectiveness of the connections (Figure 170).

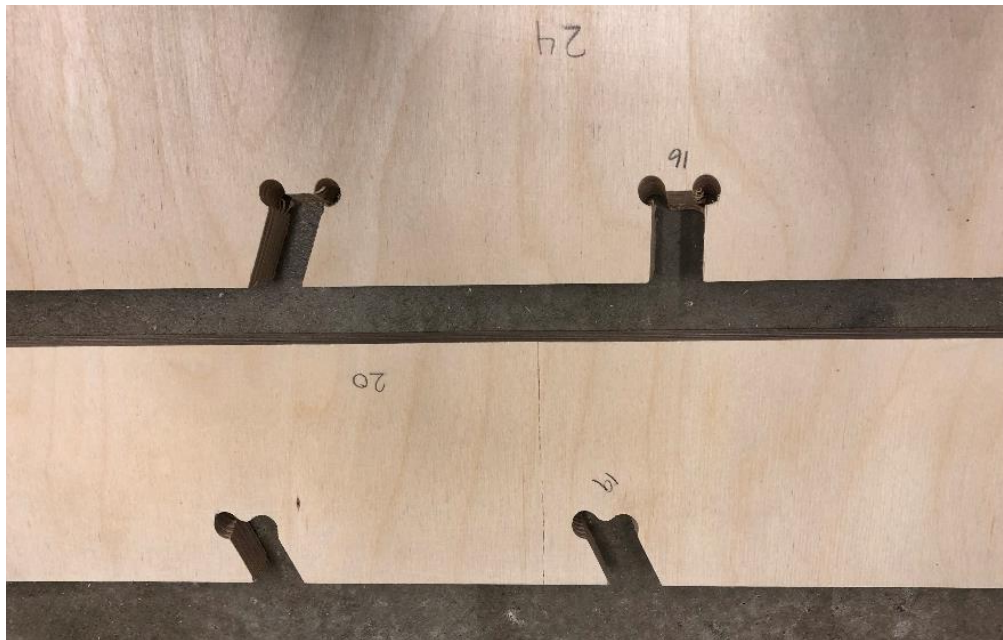


Figure 170_ Comparing dog bone cuts vs drilling. Top: drilling the corners, bottom: dog bone detailing.

The main problem with using drill holes instead of dog bone is that some of the holes may miss the acute corners which needs post processing to eliminate extra material. Toward this goal 1/2 inch drill bits where used at the acute angles to ensure complete corner cuts (Figure 171).



Figure 171_ Using 3/8 inch and 1/2 inch drill holes based on the connection angle.

Connections are an important aspect of the design in discrete systems and should be integrated in the design to fabrication process to guarantee the structural integrity and effective assembly logic, especially in an interconnected system such as reciprocal systems. Moreover, connection design always presents a compromise between different design constraints such as fabrication constraints, assembly constraints, architectural and structural functions, cost and labor.

Therefore, the connection design should address the design requirements and limitations as part of the design process. Earlier in this section four connection designs were introduced for reciprocal systems with 2-D or 3-D member connections. The applications and limitations of each design were explained. This information is helpful in decision making for connection design in different scenarios in relation to the function of the reciprocal system, choice of the digital fabrication technology, and choice of material.

For design and fabrication of the scaled prototype, the modified reciprocal connection detailing with a Kreg screw is chosen due to simplicity and elegance of the connection, cost effectiveness, application of 5-axis CNC machinery for digital fabrication and most importantly ease of assembly. Once the pieces were cut and fabrication holes are done, the pieces are ready to be assembled. Testing the assembly is significantly important to test the applicability of the connection detailing as well as ease of modular assembly, and assembly method is crucial for large scale fabrication.

The scaled half-arch geometry was assembled from bottom up using the notches as guides to determine the orientation of the members. The assembly of the pieces was straight forward, and the connection detailing facilitated effortless registry of the members and screw connections. The tests showed that pre-drilling is essential for ease of assembly (Figure 172, Figure 173).



Figure 172_ Bottom up assembly process for the scaled half arch.

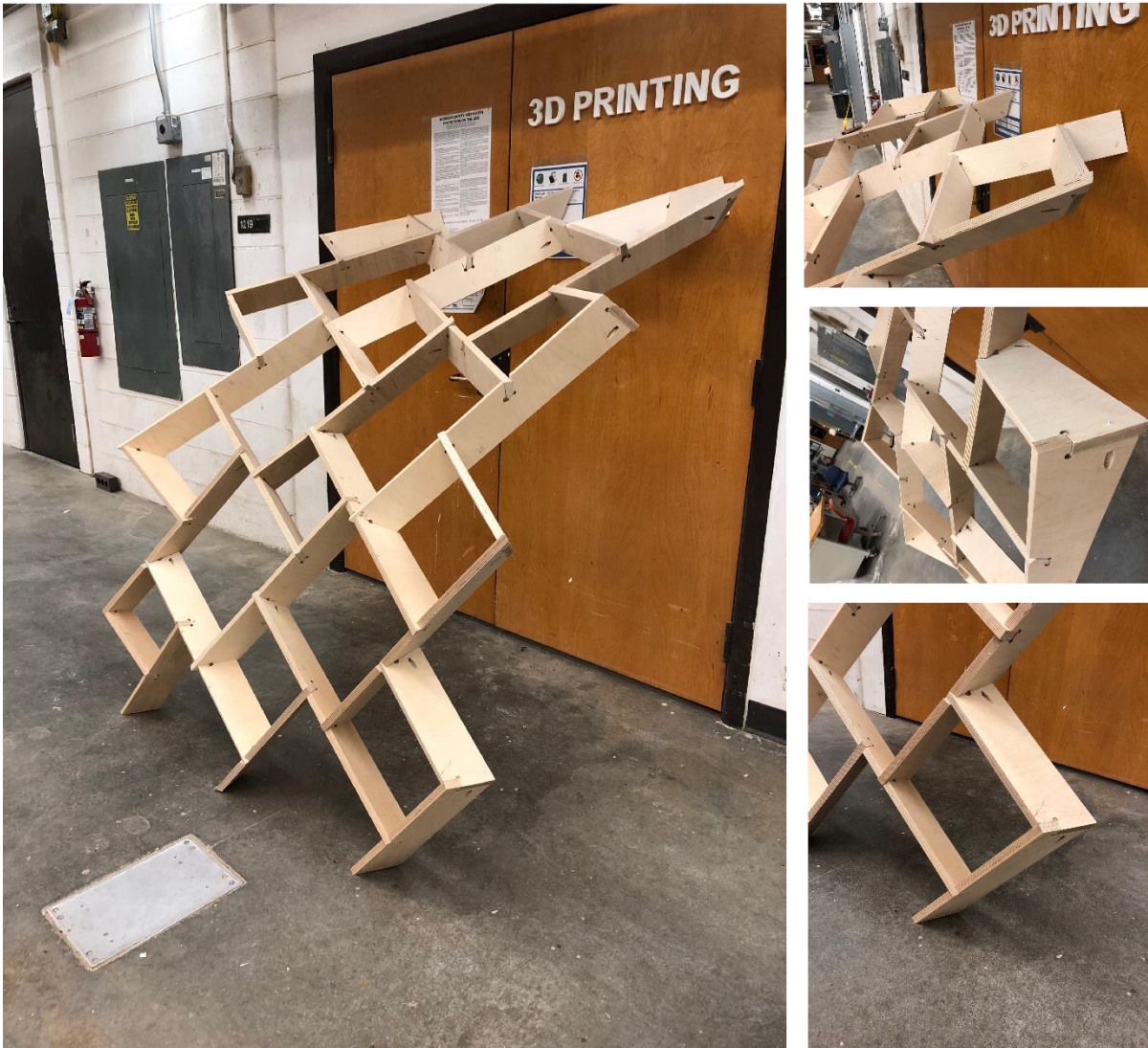


Figure 173_ Half Arch reciprocal geometry with planar rotated members.

5.7 Discussion and conclusion

Reciprocal structures are considered as a practical way to reduce the complexity of member connections, by reducing the number of connecting members to two. However this reduction in construction complexity is replaced with geometrical complexity due to numerous compatibility constraints in the form-finding process. Moreover, the interconnection between form, structural behavior and fabrication process in reciprocal structures requires an integrative design process, which can integrate form-finding, performance feedbacks and fabrication constraints into the design process, to address different design aspects as well as interconnection between the design parameters. This chapter studies the fabrication process for reciprocal structures with 2-D and 3-D configurations.

Joint fabrication and assembly process are two of the main fabrication considerations in design of reciprocal structures as modular and discrete systems. Joint design always presents a compromise between different design constraints such as fabrication constraints, assembly constraints, architectural and structural functions, precision, affordability, rapidity, aesthetics, cost and labor. Therefore, it is important to understand and address these conflicting soft and hard constraints during the design process to ensure the practicality, reliability, cost effectiveness and efficiency of the design solution. Integrating these design constraints in the computational design process can provide useful feedback to ensure the constructability of the design solutions.

In this chapter, four different connection types are proposed for reciprocal systems with 2-D and 3-D member connections and applications and limitations of each design is explained. This information is helpful in decision making for connection design in different scenarios in relation to the function of the reciprocal system, choice of the digital fabrication technology, and choice of material. Based on the studies, a modified connection detailing is proposed which

accommodates fabrication and assembly requirements of reciprocal systems with 2-D and 3-D connections and can be fabricated affordably from sheet materials.

Different design considerations of this connection are studied through digital and physical prototyping, destructive structural testing, detailed simulation, and fabrication of a scaled structure. The main design considerations include, the digital fabrication requirements, loadbearing capacity and mechanical behavior, alignment and accessibility issues of members during the assembly process, required tolerances for fabrication, requirements of external fasteners for structural integrity, and speed, cost and ease of fabrication. One of the important considerations for the digital fabrication is the fabrication tolerances. These tolerances include the specific tolerances of the digital fabrication machinery and tools, material dimensional tolerances, and geometric modeling and form-finding tolerances. These design and fabrication tolerances depend on the choice of digital fabrication, material properties, and the design method. These tolerances are studied through fabrication of multiple physical prototypes. Physical prototypes show that fabrication tolerances have direct effect on the mechanical behavior and assembly process of the connections. Destructive structural tests are carried out to study the mechanical behavior of the connections and possible failure modes of the structure. Specimens show a warping behavior in the members under symmetric loading caused by the inherent asymmetry of reciprocal module, this effect is important since this effect can cause delamination in materials with weak bonds between the parallel layers.

Detailed load-displacement measurements demonstrate a bilinear load-displacement graph which depicts the nonlinear behavior of the connections caused by the fabrication tolerances. Results show that large fabrication tolerances can reduce the stiffness of the system by up to fifty percent. Also, the test results show that the failure happens in the connection region and the

fracture is initiated at the bottom face of the crossing member under the tension induced by the bending moments. Detailed finite element structural analysis of the reciprocal module shows that maximum stress concentrations happen at this area. Moreover, the connection region is weakened by the fabrication cuts and the screw hole which guarantees the failure in this area. These observations have important implications. First, it is important to reduce the depth of the notch cuts to keep the structural depth as much as possible (in contrast, the notch geometry and depth play an important role in the alignment of the connecting members in the assembly process). Second, it is structurally beneficial to fabricate the connection cuts with minimum tolerances. Based on the observations during the loading tests, if the fabrication tolerances are small enough, they would be eliminated by the elastic deformations of the structure and the full capacity of the member cross-section would participate in the loadbearing process.

These studies define the key parameters for fabrication of reciprocal systems based on the proposed connection detailing. Also, a generalizable and efficient fabrication process is proposed for fabrication of reciprocal systems with 3-D module geometry using 5-axis CNC machinery. The fabrication and assembly process of the proposed method is tested through the design and fabrication of a scaled half-arch reciprocal geometry.

References

- Baverel, Olivier, and O. Popovic Larsen. "A review of woven structures with focus on reciprocal systems-nexorades." *International Journal of Space Structures* 26, no. 4 (2011): 281-288.
- Galjaard, Salomé, Sander Hofman, and Shibo Ren. "New opportunities to optimize structural designs in metal by using additive manufacturing." *In Advances in architectural geometry 2014*, pp. 79-93. Springer, Cham, 2015.
- Mesnil, Romain, Cyril Douthe, Olivier Baverel, and Tristan Gobin. "Form finding of nexorades using the translations method." *Automation in Construction* 95 (2018): 142-154.

Messler, Robert W. Joining of materials and structures: from pragmatic process to enabling technology. Butterworth-Heinemann, 2004.

Chapter 6: Computational Design Process and the Fabrication Case Study

6.1 The complexity of the reciprocal systems: the need for an integrative design process

In reciprocal frames, elements are geometrically interdependent in that the position of one element depends on the elements it connects to, and these dependencies form a circular graph. These interdependencies have multiple implications in the design, analysis, and fabrication of these systems (Kohlhammer et al., 2017).

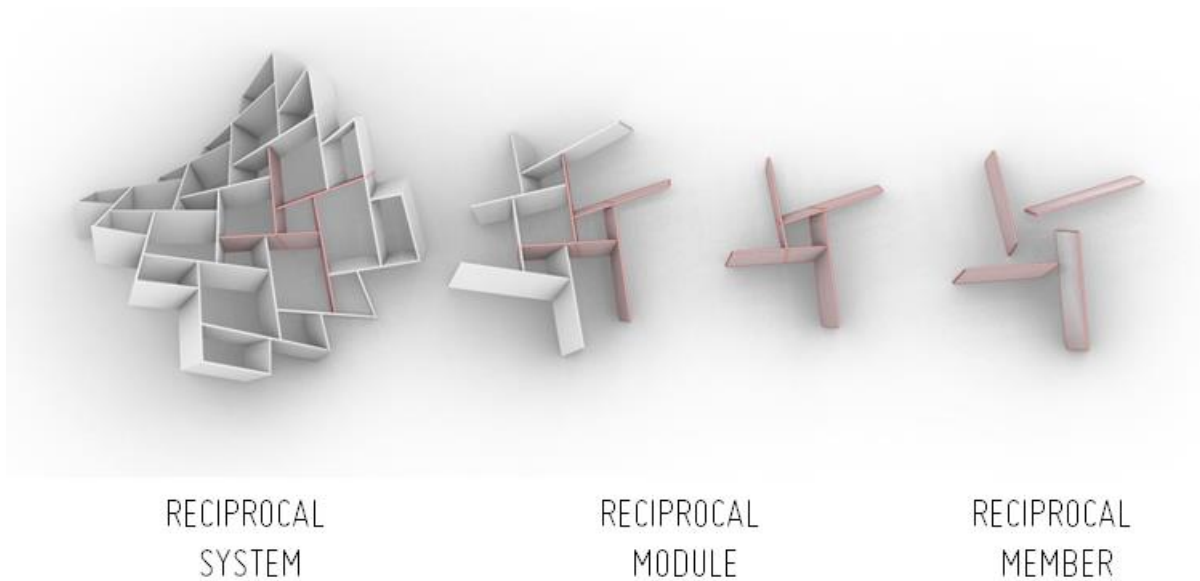


Figure 174_ The interconnected structure of the reciprocal systems illustrating the relationship between member, module, and system.

Altogether, the specific combination of geometric, structural, and fabrication-related constraints form a unique and thus far, unexplored problem setting. In other words, little knowledge exists to provide guidance to the designer to apply these constructive systems, especially with non-regular designs and structural topologies that have many unique and interdependent elements (Apolinarska, 2018). Because of the prevailing complexity, the geometric, structural, and fabrication-related aspects cannot be treated in isolation during the design process and need to be integrated within one digital workflow. As a prerequisite for such integrative design approach, the designer must not only reflect the specific build-up, but also provide meaningful methods to evaluate the results and visualize them.

In the previous chapters of this dissertation, various design aspects of reciprocal systems have been studied separately. In Chapter 3, the generative design and form-finding was examined; Chapter 4 investigated the structural behavior and the governing parameters; and Chapter 5 explored the fabrication process for non-conventional reciprocal systems with planar elements and their design constraints. These studies provided an in-depth understanding of the design and analysis process for reciprocal systems. The ultimate goal of this understanding then is to develop an integrative design to the fabrication process to address the interdependent design complexities of reciprocal systems. To this end, a computational design process is developed which integrates multiple levels of design and fabrication feedback to inform the design geometry.

Combining computation, simulation, and digital fabrication creates a rationale for new types of design and construction methods informed by the performance efficiency while guaranteeing constructability and ease of assembly. This research presents an integrative computational design

process for form-finding, analysis, and fabrication of reciprocal systems with planar elements connected with integrated notched connections allowing 3-D rotations of the members.

The proposed computational method is used to study the complex interplay of the geometric and fabrication parameters with structural performance. The results show that the optimal geometric parameter settings with respect to structural performance and fabrication constraints are neither evident nor easy to drive. Nevertheless, desirable configurations can be found with the aid of the developed computational design process. Moreover, optimal configurations can be found through the application of the proposed computational design method in a multi-objective exploration of the design space.

6.2 Computational design process: the need for computational tooling

To overcome the design complexities of reciprocal systems, custom computational methods are needed. First, the computational design process needs to address the complexities of design, analysis, and fabrication of these systems. This can be achieved through the development of custom software (or an adaptation of the standard software) that can generate the design and evaluate its performance based on the design requirement. Second, the computational design process needs to integrate different disciplines within one digital workflow to produce satisfactory designs within a combination of architectural, structural, and fabrication related requirements. Third, the confluence of data, differentiated in terms of source, content and structure, requires appropriate data management, storage, and exchange methods.

Figure 175 depicts different modules and the interoperability between them in the computational design process. This diagram shows different methods and file formats to store and view design objects and the corresponding data in each module within the digital dataflow.

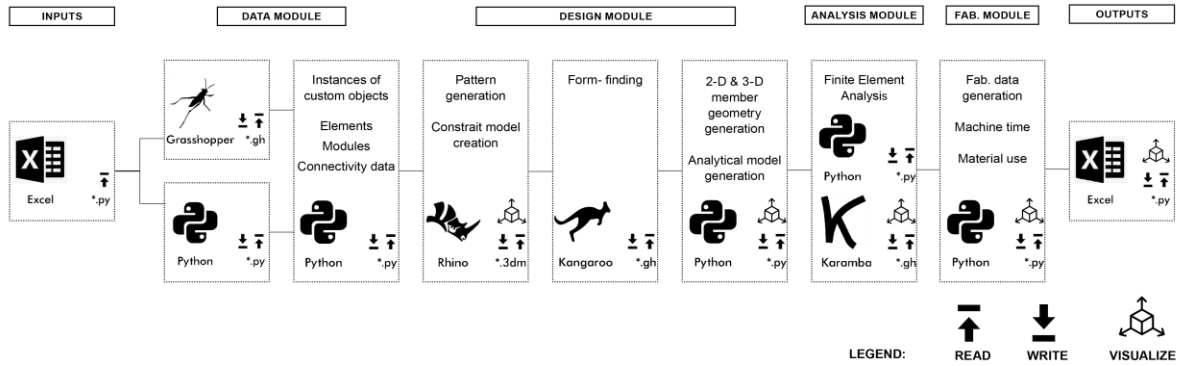


Figure 175_ Depiction of the digital dataflow: different methods and file formats to store and view design objects and the corresponding data in each module within the digital dataflow.

Reciprocal structures are complex structural systems (exposing tangled interrelations between their features), non-standard systems (consisting of large amounts of unique elements), and unexplored structural type (lacking empirical design guides) (Apolinarska, 2018). These traits challenge the capabilities of the standard modelling and analysis tools and conventional workflows. Consequently, custom design and analysis tools are needed to be developed to address the complexities and non-conventional design aspects of these systems in an integrative design process.

In this research a combination of custom software (self-made) and commercial software (standard) were used in the computational design process. Some of the custom software were developed to do a specific design or evaluation task (including pattern generation, fabrication data generation, and code based structural evaluations) and some were developed to translate and transfer different data between the self-made modules and commercial software (including analytical model development, developing performance metrics from the simulation results, data transfer, and data storage). Figure 176 shows the architecture of the computational model differentiating between self-made (custom) and ready-made (standard) components.

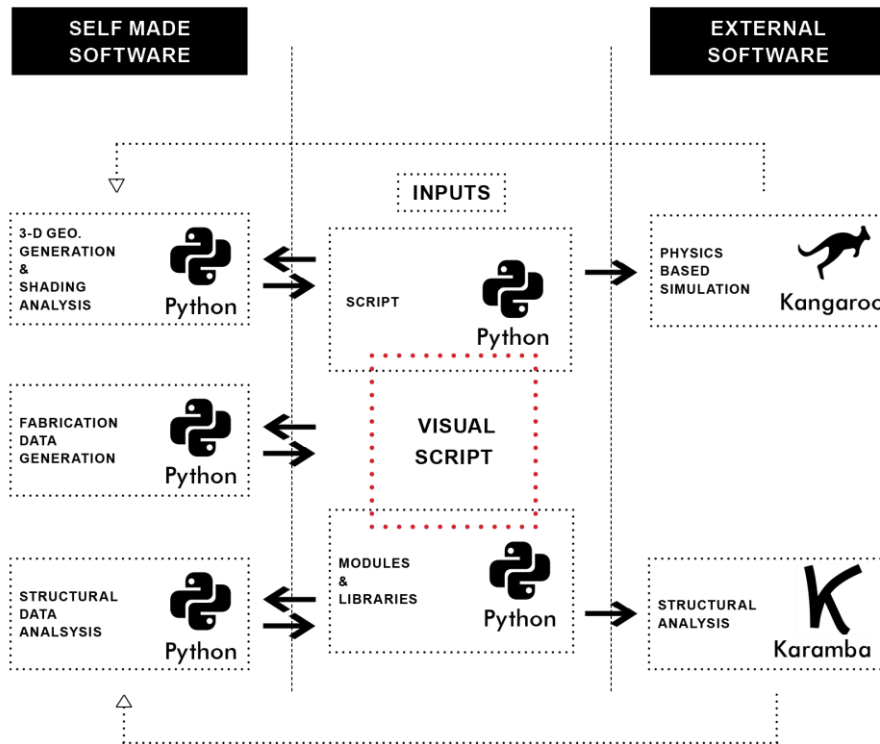


Figure 176_ Implemented software and programming tools differentiating between self-made (custom) and commercial (standard) components.

6.3 Case study: design to fabrication of the Reciprocal Shades project

To better demonstrate the application of the proposed computational design process for an architectural scale construction, a full-scale prototype of an arch was fabricated as a public pavilion located at the entrance of Matthaei Botanical Gardens in Ann Arbor, Michigan (Figure 178). The arch was located on the top of a hill in front of the Conservatory building.

A doubly curved arch geometry was used as the base surface geometry to design the reciprocal structure. The arch spanned almost 14 ft. wide with a maximum height of 6.7 ft., and a structural depth of less than 5 inches using 0.75 inch thick plywood sheets. The maximum size of the reciprocal members was limited to 4 ft. for ease of fabrication (nesting within a 4 by 8 foot

plywood sheet), as well as length and weight limitations for manual assembly. Figure 177 below shows the Reciprocal Shades sizing and dimensional constraints.

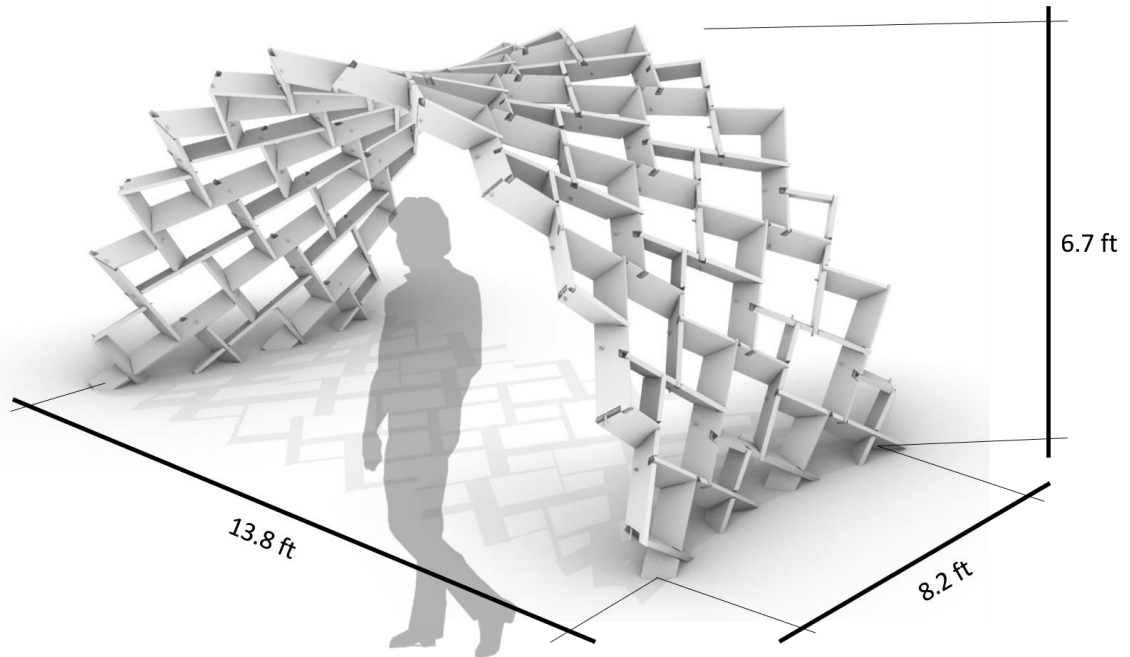


Figure 177_ Reciprocal Shades dimensions.

In addition to these adjustments, multiple design considerations including aesthetics and performance issues were taken into account for the possible positioning and orientations of the arch on the site. The arch axis was rotated 35 degrees clockwise to enhance the perception of the reciprocal pattern for the visitors as they drive by the arch from the north entrance to the west parking lot. This decision was also informed by the dominant Southwest wind direction in the area. Since this orientation allows the winds to go through the arch, it would lead to a less wind exposure area on the arch which reduces the overall wind induced loading on the structure (Figure 179). Other aesthetic aspects, including the scale of the arch and the density of the pattern, were limited by the project budget. Since these design aspects are quantifiable, they were

considered as objective metrics in the form exploration process to generate better performing design solutions.



Figure 178_ Designated site for construction of the Reciprocal Shades at Matthaei Botanical Gardens, Ann Arbor, Michigan.



Figure 179_ Accessibility from the north entrance and arch location and orientation.

Plywood was chosen as the fabrication material. Plywood is an engineered wood material composed of thin sheets of wood veneer glued together and rotated 90 degrees in respect to adjacent layers. Unlike unprocessed timber, the properties of the panel are more similar in all directions due to the layering orientation. Plywood was selected due to availability, acceptable dimensional stability, and ease of fabrication using 5-axis CNC. Figure 180 compares the various material properties for a range of materials applicable to reciprocal systems. As the chart displays, plywood has high stiffness with comparatively lower density which makes this material ideal for light weight construction.

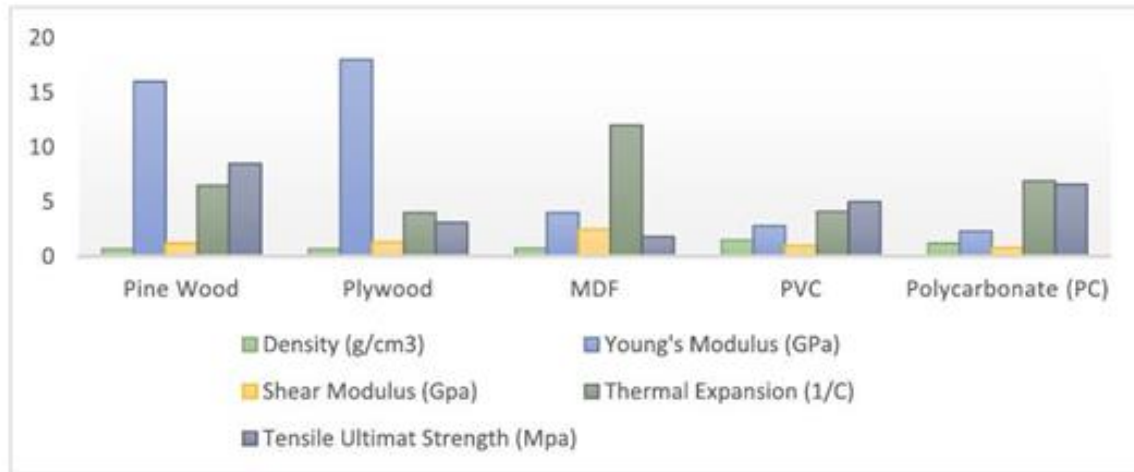


Figure 180_ Comparison of different material properties for wood, plywood, MDF, PVC and PC (Asefi and Bahremandi-Tolou, 20019).

Weathering was an important design consideration, since the designated site for this project was located outdoors, for the duration of six months including the cold season. Thus, marine grade plywood was chosen due to its high waterproof properties, and an additional waterproof and UV resistant coating was applied to all of the surfaces in order to enhance the overall weathering

resistance of the structure. Table 1 shows the material properties of the 8 layered marine grade birch plywood based on the APA standard.

6.4 Implementation of the computational design process

As was depicted in Figure 175 the computational design process was implemented in the form of a series of modules, each responsible to carry out a certain task. Each module receives specific inputs and generates expected outputs that contain geometric and numerical data depending on the module task and requirements. Each of these modules, their implementation and their application in the computational design process is explained in the following sections.

6.4.1 Computational model: The geometry module

As detailed in Chapter 3, the reciprocal pattern generation and the generative mesh-based formulation uses the quadrilateral mesh data derived from the rationalization of the design geometry to generate the reciprocal patterning. It additionally generates geometric and connectivity data to formulate the geometric and fabrication constraints based on the connection design requirements. Steps in the reciprocal pattern generation process are depicted in Figure 181. The process in the geometry module begins by discretizing the design geometry by using a quadrilateral mesh. Next, the mesh data (mesh vertices, half edge data, neighboring cell data) is generated and stored. This data is then used to implement the reciprocal pattern generation formulation. This step generates 1-D reciprocal members and the topological network data (connectivity data for each reciprocal member and each reciprocal module in the network). This data is necessary for generation of the constrained model in the form-finding process.

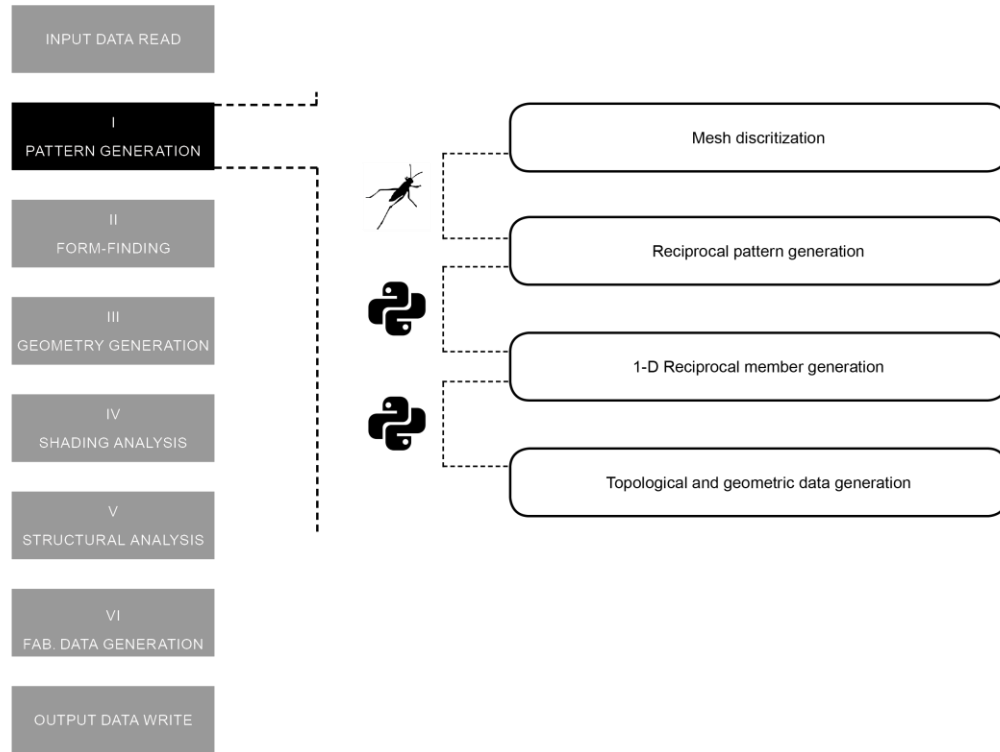


Figure 181_ Implementation of the reciprocal pattern generation module in the computational design process.

6.4.2 Computational model: the form-finding module

The proposed process of reciprocal pattern generation results in an interconnected network of reciprocal members that approximate the design geometry based on the density of the underlying mesh. However, it is important that the process of pattern generation on the free-form geometries induces varying amounts of eccentricities between the intersecting reciprocal members in the modules. These eccentricities need to be addressed in order to create analytical models for analysis or 3-D models for digital fabrication. Different steps in the form-finding process are depicted in Figure 183 .The form-finding process is defined in the form of a constraint-based model. The mathematical formulation of the constraint-based model is defined by the design constraints (eccentricity constraints, rigid body constraints, and the boundary conditions,). The

form-finding process then uses the dynamic relaxation method to solve the constraint-based model, which iteratively and simultaneously minimizes the eccentricities between the members. The form-finding module generates the final geometry with 1-D members with minimal eccentricities within the fabrication tolerances. Moreover, as explained in Chapter 5, this module generates series of structured data which is required to design the fabrication detailing including 3-D member geometry and connection detailing. The first data set identifies the reciprocal members in each reciprocal module of the reciprocal system. This data is specifically important because due to the interconnected nature of the reciprocal network, every reciprocal member is shared with two reciprocal modules. As a result, any variation (variation in member rotation or perforation depth) will propagate in the system through the shared members. The second data set identifies the four intersecting members to each reciprocal member (Figure 182).

This data is required to first to calculate each intersection point based on the existing residual eccentricities and then generate a new wireframe member for analysis purposes based on the calculated intersection points. From there, these intersection points generate connection detailing.

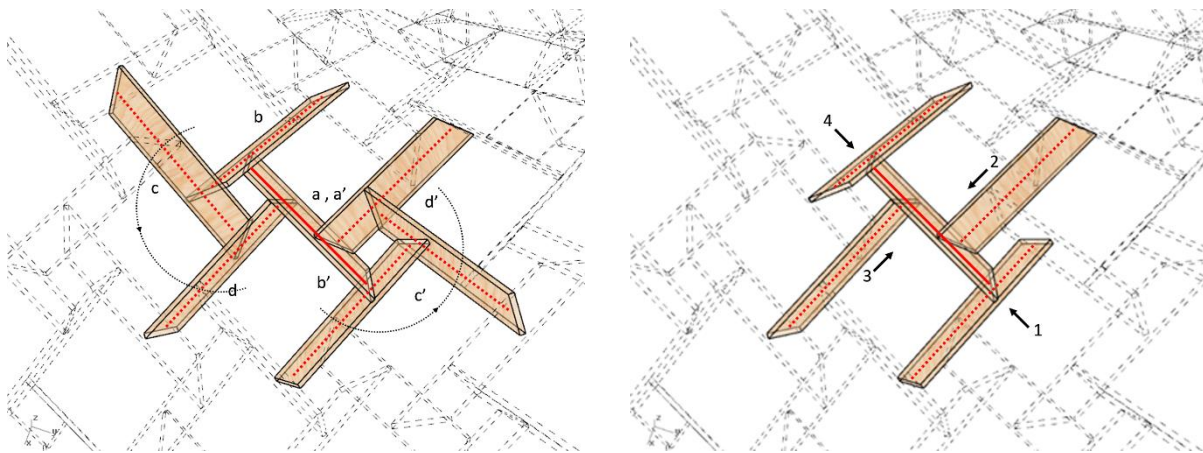


Figure 182_ Generation of the system network data.

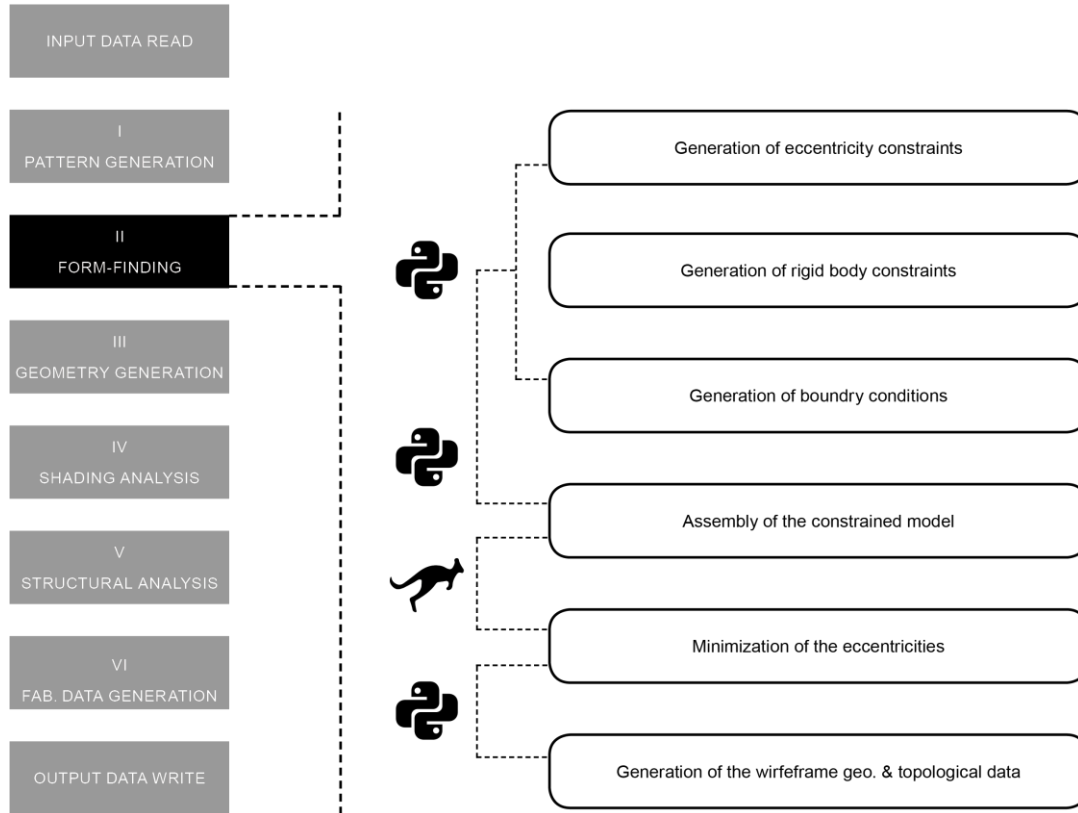


Figure 183_ Implementation of the form-finding module in the computational design process.

6.4.3 Computational model: the 3-D geometry generation module

The output of the form-finding module is a wireframe geometry which defines the center line of the reciprocal members. The wireframe geometry is used in the geometry generation module to generate the 2-D and 3-D member geometries based on the design parameters and the topology data. As described in Chapter 5, rectangular member cross-sections with large height to width ratio were considered to generate the reciprocal member geometry. These considerations relate to the construction considerations and efficiency of using flat sheet materials for fabrication. Also, a large height to width ratio guarantees the construction of reciprocal systems with perforation

depth which has applications in modulating light and generating shades. The parametric process can then be modified to accommodate any cross-section types: circular, rectangular, or irregular. Different steps in the geometry generation process are depicted in Figure 184. Cross-sections are oriented along each element following the Darboux-frame and the expansion of the reciprocal member is defined by the normal of the underlying mesh face geometry (Figure 117). Once the orientation is determined the surface geometry of the member is generated based on the depth parameter. Once the surface geometries of the members are generated, they are cut by the intersecting members at the two ends. These trimmed surfaces are used to generate the 3-D solid geometry of the members based on the member thickness parameter or the calculated member thickness based on the structural requirements.

Moreover, this module generates the geometric data required for the generation of the analytical model for structural analysis. As was mentioned in the definition of the form-finding module, the form-finding process will minimize the eccentricities but will not eliminate them for all members, however these eccentricities need to be addressed in the analytical model. Building off findings in Chapter 3, the residual eccentricities are relatively small and accurate enough to regenerate each reciprocal member from the calculated intersection points from four intersecting members. These new members are then used to generate the analytical model where each reciprocal element is discretized into three beam elements.

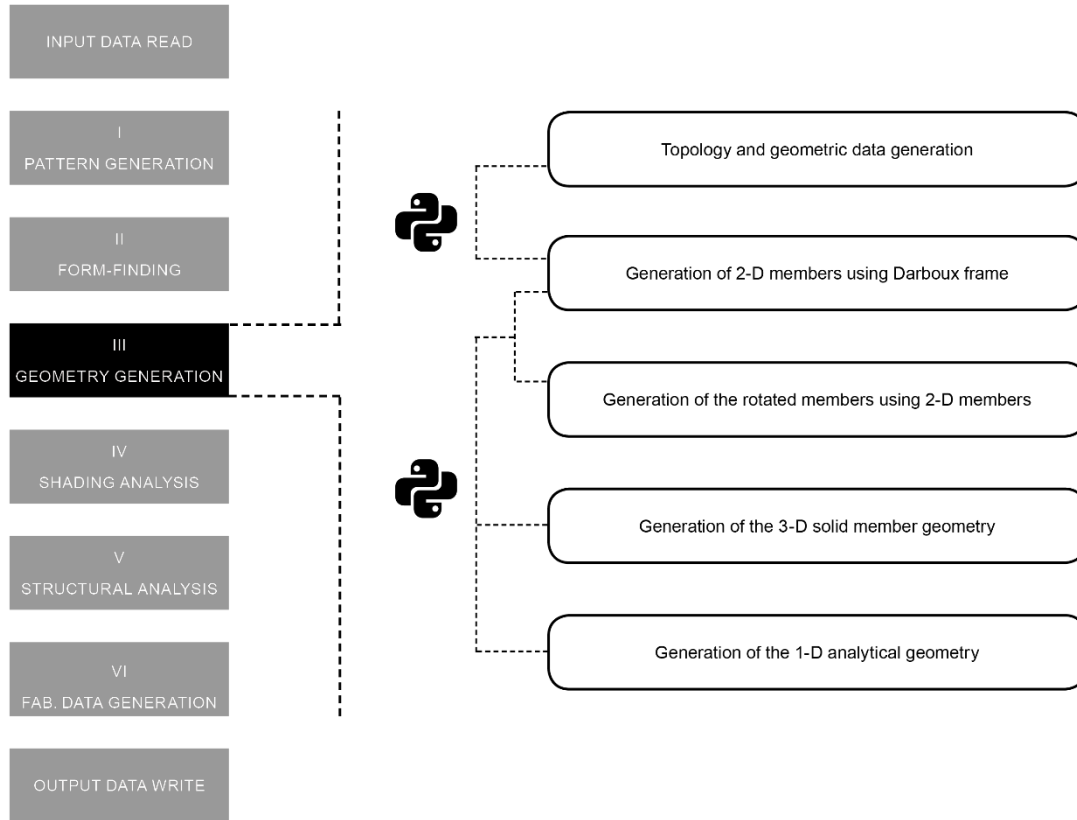


Figure 184_ Implementation of the geometry generation module in the computational design process.

6.4.4 Computational model: the structural simulation module

The geometry generation module generates the analytical wireframe geometry. This 1-D geometry defines the centerlines of the members in the analytical model. The simulation module uses this geometric data to develop the analytical model for the structural simulation. Different steps for the simulation process are depicted in Figure 185. To develop the simulation model first, the member cross-sections are defined based on the member depth and member thickness parameters. Then, plywood material properties are defined and assigned to the members. The boundary conditions of the structure are defined and assigned to the support nodes. Load cases including snow and self-weight are defined and applied to the structure. The member

connectivity stiffness is defined based on the pinned connection of reciprocal members at the joints and assigned to the end points of the reciprocal members. The simulation model of the arch is generated using the analytical data. This simulation model is used to carry out a linear static finite element analysis of the structure using Karamba3D (a structural analysis plugin for Grasshopper) (Preisinger, 2013). The structural analysis generates a series of structural data including node displacement vectors and internal forces in the reciprocal members. A custom code is developed to generate desirable performance metrics from the simulated structural analysis data. The generated structural data is then used in a custom code to generate desirable performance metrics including member utilization factors, maximum displacements, total weight of the structure, maximum and minimum member sizes. The member utilization factors are calculated using the internal forces based on bi-axial bending and axial force formulation as explained in Chapter 3 (APA code specifications). Moreover, the structural data is visualized using custom software and visualization tools in Karamba3d (Figure 186).

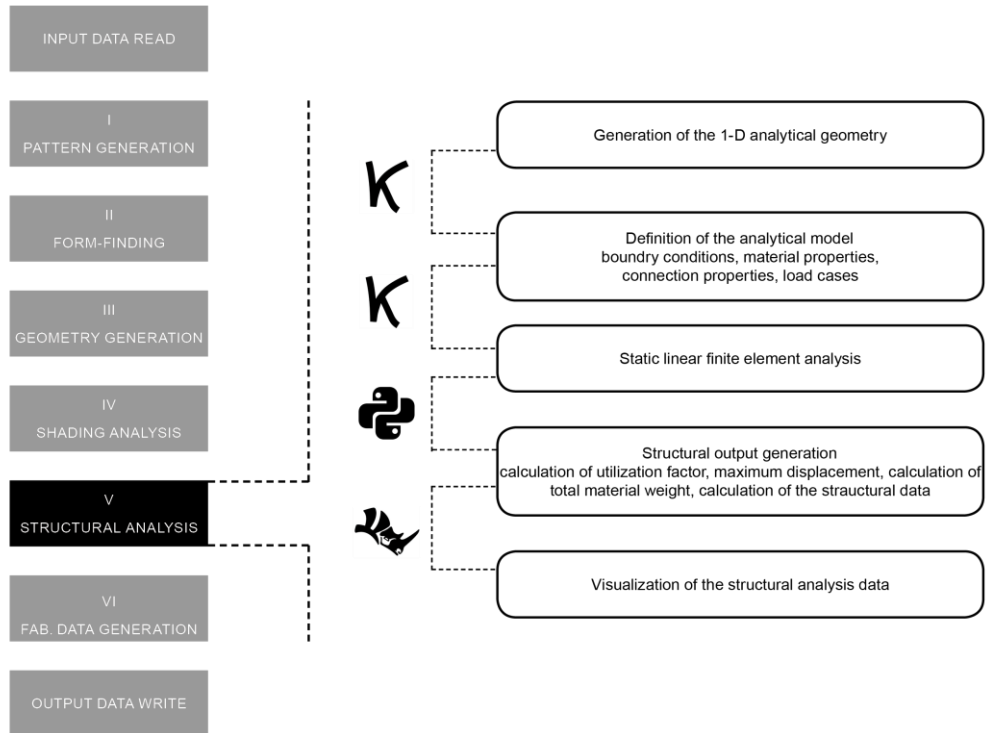


Figure 185_ Implementation of the structural analysis module in the computational design process.

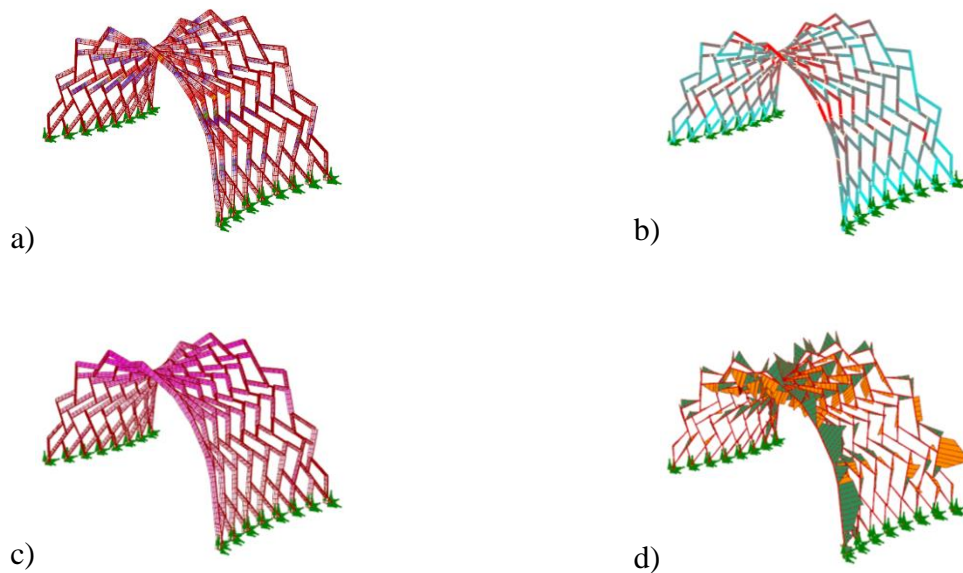


Figure 186_ Visualization of the structural analysis results a) Stress Distribution b) Member utilization generated by a custom code c) Displacement Distribution d) Bending moment distribution.

6.4.5 Computational model: the shading estimation module

The geometry generation module generates 2-D and 3-D member geometries as an output. A simple custom code generates the shading capacity and shading pattern of the structure using the projected geometry of the reciprocal members on a flat surface under the arch. The code removes the overlapping projections and calculates the uncovered area under the arch to estimate the shading capacity and develop the shading pattern. These steps for the estimation of the shading capacity are depicted in Figure 187. Although this method is not an accurate calculation of the shading performance of the system, it provides an approximated metric to compare the shading capacity and the effect of perforation size and distribution with applications in the design exploration process (Figure 188).

For a more accurate estimation of the shading capacity, daylight analysis simulations need to be carried out based on the local weather data.

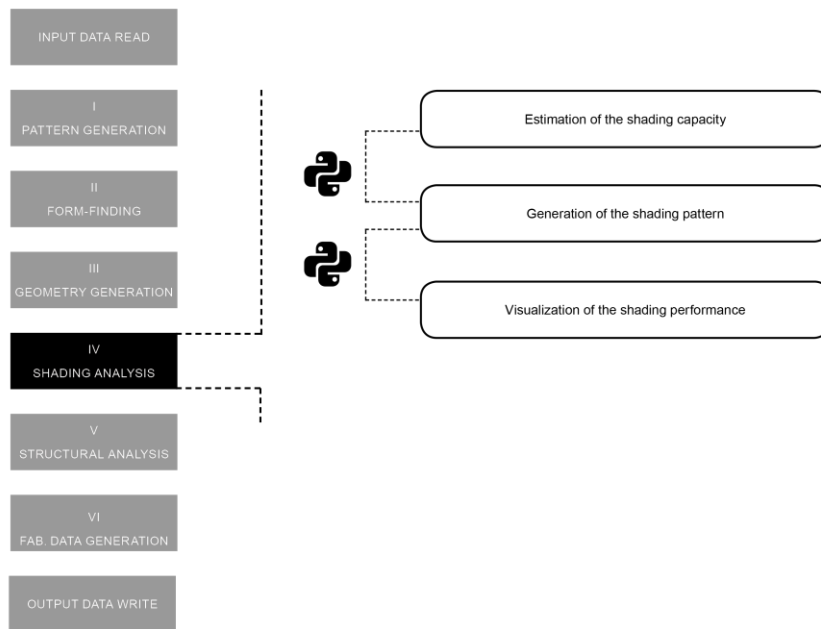


Figure 187_ Implementation of the shading estimation module in the computational design process.

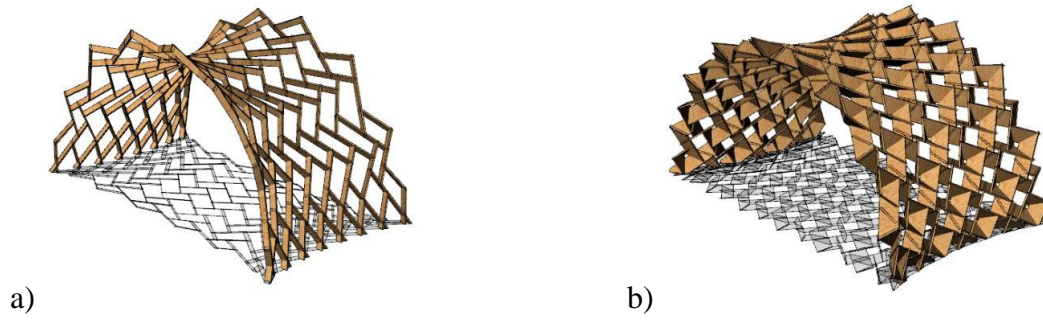


Figure 188_ Comparing shading capacity and shading pattern of two different designs. A) Shading ratio 14.7% b) Shading ratio 85%.

6.4.6 Computational model: the fabrication data generation module

In this case study, the structure is designed to take advantage of the fabrication benefits of using sheet materials (expedient for fast machining), and the lapped joint connection technique (modified notched with 3-D fabrication cuts) that is geometrically simple, easy to fabricate, structurally sound, provides guidance for assembly and can accommodate minor tolerances. (Figure 189).

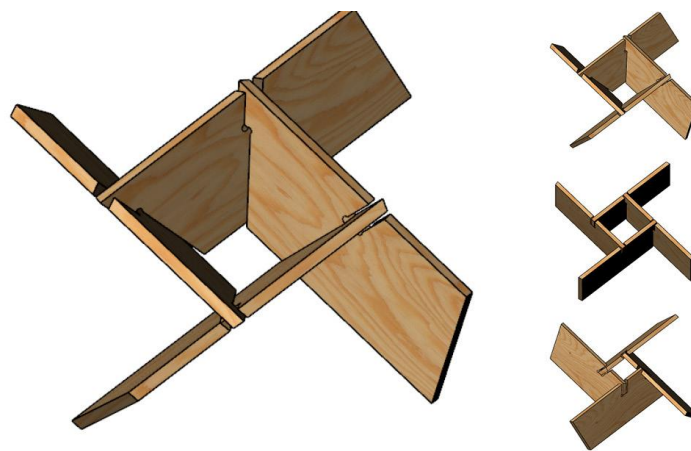


Figure 189_ Lapped notched joint: modified conventional connection adapted for rotated reciprocal members.

Using sheet material, efficiency in material usage is aided by the power of computational design and CNC manufacturing. The steps for the generation of the fabrication data in the fabrication module are depicted in Figure 190. This module uses the 2-D and 3-D member geometries, the network topological data generated in the geometry generation module and the fabrication parameters (connection type and parameters, fabrication tolerances, drill bit sizes, etc.) to create the connection detailing and connection cuts for each joint.

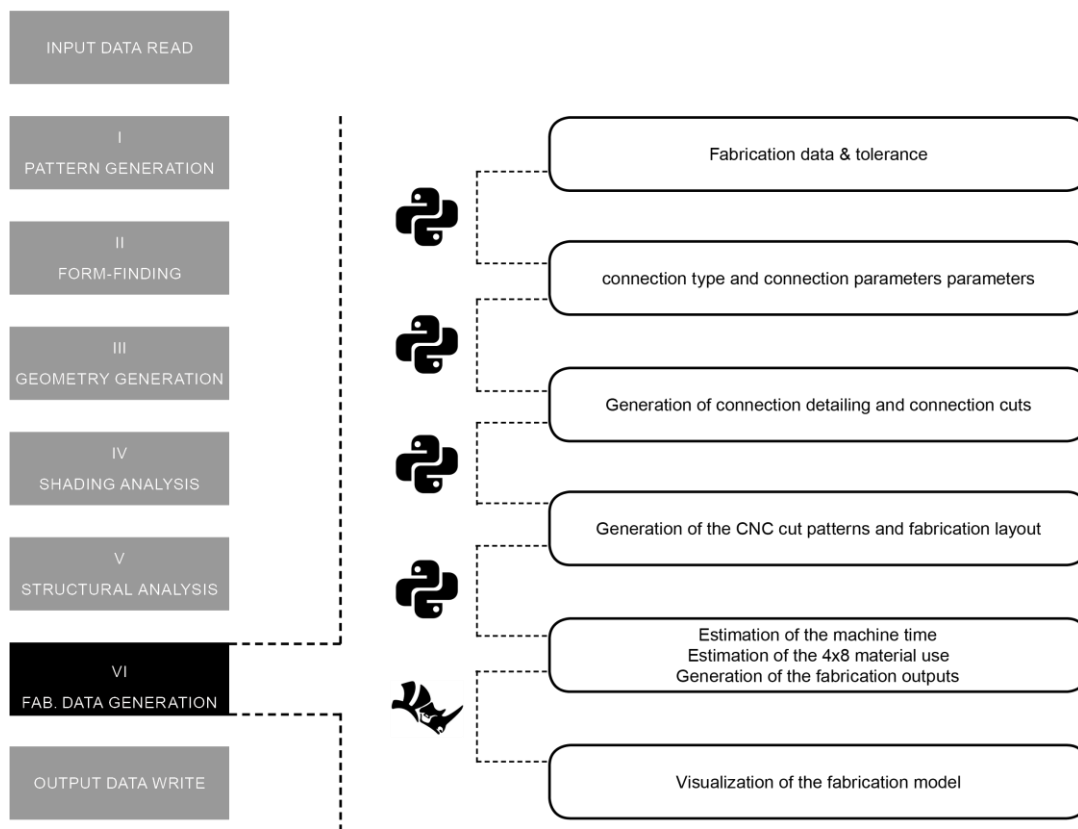
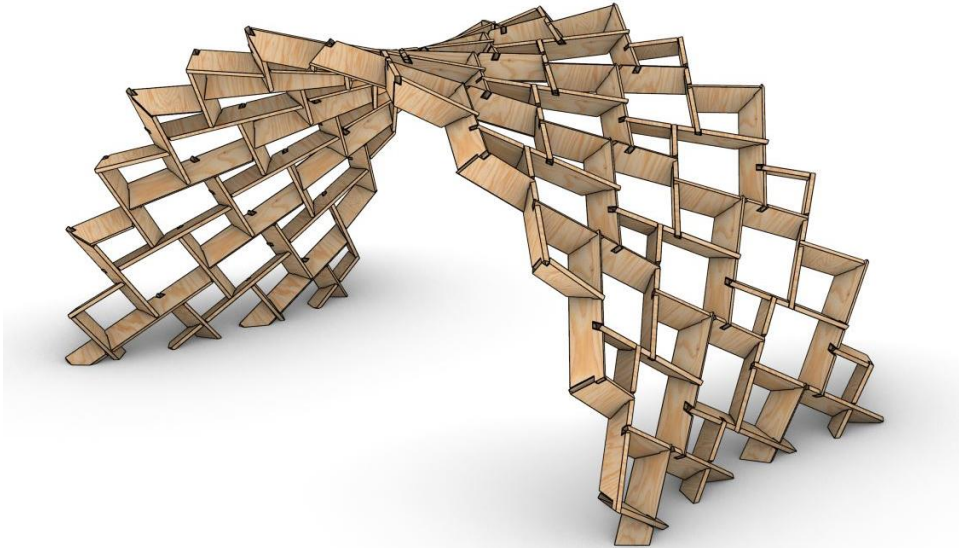


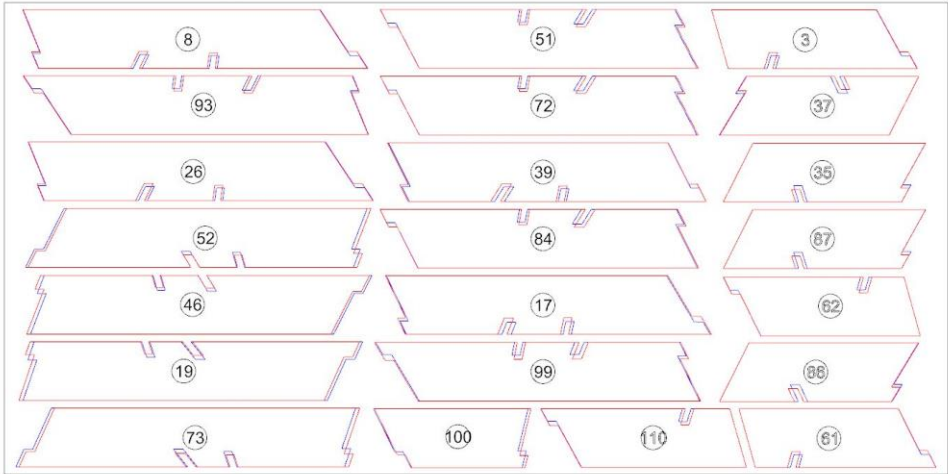
Figure 190_ Implementation of the fabrication data generation module in the computational design process.

The final geometry of the members is used to estimate the CNC machining time based on the estimation derived from the fabrication tests. The total sheet material use is estimated based on the estimated nesting capacity of a 4 by 8 sheet of plywood for planar members. Moreover, the

module visualizes the arch geometry with connection detailing and generates a layout of the cut patterns and drill hole locations for the CNC fabrication (Figure 191).



a)



b)

Figure 191_ Fabrication module visual outputs: a) Sample of the design geometry with connection detailing. b) Sample of the fabrication cut patterns nested on a 4 by 8 sheet for toolpath generation.

6.5 Design exploration: multi-objective exploration of the design space

Due to the complex nature of reciprocal systems and their interconnected design parameters and conflicting design constraints (such as structural performance, fabrication constraints, shading capacity, material use, machine time, etc.) it is impossible to attain an optimal configuration of the design parameters manually. Thus, to reach a desirable solution a systematic exploration method is required to carry out a multi-objective exploration of the design space.

The proposed computational design process generates performance and fabrication feedback (in the form of numerical and visual data) in a modular design to fabrication workflow using a seamless digital dataflow between the modules (Figure 192). Moreover, all the design modules (geometry generation, form-finding, analysis, and fabrication module) are implemented in an associative parametric environment which provides numerical and visual data for each design solution with the dataflow compatible for automation. Figure 192 shows the digital dataflow between different modules in the computational design process, describing the input data (numerical and visual) that each module operates on and the output data (numerical and visual) that each module generates and stores in the workflow. Thus, this computational model can be paired with an automation process and data storage system to perform a multi-objective exploration of the design space.

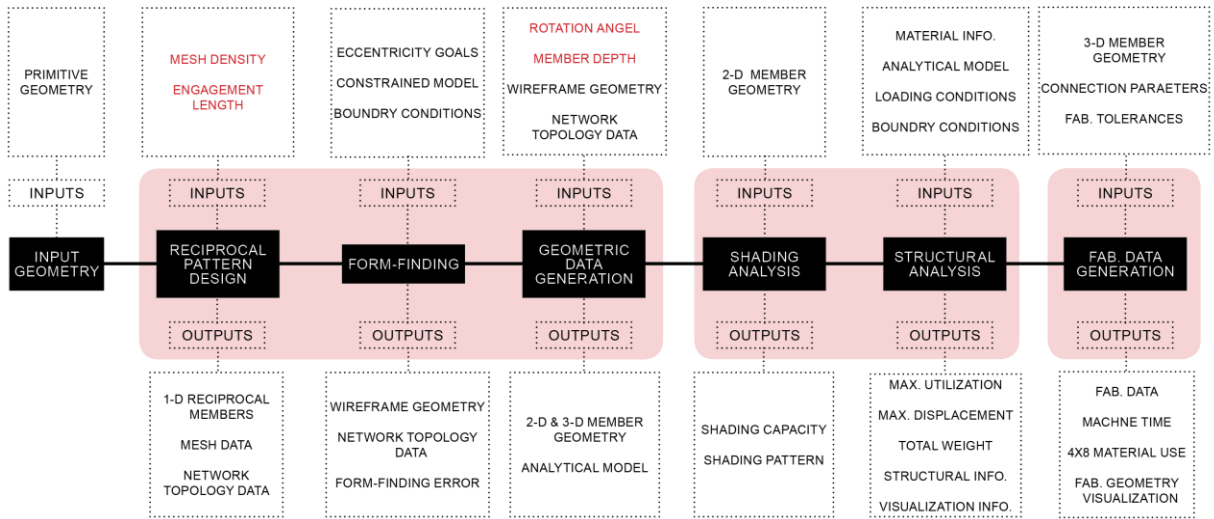


Figure 192_ Definition of inputs and outputs and the digital dataflow between different modules in the computational design process.

The choice of design parameters and their variation range significantly effects the efficiency of the design exploration. The design space needs to include enough diversity of the design solutions while also being sized within an acceptable range which can be efficiently explored with an affordable computational cost. This requires preliminary explorations to understand the sensitivity of the objective functions in relation with design parameters and to determine the acceptable variation range of the design parameters.

To this end, a series of manual explorations were carried out using the design parameters (minimum, median and maximum values) and their permutations (Figure 193). Through the manual explorations the governing design parameters and their acceptable variation ranges were determined as described in

Table 5.

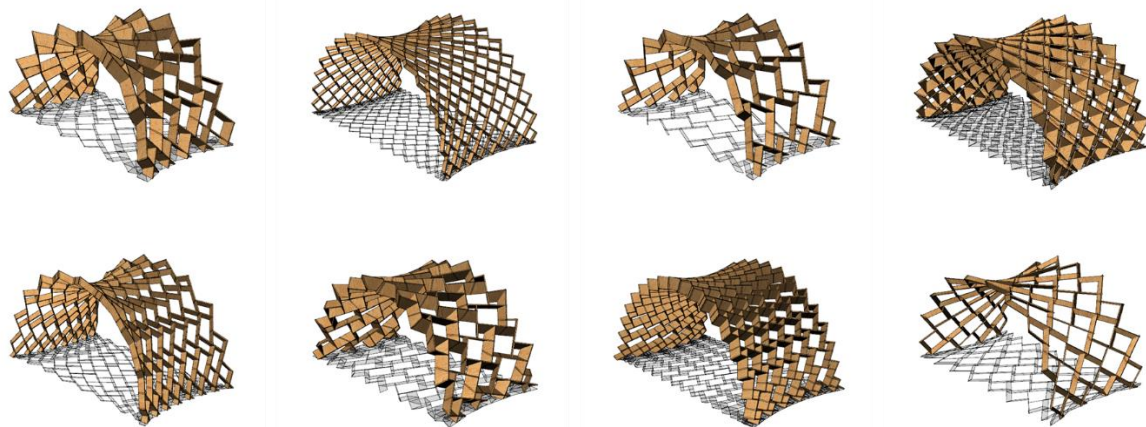


Figure 193_ Samples of design solutions generated by manual exploration showing the variation of form based on the design parameters.

Variable	Min. Value	Max. Value	Step
Meh U Size	4	8	1
Meh V Size	8	18	1
Engagement Length	0.4	0.8	0.1
Member Depth (in)	3	10	1
Rotation (degrees)	0	40	10

Table 5_ Design parameters and their variation ranges defined for design exploration.

The range of design parameters defines the dimensionality and size of the design space, and the range of the possible solutions that the computational model can generate. Thus, the choice of design parameters and their variation range along with the type of performance metrics and the

nature of output data define the usefulness and efficiency of the design exploration process. Moreover, a reliable exploration method is required to explore the design space based on both quantitative performance metrics (material efficiency, shading capacity, structural performance, machine time) and qualitative design values (aesthetics and expression). This requires a design exploration method that explores the design space using both numerical and visual feedback data. To this end, ParaGen, a web-based design exploration engine developed at the Hydra Lab at Taubman College of Architecture in the University of Michigan is used to explore the design space for this project (von Buelow, 2012). ParaGen combines a computational model with a database to store and retrieve the solutions for subsequent exploration. ParaGen can be used either as an optimization tool using a Genetic Algorithm (GA) or as an exploration tool for exhaustive exploration of the design space (brute force). Additionally, the design exploration can be enhanced by means of the interaction of the designer with the process. GA is a population-based metaheuristic optimization method inspired by the natural selection. Through an iterative process, several populations of design solutions are generated successively, and best performing solutions are passed to the next generation. This process searches the design space towards the best performing design solutions. In contrast, the brute force search generates all the possible solutions within the design space with their performance metrics and uses post processing to find the better performing design solutions based on the design criteria.

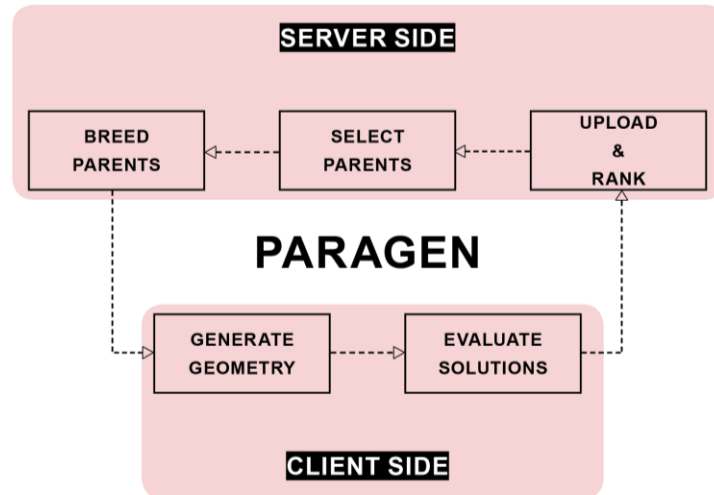


Figure 194_ ParaGen process for a GA based exploration of the design space.

In this research ParaGen was used as a form exploration tool based on performance and fabrication criteria. For this purpose, ParaGen was used on a single PC running Windows 10 and a Linux web server, to run a series of both custom written and commercial software packages.

ParaGen cycles each solution through three basic steps:

- 1) Generation of the input parameters based on the independent design parameters and their variation range.
- 2) Running the computational model based on the input parameters for each design solution. In this research the computational model contains: form generation, geometry generation, performance evaluation and simulation, and the fabrication data generation modules. Each module generates corresponding output data (numerical and visual) for the design solution as is described in Figure 192. Figure 195 shows the visual outputs generated for a sample model and the Table 6 shows the corresponding numerical data.

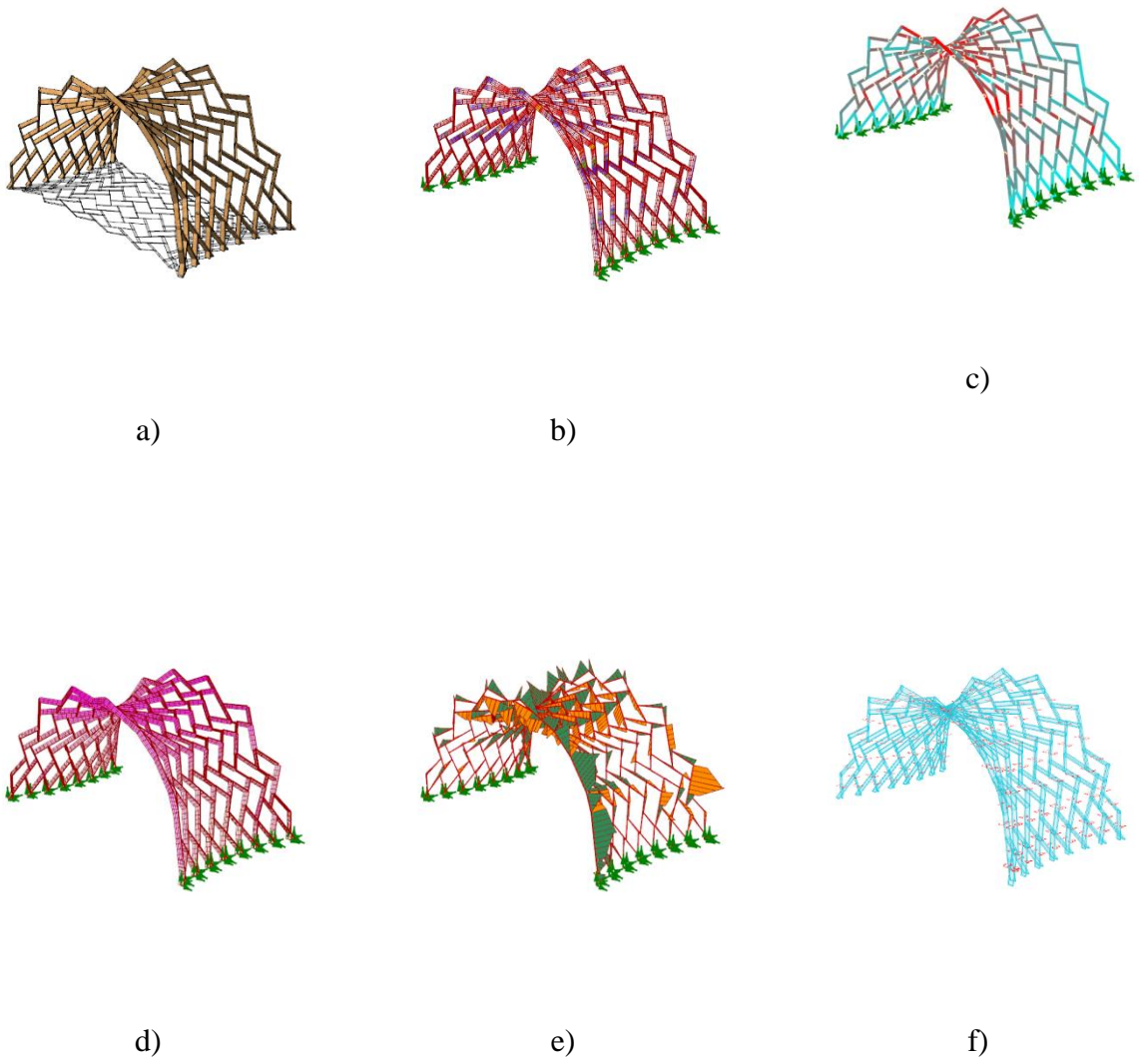


Figure 195_ Visual output generated for each design solution in the form exploration process. a) 3-D Geometry and shading pattern b) Stress Distribution c) Member utilization.

Arch Weight	167 lbs	Estimated Machine Time	104 min
Max. Displacement	0.25 in	Number of Connections	270
Max. Utilization Factor	44.1 %	Number of Elements	144
Min. Utilization Factor	3.7 %	Min. Member Length	1.13 ft
Number of 4 by 8 Sheets	4.2	Max. Member Length	3.09 ft
Max. Form-finding Error	0.18 in	Max. Height	7.1 ft
Shading Ratio	14 %		

Table 6_ Numerical output generated for each design solution in the form exploration process.

3) The design solutions along with the related performance values, fabrication data and graphic depictions are returned to the server where all solutions are maintained in a searchable SQL database. A web page provides a graphic interface to explore the generated design space using multiple queries based on the design parameters and performance values. The design cycle and the data flow are shown in (Figure 196).

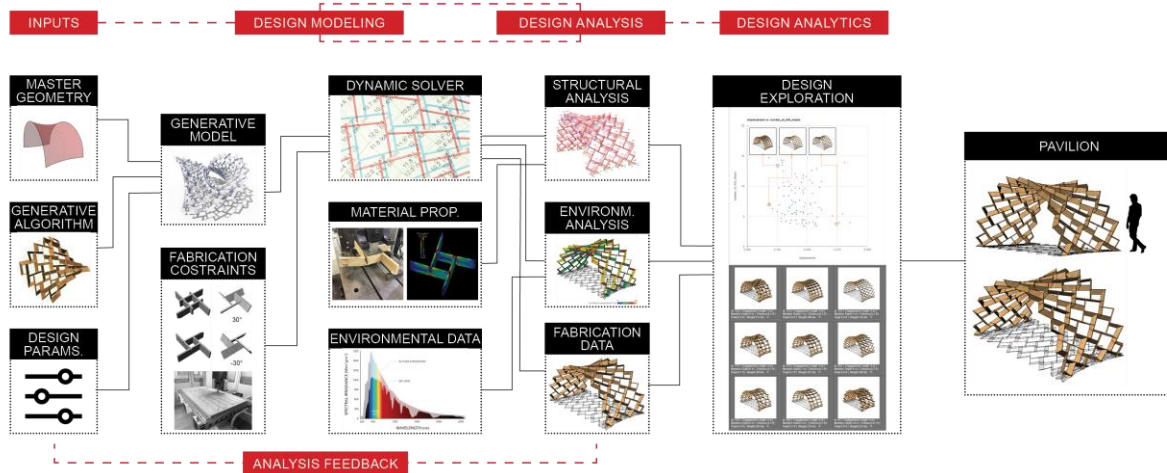


Figure 196_ Visualization of the design exploration cycle.

Once the solution space is generated and saved in the database it can be explored through the graph interface on the ParaGen webpage, which provides different queries and graphing tools to search through the design space with multiple design and performance criteria. Figure 197 to Figure 206 show different exploration schemes applied to search for desirable design solutions based on specific design parameter or performance criteria. Figure 197 to Figure 202 show sorting the design space based on a specific design parameter such as mesh density, engagement length, and rotation angle. Sorting the multi-dimensional design space based on the extremes of a single design parameter shows the variation of the geometry at the extremes of the parameter which is a useful measure to examine the diversity of the solutions in the design space based on the aforementioned parameter.

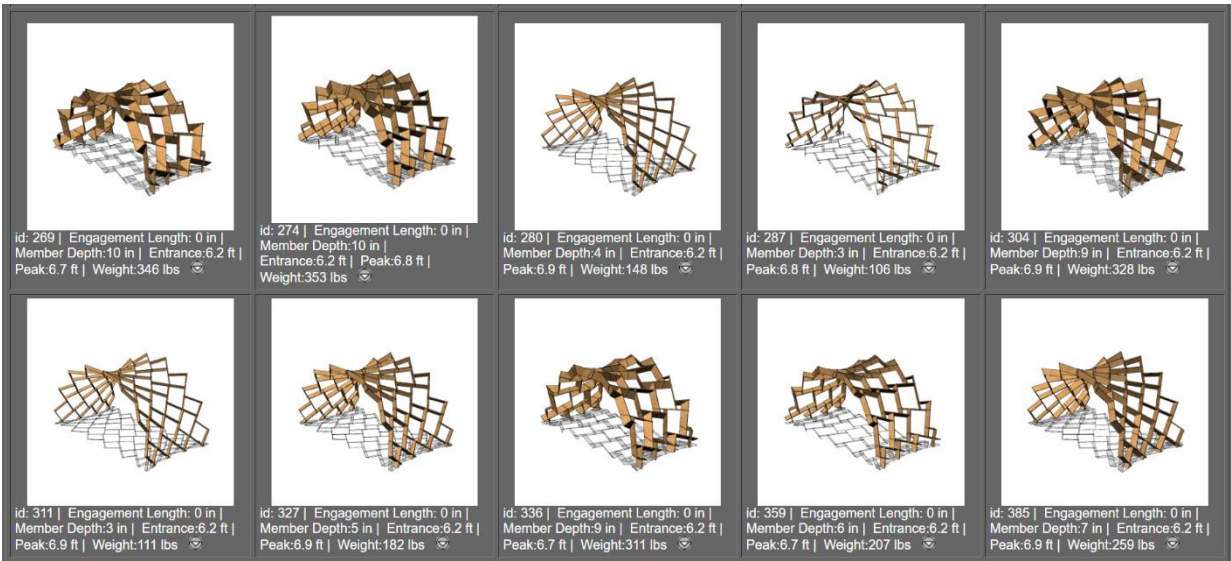


Figure 197_ Design exploration using design parameters: design solutions with lowest mesh density in the design space, sorted using the ParaGen interface.

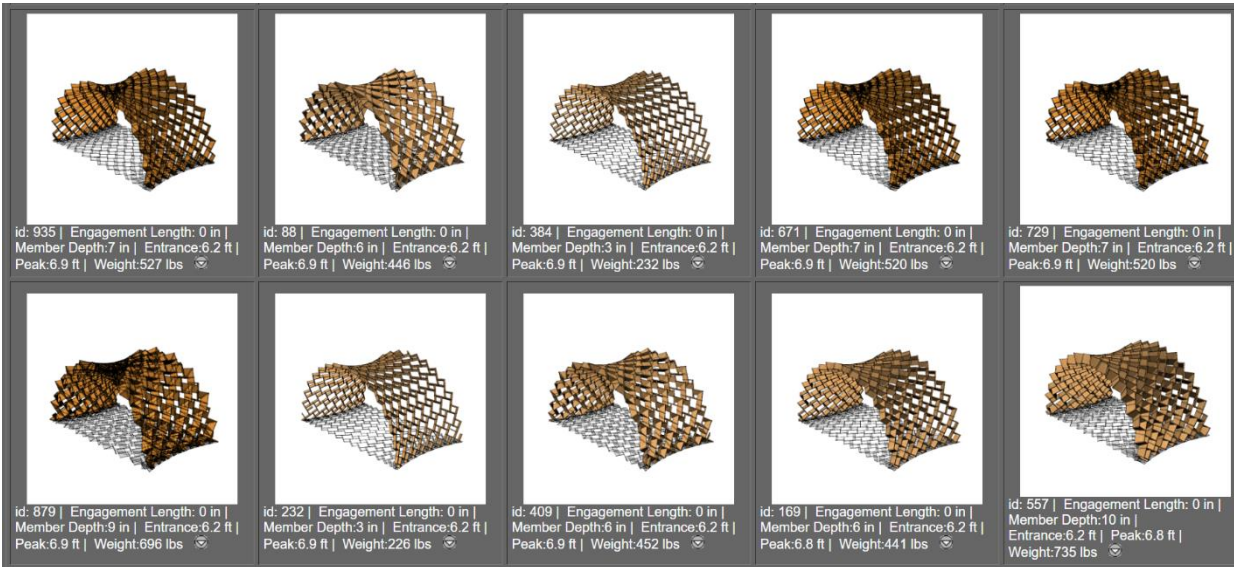


Figure 198_ Design exploration using design parameters: design solutions with the highest mesh density in the design space, sorted using the ParaGen interface.

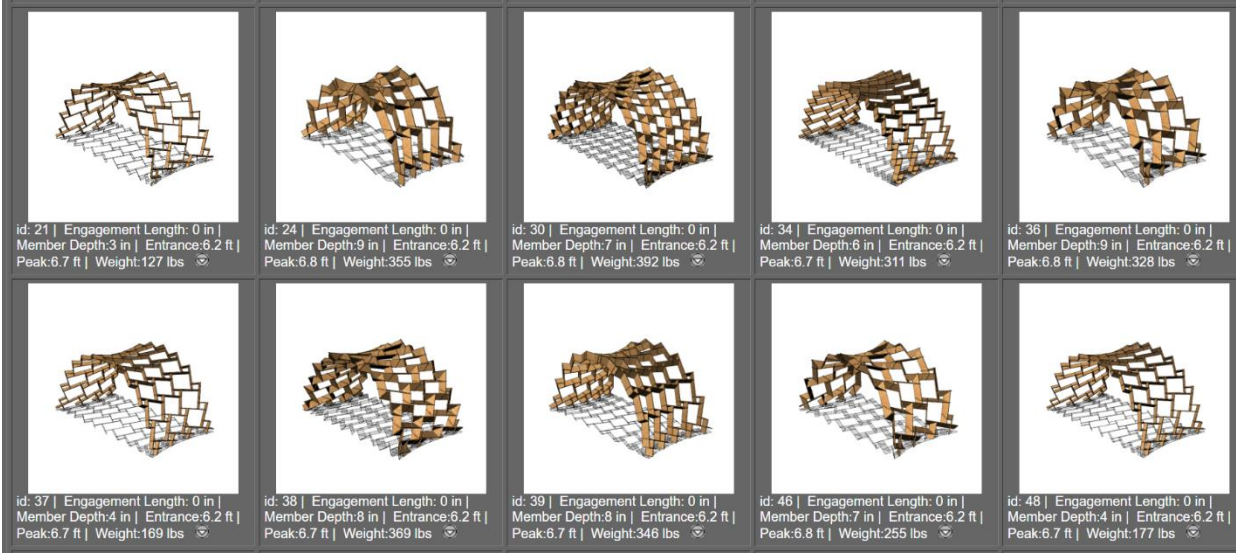


Figure 199_ Design exploration using design parameters: design solutions with the smallest engagement length in the design space, sorted using the ParaGen interface.

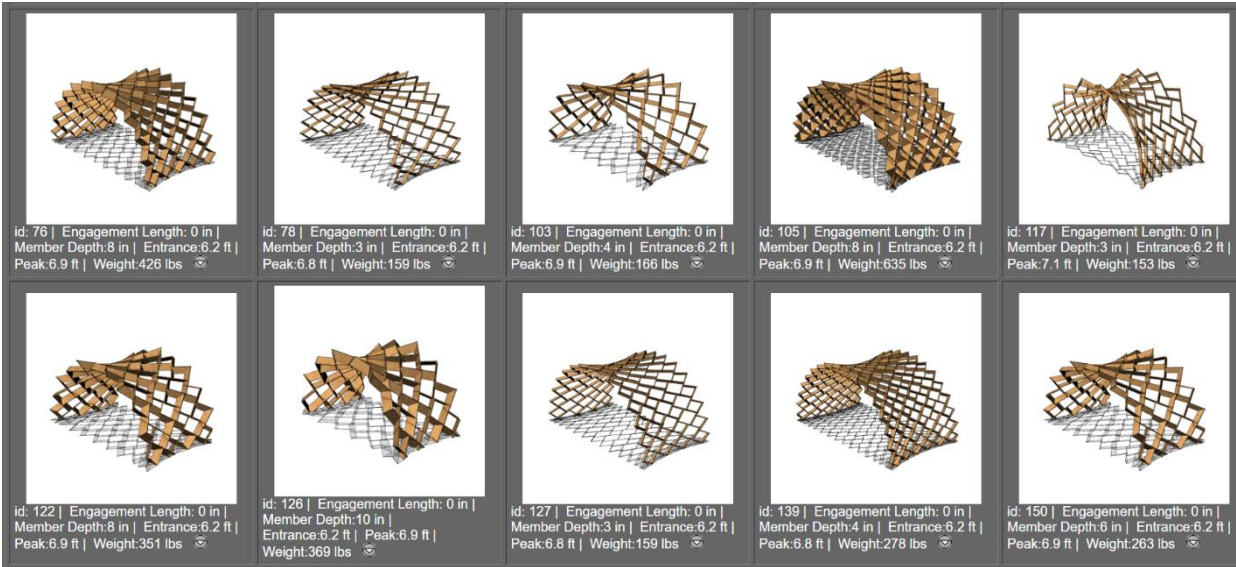


Figure 200_ Design exploration using design parameters: design solutions with the largest engagement length in the design space, sorted using the ParaGen interface.

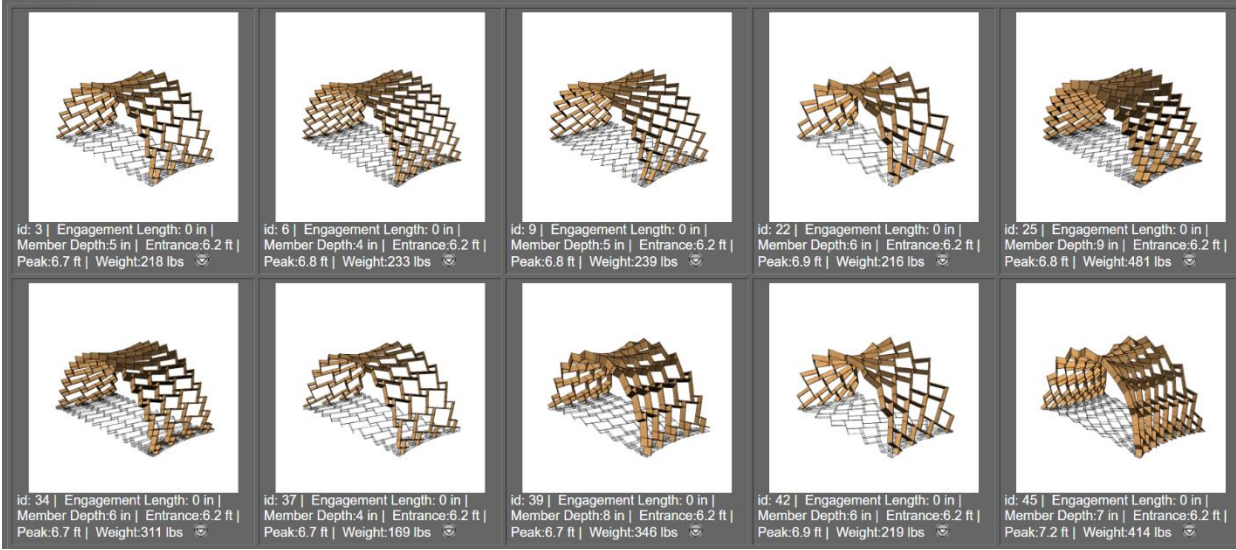


Figure 201_ Design exploration using design parameters: design solutions with the smallest rotation angle in the design space, sorted using the ParaGen interface.

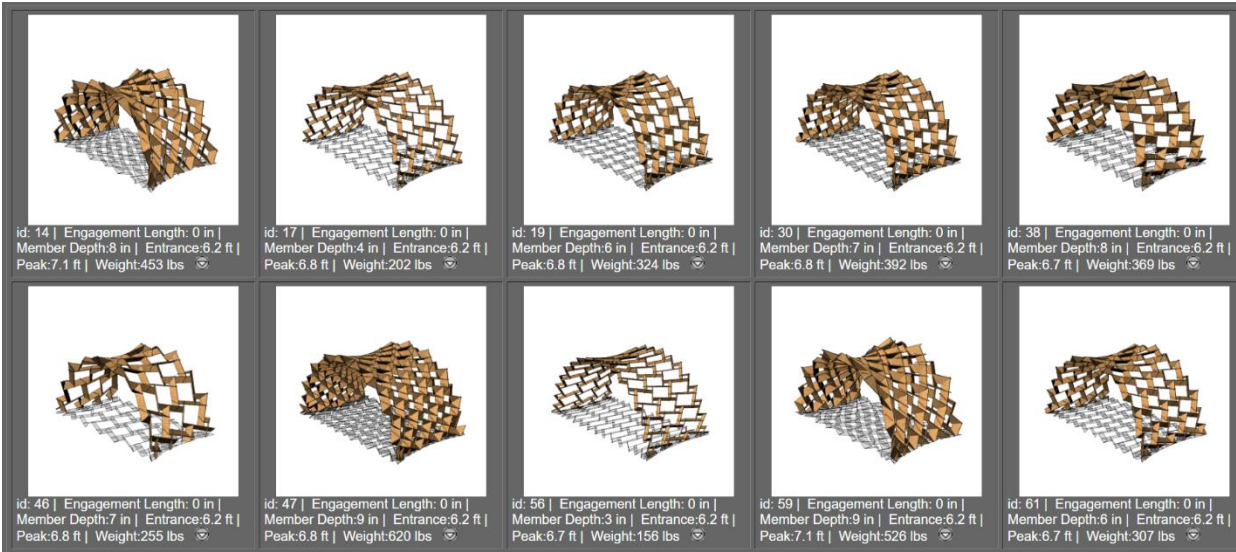


Figure 202_ Design exploration using design parameters: design solutions with the largest rotation angle in the design space, sorted using the ParaGen interface.

Figure 203 to Figure 206 show sorting the design space based on a specific performance criterion (total weight and form-finding error). Figure 203 and Figure 204 show a range of the lightest and the heaviest design solutions and their geometry variations.

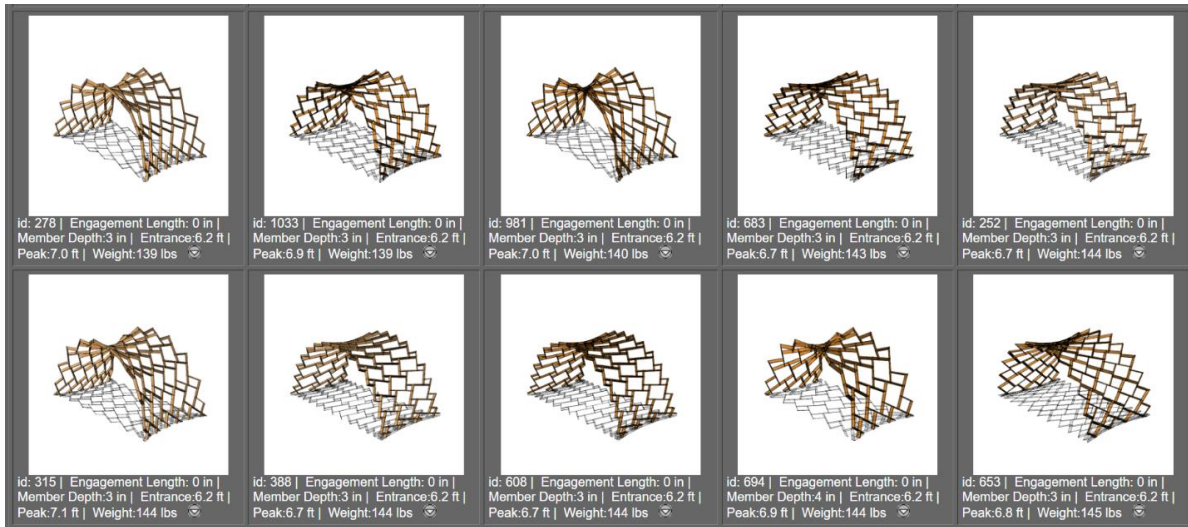


Figure 203_ Design exploration using performance criteria: design solutions with the smallest total weight in the design space, sorted using the ParaGen interface.

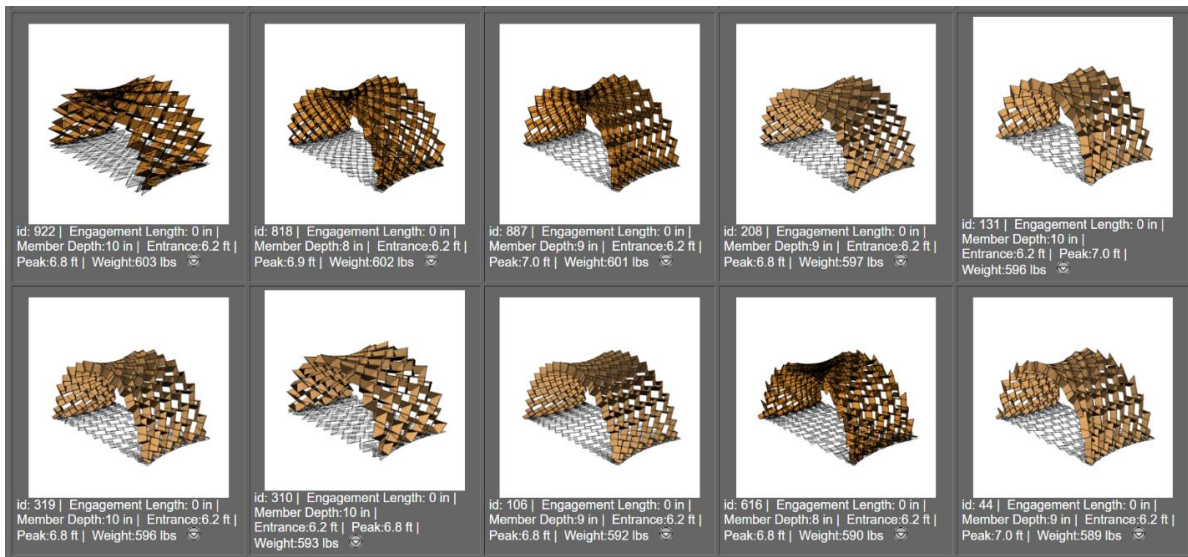


Figure 204_ Design exploration using performance criteria: design solutions with largest total weight in the design space, sorted using the ParaGen interface.

Figure 205 and Figure 206 show the design solutions with minimum and maximum form-finding error respectively. As it is depicted by the sorted pallet of design solutions, the design solutions with minimum form-finding error (residual eccentricities remained at the end of the form-finding process) tend to have a higher mesh density which approximates the base geometry more closely. However, as investigated in Chapter 3, this is not a generalizable rule and the eccentricities are not necessarily lower in grids with higher mesh density. The minimum form-finding error is an important fabrication constraint since the eccentricities need to be below the fabrication tolerances for fabrication of connection details with small tolerances. As a result, design solutions with minimum eccentricities are more desirable, however due to the nonlinear connection between the design parameters and the form-finding error, the choice of geometry with minimum form-finding error is not intuitive and requires a practical design exploration as is implemented in this research.

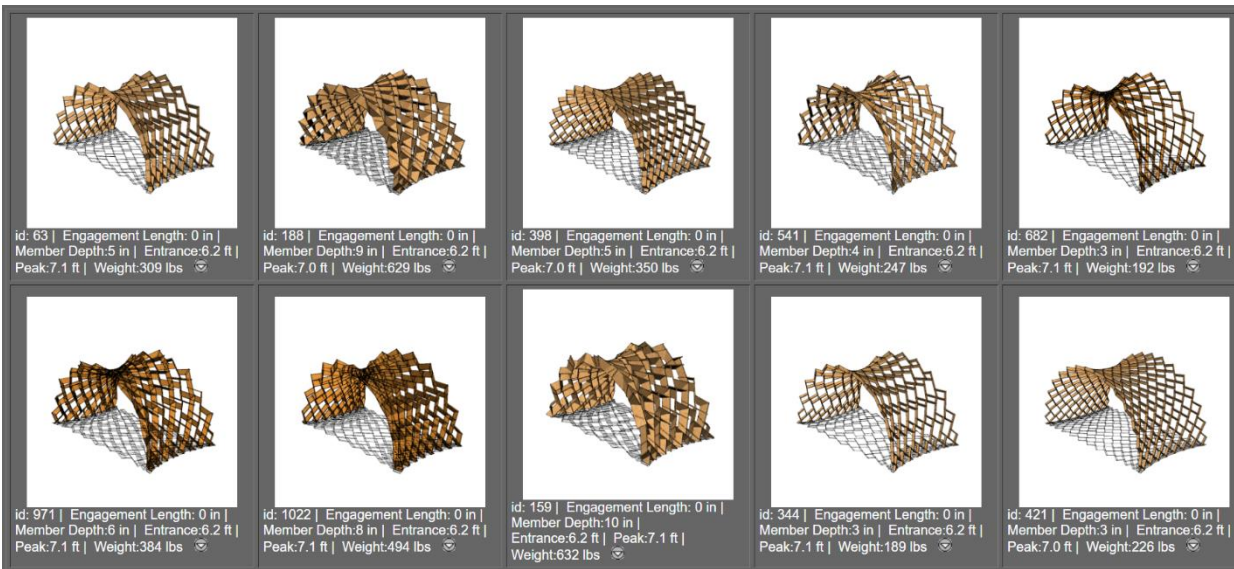


Figure 205_ Design exploration using performance criteria: design solutions with the smallest form-finding error in the design space, sorted using the ParaGen interface.

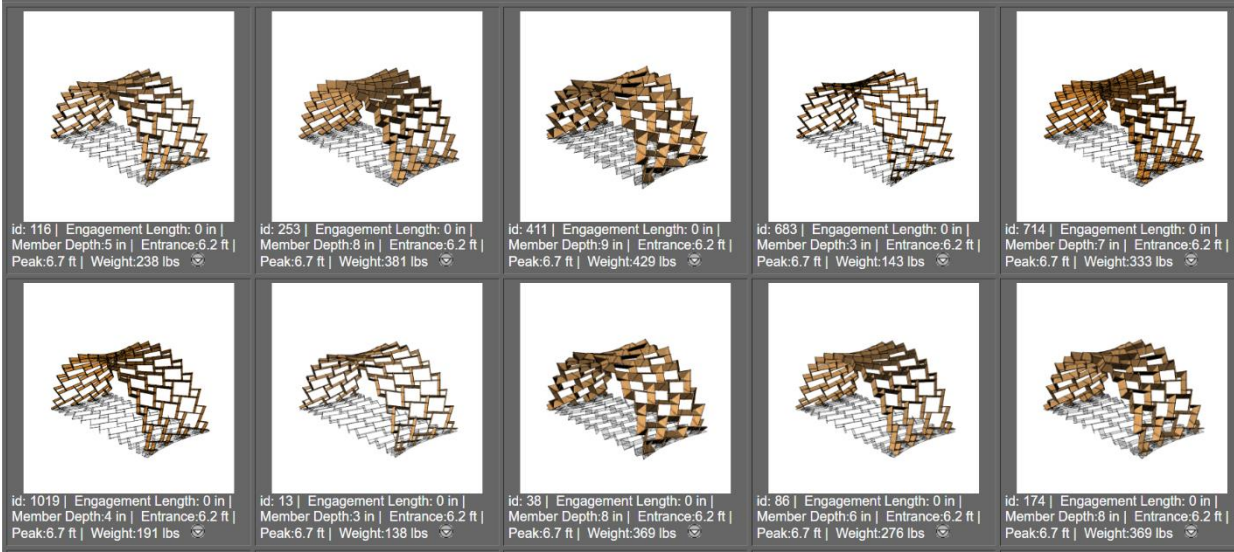


Figure 206_ Design exploration using performance criteria: design solutions with the largest form-finding error in the design space, sorted using the ParaGen interface.

The ParaGen interface allows the generation of 2-D graphs as well. In this section 2-D graphs are used to study the variation of different performance criteria (total weight, shading capacity, machine time and material use) based on the design parameters (mesh density, engagement length and rotation angle).

Figure 207 depicts a 2-D graph describing shading capacity versus engagement length. The design solutions with maximum shading capacity are visualized for each engagement length value. As expected, the arch with the maximum shading capacity has maximum engagement length and a high rotation angle which reduces the perforations significantly and produces the maximum coverage of the footprint.

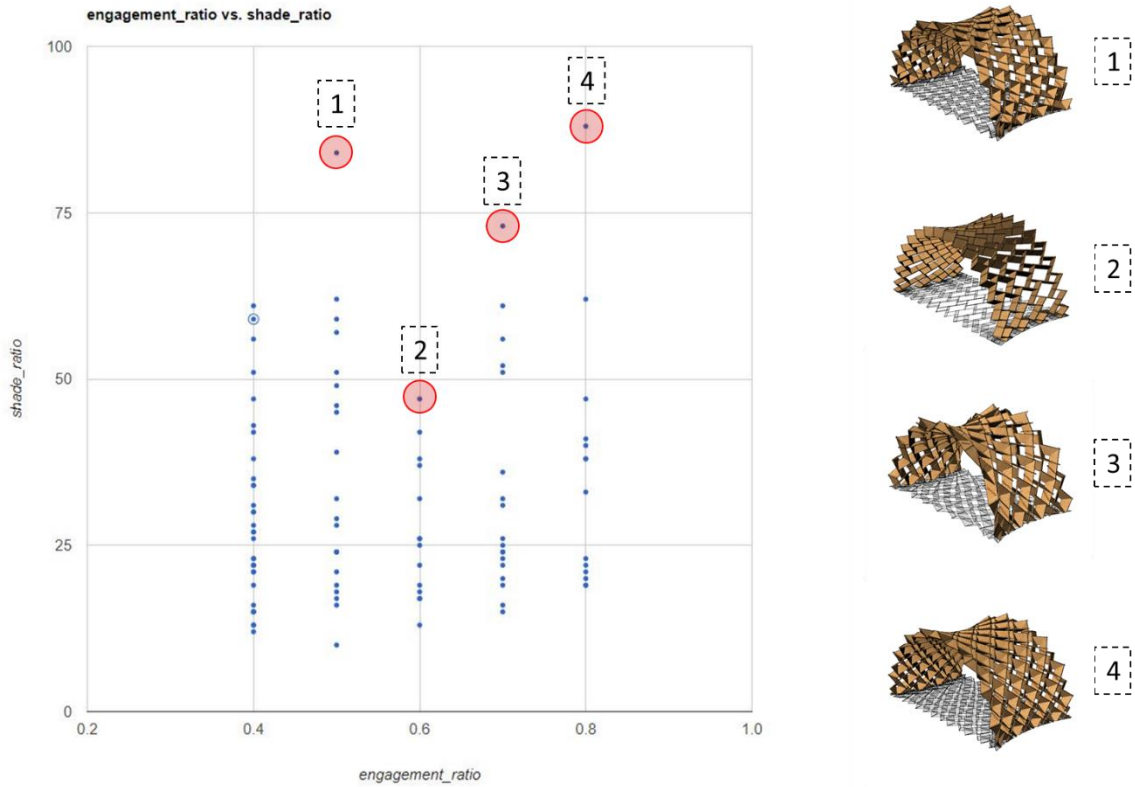


Figure 207_ 2-D graph describing shading capacity vs. engagement length. The design solutions with maximum shading capacity are visualized for each engagement length value.

Figure 208 depicts a 2-D graph describing shading capacity vs rotation angle. The design solutions with maximum shading capacity are visualized for each rotation angle. Solutions with maximum capacity have high mesh density, which reduces the size of the perforations in the arch geometry. The maximum shading capacity belongs to the arch geometry with maximum rotation angle and high mesh density.

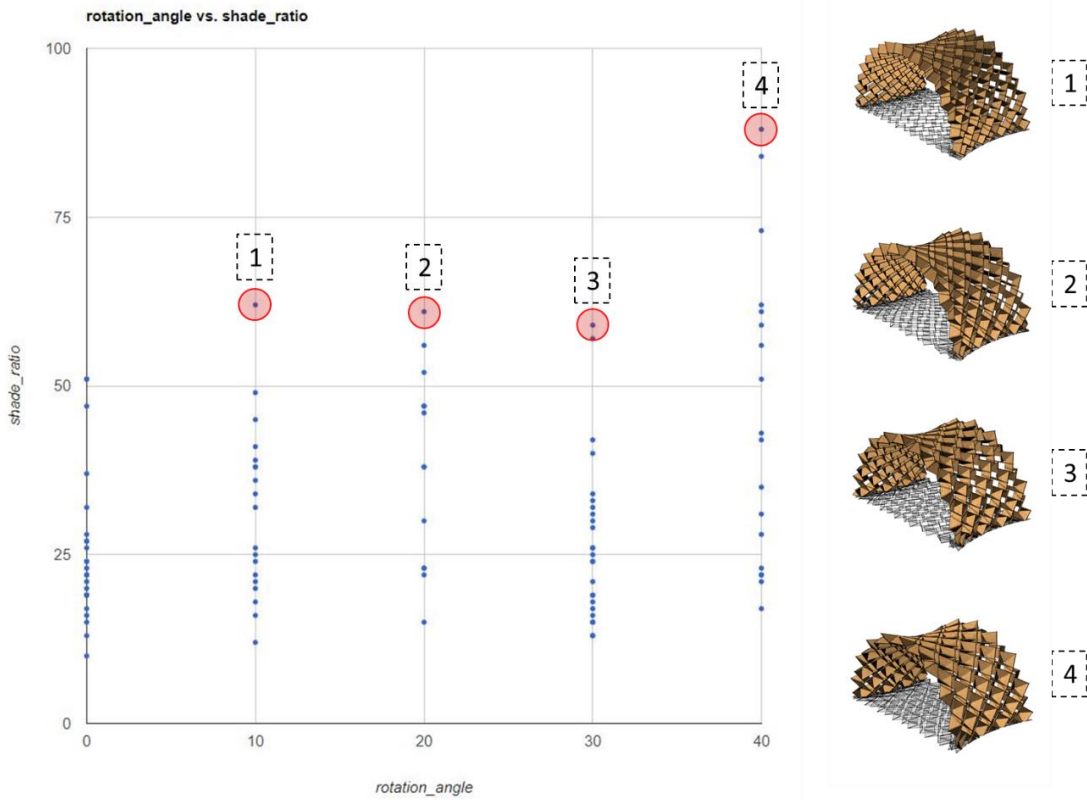


Figure 208_ 2-D graph describing shading capacity vs. rotation angle. The design solutions with maximum shading capacity are visualized for each rotation angle.

Figure 209 and Figure 210 depict 2-D graphs describing total arch weight versus engagement length and rotation angle respectively. The design solutions with minimum weight are visualized for each engagement length and rotation angle. Low shading capacity corresponds with low mesh density and low rotation angle as depicted in the Figure 210. Moreover, this graph shows the effect of different mesh types (mesh cells aspect ratio) on the curvature variation of the arch geometry after form-finding in low density meshes. While all of these four solutions are generated from a similar base geometry and they have similar low mesh density, they have significantly different variation of curvature in the doubly curve geometry which relates to the effect of the reciprocal member configuration (induced by the mesh cells aspect ratio) on the result of the form-fining process.

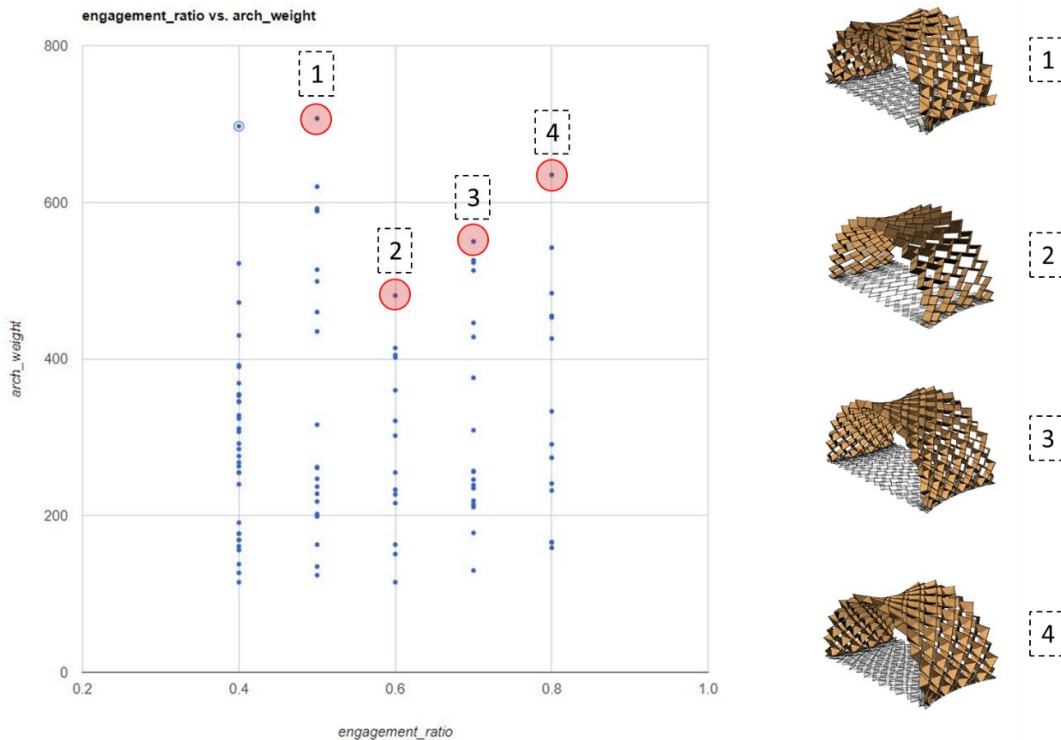


Figure 209_ 2-D graph describing total arch weight vs. engagement length. The heaviest arch geometries and shading patterns are visualized for each engagement length value

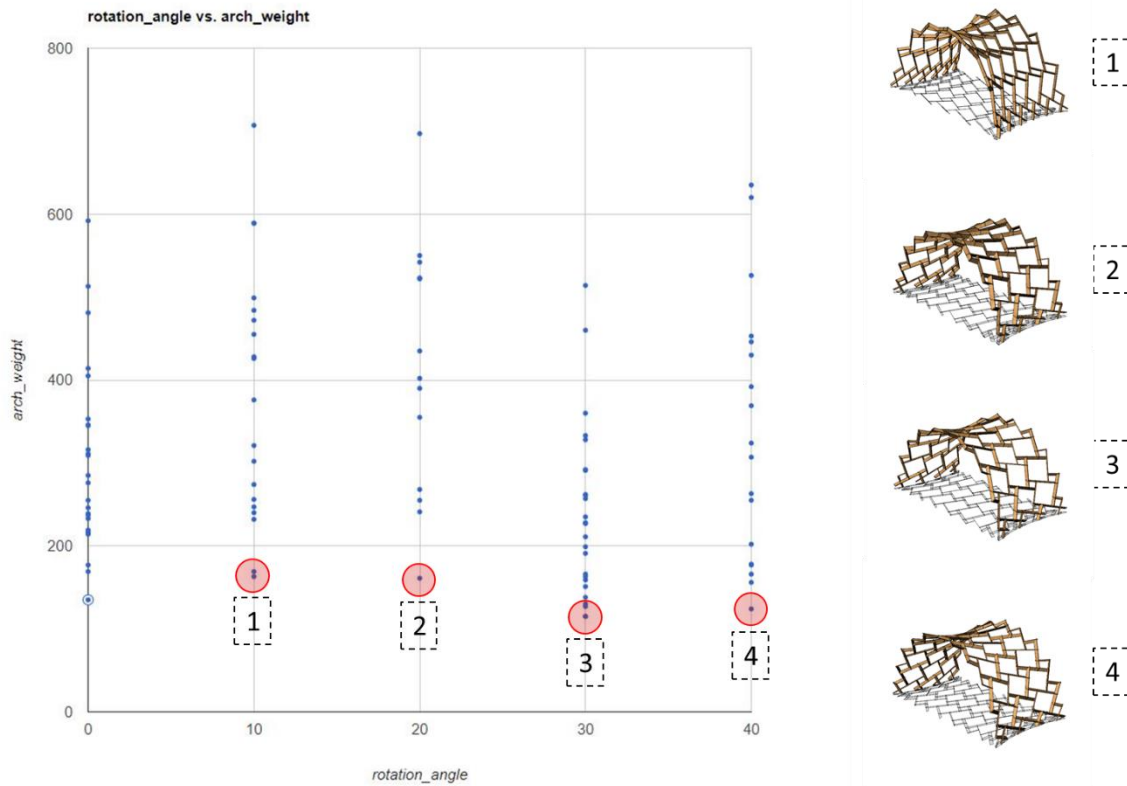


Figure 210_ 2-D graph describing total arch weight vs. rotation angle. The design solutions with minimum weight are visualized for each rotation angle.

Figure 211 depicts a 2-D graph describing estimated machine time versus maximum member size. Maximum member size is considered as an independent parameter for two reasons: first, the maximum member size is an assembly constraint for the human-led assembly process, second, maximum member size corresponds with the mesh density. The estimation of the CNC machine time is based on the geometry and fabrication cuts for each member which is controlled by the mesh density and the member cross-section. Figure 211 shows the nonlinear relation between the machine time against mesh density and depicts the geometry of four design solutions with decreasing mesh density.

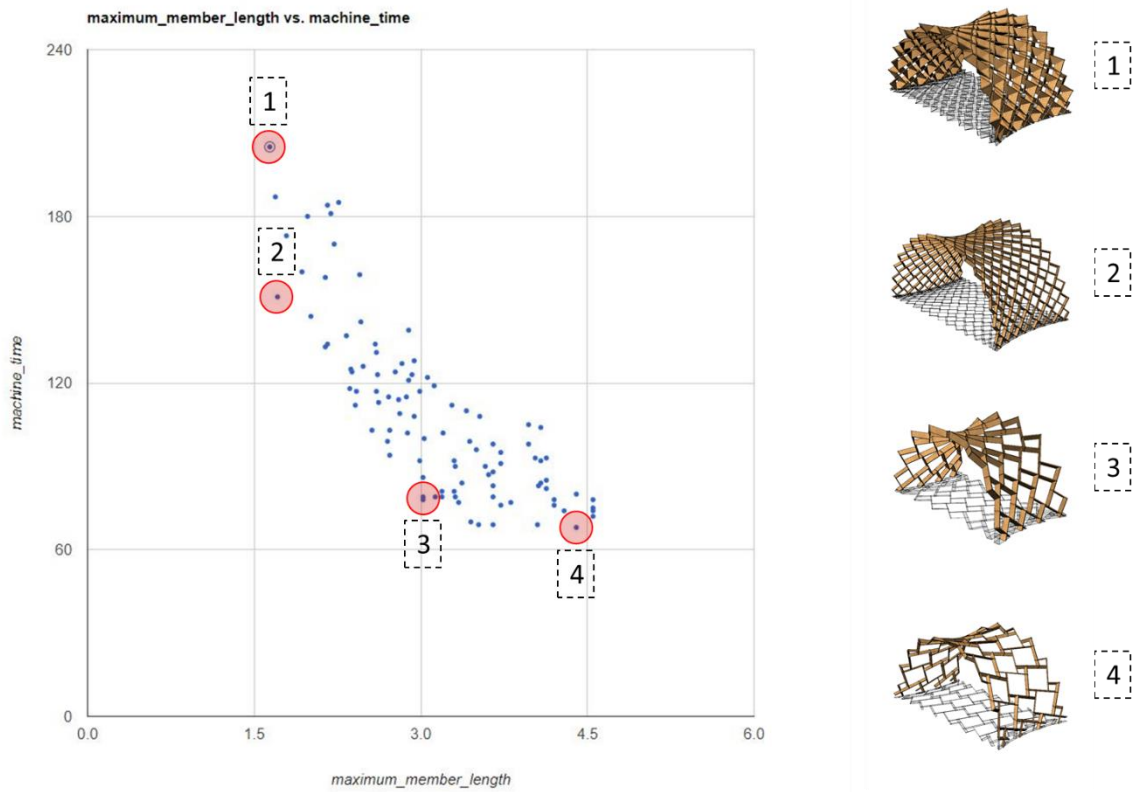


Figure 211_ 2-D graph describing estimated machine time vs. mesh density.

Similarly, Figure 212 depicts a 2-D graph describing estimated machine time versus maximum member size. The shading capacity depends on the size of the perforations and the rotation angle. As Figure 212 shows, shading capacity decreases as the mesh density decreases. Consequently, the minimum shading capacity belongs to a design solution with lower mesh density and small rotation angle.

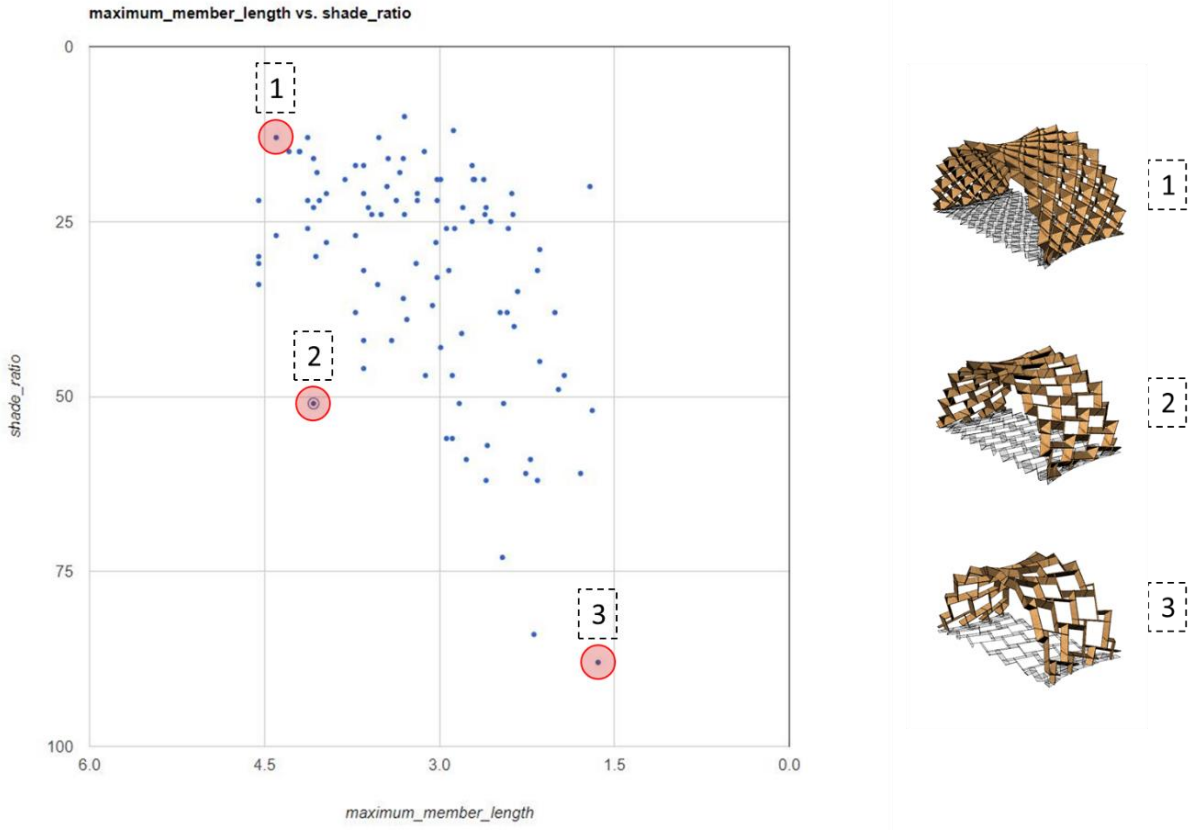


Figure 212_ 2-D graph describing shading capacity vs. mesh density.

Similarly, Figure 213 depicts a 2-D graph describing estimated 4 by 8 sheet material use versus mesh density. Estimation of the amount of sheet material use is based on the total 2-D surface of the reciprocal members and the nesting effect which is derived from the fabrication tests. The nonlinear dependency of the material use and the mesh density is depicted in Figure 213. The higher the mesh density and member depth the higher the number of 4 by 8 sheet material use.

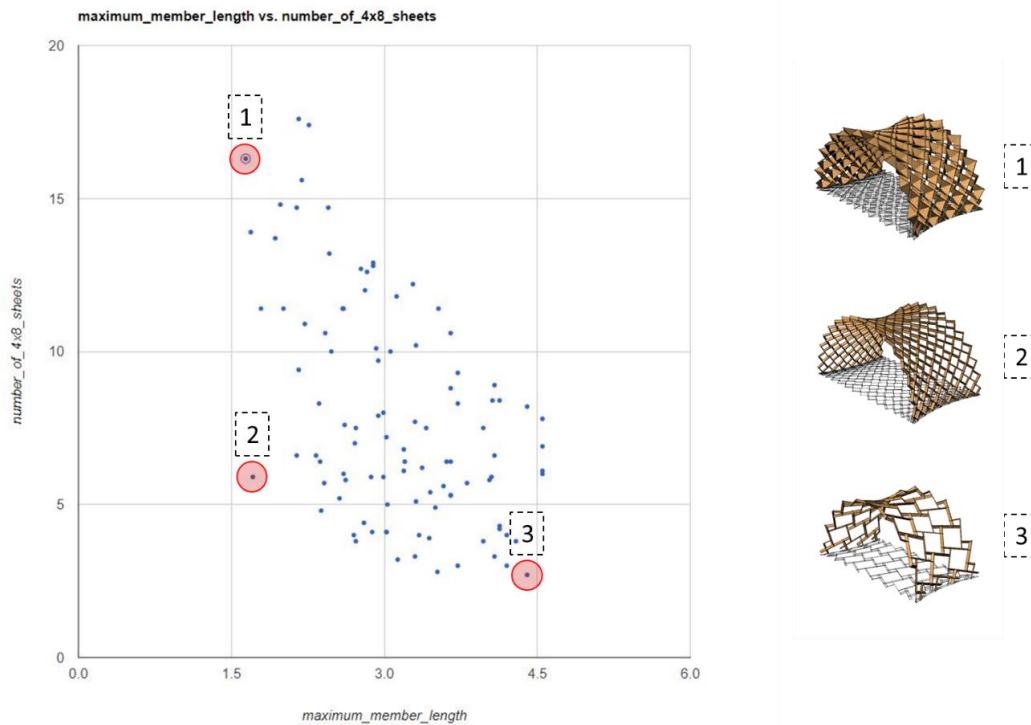


Figure 213_ 2-D graph describing estimated 4 by 8 sheet material use vs. mesh density.

The complex nature of reciprocal systems, their interconnected design parameters, and conflicting design constraints (such as structural performance, fabrication constraints, shading capacity, material use, machine time, etc.) require a multi-objective exploration scheme which responds to different design criteria. ParaGen provides multi-objective exploration of the solution space through application of multiple sorting criteria to the solution space.

Figure 214 shows six sorting criteria that are applied to the solution space and Figure 215 shows the reduction in size of the design space due to application of each sorting criteria. The first criterion is the estimated number of 4 by 8 plywood sheets needed for fabrication, which is kept below eight sheets based on the available budget. This design constraint reduces the design solution space in half as shown in Figure 215. The second criterion is the mesh density which is kept above 40 cells to have a better expression of the reciprocal pattern and also to limit the maximum member size to facilitate human-led assembly. The engagement ratio is kept above 0.5 for better design expression, as well as to accommodate reciprocal patterns with more uniform perforations. The rotation angle is kept above 20 degrees for better design expression and to find design solutions with higher shading capacity. Member depth is kept above 5 in for structural depth and the shading capacity is kept above 30 percent. All of these design criteria are applied to the solution space which reduced the desirable design solutions to 15 solutions which meet all of the design criteria (Figure 215).

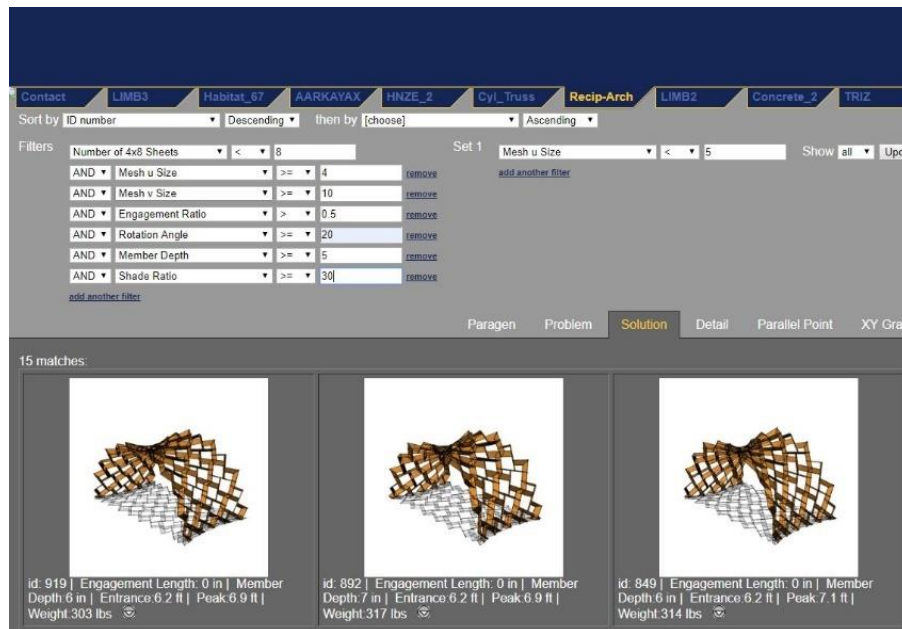


Figure 214_ Application of multiple queries in ParaGen to explore the design space.

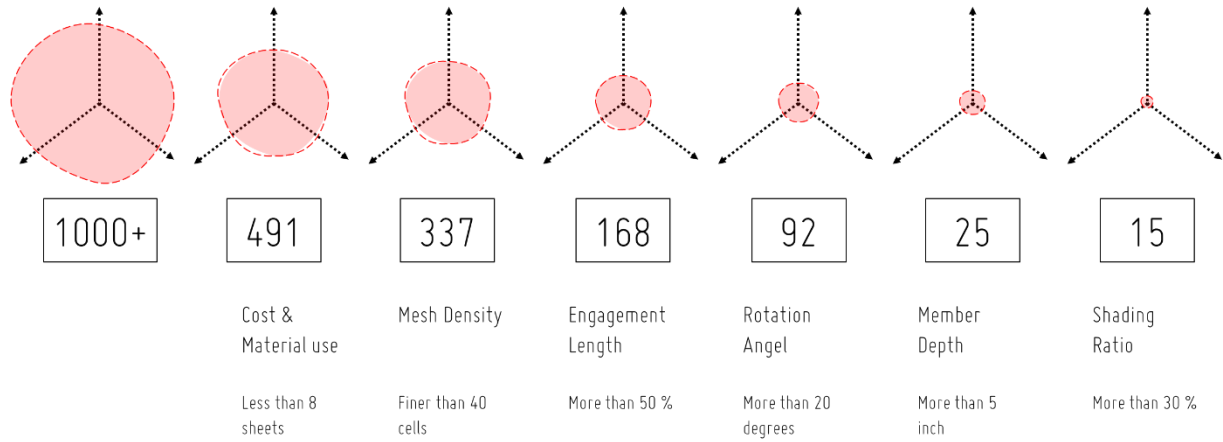


Figure 215_ Visualization of the design space reduction due to the application of different design constraints.

The exploration process produced a pallet of well performing design solutions which provided feedback on the formal variations within the design constraints. This feedback was highly informative to choose the best configuration for the design parameters with such conflicting design constraints. The final design was selected based on this feedback and is depicted in Figure 216.

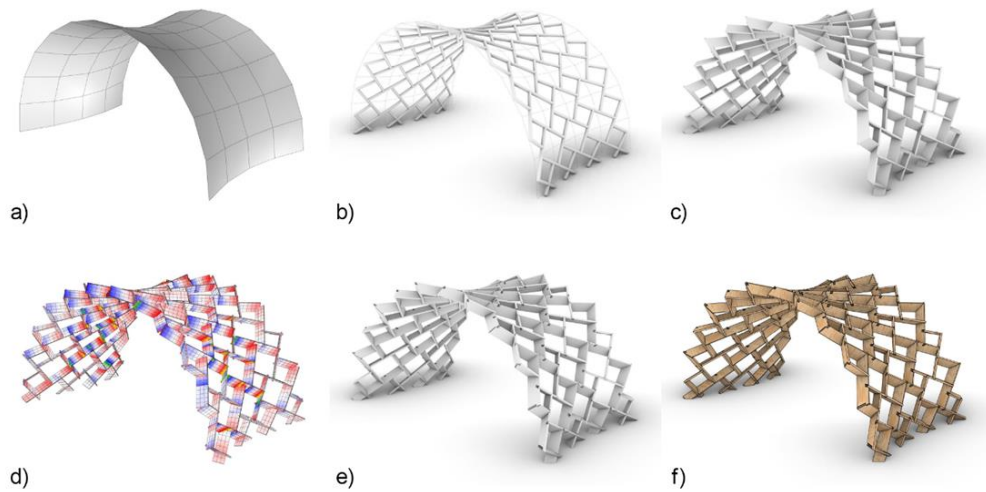


Figure 216_ Final arch geometry and the design process: a) mesh approximation of the base geometry b) reciprocal pattern generation and form-finding results c) 3-D member geometry generation d) analytical model and finite element analysis results e) 3-D member geometry.

Using the computational model, the visual and numerical data for the final design is generated as shown in Figure 217 and Figure 218. Moreover, the computational model generated the fabrication data which was used for fabrication and assembly of the arch as is described in the next section.

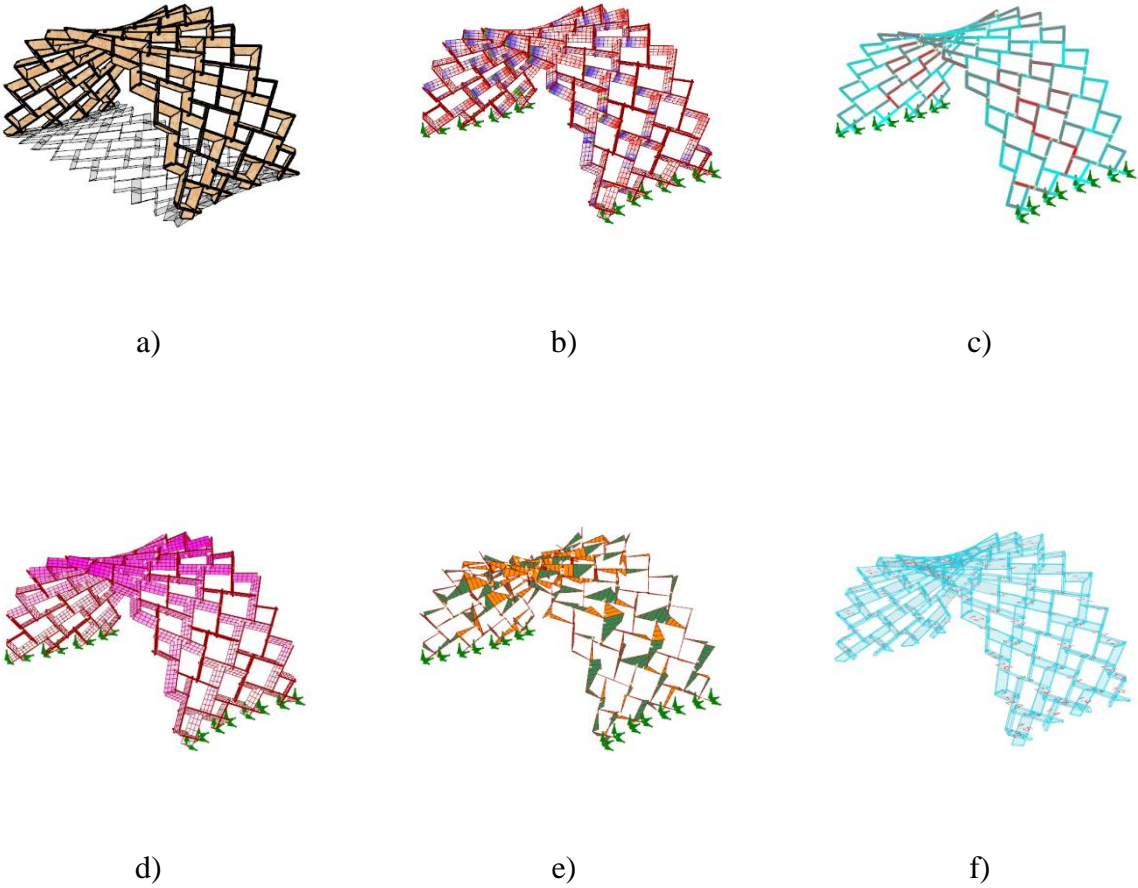


Figure 217_ Visual data for the selected arch geometry. a) 3-D Geometry and shading pattern b) Stress Distribution c) Member utilization d) Displacement Distribution e) Bending moment distribution f) Member geometry and labeling.

Arch Weight	278 lbs	Estimated Machine Time	140 min
Max. Displacement	0.263 in	# Connections	200
Max. Utilization Factor	83.7 %	# Elements	112
Min. Utilization Factor	3.7 %	Min. Member Length	1.1 ft
# 4 by 8 Sheets	8.4	Max. Member Length	3.4 ft
Max. Form-finding Error	0.13 in	Max. Height	6.7 ft
Shading Ration	32 %		

Table 7_ Numerical design data for the selected arch geometry.

6.6 Fabrication process for the Reciprocal Shades project

The fabrication and erection process were informed by several constraints in this prototype. These constraints encompass assembly and erection, digital fabrication, and weight limitations for the reciprocal members. No lifting equipment was available for the assembly process, thus limiting the size and weight of the members. The final geometry was designed to have members weight less than 5 pounds and to be easily assembled by one person. The members were assembled onsite manually which required pre-drilling of the holes and fabrication of guides to facilitate the process. The three-dimensional notched geometry of the connection cuts was designed to guide the assembly and orientation of the rotated reciprocal members. The three dimensionality of the connection detailing required 5-axis CNC routers to cut the connection notches. All of the members were cut out of 0.75 inch sheet marine grade plywood.

The proposed computational design process was used to model the arch geometry and perform a design exploration process to address all of the constraints within the design space.

The trapezoidal geometry of the planar reciprocal members facilitated the nesting process on the 4 by 8 sheet plywood. Two Kreg screws were used for each connection to strengthen the connection and reduce the potential assembly gaps. The screw holes were pre-drilled to facilitate the assembly process. The thickness variation of the procured plywood was within a 0.02 inch range so it was important to find a working tolerance that would accommodate this thickness variation across the sheet. Considering the modified connection detailing for fabrication, tight connection tolerances were used (Figure 218). In this process, a 0.01 inch tolerance was used on each side of the connection cuts ($0.01 < 1/64$ inch conventional tolerance). The integration of the connection design with fabrication constraints into a completely parametric environment allowed for the verification and customization of the connection detailing across the structure.

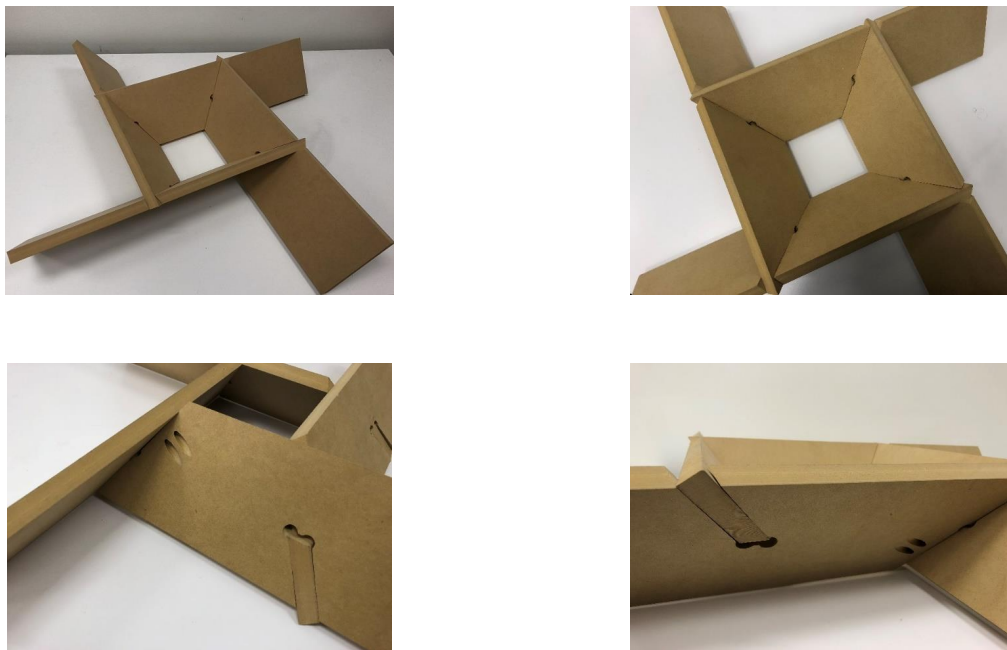


Figure 218_ Sample of lapped reciprocal connection design stabilized with two Kreg screws using MDF material.

The selection of the final design was informed by the multi-objective design exploration process that takes account of multiple conflicting design objectives within the design space. Once the final design was selected, the fabrication data was automatically generated. All of the members are numbered, and the fabrication cuts are generated based on the fabrication parameters and tolerances.

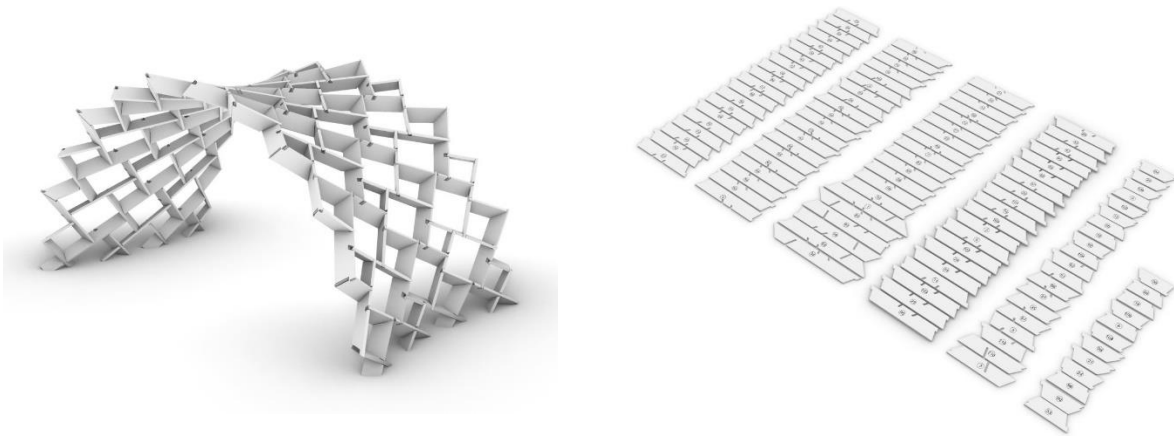


Figure 219_ Arch geometry and the members layout and the final arch geometry 112 reciprocal members.

112 planar reciprocal members are nested on eight 4 ft. by 8 ft. marine grade plywood sheets with 0.75 inch thickness. Tool pathing was done in Mastercam software for 5-Axis CNC router machine, available at Taubman College of Architecture.



Figure 220_ Cutting the reciprocal members out of plywood sheets using 5-Axis CNC.

The fabrication process was very efficient and manageable by one person. The routing process for each 4 by 8 sheet took around an hour using the 5-axis CNC. The overall fabrication process took around two hours for each sheet, including the setup time prior to the routing and the cleanup, labeling and storage of members afterwards.

All of the members were labeled to include the member number, the crossing member number(s), and direction for each connection. This numbering system facilitated the manual assembly process significantly. The routing process was done in three days and the reciprocal members were stored for post-processing and predrilling (Figure 221).



Figure 221_ Labeling and storage of the members.

All of the members are predrilled with two Kreg screws at each connection. As previously mentioned, pre-drilling is necessary to facilitate the assembly process (Figure 222).



Figure 222_ Predrilling the screws and pre-assembly of connecting members.

The arch was first assembled temporarily in the student research room at the Taubman College of Architecture. Multiple assembly sequences were tested. The final assembly sequence started with the construction of the central node of the arch resting on two ladder supports. The structure was then built by cantilevering reciprocal members from the central part on two sides.

Starting from the central node of the structure, the assembly process was straightforward and manageable with three people. The connection detailing allowed ease of assembly even with tight fabrication tolerances (0.1 inch on each side of the fabrication cuts). The whole assembly process took less than a day and the support members were held in place with bracing ropes connecting the two sides of the arch (Figure 223).

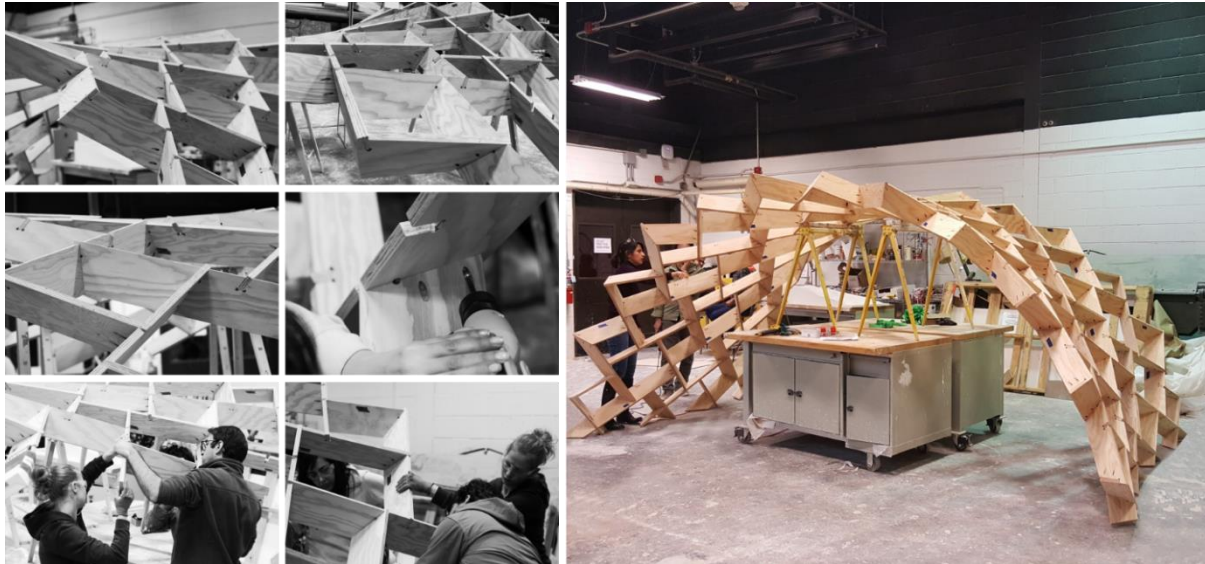


Figure 223_ Assembling the arch at the Taubman College of Architecture. Assembled arch with temporary supports.

The arch was then disassembled into three pieces (a central piece and two side pieces) for storage and the application of anti-weathering coating. Although the marine grade plywood has waterproof adhesive between the layers, anti-weathering coating (Minwax Helmsman Satin Oil-Based Spar Urethane Varnish) was applied to enhance the overall waterproofness and the UV resistance of the material. One coat of the sealant was applied to all surfaces of the reciprocal members with special attention to the end grains (Figure 224).



Figure 224_ Application of waterproof and anti UV sealant to the arch.

For the permanent set up of the arch on the site location, a custom support system was needed to secure the structure safely to the ground with minimal invasion to the site. Thus, custom support plates were designed to facilitate the erection, as well as distribute the load on the ground (Figure 225). The support plates were cut out of 12-gauge steel plate using the CNC water jet cutter at Taubman College (Figure 226). The support plates were bent to the custom angles of the support members using a break. Bending angle guides were cut out of cardboard to direct the bending angles (Figure 227 and Figure 228).



Figure 225_ Custom support palate design.

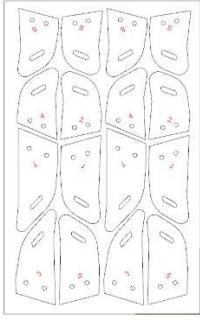


Figure 226_ Fabrication of the support plates using water jet cutter.



Figure 227_ Bending the supports plates to custom angles using break.



Figure 228_ Connection detailing of the support members and the base plates.

The support plates were designed to connect to each of the support members (eight on each side of the arch) with one bolt (a Zinc plated half inch hex bolt) and connect to the ground with a one-foot earth screw (total of sixteen earth screws). The bolt holes and earth screw slots were cut with CNC water jet cutter. The slotted holes would provide half inch movement room to ease the setup process (Figure 229).

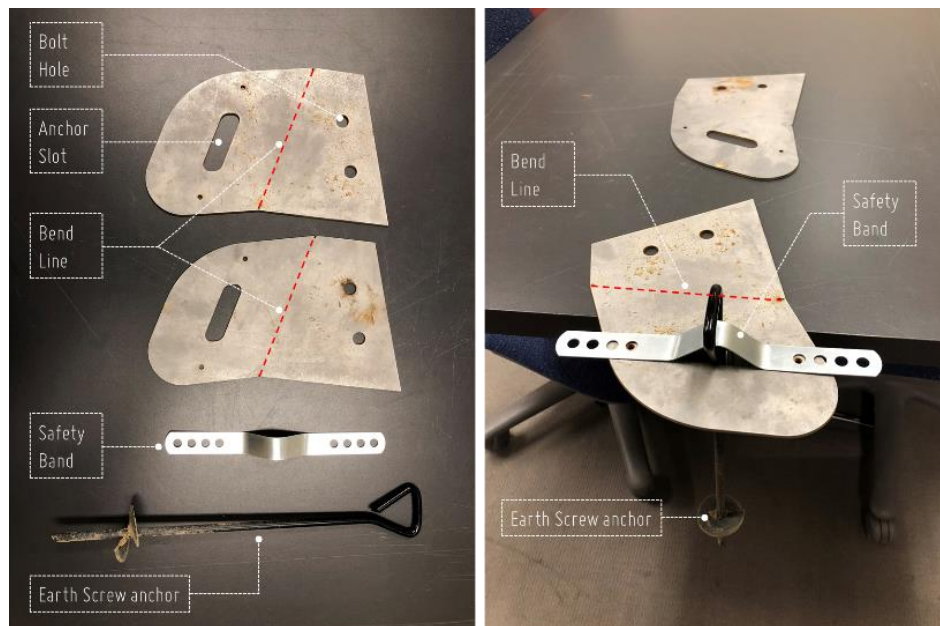


Figure 229_ Base plate connection detailing and connection pieces.

The half inch bolt size was chosen so that the members would not fail under bearing stresses at the support. The one-foot earth screws would support the structure against possible uplift loads induced by wind.

Once the support detailing was resolved, the arch was transported to the site in three pre-assembled pieces and reassembled on-site using two ladders. The arch was constructed adjacent to the site with the plates attached to the support members, and supported using four bracing ropes (Figure 230, Figure 231 and Figure 232).



Figure 230_ Moving the preassembled pieces of the arch to the site location for setup.



Figure 231_ a) Erecting the arch from three pre-assembled pieces using two support ladders. b) assembling the connecting pieces using screws c) assembling the last pre-assembled piece of the arch. d) supporting the arch using bracing ropes.



Figure 232_ Connecting the base plates to the arch support members.

The earth screws were then put in place at the designated support locations and the arch was transferred to the site location. The bracing ropes were removed after securing the arch in place by the earth screws. The details of the support connection are depicted in Figure 233.



Figure 233_ Base plate connection detailing.

The arch geometry and the fabrication details are depicted in Figure 234 to Figure 238.



Figure 234_ The arch geometry (South view), Matthaei Botanical Gardens, Ann Arbor, Michigan.



Figure 235_ The arch geometry (North view), Matthaei Botanical Gardens, Ann Arbor, Michigan.



Figure 236_ Arch connection detailing.



Figure 237_ Arch connection detailing.

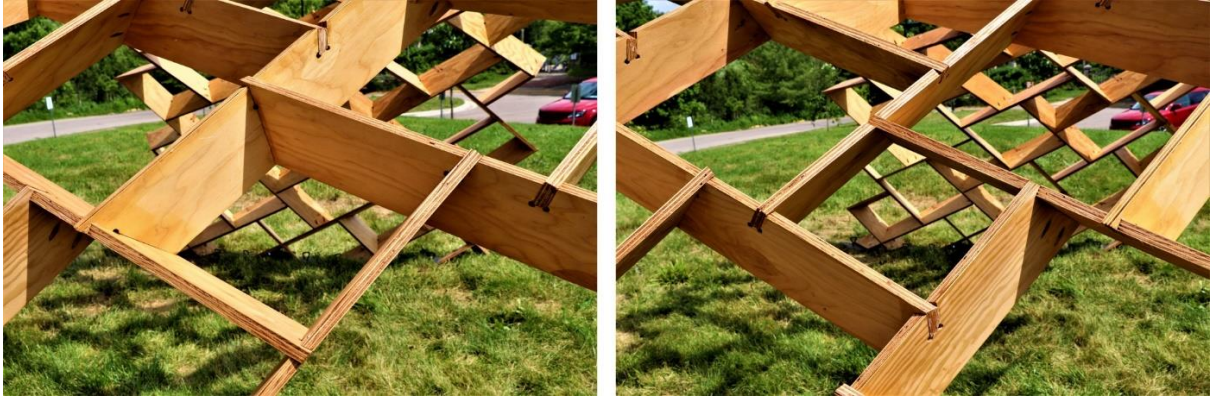


Figure 238_ Convex and concave reciprocal modules in the system.

6.7 Post-construction inspections

The reciprocal shade project was set up on the site on June 17th, 2018 and was initially intended to be on the site for a six month duration. However, the display time for the arch was extended by the Botanical Garden administration until the end of 2019. This extension was a great opportunity to study the long-term behavior of the reciprocal system under different environmental conditions. Multiple inspections were carried out over the course of eighteen months. Through these inspections multiple issues were observed in the structure including material discoloring and deterioration due to UV exposure and humidity, permanent deformations of the members under self-weight and environmental loads, and failure of the connections due to material deterioration and defects (Figure 241).



a)



b)

Figure 239_ Discoloration due to UV exposure. a) Arch condition after eight months. b) Arch condition after sixteen months.



a)



b)

Figure 240_ a) Reciprocal member deformations after sixteen months, b) warping of reciprocal members.



a)



b)

Figure 241_ a) Connection failure due to excessive deformations, b) connection failure due to material defect.

After nine months, the reciprocal arch geometry started to sag. Since the Botanical Garden was still interested in having the arch on the site, steps were taken to reshape the arch to retrieve the initial height. Due to the low degree of indeterminacy in reciprocal systems, they are less sensitive to support settlements which means their supports can move with little increase in the forces within the system. This property allowed for the retrieval of the initial arch height by moving the supports to a pre-defined configuration. Determining the exact displacement patterns to generate a desired form is not a trivial task which further requires consideration of limiting the stress level in the critical members to withstand the desired displacement pattern. To this goal, the analytical model which was initially developed in Chapter 3 was adapted to simulate the structural behavior and calculate the internal member forces induced by the movement of the supports.

The deformed geometry of the arch was measured using the radial distance of each member center point from the base center point (Figure 242). This data was used to generate a digital 3-D geometry of the arch (Figure 243) which then informed the creation of an analytical model that

could predict the member forces in the system due to a series of imposed support displacements and predict the final geometry of the arch. This model explored the set of support movements to fit the maximum height of the sagging arch geometry to the initial arch geometry. The member stress levels were checked to ensure the feasibility of the support movements without failure of the members.

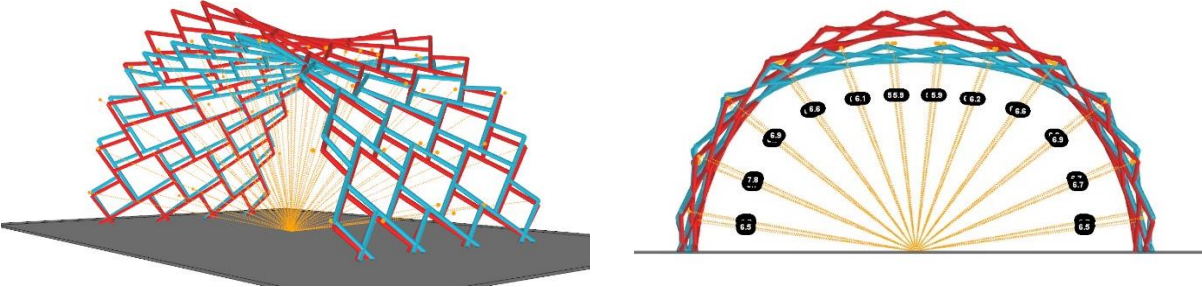


Figure 242_ Using the radial distance measurement data to generate the digital arch geometry. The deformed geometry is depicted in blue and the initial arc geometry is depicted in red.

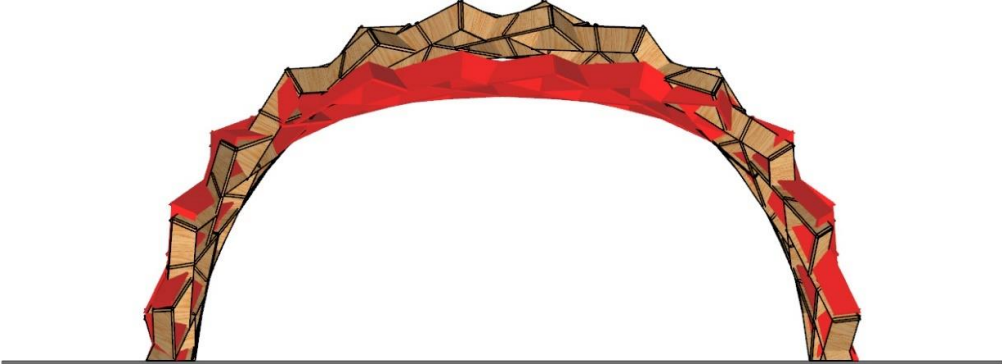


Figure 243_ Comparison of the measured geometry and the initial geometry.

Through series of simulation tests, the proposed support displacement scheme was chosen as depicted in Figure 244. The displacement pattern included gradual and simultaneous movement of the supports on the right side of the arch (8 supports) to the left side for 30 cm, while the top central members of the arch (8 members) were moved upwards for 15 cm.

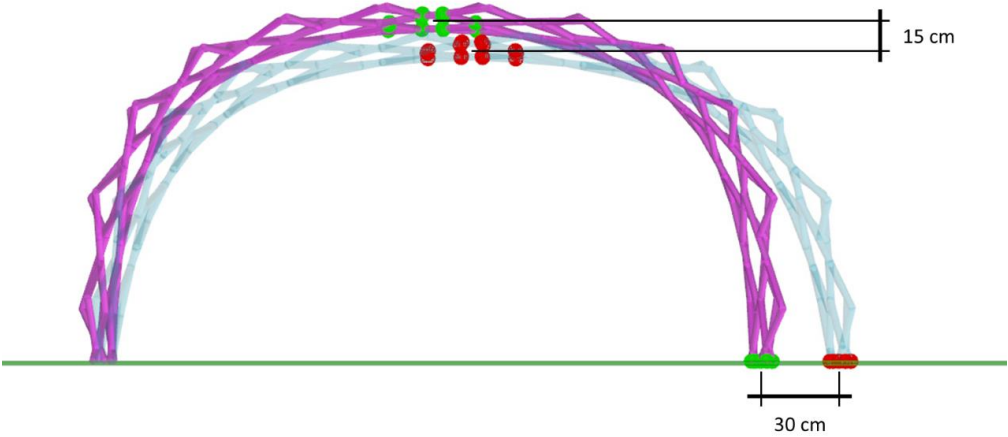


Figure 244_ Support displacement scheme to retrieve the initial height. Gradual and simultaneous movement of the right support to the left side (30 cm) and the top center members upwards (15 cm).

Figure 245 shows the bending moment distribution in the arch as the displacement values increase based on the support displacement pattern.

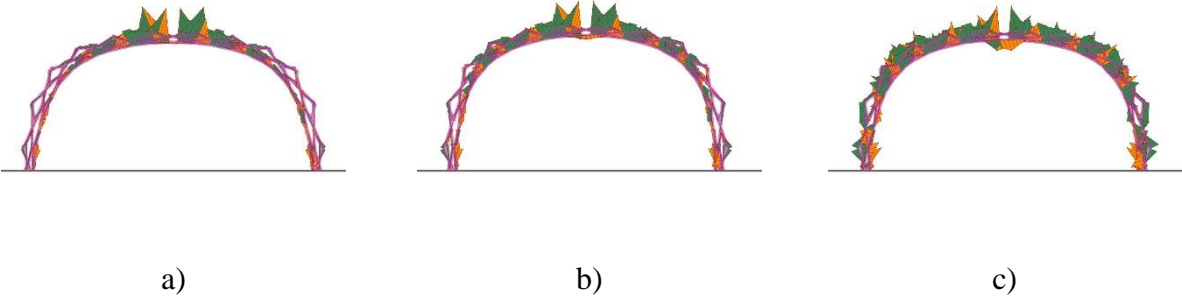


Figure 245_ Internal member moments in the arch structure induced by the gradual support movements. a) step one: support movements 15 cm to left and 5 cm upwards. b) step two: support movements 30 cm to left and 10 cm upwards. c) step three: support movements 45 cm to left and 15 cm upwards.

Using the analytical model internal forces of reciprocal members and their utilization factors were calculated and visualized as depicted in the Figure 246.

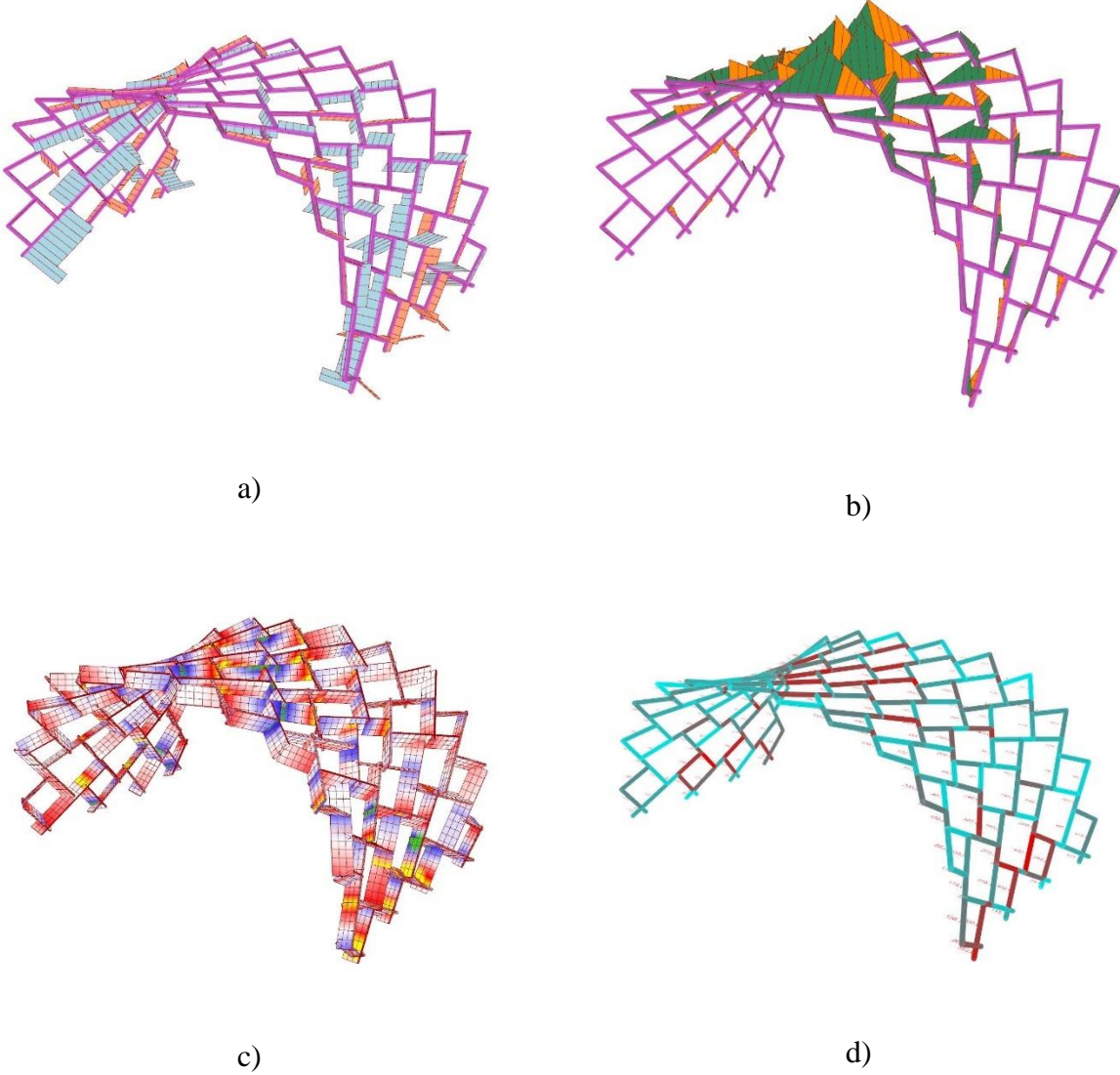


Figure 246_ Internal member forces in the arch induced by the support movements (30 cm to left, 15 cm upwards). a) axial member forces, b) bending moments, c) stress distribution, d) member utilization factor.

A custom code was developed to calculate and visualize the utilization factor based on the combined bi-flexural and axial loading formulation. This visualization was used to determine the

critical members before the application of the support displacement so the joints could be reinforced using high strength tape (Figure 247).

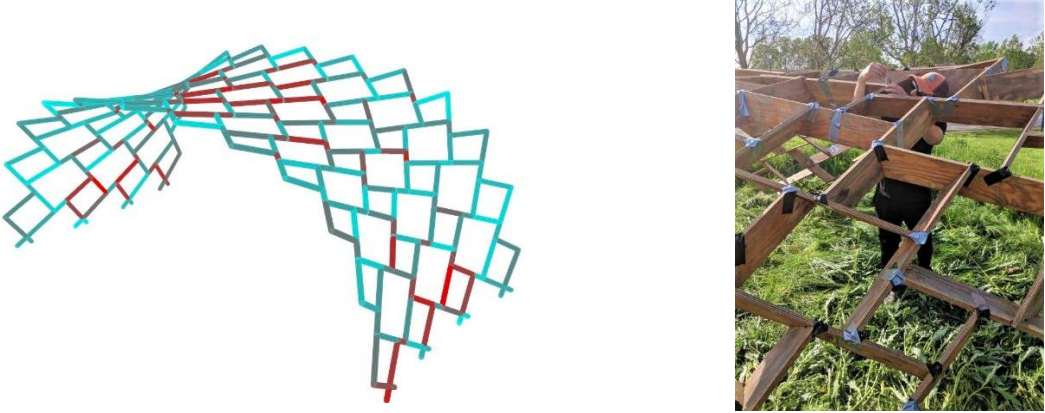


Figure 247_ Using the simulation results to reinforce the joints with maximum utilizations prior to supports displacement.

The displacement pattern was marked for each support base plate on the ground under the arch, and for each top central member using hanging measures. The displacements were gradually applied to the structure as shown in Figure 248.

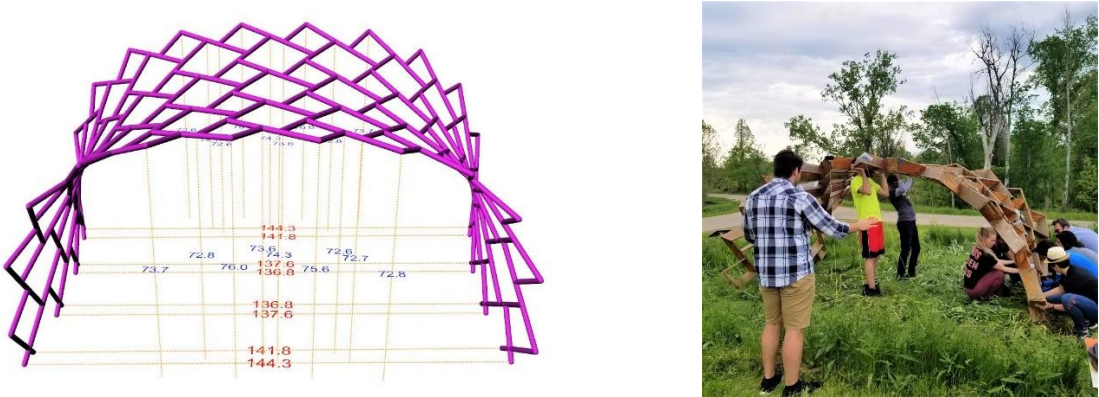


Figure 248_ Support displacement scheme and target support locations.

Figure 249 and Figure 250 depict the results of the arch geometry after the support displacement and compares it with the initial arch geometry.

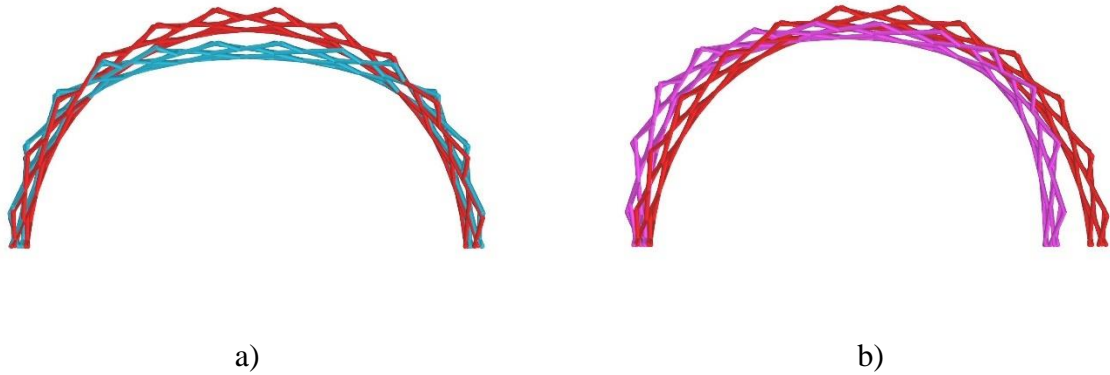


Figure 249_ Arch geometry: a) deformed arch (blue) vs initial arch (red), b) arch geometry after moving the supports to the target locations (purple) vs initial arch (red).

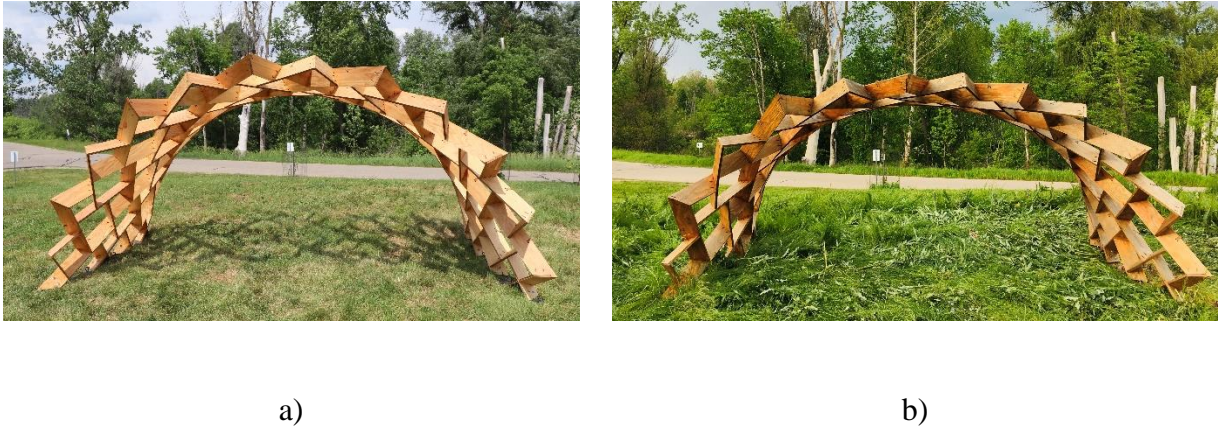


Figure 250_ Arch geometry. a) initial arch geometry right after erection, b) arch geometry after moving the supports to the target locations.

The physical measurements data paired with the simulation model made it possible to try different support displacement scenarios to choose a desirable displacement scheme that

retrieved the initial height of the arch while keeping the members stress levels below the critical level. The process of the support displacement partially retrieved the initial arch height.

6.8 Discussion and conclusions

This chapter explains the process and the structure of the computational design process for design to fabrication of reciprocal systems with planar elements. A modular computational method was developed to address the interconnected design constraints of reciprocal systems. Each of the design modules were developed in the previous chapters and used to study different design parameters individually. In this chapter, these design modules were connected with an efficient digital dataflow to create an integrative design to fabrication process.

The computational model is comprised of different modules, combining custom software (self-made) and commercial software (standard). Some of these software were developed to do a specific design or evaluation task (pattern generation, fabrication data generation, or code based structural evaluations) and some were developed to translate and transfer data between the self-made modules and commercial software (analytical model development, developing performance metrics from the simulation outputs, data transfer, and data storage). The structure and the implementation of each design module was explained, along with their role and applications within the computational design process. An efficient digital workflow was developed to integrate these design modules and to implement a practical performance-based and fabrication-aware design process. Furthermore, all the design modules (geometry generation, form-finding, analysis, and fabrication module) were implemented in an associative parametric environment that generated numerical and visual data feedback based on the design parameters. This computational model is compatible for automation using design exploration and optimization methods to address the complexity of the interconnected design parameters and

conflicting design constraints (such as structural performance, fabrication metrics, shading capacity, material use, machine time, and etc.). The computational model was then used for the design and fabrication of a full-scale arch prototype as a public pavilion located at Matthaei Botanical Gardens in Ann Arbor, Michigan.

To this end, the design constraints were defined based on the project goals and performance and fabrication metrics. Then, the computational model was used in a multi-objective design exploration to find the range of better performing design solutions within the design constraints. The final design geometry was informed by the results of the exploration process. The computational model generated all the required fabrication data. The fabrication process of the arch was explained through different steps including: 5-axis CNC routing of reciprocal members, sorting and labeling, predrilling, coating, support connection detailing and fabrication, assembly, and erection.

To study some of the long-term issues of using plywood as the construction material for this project a series of post-construction inspections were carried out in the duration of 16 months after the arch setup. Multiple issues were observed through these inspections including: material discoloring and deterioration due to humidity and UV exposure, permanent deformations of the members under self-weight and environmental loads, and failure of the connections due to material deterioration and defects.

Finally, the physical measurements data paired with the simulation model made it possible to try different support displacement scenarios to choose a desirable scheme that retrieved the initial height of the arch (which sagged after nine months) while keeping the members stress levels below the critical level.

References

APA – The Engineered Wood Association. <https://www.apawood.org/plywood>

Apolinarska, Aleksandra A. "Complex Timber Structures from Simple Elements: Computational Design of Novel Bar Structures for Robotic Fabrication and Assembly." PhD diss., ETH Zurich, 2018.

Asefi, Maziar, and Mahnaz Bahremandi-Tolou. "Design challenges of reciprocal frame structures in architecture." *Journal of Building Engineering* 26 (2019): 100867.

Kohlhammer, Thomas, Aleksandra Anna Apolinarska, Fabio Gramazio, and Matthias Kohler. "Design and structural analysis of complex timber structures with glued T-joint connections for robotic assembly." *International Journal of Space Structures* 32, no. 3-4 (2017): 199-215.

Preisinger, Clemens. "Linking structure and parametric geometry." *Architectural Design* 83, no. 2 (2013): 110-113. (Karamba (Karamba, Parametric Engineering, Available: www.karamba3d.com)

Von Buelow, Peter. "ParaGen: Performative Exploration of generative systems." *Journal of the International Association for Shell and Spatial Structures* 53, no

Chapter 7: Conclusions

7.1 Summary

Using the capacities of computation and digital fabrication this dissertation provides a basis for a novel process of design to fabrication for reciprocal systems. Specifically, the focus lies in self-supporting systems based on planar elements which have a high fabrication efficiency from sheet materials. This research demonstrates the essential need for the application of an integrative design process to address the complex coupling of geometry, structural performance and fabrication and presents a novel computational process for design to fabrication of these systems. The proposed computational design process is developed by rethinking and replacing the conventional direct incremental development by a modular integrative computational process using multi-directional dataflow between modeling, analysis and fabrication modules. Finally, the proposed framework is used for a full-scale design to fabrication case study to validate the applicability of the design process.

A synopsis of the research is provided in this chapter which explains the contributions of the research and the conclusions derived from the results.

7.2 Conclusions, Contributions and synthesis

In addressing different design aspects of reciprocal systems, new design methods and tools are required. This dissertation identifies the main limitations of the existing methods and proposes practical solutions for an efficient design development, including modelling, analysis and

fabrication. The results demonstrate the complex coupling of geometry, structural performance and fabrication in these systems, hence an essential need for application of an integrative design process. Though application of computation, simulation, and digital fabrication this research proposes an integrative computational design process which can effectively address the coupling of design, analysis and fabrication of reciprocal systems and accommodate design exploration and optimization. This chapter summarizes the key contributions and findings of each dissertation chapter and provides a synthesis of the research.

Chapter 2 introduces some of the main concepts and strategies in the field of computational design and explores their scope and applications within the academic and industry driven research. In this regard, architectural representations of generative design are explained through the ways the geometry and organization of space is informed based on the underlying rules defined by the main design drivers including performance, tectonic, material, and fabrication. The application of these design methods is investigated through study of pre-, post-, and co-rationalization methods in academic and industrial research and qualities, timing and the scope of application of each of these methods are investigated. The review shows the necessity for the implementation of flexible computational design processes with capacities to integrate real-time and continuous data feedback including performance goals (performance-based design) and fabrication constraints (fabrication-aware design). This analytical review establishes the theoretical framework for the proposed performance-based and fabrication-aware design process of reciprocal systems.

In Chapter 3 the complexities of the design and form-finding of reciprocal systems are explored, and a generalizable design method is proposed. First, the limitations of the existing design methods (such as case specificness and lack of generalizability, limitations in formal complexity,

lack of capacity for the integration of performance and fabrication parameters) are studied, and a generalizable computational method is proposed for geometric design and form-finding of these systems. It is shown that the proposed method is applicable to different geometry types (synclastic and anticlastic surfaces) and accommodates varying degrees of formal complexity.

The proposed design method consists of two steps, a generative modelling process and a dynamic form-finding process. The modelling process uses a geometric formulation using the quadrilateral mesh data derived from the rationalization of the base geometry to generate the reciprocal patterning. This novel method uses the neighboring cell mesh data in the formulation which eliminates the limitations of similar methods that only operate on ordered meshes. The form-finding process uses the dynamic relaxation method to solve the constraint-based model, which iteratively and simultaneously minimizes the eccentricities between the members to generate the proper geometric model for analysis and fabrication of 2-D and 3-D reciprocal systems. Finally, effectiveness and speed of the proposed method is studied quantitatively, and visualization techniques are developed for post-processing of the form-finding results.

Chapter 4 investigates the structural behavior of the reciprocal systems. To this end, a geometric method is proposed to generate an analytical model that can address the geometric complexity of the reciprocal systems and the different member connectivity conditions between their members affected by member eccentricities. This analytical model is then analyzed using a finite element method to study the effect of different design parameters (mesh density, engagement length, rotational angle and member connectivity conditions) on the structural behavior and flexibility of the reciprocal systems. Through the application of the proposed method a comprehensive parametric study of reciprocal structures is carried out on different scales including: reciprocal member, reciprocal module, and reciprocal structure. The results reveal a complex relationship

between the governing parameters (mesh density, engagement length and connection type) and the structural performance even in regular flat reciprocal systems. Although, these studies provide significant insight into the structural behavior of the reciprocal systems, however the results remain inconclusive, showing that it is impossible to derive a generalizable design guideline applicable to all design typologies, hence there is an urgent need for a real-time performance feedback for optimal design of irregular and free-form reciprocal systems.

Finally, the cumulative effects of the design parameters are studied through an optimization process for a flat reciprocal system. The results of the optimization show that, a design approach purely driven by structural response would result in minimizing the engagement length as the flat reciprocal system converges to its gridshell counterpart. However, integrating the fabrication and assembly parameters (minimum engagement length for accessibility for assembly, connection type, material use, and CNC machine time) can significantly change the optimal solution. It becomes clear that, due to the complex interconnection between geometry, structural performance and fabrication constraints, the optimal configuration of the design parameters is neither trivial nor intuitive. As a result, a design process with real-time fabrication and performance feedback is essential to address the design complexity of the reciprocal systems.

Chapter 5 studies the fabrication process for reciprocal structures with 2-D and 3-D configurations and provides guidelines for selection of the main fabrication parameters including: joint detailing parameters, material dimensional tolerances, and digital fabrication parameters and tolerances. This chapter argues that integrating these design parameters in the design process can provide essential feedback to ensure the constructability of the design solutions and proposes a scalable and efficient fabrication process for reciprocal systems with 3-D module geometry using 5-axis CNC machinery.

In this chapter, four different connection types are studied for reciprocal systems with 2-D and 3-D member connections, and applications and limitations of each connection design is explained. This information is helpful in decision making for connection design in different scenarios in relation to the function of the reciprocal system, choice of the digital fabrication technology, and choice of material.

It is argued that, one of the important considerations for the digital fabrication of reciprocal structures is the fabrication tolerances including: tolerances specific to the digital fabrication machinery and tools, material dimensional tolerances, and geometric modeling and form-finding tolerances. It is demonstrated that, these design and fabrication tolerances depend on the choice of digital fabrication, material properties, and member connection type. These tolerances are studied through fabrication of multiple physical prototypes. Moreover, destructive structural tests are carried out to study the mechanical behavior of the connections and possible failure modes of the structure. Physical prototyping paired with destructive structural tests and a detailed finite element analysis provide valuable insight into behavior of reciprocal systems connections, and indicate that fabrication tolerances have a substantial and complex effect on the mechanical behavior and assembly process of connections. Based on the observations regarding the vulnerability of the connections, it is beneficial to reduce the depth of the notch cuts to keep the structural depth as much as possible, in contrast the notch geometry and depth play an important role in the alignment of the connecting members in the assembly process. Additionally, it is structurally beneficial to fabricate the connection cuts with minimum tolerances, however minimum tolerances are restricted due to assembly requirements. It is argued that integrating fabrication parameters into the computational model is an effective way to evaluate different scenarios to make compromises between conflicting design criteria.

Chapter 6 responds to the necessity of developing an integrative design process to address the complexities and exploit the multi-disciplinary potentials of reciprocal systems. This chapter introduces a practical synthesis of the computational methods developed for modeling, form-finding, performance evaluation and fabrication data generation in a computational design process. Moreover, a multi-directional dataflow is implemented to integrate multi-disciplinary performance feedbacks into the computational design process. This chapter explained the structure of the proposed computational design process for design to fabrication of reciprocal systems with planar elements. A modular computational method was developed in a fully associative parametric environment to address the interconnected design constraints of reciprocal systems. Multiple design modules were developed and connected with an efficient multi-directional digital dataflow to create an integrative design to fabrication process. Finally, the proposed computational model has been paired with a design exploration method to address the complexity of the interconnected design parameters and conflicting design criteria in a full-scale design to fabrication case study project to validate the applicability of the proposed design process. The case study project demonstrates the effectiveness of the proposed computational design method in integrating design, analysis and fabrication considerations to explore well performing design solutions and guaranteeing the constructability using 5-axis CNC fabrication. Moreover, integrating fabrication data (3-D member geometry, fabrication cut patterns, and material use) made it possible to estimate the sheet material use and machine time and fabrication cost and use them as a design feedback, which made it possible to find affordable design solutions within the limited budget of the project.

This research demonstrated the necessity of developing an integrative design process to respond to the complex and interconnected design aspects of reciprocal systems which is not feasible

with direct incremental design methods. This research presented new methods for design, analysis and fabrication of reciprocal systems and proposed a novel integrative computational process for design to fabrication of these systems. Moreover, this research validated the applicability of the proposed computational design process through design to fabrication of a full-scale project. It is shown that the proposed computational method can handle the complex coupling of geometry, structural performance, and fabrication constraints in these systems and elevate the process of design to fabrication through intensive application of computation, simulation, and digital fabrication.

7.3 Outlook and future works

Developed at an intersection of multiple disciplines, the implementation of the proposed integrative computational design process opens new venues for further developments and applications both in research and practice. This thesis approaches the general problem of entanglement between form, structure and construction through an in-depth study of reciprocal structures. The resulting tools and methods developed for design, analysis and fabrication, and the implementation of the computational process, offer a practical and flexible design method for reciprocal systems. Moreover, the flexible structure of the modular computational design method with multi-disciplinary feedback systems demonstrates the implications of generalizable application of this approach to address the general problem of coupling of design constraints. This section proposes different venues to enhance the proposed computational design process for practical design to construction of reciprocal structures, and new venues to envision novel integrative design to fabrication processes with application and integration of digital and robotic technologies.

In this research linear, elastic analysis method is used to evaluate the structural performance of the reciprocal systems. Application of nonlinear and large deformation analysis methods would lead to a more accurate structural analysis results for large-scale reciprocal structures. This can be achieved by integration of appropriate software (commercial or custom) with nonlinear analysis capabilities into the proposed computational design method.

The proposed computational design method generates the required fabrication data including member geometries and cut patterns, however a post processing procedure is needed to generate the G-code using commercial software for CNC fabrication, depending on the size of the structure this process can be time consuming. Therefore, it would be efficient to implement the G-code generation in the computational design method, moreover, this development would provide a more accurate estimation of material use and machine time.

This research is focused on design of reciprocal systems for human-led assembly, which is studied through extensive digital and physical prototyping of connection detailing and the assembly process, however the assembly sequencing is not integrated in the computational design process. Developing assembly sequencing algorithms using graph-based methods can significantly enhance the computational design process to evaluate different constructions approaches and verify assembly feasibility.

One of the areas of research on reciprocal systems, that has received significant attention in the recent years, is the field of robotic fabrication and robotic assembly. The main reason for this attraction is the capacity of reciprocal systems to reduce the complexity of connections by reducing the number of members connecting at each joint. Using T-joint connections for fabrication, reciprocal configurations produce minimal assembly constraints for robotic assembly. Typically, T-joint connections require application of external fasteners or glue which

requires manual post processing. However, with integration of feedback from sensors and scanners the assembly tool pathing can be informed to allow application of more reliable and self-supporting connection types which reduce the post processing time and labor. Moreover, integration of structural feedback paired with assembly sequencing algorithms and smart tool pathing mechanisms can lead to development of autonomous robotic fabrication methods for design to fabrication of self-supporting systems taking advantage of reciprocal configurations. Another area for future enhancement relates to capacities for sharing the tools and transferability of the technology. The modular nature of the proposed computational design method supports further developments through addition of modules with new functionalities. More importantly, it supports releasing the method in the form of a plug-in to make it accessible to a wider group of prospective users and facilitate further research in this topic. However, a more flexible software structure is required to address the transferability of the proposed tools and methods to other use-cases or different structural topologies.

Finally, this thesis provides a basis for further developments in the application of reciprocal configurations for lightweight and modular construction. Moreover, this research proposes new venues to revisit the question of entanglement of form, structure and fabrication from both design and technological point of view through application of computational design process.